Antimicrobial potential of diverse nature-based synthetic analogues and bio-fabricated nanoparticles derived from ethnomedicinal plants *Albizia lebbeck* and *Oxalis corniculata*

THESIS SUBMITTED FOR THE DEGREE OF

DOCTOR OF PHILOSOPHY (SCIENCE)

JADAVPUR UNIVERSITY

KOLKATA – 700032,

WEST BENGAL, INDIA

BY

Ananya Das Mahapatra, M. Sc.

Registration No- SLSBT1123516

ICMR -NICED,

Kolkata-700010, West Bengal, India

Declaration of the Scholar

I declare that this written submission suggests my creative approaches in my own words and where other's ideas have been included. I have properly cited with suitable reference from authentic sources. I also declare that I have adhered to all origins of academic principle and honesty and have not misled or fabricated or falsified any approach/ data/ origin in my submission. I understand such violation of the above will cause disciplinary action by University and can evoke penal action from the sources which have thus not been properly cited or from whom proper permission has not been taken when needed.

Ananya Das Mahapatra

Ananya Das Mahapatra

Dedicated to my

Parents

Acknowledgement

It is one of the achievements in my life when I have an opportunity to express my warm regards and gratitude to those people, to whom I am very much grateful. I take this opportunity with much pleasure to thank all the people who have helped me a lot and inspired me through the course of my journey during my entire research work leading to the final form of thesis being submitted for my Ph.D. degree. It is a great pleasure and satisfaction to convey my gratitude to all of them in my humble acknowledgment.

Firstly I would like to express my heartiest gratitude, deepest regard and beloved thanks to my respected supervisors as well as my mentors Dr. Debprasad Chattopadhyay (former Director of ICMR-National Institute of Traditional Medicine, Belagavi, Karnataka and Scientist F, ICMR-NICED, Virus Laboratory, Beliaghata, Kolkata, India), a renounce Scientist with gentle behaviour and havoc power of perception, motivation, positive attitude along with good mentality for helping and supporting during my entire research work and I humbly offer my deepest obeisance to me another Supervisor Professor Chittaranjan Sinha, Department of Chemistry, Jadavpur University, Kolkata - 700 032, who offered me the scope to be one of the Research Scholars under his supervision. His constant guidance, perpetual inspiration with occasional reformatory thrashings always acted as motivating factors to my research works. It is a great honor and a matter of pride to be a research scholar of an exceptionally brilliant scientist and wonderful person. I am indebted to him for teaching me with his innovative ideas the way to address a problem and shaping me scientifically as a researcher. Sir, your passion and dedication in science and your "never give up attitude" has always inspired me and enriched my growth as a student and researcher. Above all and the most needed thank you Sir, for keeping faith in my abilities.

I would like to duly acknowledge Vice Chancellor, Pro Vice Chancellor, Secretary of Science, and Registrar, Jadavpur University for my academic affiliation and Ph.D. registration.

I am grateful to the Director, ICMR-NICED, Beliaghata, Kolkata for providing all laboratory facilities to do my research work. I would like to express my regard to all scientists and employees of ICMR Virus Laboratory for their cooperation and help.

I am very much thankful to the staff members of the Dept. of Chemistry, for their help in different respect and help are render from my research group Continuous help rendered by the researchers of this research group *viz*., Dr. Chiranjit Patra, Dr. Rakesh Purkait, Dr. Sunanda Dey, Dr. Kousik Naskar, Dr. Basudeb Dutta, Mr. Srikanta Jana, Dr. Angeera Chandra, Miss. Sukanya Paul, Mr. Joy Mondal and others.

Words are not enough to convey my deepest thank to my grandparents, my parents, my spouse and my sisters. My thesis is dedicated to their prayers, sacrifices, patience, love and unconditional support. Thank you so much for accepting me the way I am for supporting me throughout. This thesis would never be possible without your help and support.

Last but not least I would like to express my warm thanks to God almighty for giving me strength, courage and patience to complete my thesis and for bringing me so far in my academic career.

.

(Ananya Das Mahapatra)

ICMR- NICED, Virus Laboratory

Beliaghata, Kolkata

CONTENTS

Abstract

Title: Antimicrobial potential of diverse nature-based synthetic analogues and bio- fabricated nanoparticles derived from ethnomedicinal plants *Albizia lebbeck* and *Oxalis corniculata*.

The main motivation of this research is the exploration of more efficient less toxic antimicrobial drugs using less expensive biofriendly materials following semi-synthetic green techniques. Synthesis of silver nanoparticles has been carried out by using two folk-lore of Jangalmohal, West Bengal. These are *Albizia lebbeck* (local name, Sirish) and *Oxalis corniculate* (local name, Amrul) and the antibacterial activities of the crude extracts of *Albizia lebbeck* and *Oxalis corniculata* lie at 250-1000μg/ml. The antibacterial activities of AgNPs@*Albizia lebbeck Oxalis corniculata* have been significantly improved. A series of new sulfonamide derivatives incorporating nature-based analogues of Coumarin is reported in this Thesis. On the other hand, different nucleoside and non-nucleoside analogues have been synthesized, characterized, and used to discover less toxic better antimicrobial agents. The characterizations of the derivatives have been done by spectroscopic and other photo physical techniques and bio-fabricated nanoparticles have been characterized by both spectroscopic and microscopic techniques. The antibacterial susceptibility was evaluated by standard disc-diffusion, agar and broth-dilution methods. Some of the derivatives are used to

investigate the interaction with surface glycoprotein of Herpes Simplex Virus (HSV)-1 to discover their antiviral activity, if any, in virus-infected Vero cells.

The thesis consists of six chapters. **Chapter 1** is the review of literature for ethnomedicine and *in vitro* anti-microbial activity of green synthesized nanomaterials and different semi-synthetic compounds including new Schiff bases incorporated with coumarin moiety and Sulfonamide derivatives to discover new lead molecules with high activity and less cellular toxicity. The **Chapter 2** describes the synthesis, structure and bioactivity studies including antimicrobial and anti-oxidant activities of silver nanoparticle (AgNPs) synthesized using the bark extract of *Albizia lebbeck*. **Chapter 3** includes the spectral characterization and anti-bacterial activities of bio-fabricated silver-nanoparticles AgNPs from the herb *Oxalis corniculata*. Here, we also include the significant anti-biofilm activities, followed by and cell viability assay of AgNPs in Vero cell. The **Chapter 4** represent the synthesis characterization of novel nucleoside-based pyridine functionalized derivatives, along with their anti-HSV activity. Here, we have re-examined the anti-HSV-1 activity of certain amides compounds having nucleoside-moiety by cytopathic effect (CPE) and standard Plaque reduction assays, with the possible mode of action in HSV-infected Vero cells *in vitro*. While the **Chapter 5** depicts the antimicrobial activity of Schiff's base derived from 7-Hydroxy-4-methyl-2-oxo-2H-chromene-8-carbaldehyde and four different sulphonamides (Sulfapyridin, Sulfathiazole, Sulfa-methoxazole, Sulfamerazine). The last chapter, **Chapter 6**, contained supramolecular assembly of an Au (III)-complex and its biological activities. Here, 2-(3-Phenyl-1H-1, 2, 4-

triazol-5-yl) pyridine acts as bidentate N, N$^/$-chelator, and forms Au (III)-complex

[**Au** (2-ptp)$_2$]Cl (**1**). The structure has been characterized by single-crystal X-ray

diffraction technique and other spectroscopic data.

Dr. **Debprasad Chattopadhyay**

Former Founder-Director & Scientist G
ICMR-National Institute of Traditional
Medicine Belagavi, Karnataka
 And Scientist F, ICMR-Virus Unit
Kolkata (Now ICMR-NICED)

Prof Dr. **Chittaranjan Sinha**

Department of Chemistry
Jadavpur University, Kolkata
(Signature of the Supervisors, date with Seal)

Ananya Das Mahapatra

Senior Research Fellow, DST-INSPIRE
(Signature of the Candidate)

Abbreviation

AE: Aqueous extract

ALP: Alkaline phosphatase

ATCC: American type culture collection

BSA: Bovine serum albumin

CFU: Colony forming unit

CC_{50}: Cytotoxic concentration that is toxic to 50% cells

CMC: Carboxy methyl cellulose

CMV: Cytomegalovirus

CPE: Cytopathic effect

$CHCl_3$: Chloroform

DLS: Dynamic Light Scattering

DMSO: Dimethyl sulfoxide

DMEM: Dulbecco's minimum essential medium

EC_{50}: effective concentration required to achieve 50% protection

ELISA: Enzyme-linked immunosorbent assay

EMEM: Eagle's minimum essential medium

FBS: Fetal bovine serum

FCS: Fetal calf serum

FTIR: Fourier Transform Infrared Spectroscopy

HCl: Hydrochloric acid

HPLC: High-performance liquid chromatography

HSV: Herpes simplex virus

HIV: Human immunodeficiency virus

IL: Interleukin

IR: Infra-red

LD$_{50}$: 50% or median lethal dose

MBC: Minimum bactericidal concentration

ME: Methanol extract

MeOH: Methanol

MgCl$_2$: Magnesium chloride

MIC: Minimum inhibitory concentration

MOI: Multiplicity of Infection

MS: Mass spectrometry

MTT: (3-(4, 5-Dimethylthiazol-2-yl)-2, 5-diphenyltetrazolium bromide

NMR: Nuclear magnetic resonance

OC: *Oxalis corniculata*

PBS: Phosphate buffer saline

PGE2: Prostaglandin E2

POL: Polymerase

RPMI: Roswell park memorial institute medium

RTPCR: Reverse transcriptase polymerase chain reaction

SEM: Scanning Electron Microscopy

SI: Selectivity index (CC$_{50}$/EC$_{50}$)

SMX: Sulfamethoxazole

TEM: Transmission Electron Microscopy

TLC: Thin Layer chromatography

TK: Thymidine kinase

TNFα: Tumor necrosis factor

UV: Ultra Violet

Rights and Permission

Chapter 1:

Figure reprinted with permission from *Scientific Reports* 2017, 7, 1–3.

Copyright: Spinger Nature.

Figure reprinted with permission from *J. pharmacogn. Phytochem*, 2018, 7, 1020–1023.

Copyright: Journal of Pharmacognosy and Phytochemistry.

Chapter 2:

Figure reprinted with permission from *Chemistry Select* 2020, 5: 4770–4777.

Copyright: Wiley.

Chapter 3:

Figure reprinted with permission from *Journal of Indian Chemical Society* 2022, 99: 100529.

Copyright: Elsevier.

Chapter 6:

Figure reprinted with permission from *Applied Organometallic Chemistry* 2022. e6754.

Copyright: Wiley.

Research Publications

Included in Thesis:

1. **Das Mahapatra A**, Patra C, Mondal J, Pal K, Sinha C, Chattopadhyay D (2022).Green synthesis of AgNPs from aqueous extract of *Oxalis corniculata* and its anti-biofilm and antimicrobial activity. *Journal of Indian Chemical Society.* 99:100529.

2. **Das Mahapatra A**, Patra C, Mondal J, Sinha C, Sadhukhan PC, Chattopadhyay D (2020). Silver Nanoparticles Derived from *Albizia lebbeck* Bark Extract Demonstrate Killing of Multidrug- Resistant Bacteria by Damaging Cellular Architecture with Antioxidant Activity. *Chemistry Select*. 5: 4770–4777.

3. Shit M, Dey A, **Das Mahapatra A**, Dutta B, Naskar K, Ray PP, Sinha C. Supramolecular assembly of an Au (III) complex of 2- (3- phenyl- 1H- 1, 2, 4- triazol- 5- yl) pyridine: structure, biological studies and charge transportation. *Applied Organometallic Chemistry*. e6754.

Not Included in Thesis:

1. Mondal J, Patra C, **Das Mahapatra A**, Mandal KC, Chattopadhyay D (2022). Ethnomedicinal Plant Stephania hernandifolia and its Active Fraction 2- Chloroethyl Linoleate Inhibits HSV-2 Infection by Blocking Viral Immediate Early and Early Transcription. *Current Drug Therapy.*

2. Mondal J, **Das Mahapatra A**, Mandal KC, Chattopadhyay D (2021). An extract of *Stephania hernandifolia*, an ethnomedicinal plant, inhibits herpes simplex virus 1 entry. *Archives of Virology*. 26:1–2.

3. Das B, Dolai M, Ghosh A, Dhara A, **Das Mahapatra A**, Chattopadhyay D, Mabhai S, Jana A, Dey S, Misra A (2021). A bio-compatible pyridine–pyrazole hydrazide

based compartmental receptor for Al $^{3+}$ sensing and its application in cell imaging. *Analytical Methods.* 13: 4266–4279.

4. Dey S, Maity S, **Das Mahapatra A**, Chattopadhyay D, Sinha C (2019). A Phenyl Thioether- Based Probe: Zn^{2+} Ion Sensor, Structure Determination and Live Cell Imaging. *ChemistrySelect.* 4: 4472–4477.

5. Das B, Jana A, **Das Mahapatra A**, Chattopadhyay D, Dhara A, Mabhai S, Dey S (2019). Fluorescein derived Schiff base as fluorometric zinc (II) sensor via 'turn on' response and its application in live cell imaging. *Spectrochimica Acta Part A: Molecular and Biomolecular Spectroscopy.* 212: 222–231.

6. Purkait R, **Das Mahapatra A**, Chattopadhyay D, Sinha C (2019). An azine-based carbothioamide chemosensor for selective and sensitive turn-on-off sequential detection of Zn (II) and H2PO4−, live cell imaging and INHIBIT logic gate. *Spectrochimica Acta Part A: Molecular and Biomolecular Spectroscopy.* 207:164–172.

7. Purkait R, Patra C, **Das Mahapatra A**, Chattopadhyay D, Sinha C (2018). A visible light excitable chromone appended hydrazide chemosensor for sequential sensing of Al^{+3} and F− in aqueous medium and in Vero cells. *Sensors and Actuators B: Chemical.* 257: 545–552.

8. Goswami D, **Das Mahapatra A**, Banerjee S, Kar A, Ojha D, Mukherjee PK, Chattopadhyay D (2018). *Boswellia serrata* oleo-gum-resin and β-boswellic acid inhibits HSV-1 infection in vitro through modulation of NF-κB and p38 MAP kinase signaling. *Phytomedicine.* 51: 94–103.

9. Sahu N, Mondal S, Naskar K, **Das Mahapatra A**, Gupta S, Slawin AMZ, Chattopadhyay D, Sinha C (2018). Spectroscopic characterization, antimicrobial activity and molecular docking study of novel azo-imine functionalized sulfamethoxazoles. *Journal of Molecular Structure.* 1155: 152–164.

10. Patra C, Sen C, **Das Mahapatra A**, Chattopadhyay D, Mahapatra A, Sinha C (2017). Pyridylthioether-hydroxycoumarin Schiff base as selective Zn2+ fluorescence sensor, application in life cell imaging and uses of resulting complex as secondary probe for ATP sensing. *Journal of Photochemistry and Photobiology A: Chemistry.* 341: 97–107.

Book Chapter

Das Mahapatra A, Bhowmik P, Banerjee A, Das A, Ojha D, Chattopadhyay D (2019). Ethnomedicinal Wisdom: An Approach for Antiviral Drug Development. *In New Look to Phytomedicine,* 35-61 (Academic Press, Elsevier Science).

Kar A, **Das Mahapatra A,** Das Gupta A, Chattopadhyay D (2022).Validation of antiviral potential of herbal ethnomedicine, *Science Direct*, 251-281

Conference Attended

Poster Presentation

1. **Das Mahapatra A**, Sinha C, Chattopadhyay D, Exploration of Anti-HSV potential of nucleoside Analogue, 58th Annual Convention of Chemists and International Conference on "Recent Trends in Chemical Sciences (RTCS-2021)" organized by the Indian Chemical Society, Kolkata, December 21st – 24th, 2021.

2. **Das Mahapatra A**, Sinha C, Chattopadhyay D, A fight between Defense Weapons of the Immune System and COVID-19 virus, International Seminar on Recent Advances in Chemistry & Material Sciences 2020 organized by the Indian Chemical Society August, 2020. (**S. S. Bhatnagar Young Scientist Award**).

3. **Das Mahapatra A,** Goswami D, Chattopadhyay D, *Boswellia serrata* gum-resin inhibits HSV-1 infection by modulation of NF-κB signalling, International Conference by New Horizons in Biotechnology, 20th to 24th November 2019, Thiruvananthapuram, Kerala. (Poster Presentation)

4. **Das Mahapatra A**, Patra C, Mitra A, Chattopadhyay D, Sinha C, Antibacterial and safety potential of selected smx and non-smx derivatives: A prospectus study, Fifty fifth Annual Convocation of Chemists by Indian Chemical Society, 2018, Bhagalpur, Bihar. (Poster Presentation)

Oral Presentation

1. **Das Mahapatra A**, Mitra A, Mondal J, Ghosh A, Ojha D, Mondal KC, Chattopadhyay D, Evaluation of Antimicrobial potential of an Ethnomedicinal formulation of Jangalmohal against selected MDR-bacteria and Herpes Simplex Virus, 27th West Bengal State Science & Technology Congress, 2019-20, (MAKAUT), Haringhata, Nadia.

Awards and Recognition

1. M.Sc. Biochemistry, 1st Class 1st from Vidyasagar University, West Bengal, India.

2. DST-INSPIRE Fellowship, DST, India (IF160144).

3. Qualified GATE with AIR-209.

Chapter 1

INTRODUCTION

Partial Review of literature on ethnomedicine and use of AgNPs obtained from green synthesis and their antimicrobial activities. A literature survey is focused on synthetic sulphonamides and coumarinyl amides for their application in antibacterial and antiviral programs. Concerning the literature report, the present research work is designed.

1.1 Introduction

People and plants' communication is too intimate all throughout the advancement of human civilization. At present human is the most affluent species among all animals on Earth. Among the plants, the richest species are those that are cultivated. The evolutionary success of human and useful plant symbionts is connected with the rise of a strong mutual dependence between the partners [1]. The production of plant-based food provides not only complete nutrition in terms of carbohydrates, plant proteins containing amino acids, and fats but also vitamins, minerals, micronutrients, and phytofactors, required for good health. A huge number of natural compounds derived from plants and microbes also have broad pharmaceutical applications [2]. The use of plants for various ailments by our ancestors specifies that plant-derived medication is a rich tradition of our civilizations. Even though a large no of compounds are derived from medicinal plants using the modern drug discovery process, their availability in rather small quantities imposes several challenges like insufficient to optimize, develop, and test leads. Therefore, compared to procedures based on chemicals, methods for discovering new drugs utilising medicinal plants typically take significantly longer and are more difficult [3]. However challenging it may be to isolate natural products from medicinal plants for use as drugs, these products may remain a vital part of the quest for new therapeutics.

गृहकृत्वानिकाष्ठानिक्षुद्रजन्तुगृहंतथा।सत्रनिवर्त्तनंप्रोक्तंभिक्षापात्रैःसमाकृताः।।फलन्तिवत्सरेमध्येद्वौवारौ शकुनादयः।सांवत्सरंपितुमातुरुपकारंफलैःकृतम्।।एवंपुत्रसमारोपाएवंतत्त्वविदोविदुः। (बराहःपुराण, 170-40-41) [4].

1.2 Ethnomedicine

Ethnomedicine is the knowledge of the composite multifaceted long-term medical practices where the activity or function of plants, spirituality, belief, as well as nature,

2

and surrounding environment collectively contributed to the healing process, worried with the cultural perceptions of health and diseases [5]. In the last few decades, research interest and studies in ethnomedicine have increased massively.

Scientists began unravelling the chemistry of ethnomedicines as natural products chemists, pharmacologists, microbiologists, and biochemists began examining them. Since its inception, research in ethnomedicine immensely contributed to the understanding of traditional, medical knowledge and practice. The study of the ethnomedicine literature was motivated by increased awareness of health and disease by the indigenous people and maintaining ethnic identities as well as the search for new treatments and technologies [5]. The systematic study of drugs used by the ethnic groups leads to the development of a new branch named **Ethnopharmacology**, which is together linked to the use of plants, their botany, and pharmacology [6]. India and China are two major countries in Asia that are involved in the production and trade of herbal products and ethno-pharmaceuticals. In India total of 45,000 vascular plant species have been reported and among them, our folk medicine system has utilized 5000 plant species for different formulation preparation. Most tribal communities still depend on local traditional medicines for their survival [7, 8]. The forests of the Himalayas provide a rich reservoir of diverse medicinal plants that are vital to the native people [9]. More than half of the medications used in modern medicine come from natural sources or their derivatives. At least 25% of the contribution comes from higher plants. The tropical woods are home to around half of the species of flowering plants in the world, creating a huge diversity of species that can be used as medication sources. These plant species will continue to provide useful natural products to the chemists as the initial materials to develop-new lead molecules [10].

1.3 Nanotechnology

Nanotechnology is an expeditiously growing field and shows a key function in the areas of science, medicine, and technology because of its elevated charge density, smaller size, greater surface-to-volume ratio, lower melting point, diverse magnetic properties, higher catalytic rate, and higher solubility in suspensions.

The concept of "Nanotechnology" was developed in the late19[th] Century by the German Nobel Laureate Physicist Professor **Richard Feynman** who revealed nanoparticles when describing molecular machines designed with atomic precision entitled *"There's plenty of space at the bottom"* for the first time in 1959.
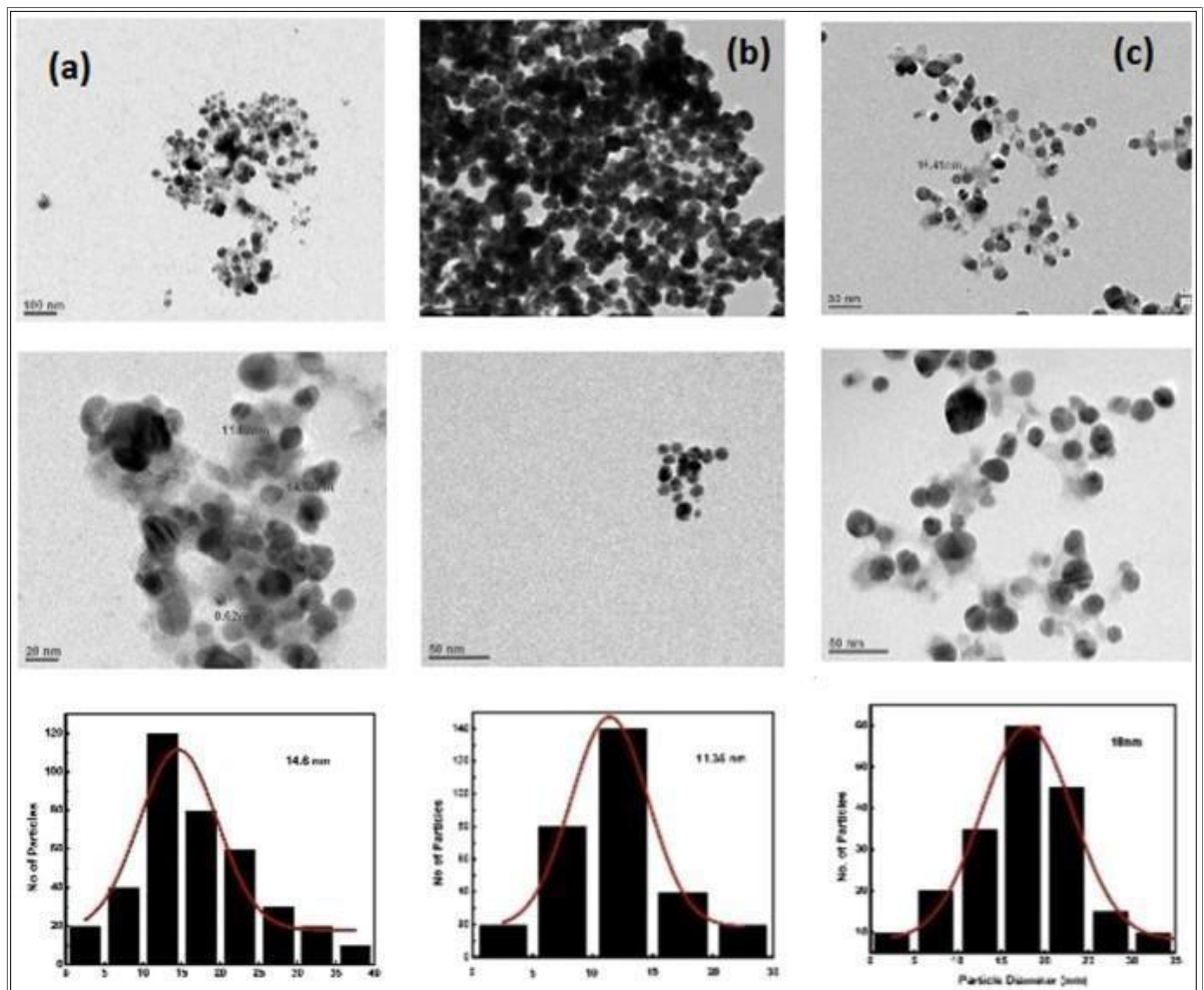

Fig. 1.1 Transmission Electron Microscopy image of silver nanoparticle(s) according to their size [11]. Reprinted with permission.

Generally, the "top to bottom" and "bottom to up" approaches are concerned with the creation of silver nanoparticles. In the 'bottom-to-top' approach, nanoparticles can be cultivated via biological and chemical way by self-assembly of atoms to new nuclei which raise into a particle of nanoscale; while in the 'top-to-bottom' approach, appropriate bulk material rupture by using various lithographic techniques like grinding to reduce the size into fine particles, milling, etc. [12]. Among all the noble metal nanoparticles, the silver nanoparticle has obtained boundless interest because of their exceptional properties of chemical stability, good conductivity, catalytic ability, and significant antiviral, antibacterial, antifungal, and anti-inflammatory activities that help silver nanoparticles to be included in composite fibers, cryogenic superconducting materials, cosmetic and food products, and electronic components [13]. Silver ions (Ag^+) in aqueous or non-aqueous solutions can be reduced using a variety of organic and inorganic reducing agents, including sodium borohydride $(NaBH_4)$, sodium citrate, ascorbate, elemental hydrogen, and polyethylene glycol block copolymers [14]. Among all metal nanoparticles, the silver nanoparticle is considered a central product in nanotechnology for its boundless interests due to its unique properties most importantly diverse bioactivities. Thus, nanoparticles can be incorporated into diverse use like composite fibers, cryogenic super-conducting materials, cosmetic and edible products, and electronic components [15]. AgNPs' bioactivity is influenced by a number of variables, such as their surface chemistry, size distribution, shape, coating or capping, agglomeration, dissolution rate, particle reactivity in solution, ion release efficiency, cell type, and the type of reducing agents used in their synthesis, which is an important factor in determining their cytotoxicity [16]. Smaller particles keep away from accumulation and precipitation because they have smaller Van der Waals attraction.

1.3.1 Importance of Green synthesized Nanomaterial

There are various physical, chemical, and biological processes that can be used to create nanoparticles. The plant-mediated nanomaterial has recently gained increasing attention for its extensive use in a variety of industries due to its physic-chemical characteristics. Routinely, nanoparticles are made by a method where chemicals are used as reducing and stabilizing agents, found to be responsible for various bio-risks due to the toxicity of many chemicals; causing serious ecological concerns that forced the chemists to develop environment-friendly processes [17]. In comparison to other synthetic techniques, bio-synthetic or "green synthesis" appears to be straightforward, quick, non-toxic, predictable, and capable of producing materials with well-defined sizes and morphologies under ideal circumstances for translational research [18, 19]. There are different metals such as gold, silver, platinum, zinc, copper, titanium oxide, magnetite, and nickel which can be combined with plant extracts to prepare biogenic nanoparticles [20]. The different parts of a plant such as a stem, root, fruit, seed, callus, peel, leaves, and flower are used as a natural source of stabilizing and capping agents during syntheses of metallic nanoparticles [21, 22]. Depending upon the nature of the extract derived from different plant resources the nanoparticles are in various shapes and sizes. The biological molecules undergo highly controlled assembly for creating them suitable for metal nanoparticle synthesis which was found to be reliable and eco-friendly [18]. Additionally, plant-mediated nanoparticles are employed as possible medicinal agents for bacteria with drug resistance [23].

Plant-based biomolecules undergo highly controlled assembly to suit metal nanoparticle synthesis. Although various physical and chemical processes are commonly used for the production of nanoparticles, they come with disadvantages such as the use of hazardous

6

chemicals, high energy consumption and low efficiency. In addition, there is a lot of waste produced that pollutes the environment. Due to their compliance with the environment and practical benefits, biosynthesis of nanoparticles has garnered considerable interest among scientists searching for novel ways to produce nanoparticles. Table 1.1 displays some significant uses of AgNPs in pharmaceutics, medicine, and dentistry.
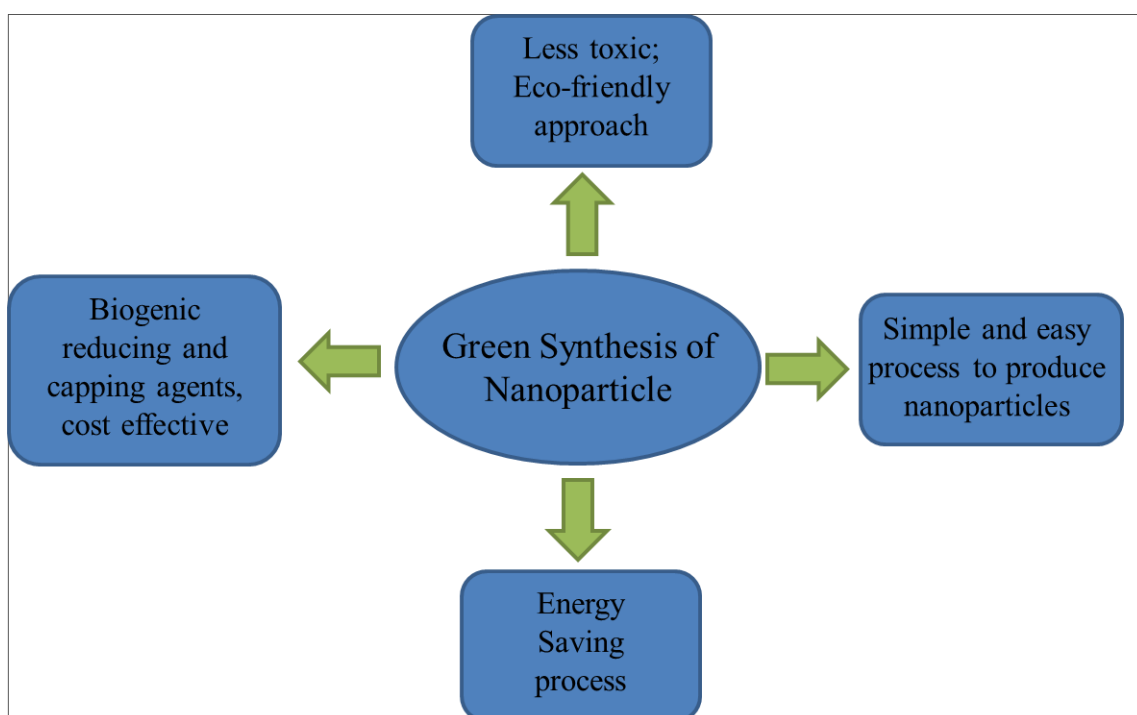

Fig. 1.2 Importance of Green synthesized nano particles.

Silver nanoparticles are potent nano-weapons in the destruction of growing multidrug-resistant bacteria [24]. Despite the development of hundreds of antimicrobial compounds and their derivatives, especially antibiotics, routine management of infections generated by microbes is still difficult [24]. Medicinal plants are one of the predominant natural resources for drug development and plants used as ethnomedicines of diverse cultures are believed to possess antimicrobial activities [25]. Multidrug resistance (MDR) organisms emerging rapidly are posing threat as many pathogenic microbes can protect them from the conventional as well as routinely used antimicrobial agents. Therefore,

there is a necessity for continuous investigation of new drugs to fight microbial infections.

The development of the discipline of ethnopharmacology is closely related to the history of botanical studies in West Bengal and the growing interest of the local population in plants. The only comprehensive and practical information about the flora of the former Bengal was published in 1903 by David Prain as "Bengal Plants" in two volumes. Since then, several publications have dealt with the flora of various regions of West Bengal and there is an continuous updation of the related information. Among them locally used two plants such as *A. lebbeck* stem bark and *Oxalis corniculata* were used here for nanoparticle preparation. They were collected from the forests of the Jangalmohal area (Belpahari, Similipal, and Jhargram), West Medinipur, West Bengal, India.

1.3.1.1 Bio-fabricated nanoparticles preparation using ethnomedicinal plant(s); *Albizia lebbeck*

A perennial, deciduous tree of the family Fabaceae popularly known as Siris, achieve a height of about 30 m with a 1.0 m stem diameter. This plant can raise 5m/year under proper climatic conditions. *A.lebbeck's* growth pattern depends on the agro-climatic and seasonal changes and is distributed in Australia, Asia, Central America, and South America, etc. There are reports that the Indian folk medicine, *A. lebbeck* can treat multiple inflammatory conditions such as burns, asthma, and arthritis [26]; while the ethnic people of Kashmir and Himachal Pradesh use *Albizia* to treat inflammation [27, 28]. According to the report of Balasubramaniam (1992) the tribal of point Cali mere wildlife sanctuary, Tamilnadu used this plant to manage the fractured bones [29]. The bark of *A. lebbeck* is also used to heal edema, asthma, diarrhoea, bronchitis, and poisoning as mentioned in the ayurvedic system [30].
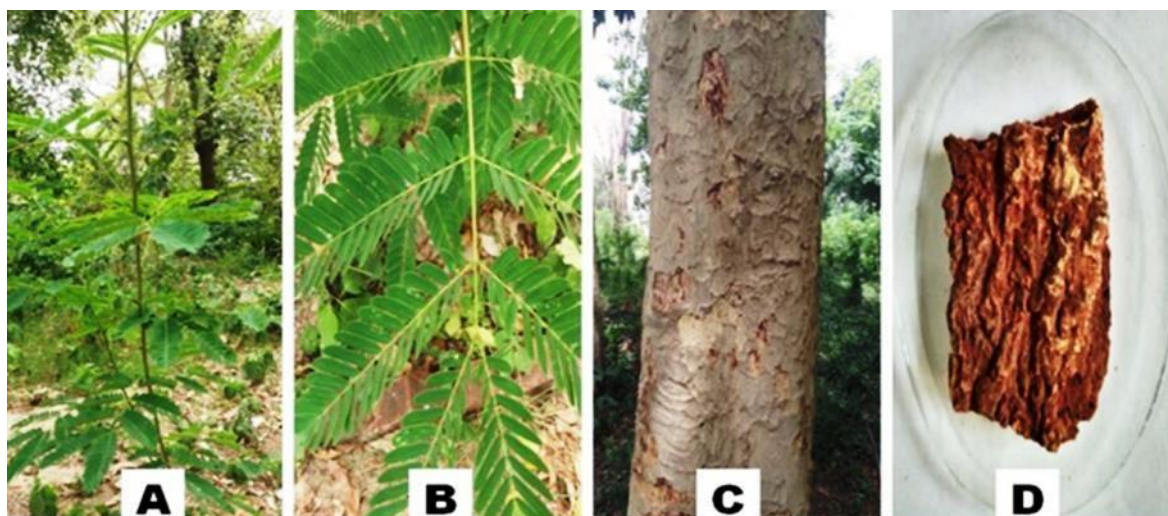
Fig. 1.3 Image of *Albizia lebbeck* bark [31]. Reprinted with permission.

Table1.1: Phytochemical components isolated from Stem Bark of *Albizia sp.*

Group of the Secondary Metabolites	Name of the phyto-constituents	Reference
Saponins	Lebbekanin A–H Albizzia saponin A, B and C	[32, 33, 34]
Triterpenoid	Acacic acid	
Sapogenins	Oleanolic acid Echinocystic acid	
Alkaloids	Budmunchiamines L1–L6	
Sterols	β-sitosterol	
Tannins, steroids, phenols, leucocyanidin, glycosides, protein, and carbohydrates	Galactopyranoside	
Flavonoids	d-catechin, quercetin, kaempferol	

Chemically *A. lebbeck* bark contains 7-11% condensed tannins, friedellin-3-one, acacic acid, along with oleanane-type triterpene libbekenin (A, B) and albiziasaponins A-C [32]. Condensed tannins are water-soluble poly-hydroxy phenols (polyflavonoids), with anticancer and inducible antioxidant activities [35]; while catechin is an antioxidant, libbecacidin and leucocyanidin increase the thickness of the mucous layer in stomach to neutralize acidity, but libbekenin and albiziasaponins have anticancer activity [36]. β-

sitosterol is another ubiquitous plant sterol and it induces proliferation of epithelial cells and marginal blood lymphocyte with increased T-cell production [37, 38].

1.3.1.2 Oxalis corniculata

This sub-tropical herb of the Oxalidaceae family is native to India, commonly known as creeping woodsorrel. The genus *Oxalis* has 500 species, which can be found throughout Europe, Africa, Asia and America [39, 40]. The herb is delicate, low growing, and and found across the warmer regions of India in damp shady areas and specifically in the Himalayas up to 8,000 feet [41, 42]. The multifunctional medicinal plant Oxalis corniculata has a wide range of bioactivities and a vast variety of phytochemicals in it that support well health. *Oxalis corniculata* is a multifunctional medicinal plant having a wide spectrum of bioactivities and diversified phytochemicals that help to promote good health [43]. In Ayurveda this herb is used as a good appetizer, to remove Kapha, vata, and piles. Traditionally it is used as an astringent, to cure dysentery and diarrhoea, skin diseases and fevers; while an infusion of leaves help to remove warts and opacities of the cornea and has anti-inflammatory activity [42].

Fig. 1.4 Image of *Oxalis corniculata* Linn. plant.

Natives of West Bengal use *Oxalis corniculata* Linn in various ailments which is a rich source of niacin, vitamin C and β-carotene [44]. The raw juice of this plant is effective in treating jaundice and stomach issues. While the juice and butter mixture is used to reduce muscle swellings, boils, and pimples. It also functions as an antibacterial, a refrigerant, a diuretic, a gastro protective, and an anti-diabetic agent. [44, 45, 46]. The whole plant is used in wound healing, anemia, dyspepsia, cancer, piles, dementia and convulsions [47]. Other use of this plant are anti-inflammatory, anti-helminthic, astringent, depurative, diuretic, emmenagogue, febrifuge, lithontriptic, stomachic, styptic infections, enteritis, diarrhoea, traumatic injuries and sprains [48]. *Oxalis corniculata* also reported to have antihypertensive, hypoglycemic, antipsychotic, chronotropic, nerve stimulant, and inotropic effect [49]. Chemically the plant contain glyoxylic acid, oxalic acid, pyruvic acid, vitexin, isovitexin, vitexin- 2- O- beta- D- glucopyranoside, neutral lipids, glycolipids, vitamin C, phospholipids, fatty acids (18:2, 18:3, 16:0; saturated C10- C14 acids), alpha and beta tocopherols etc. [48].

Table1.2 Phytochemical components isolated from *Oxalis corniculata.*

Name of the group	Phytochemical Components Present in *Oxalis corniculata* plant	References
Essential fatty acids	Palmitic acid, linoleic acid, linolenic acid, stearic acid	[49, 50, 51, 52]
Vitamins	Ascorbic acid, alpha and beta tocopherols	
Acids	glyoxylic acid, oxalic acid, pyruvic acid,	
Glucopyranoside	vitexin, isovitexin,vitexin- 2- O- beta- D- glucopyranoside	
Phospholipids, glycolipids,	Present	
Tannins, flavonoids, polyphenols, steroids, alkaloids, volatile oil,	Present	

In some areas of Madhya Pradesh, the leaf decoction is used to cure fever and dysentery [50]. The locals in Tehsil Chakwal (Pakistan) utilize the plant sap to treat skin conditions, while the leaves are also used to treat snake bites and stomach ailments as well as to treat fever and acute headaches [53]. In addition to being used for sensitive teeth, a plant crushed with cumin seeds is taken three times day with water to treat diarrheal symptoms [54]. The whole plant parts are used as anti-scorbutic in the treatment of scurvy [55].

This study aimed to investigate the antibacterial potential of *Oxalis corniculata* derived silver nanoparticles against human pathogenic bacterial species *Escherichia coli*, *Pseudomonas aeruginosa*, *Klebsiella pneumoniae*, *Serratia marcescens*, and *Bacillus subtilis*, *Streptococcus pneumonia*, *Staphylococcus aureus*. We have opted for different types of pathogenic bacteria because of the following reasons:

- ***E. coli***: Gram-negative, virulent strain causes food poisoning, urinary tract infection, and even neonatal meningitis.

- ***Pseudomonas aeruginosa***: Gram-negative rod-shaped bacteria infects the pulmonary and urinary tract, as well as burns, wounds and, other blood-borne infections.

- ***Serratia marcescens***: Gram-negative bacteria is a member of the genus *Serratia*, which is a part of the *Enterobacteriaceae* family, which causes generally urinary tract and ocular lens infections. It has capability to produce a beta-lactamase for development of drug resistance property.

- ***Klebsiella pneumonia***: Gram-negative, non-motile, encapsulated bacterium exhibit in the environment and has been correlated with pneumonia.

- ***Bacillus subtilis***: Gram-positive coccus that causes pneumonia, sepsis, meningitis.

- ***Streptococcus pneumonia***: Gram-positive rod shaped responsible for food poisoning.

- *Staphylococcus aureus***:** Gram-positive round shaped bacterium can cause skin infections and sometimes pneumonia.
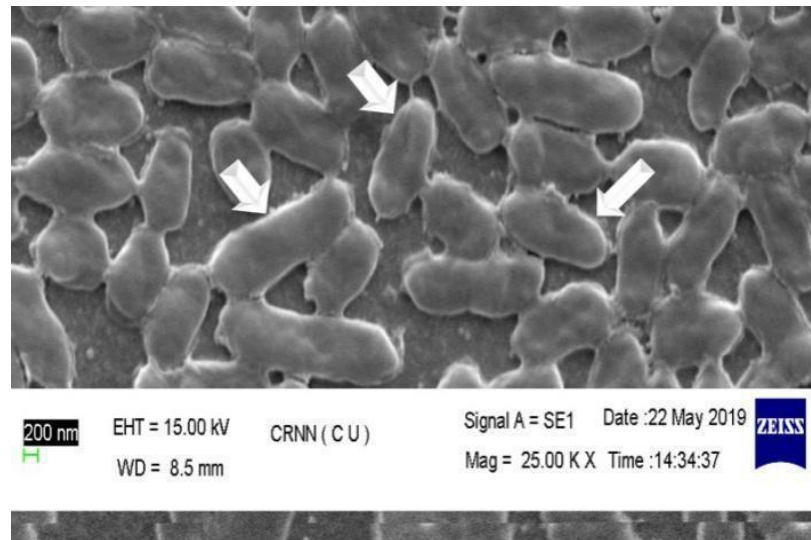

Fig. 1.5 FE-SEM image of *E.coli* (gram negative) bacteria.

Herpes Simplex **virus***:*

The Latin word *virus* means poison or fatal substances. A virus is a small infectious agent that can replicate only inside the living cells of the host, and a complete virus particle is known as a *virion*. Viruses infect almost all types of organisms, from bacteria and archaea to plants to animals. Herpes simplex virus (HSV) is one of the most serious public health troubles that cause a variety of diseases including kerato conjunctivitis, recurrent cold sores, genital herpes, and encephalitis [56]. The Herpes viruses belong to the family of double-stranded DNA viruses, *Herpesviridae* (Class I, Baltimore Classification) that cause diseases in humans and animals [57]. In Greek, the word herpein means "to creep", which explain the several typical features of these viruses like latency, re-occurrence and lytic infections. The Herpesviridae family consists of eight viruses that are divided into the alpha, beta, and gamma subfamilies, respectively. These Herpes Virus types are known to infect humans frequently. Herpes viruses are morphologically similar and share a number of intracellular development aspects, although they differ greatly in their biological characteristics [58, 59]. HSV, having two serotypes HSV-1 and HSV- 2,

targets the oral and genital mucosa of humans, and establishes latent infections in the sensory ganglia that may reactivate to cause recurrent infections at the primary site [60]. Though HSV infections are often subclinical, its incidence and severity have increased over the past decades due to the increasing number of HIV patients [61]. The impact of genital herpes as a public health threat is amplified because of its epidemiological co-pathogenesis with HIV in particular [62]. Since 1970, HSV has been successfully treated with acyclovir, which decreases the severity of disease [61].
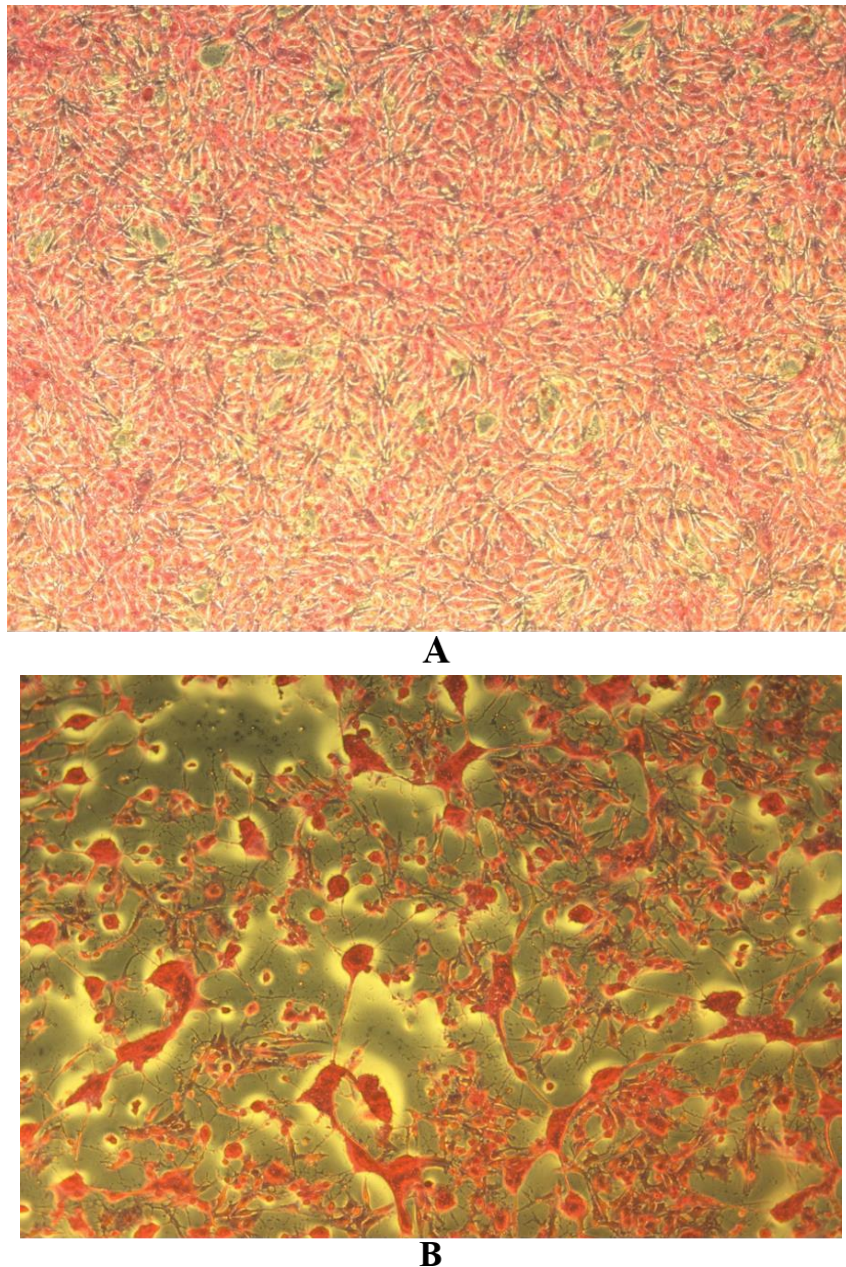

A

B

Fig. 1.6 Cytopathic effect of HSV-1F on Vero cell before (A) and after infection (B).

Other licensed anti-herpes virus agents includes acyclovir, ganciclovir, foscarnet and cidofovir also target herpesvirus DNA polymerases also have long-term use toxicity [63]. Moreover, the vaccines developed so far against HSV failed to induce antibody-specific responses to protect recivers [64]. Thus, new antiviral agents from natural source exhibiting different mechanisms of action are urgently needed. HSV infections are managed with the nucleoside analogue acyclovir (ACV) as a gold standard antiviral which undergoes phosphorylation in the infected cells by viral thymidine kinase into ACV-ATP [65]. However, ACV is neither able to eradicate the virus from the infected cell nor prevent the recurrences of HSV, which may be due to in its inability to counteract in the early stage of viral infection [66]. The frequent emergence of drug-resistant viruses, particularly in immune compromised patients, is another side effect of long-term use of ACV or related medications. This increases the chance of HSV recurrence and treatment failure [63, 67]. Furthermore, no efficient treatment or vaccine is available as of yet.

Silver nanoparticles as antibacterial:

Worldwide synthesis of silver nanoparticles has been estimated to be 55 tons per year [68]. Previous studies suggested that the optical properties of nanoparticles mainly depend on the concentration of metal salts taken initially and the bioactive reductant molecule of plant extract which may have contributed to the reduction of the metal ions and formation of the nanoparticles [69]. It is also reported that chemical synthesis of silver colloids mostly leads to aggregation as the period of storage increases [70].

Table 1.3: The biogenic synthesis of silver nanoparticles using different plant extracts and principal applications:

Precursor Plant extract	Amount of extract	Size	Morphology	Application	References
Chelidonium majus L.	1:1 plant extract:1 mM silver nitrate	90 nm	Spherical	Antioxidant, Antimicrobial	[70]
Solanum tuberosum (Potato starch)	85 mg soluble starch and 15 ml glucose solution (0.06/0.12M) in 10 ml of 60 mM Silver nitrate	20–50 nm	Spherical	Antimicrobial, biomedicine, and sensors	[71]
Sambucus nigra Fruit	16.6 ml extract in 6.6 ml 1% Silver nitrate	20–80 nm	Spherical	Anti-inflammatory	[72]
Tragopogon collinus Leaf	0.0025 M Silver nitrate in 20 cc extract, at 40°C, pH 10	7 – 18 nm	Spherical	Antimicrobial	[73]
Musa paradisiaca (Bananna peel)	3ml peel extract in 1.75mM AgNO$_3$	23.7nm	Spherical	Antimicrobial	[74]
Azadirachta indica (Neem) Leaves	1 mM AgNO3 in 1mM *A. indica* leaf extract	34 nm	Round	Antimicrobial	[75]
Arbutus unedo Leaf	50 ml leaf extracts in 50 ml 1 mM Silver nitrate	3–20 nm	Spherical	Biotechnological applications	[76]

Picrasma quassioides Bark	5 ml extract in 95 ml of 1 mM Silver nitrate	17.5–66.5 nm	Spherical	Catalytic activity	[77]
Arachis hypogaea (Pea nut shell)	5 ml extract in 45 ml of 10 mM Silver nitrate	10–50 nm	Spherical	Antifungal	[78]
Illicium verum (Star anise) seed	10 ml extract and 10 ml of 0.5, 0.05 or 0.01 M Silver nitrate	19–32 nm	Spherical	Molecular sensors and Nano photonic devices	[78]
Corn husk extracts	1, 3, 5, 8, 12 ml with 25 ml of 2 mM Silver nitrate	20 nm	Spherical	Antibacterial	[79]
Cassia tora leaf extract	50 ml diluted extract into100 m of 0.1 M Silver nitrate	400–450 nm	Spherical	Antibacterial	[80]
Allium ampeloprasum leaf	1 ml extract into 50 ml of an aqueous solution of AgNO3 (1 mM) at 60 °C	8–50 nm 2-43nm	Spherical	Antioxidant, Antibacterial	[81, 82]
Solanum torvum Fruit	10% extract was added to 100 ml aqueous AgNO3 (1 mM)	27 nm	Spherical	Antibacterial against Phyto pathogen	[83]
Caralluma tuberculate	200 µl extract in (2.5, 5, 7.5, 10, 15 mM) Silver nitrate	4 to 70 nm	Spherical	Antibacterial, Antioxidant	[84]

Phlogacanthus thyrsiformis Nongmangkha Leaf	30 ml extract in 15 ml of 60 mm AgNO3 solution	Not detected	Not detected	Antibacterial	[85]
Catharanthus roseus leaf	10 ml extract in 2 mM AgNO$_3$ at 70 °C, stirred magnetically at 1000 rpm for 3 min	49 nm	Spherical	Anti-plasmodial against *P. falciparum*	[86]
Piper longum catkin	Extract and AgNO$_3$ solution (1 mM) mixed in 1:1–1:6 ratios	67 nm	Spherical	Anticancer, Antioxidant, Antibacterial, Antifungal	[87]
Padina tetrastromatica Leaf	10 ml aqueous extract into 90 ml of 1 mM aq AgNO$_{33}$ solution for 72h at 120 rpm	20 nm	Spherical	Antibacterial activity	[88]
Melia azedarach L. leaves	100 ml extract in 100 ml of Silver nitrate	34– 48 nm	Spherical	Antibacterial	[89]
Plukenetia volubilis L. Sacha Inchi nut oil	140 µl with aqueous Silver nitrate (1 mM, 10 ml), and acetone (1.86 ml) stirring at 70 ∘C.	60 nm	Irregular Shape	Antioxidant activity	[90]

The mechanism of the bactericidal effect of AgNPs remains to be understood. According to several research, AgNPs may adhere to the microbial cell membrane and thus disrupt the cell's permeability and respiration. Smaller AgNPs would have a greater bactericidal impact than larger AgNPs because they have a larger surface area accessible for interaction [91]. It is also possible that AgNPs not only interact with the surface of the microbial cell membrane but can also penetrate inside the bacteria to hamper cellular pathway [92]. After synthesis of nanoparticles, their characterization is also important. Nanoparticles are usually characterized by their shape, size, disparity, and surface area etc. [93]. The performance, bio-distribution, safety, and efficacy of the nanoparticles are largely defined by their physicochemical qualities. Therefore, to assess the functional characteristics of the produced particles, it is crucial to characterize AgNPs. A number of analytical methods are used for characterization, including scanning electron microscopy (SEM), transmission electron microscopy (TEM), Fourier transform infrared spectroscopy (FTIR), dynamic light scattering (DLS), and X-ray photoelectron spectroscopy (XPS). These techniques can also be used to study the sizes and structures of individual plant-derived orally used nanoparticles. Transmission electron microscopy (TEM) has been used to characterize plant-derived edible nanoparticles. Dynamic light scattering (DLS, also known as photon correlation spectroscopy or quasi-elastic light scattering) can be used to determine the size-distribution profiles of small particles in suspension.

1.4 Synthetic Antimicrobial compounds: Workout in this research

Coumarin (1,2-benzopyrone or 2H-1-benzopyran-2-one) and coumarin derivatives are natural product found in some plant sources as a heteroside or free form, including the sweet clover and Tonka bean. Total number of naturally found coumarin derivatives are 800 that were obtained from near about 600 genera of 100 families to date [94, 95].

Coumarin and its derivatives have been found to possess antiviral, antioxidant, antimicrobial, anti-inflammatory, anti-cancer, anticoagulant and enzyme inhibition activities [96, 97, 98]. Coumarins (benzopyrones) are compound containing two rings of six membered heterocycle rings with two oxygen atoms. Coumarins display vitamin K antagonist activity to exert their anticoagulant effect by involving the cyclic generation of vitamin K [99]. Long-chain hydrocarbon substituted Coumarin, such as ostruthin and ammoresinol, displays very high antibacterial activity against a wide spectrum of Gram positive pathogenic bacteria such as *Micrococcus luteus*, Bacillus *megaterium*, *Micrococcus lysodeikticus*, and *Staphylococcus aureus* etc. [100]. Coumermycin has a bacteriostatic effect against *Escherichia coli* and *Staphylococcus aureus* and is essentially comparable to novobiocin, but coumermycin is over 50 times more potent. It also inhibits the supercoiling of DNA mediated by *Escherichia coli* DNA gyrase [101]. A large diversity of naturally derived coumarin products have been described as anti-HIV agents, and compounds having coumarin nucleus are among them such as inophyllums A, B, C, E, E, P, G1 and G2 and calanolides [102]. In addition, it has been discovered that coumarins have weak estrogenic activity and hence coumarins prevent menopausal distress [103]. However, FDA has banned the use of coumarin derivatives, which are used as fixative and flavouring agents in tobacco, due to their negative side effects such as moderate diarrhoea, mild nausea, and hepato toxicity [104].
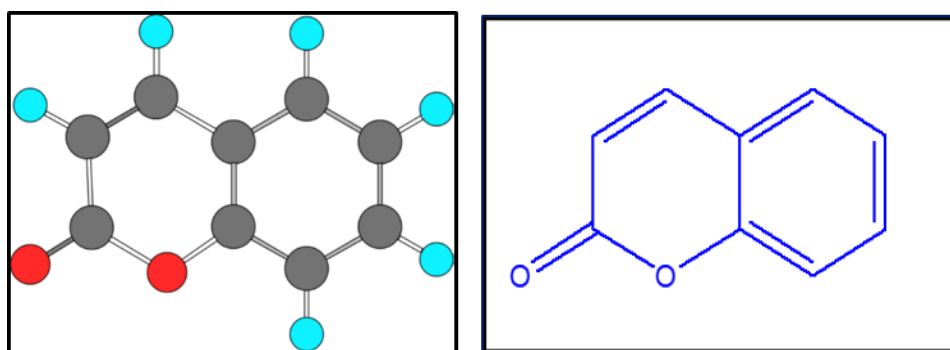

Fig. 1.7 Basic structure of Coumarins (2*H*-1-benzopyran-2-one).

The condensation reaction between a primary amine with a carbonyl compound forms an azomethine group (-CH=N-), known as **Schiff bases**. Among Schiff bases of aliphatic and aromatic aldehydes, the second one i.e. aromatic is relatively more stable than the first due to the presence of a conjugation system in it [105]. Schiff bases become visible to be an important middle product in a number of enzymatic reactions involving contact of an enzyme with a carbonyl or an amino group of the substrate. Otherwise, the condensation reaction of a primary amine of a lysine residue in an enzyme frequently reacts with a carbonyl group of the substrate to form an imine, or Schiff base [105, 106]. In a biological system, Schiff base is formed between an amino group of lysine side chains of proteins and methylglyoxal. Methylglyoxal has the ability to twist back toward the peptide bond's nitrogen atom in such a way that a charge transfer between these groups and the oxygen atoms of the Schiff bases can occur [105]. Functionality of many proteins depend upon fixation of cofactors to the Apo protein, where Schiff base plays significant role in this fixation. Different enzymes in biological system bind with their cofactors by Schiff base linkage. Schiff bases exhibit variety of valuable biological role along with activity against different microorganisms [107, 108]. It has been recorded that different Schiff bases complexes show significant antimicrobial effects on different species of pathogenic fungi and bacteria [109].
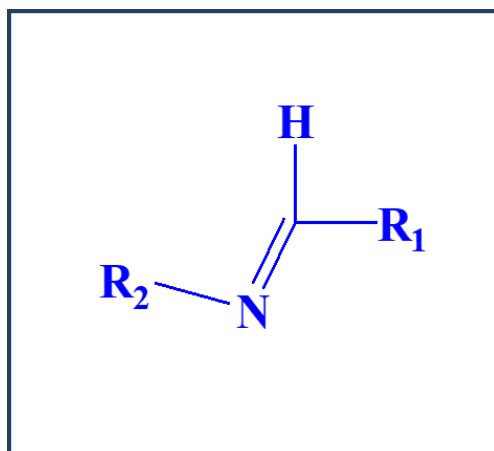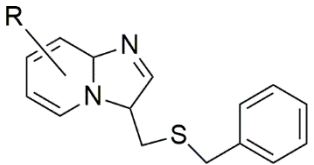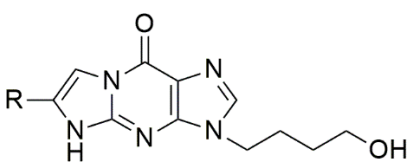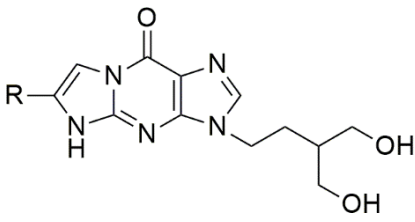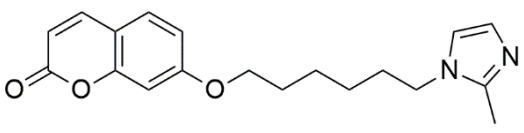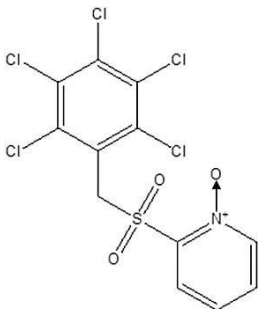

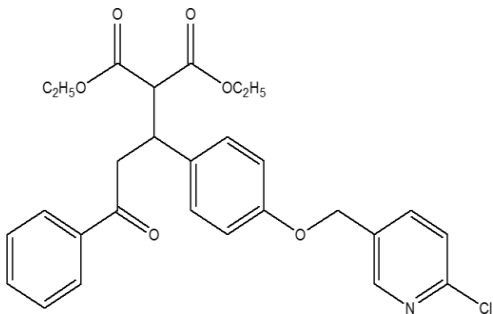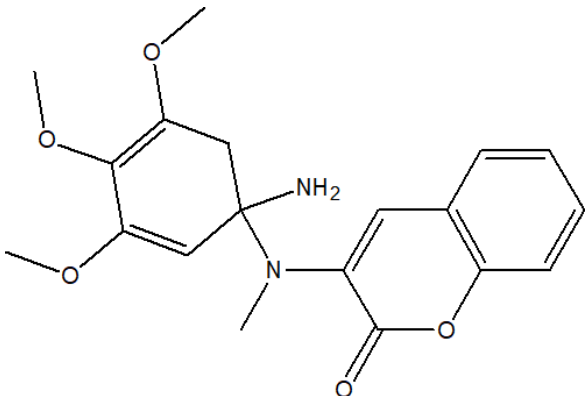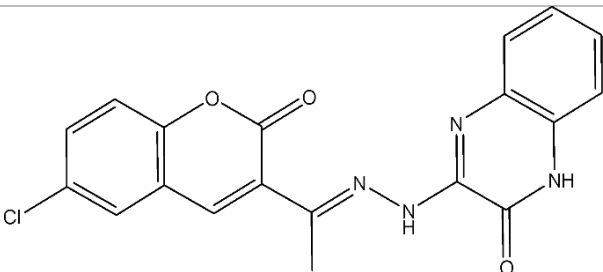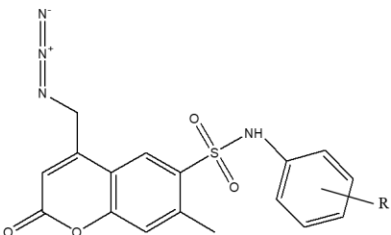**Fig. 1.8** Structure of Schiff base synthesized by the reaction between aromatic aldehyde and aromatic amine.

Sl. no	Chemical structure of synthetic Compound	Biological activity	References
1		Activity against CMV and varicella-zoster virus (VZV) at EC_{50} of 0.2 and 40 μg/ml respectively.	[110]
2		Antiviral activity against HSV-1 (KOS), HSV-2 (G) and HSV-1 TKKOS ACV	[111]
3		Antiviral activity against HSV-1 (KOS), HSV-2 (G) and HSV-1 TK(KOS) ACV having EC_{50} 1.5 μM (HSV-1), 0.8 μM (HSV-2) and 0.8 μM (HSV-1 TK- cells)	[111]
4		1. *In vivo* antiviral activities against TMV having EC_{50}54.2±2.8 to 232.9±2.6 mg/L 2. Antiviral activities against Infectious hematopoietic necrosis virus	[112, 113]

Sl. no	Chemical structure of synthetic Compound	Biological activity	References
		(IHNV) IC_{50} of 2.53 μM	
5	7-[6-(2-methylimidazole) hexyloxy] coumarin	Antiviral activity on rhabdovirus, spring viraemia of carp virus (SVCV), by interfering on SVCV replication	[114]
6		Antiviral activity against HIV-1, Feline infectious peritonitis virus FIPV and SARS-CoV having EC_{50} (0.63 − 0.29)mg/l, (0.79 − 0.18) mg/l and (17 − 7) mg/l.	[115]
7		The compounds possess good *in vivo* antiviral activity against CMV having EC_{50} 186.17 ± 3.2 μg/ml	[116]

Sl. no	Chemical structure of synthetic Compound	Biological activity	References
8		Novel anilinocoumarins possess anti hepatitis C virus (HCV) activities at EC_{50} value of 12 ± 0.3.	[117]
9		Antibacterial activity against *E. coli* and *S. aureus* at 30 and 32 mm as zone of inhibition respectively.	[118]
10		It shows *in vitro* anti-bacterial and anti-fungal activities.	[119]

On the other hand, **Sulfonamides** and their derivatives persist as a considerable branch of novel pharmacophore developed against a variety of complex diseases and the continued advancements in the use of this medication as antibacterial, antiviral, or antifungal medicines [122, 123].

An arsenical – diamino dihydroxy arseno benzol, named as Arsphenamine (known as Salvarsan) was discovered by an organic chemist, Alfred Bertheimc co-worker of Dr.

Paul Ehrlich had been used as an antisyphilitic drug since 1909 [120]. Sulphonamides, first clinically existing antibacterial agent, was discovered as by-products of the azo dye, Prontosil **Fig.1.8** [121].
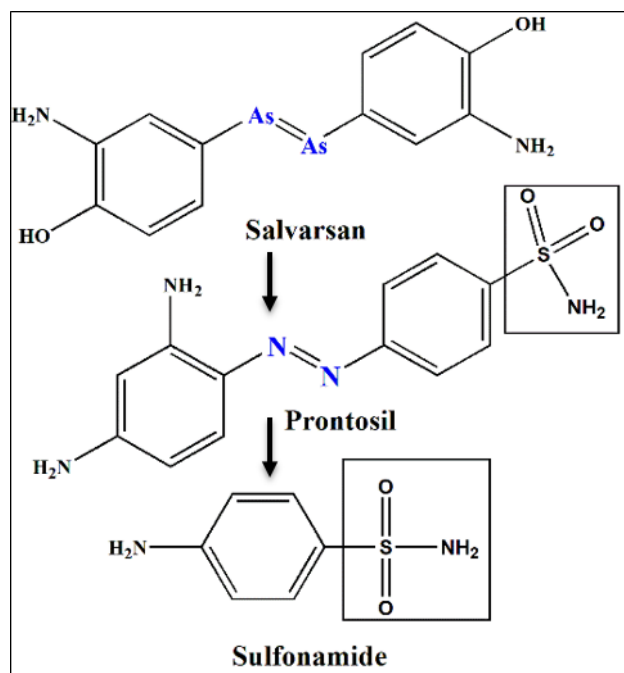

Fig. 1.8 Origin of Sulfonamides from Salvarsan.

This sulfa drugs were introduced by a German Bacteriologist, Gerhard Domagk [124, 125]. Clinically they have been utilized as antimicrobial lead for over 75 years, with confirmed effectiveness [125, 126]. Among the sulfa drug sulfamethoxazole (SMX) shows bacteriostatic activities not the bactericidal so when incorporated into the bacterial cell, they stop the synthesis of Folic acid by mimicking with para-amino benzoic acid (PABA) produced by bacterial cell [127]. Sulfa drugs mainly bind and hinder a specific enzyme named dihydropteroate synthase (DHPS). By inserting sulfa drugs into the enzyme crystals, the scientists found that the sulfa drugs are held in place by the structures called floppy loop. Folate, synthesized by *de novo* synthesis pathway, is an important metabolite for Prokaryotes and lower eukaryotes. By distracting biosynthesis of folate, SMX can hamper their growth [126]. On the other hand, higher eukaryotes

acquire folate directly from their diet and got read of the pathway. In lower organisms, the universal existence of DHPS and its absence in higher organisms explains why sulfonamides have been fruitful as broad-spectrum antimicrobials. Recently Griffith *et al.*, 2018 gave attention on the structural and mechanistic basis of sulfonamide resistance in *S. aureus* DHPS (*Sa*DHPS), and analyzed how reappearing resistance mutations can selectively unfavor the binding of sulfonamides [127]. It was reported that derivatized sulfa drug (N-(2-methoxy phenyl)-4-methylbenzenesulfonamide and N-ethyl-4-methyl-N-(3-methyl phenyl) benzene sulfonamide) have antibacterial activity against both Gram-positive and Gram-negative bacteria [128]. As multi-target methodologies in drug development gained much-deserved prominence, so did the application of sulfonamide derivatives as multi-target drugs [129].

During synthesis of genetic material bacteria require Folic acid as an important key element. This steps is inhibited by Sulfonamides and thus, the production of DNA and RNA is diminished due to insufficiency of tetra hydro folate [130]. As bacteria by mistake used sulfonamide instead of *p*-amino benzoic acid during folic acid synthesis, leading to death [131].

The six-membered heterocyclic molecules commonly known as pyridines are produced from both synthetic and naturally occurring heterocyclic chemicals and have diverse range of therapeutic uses [132, 133]. Many natural products including vitamin B3, B6, coenzymes such as nicotinamide adenine dinucleotide (NAD), and alkaloids Trigonelline contain Pyridine skeleton. Pyridine rings are present in Trigonelline, is a metabolite of niacin. Many drug and pesticides have a pyridine backbone. This scaffolds act as antiviral, antimicrobial, antidiabetic, antioxidants, anti-malarial, anti-inflammatory, antiamoebic agents due to their lower basicity and aqueous solubility [134, 135]. Moreover, another interesting action of this scaffold is against cancer, a threat to public

health [136, 137, 138]. Sulfapyridine and 5-aminosalicylic acid react with each other and make azo linkage to form compounds called sulfasalazine. Due to the strong water solubility of this compound, it is often utilised in clinical settings as a therapy for rheumatoid arthritis, ulcerative colitis, and Crohn's disease [139]. Therefore, the development of effective new lead is a very significant goal and we effort in this field and give focus towards the design of new agents.

1.5 Present Work

In this present investigation, we have evaluated the *in vitro* anti-microbial activity of green synthesized nanomaterials and different semi-synthetic compound including new Schiff bases incorporated with coumarin moiety and Sulfonamide derivative to found new lead molecule with high activity and less cellular toxicity. Chapter 2 and chapter 3 are also directed along this direction, viz. structural modification of nature-based synthetic analogues for increased bioactivity with reduced toxicity and synthesis of biofabricated silver nanoparticles using aqueous extracts of *Albizia lebbeck* Bark and *Oxalis corniculata* whole herb as an antimicrobial, anti-biofilm agent followed by complete spectral characterization, determination of cell viability at different concentrations and evaluation of antimicrobial activity against selected wild-type and drug-resistant microbes. Chapter 4 deals with the design and synthesis of nucleoside and non-nucleoside molecules HL1, HL2 and HL3.The study against Herpes simplex virus has been discussed in detail. Here we have re-examined the anti-HSV-1 activity of certain amides compound having nucleoside moiety by the cytopathic activity and Plaque reduction assays, with the possible mode of action in the HSV-infected Vero cells *in vitro* model. Time-of-addition assays displayed that pre-treatment of virus-infected cells with the pyridine derivatives and its removal before infection lowered the number of plaques

without toxicity to the cell, indicating that the pyridine derivatives affected the early stage in the viral life cycle. Docking studies has been performed to know the most preferred binding site with the gB and gD surface glycoproteins of virus. Chapter 5 depicts the fabrication of sulfonamides and exploration of their biological activities. Antibacterial activities have been studied against Gram-positive and Gram-negative bacterial strains. In Chapter 6, bidentate N, N$^/$-chelator 2-(3-Phenyl-1H-1, 2, 4-triazol-5-yl) pyridine has been prepared and this ligand has been used for the preparation of their Au (III) complex, [**Au** (2-ptp)$_2$]Cl (**1**). This ligand and complex have been spectroscopically characterized and biochemical properties (mostly antimicrobial, toxicity) have been studied.

1.6 Physicochemical Performance on molecule Characterization

The Fourier-transform infrared spectroscopy (FTIR) spectroscopy data is generally used to analyze the functional group (bond) of the organic compound present in plant extract or others and it was recorded from a Perkin Elmer LX-1FTIR spectrophotometer when run under IR region (KBr disk, 4000–400 cm^{-1}).

The absorption spectra of the nanoparticles at **UV–Visible spectrum** was recorded by a Perkin-Elmer Lambda 25 Spectrometer between 200 and 800 nm and these spectroscopic data are very much useful for the structure elucidation of an organic compound and also give qualitative information about size, shape, and concentration of nanoparticles.

Nuclear Magnetic Resonance (NMR) spectrometry was performed by using Bruker (AC) 300 MHz FT-NMR spectrometer. ^{1}H-NMR data helps to determine the actual structure of compounds, different types of hydrogen atoms, and the purity of compounds.

Dynamic Light Scattering (DLS) analysis spectra were recorded by using a DLS Analyser (Zetasizer® Nano ZS, Malvern Instrument Ltd., U.K) to determine the average size of nanoparticles and their average distribution.

Mass spectrometry has become a vital tool for qualitative and quantitative information on molecules based on their structural compositions and it was recorded from a Water HRMS model- XEVOG2QTOF# YCA351 Spectrometer.

The powder X-ray diffraction analysis of bio-synthesized nanoparticles were done by a Bruker D8 Advanced X-ray diffractometer using Cu Ka radiation (λ=1.5418 Å), and the data was taken for the 2θ range of 10° to 100° using Lynxeye detector (1D mode). This experiment is used for the identification of unknown crystalline materials such as nanoparticles. The crystalline structure was determined by comparing the data with the Joint Committee on Powder Diffraction Standards (JCPDS) library.

Morphology of bio-fabricated nanoparticles was recorded by using Scanning **Electron Microscope** (Zeiss EVO 18 Special Edition, ZEISS, Germany).

1.7 References

[1]   O. S. Ksenzhek and A. G. Volkov, *Plant Energetics.*, Elsevier, Burlington, 1998.

[2]   B. Schaal, *Plants, People, Planet.*, 2019, **1**, 14–19.

[3]   A. G. Atanasov, S. B. Zotchev, V. M. Dirsch and C. T. Supuran, *Nat. Rev. Drug Discov.*, 2021, **20**, 200–216.

[4]   D.V. Dwivedi, *Indian J. Hist. Sc.*, 2017, **52**, 251–274

[5]   S. Krippner, *In: Ethnomedicine Conferences.*, Munich, Germany, 2003, 26–27.

[6]   Farnsworth, O. Akerele, A. S. Bingel, D. D. Soejarto and Z. Guo, *Bull World Health Organ.*, 1985, **63**, 965–981.

[7]   S. K. Jain and R. R. Rao, *Today and tomorrow printers and publishers*, 1976, New Delhi.

[8]   A. Abu-Rabia, *J. Ethnobiol. Ethnomed.*, 2005, **1**, 4.

[9]   S. Vidyarthi, S. S. Samant and P. Sharma, *Int. J. Biodivers. Sci. Ecosyst. Serv. Manag.*, 2013, **9**, 185–200.

[10]   A. Gurib-Fakim, *Mol. Aspects Med.*, 2006, **27**, 1–93.

[11]   S. Jain and M. S. Mehata, *Sci. Rep.*, 2017, **7**, 1–3.

[12]   P. Iqbal, J. A. Preece and P. M. Mendes, in *Supramolecular Chemistry*, eds. P. A. Gale and J. W. Steed, John Wiley & Sons, Ltd, Chichester, UK, 2012, p. smc195.

[13]   I.-M. Chung, I. Park, K. Seung-Hyun, M. Thiruvengadam and G. Rajakumar, *Nanoscale Res. Lett.*, 2016, **11**, 40.

[14]   C. Lin, K. Tao, D. Hua, Z. Ma and S. Zhou, *Molecules.*, 2013, **18**, 12609–12620.

[15]   J. S. Moodley, S. Babu Naidu Krishna, K. Pillay and P. Govender, in *Novel Nanomaterials*, ed. K. Krishnamoorthy, *Intech Open.*, 2021.

[16]   Y. Sun and Y. Xia, *Science.*, 2002, **298**, 2176–2179.

[17]   A. M. Abdel-Mohsen, A. S. Aly, R. Hrdina and A. T. El-Aref, *J. Polym. and the Environ.*, 2011, **20**, 459–468.

[18]   Q. H. Tran, V. Q. Nguyen and A.-T. Le, *Adv. Nat. Sci: Nanosci. Nanotechnol.*, 2013, **4**, 033001.

[19]   S. Gurunathan, J.-K. Jeong, J. W. Han, X.-F. Zhang, J. H. Park and J.-H. Kim, *Nanoscale Res. Lett.*, 2015, **10**, 35.

[20]   A. M. Fayaz, K. Balaji, M. Girilal, R. Yadav, P. T. Kalaichelvan and R. Venketesan, *Nanomed: Nanotechnol, Biol. Med.*, 2010, **6**, 103–109.

[21]   P. Kuppusamy, M. M. Yusoff, G. P. Maniam and N. Govindan, *Saudi Pharm. J.*, 2016, **24**, 473–484.

[22]   S. Ahmed, M. Ahmad, B. L. Swami and S. Ikram, *J. Adv. Res.*, 2016, **7**, 17–28.

[23]   S. Gómez-Graña, M. Perez-Ameneiro, X. Vecino, I. Pastoriza-Santos, J. Perez-Juste, J. M. Cruz and A. B. Moldes, *Nanomaterials (Basel)*, 2017, **7**, E139.

[24]   A. K. Epstein, A. I. Hochbaum and P. Kim, *J. Aizenberg Nanotechnol.*, 2011, **22**, 494007.

[25]   A. R. McCutcheon, T. E. Roberts, E. Gibbons, S. M. Ellis, L. A. Babiuk, R. E. Hancock and G. H. Towers, *J. Ethnopharmacol.*, 1995, **49**, 101–110.

[26]   N. P. Babu, P. Pandikumar and S. Ignacimuthu, *J. Ethnopharmacol.*, 2009, **125**, 356–360.

[27]   S. K. Jain, 1991, Deep Publications, Lucknow, pp. 17.

[28]   T. N. Srivastava, S. Rajesekaran, D. P. Badola, D. C. Shah, 1986. *Ancient Science of Life.*, 1986, **6**, 49–63.

[29]   P. Balasubramaniam, *Bulletin of Botanical Survey of India*, Tamilnadu. 1992, **34**, 100–111.

[30]   R. S. Gupta, J. B. Kachhawa and R. Chaudhary, *Group.*, 2004, **243**, 6–89.

[31]   A. Pandey and A. K. Chaudhary, *J. pharmacogn. phytochem.*, 2018, **7**, 1020–1023.

[32]   B. C. Pal, B. Achari, K. Yoshikawa and S. Arihara, *Phytochem.*, 1995, **38**, 1287–1291.

[33]   S. El-Hawary, K. El-Fouly, N. M. Sokkar and Z.Talaat, *Asian J. Biochem.*, 2011, **6**, 122–141.

[34]   M. Aisha, A. Kalid and A. O. *John. Int. J. Integrat. Edu.*, 2020, **3**,112–116.

[35]   G. Gourlay and C. P. Constabel, *Tree Physiol.*, 2019, **39**, 345–355.

[36]   A. S. Raj and M. Katz, *Mutation Research/Genetic Toxicology.*, 1984, **136**, 247–253.

[37]   S. A. Janezic and A. V. Rao, *Food Chem. Toxicol.*, 1992, **30**, 611–616.

[38]   P. J. D. Bouic, S. Etsebeth, R. W. Liebenberg, C. F. Albrecht, K. Pegel and P. P. Van Jaarsveld, *Int. J. Immunopharmacol.*, 1996, **18**, 693–700.

[39]   A. Lourteig, *Bradea.*, 2000, **7**, 201–629.

[40]   D. J. Mabberley, *Mabberley's plant-book: a portable dictionary of plants, their classification and uses*, Cambridge University Press, Cambridge, 2008.

[41]   K. R. Kirtikar and B. D. Basu, *Indian Medicinal Plants 2nd ed. Dehradun: International Book Distributors*, 1999, 1012.

[42]   K. R. Kirtikar and B. D. Basu, *Indian Medicinal Plants, 1st edition*, The Indian Press, Allahabad, 1988, 437–438.

[43]   A. Kathiriya, K. Das, E. P. Kumar and K. B. Mathai, *Int. J. cancer manag.*, 2010, **3**, 157–165,

[44]   N. P. Manandhar, *Plants and people of Nepal*. Timber press, 2002.

[45]   K. Hussain, A. Shahazad and Z. U. Hussnain, An ethnobotanical survey of important wild medicinal plants of Hattar, District Haripur, Pakistan. *Ethnobotanical Leaflets*., 2008, **12**, 29–35.

[46]   S. S. Sakat, P. Tupe and A. Juvekar, *Indian J. Pharm. Sci.*, 2012, **74**, 48–53.

[47]   A. D Taranalli, S. V Tipare, Shiv Kumar and S. S Torgal, *Ind. J. Pharmaceutical Sci.*, 2004, **66**, 444.

[48]   R. N. Chopra, S. L. Nayar and I. C. Chopra. Glossary of Indian medicinal plants (including the supplement). Council of Scientific and Industrial Research, New Delhi, 1986.

[49]   M. P. Raghvendra, S. Satish and K. A. Raveesha, *My Science*., 2006, **1**, 72–78.

[50]   A. S. Achuta, S. Srivatsava and A. K. S. Rawat, *Ind. J. Madhya Pradesh*., 2010, **9**,191–202.

[51]   M. Hioki, T. Kaori and Y. Yokotani Kunijiro, *J. plant res*., 2008; **121**,133–136.

[52]   S. Saha, *J. Appl. Nat. Sci*., 2017, **18**, 16–19.

[53]   R. Qureshi, A. Waheed, M. Arshad and T. Umbreen, *Pak. J. Bot*., 2009 **41**, 529–538.

[54]   H. Badwaik, M. K. Singh and D. Thakur, *Int. J Phytomed*., 2011, **3**, 01–08.

[55]   S. Saini, H. Kaur, B. Verma, Ripudaman and S. K. Singh, *Nat. Prod. Radiance*., 2009, **8**, 190–197.

[56]   P. M. Ridker, C. H. Hennekens, M. J. Stampfer and F. Wang, *Circulation*, 1998, **98**, 2796–2799.

[57]   B. Roizman B. *Virol. J.*, 1996, 2231–95.

[58]   J. G. Stevens and M. L. Cook, *Science.*, 1971, **173**, 843–845.

[59]   A. J. Nahmias, F. K. Lee and S. Bechman-Nahmias, *Scand. J. Infect. Dis.*, 1990, 69,19–36.

[60]   F. J. Jenkins and A. Baum, *Ann. Behav. Med.*, 1995, **17**, 116–123.

[61]   B. Roizman and R. J.Whitley, *Herpes-Cambridge.*, 2001, **8**, 23–26.

[62]   A. Munawwar and S. Singh, *J. Lab. Physicians.*, 2016, **8**, 5–18.

[63]   E. De Clercq, L. Naesens, L. De Bolle, D. Schols, Y. Zhang and J. Neyts, *Rev. Med. Virol.*, 2001, **11**, 381–395.

[64]   J. Fricker, *Lancet.*, 1996, **348**, 1576.

[65]   H. H. Balfour Jr, *N. Engl. J. Med.*, 1999, **340**, 1255–68.

[66]   C. S. Crumpaker, I. E. Schnipper and S. I. Marlowe, *N. Engl. J. Med.*, 1982, 306, 343 –346.

[67]   C. Dekker, M. N. Ellis and C. McLaren, *J Antimicrob. Chemother.*, 1983, 12, 137–152.

[68]   O. Bondarenko, K. Juganson, A. Ivask, K. Kasemets, M. Mortimer and A. Kahru, *Arch. Toxicol.*, 2013, **87**, 1181–1200.

[69]   S. P. Dubey, M. Lahtinen and M. Sillanpää, *Colloids Surf. A Physicochem. Eng.*, 2010, **364**, 34–41.

[70]   K. M. M. Abou El-Nour, A. Eftaiha, A. Al-Warthan and R. A. A. Ammar, *Arab. J. Chem.*, 2010, **3**, 135–140.

[71]   M. E. Barbinta-Patrascu, I.-R.Bunghez, S. M. Iordache, N. Badea, R. C.Fierascu and R. M. Ion, *J. Nanosci. Nanotechnol.*, 2013, **13**, 2051–2060.

[70] M. A. dos Santos, L. G. Paterno, S. G. C. Moreira and M. J. A. Sales, *SN Appl. Sci.*, 2019, **1**, 554.

[71] L. David, B. Moldovan, A. Vulcu, L. Olenic, M. Perde-Schrepler, E. Fischer-Fodor, A. Florea, M. Crisan, I. Chiorean, S. Clichici and G. A. Filip, *Colloids Surf. B Biointerfaces.*, 2014, **122**, 767–777.

[72] R. Seifipour, M. Nozari, L.Pishkar, *J. Inorg. Organomet. Polym. Mater.*, 2020, 1–1.

[73] H. M. M. Ibrahim, *J. Radiat. Res. Appl. Sci.*, 2015, **8**, 265–275.

[74] N. Nagar, S. Jain, P. Kachhawah and V. Devra, *Korean J. Chem. Eng.*, 2016, **33**, 2990–2997.

[75] P. Kouvaris, A. Delimitis, V. Zaspalis, D. Papadopoulos, S. A. Tsipas and N.Michailidis, *Mater. Lett.*, 2012,**76**, 18–20.

[76] T. V. M. Sreekanth, G. R. Dillip and Y. R. Lee, *Ceram. Int*., 2016, **42**, 6610–6618.

[77] P. Velmurugan, M. Iydroose, S.-M.Lee, M. Cho, J.-H.Park, V. Balachandar and B.-T. Oh, *Indian J. Microbiol.*, 2014, **54**, 196–202.

[78] C. Luna, V. H. G. Chávez, E. D. Barriga-Castro, N. O. Núñez and R. Mendoza-Reséndez, *Spectrochim. Acta A Mol. Biomol. Spectrosc.*, 2015, **141**, 43–50.

[79] M. Villanueva-Ibáñez, M. G. Yañez-Cruz, R. Álvarez-García and M. A. Hernández-Pérez, *Mater. Lett.*, 2015, **152**, 166–169.

[80] A. Saravanakumar, M. Ganesh, J. Jayaprakash and H. T. Jang.*J. Ind. Eng. Chem.*, 2015, **28**, 277–281.

[81] F. Jalilian, A. Chahardoli, K. Sadrjavadi, A. Fattahi and Y. Shokoohinia, *Adv. Powder. Technol.*, 2020, **31**, 1323–1332.

[82] M. Khoshnamv and, C. Huo and J. Liu, *J. Mol. Struct.*, 2019, **1175**, 90–96.

[83] G. L.Vanti, M. Kurjogi, K. N. Basavesha, N. L.Teradal, S. Masaphy and V. B. Nargund, *J. Biotechnol.*, 2020, **309**, 20–28.

[84]   Z. Zarei, D. Razmjoue and J. Karimi, *J. Inorg. Organomet. Polym.*, 2020, **30**, 4606–4614.

[85]   A. Kumar, T. Bidyapani, S. Digvijay, N.R. Sharma and A. Mohan, *J. Pharm. Res.*, 2017, **11**, 1513–1517.

[86]   K. S. Mukunthan, E. K. Elumalai, T. N. Patel and V. R. Murty, *Asian Pac. J. Trop. Biomed.*, 2011, **1**, 270–274.

[87]   M. Jayapriya, D. Dhanasekaran, M. Arulmozhi, E. Nandhakumar, N. Senthilkumar and K. Sureshkumar, *Res. Chem. Intermed.*, 2019, **45**, 3617–3631.

[88]   P. Jegadeeswaran, R. Shivaraj and R. Venckatesh, *Dig. J. Nanomater. Biostructures*, 2012, **7**, 991-998.

[89]   A. Mehmood, G. Murtaza, T. M. Bhatti and R. Kausar, *Arab. J. Chem.*, 2017, **10**, S3048–S3053.

[90]   B. Kumar, K. Smita, L. Cumbal and A. Debut, *Saudi. J. Biol. Sci.*, 2014, **21**, 605–609.

[91]   L. Kvítek, A. Panáček, J. Soukupova, M. Kolář, R. Večeřová, R. Prucek, M. Holecová and R. Zbořil, *J. Phys. Chem. C.*, 2008, **112**, 5825–5834.

[92]   J. R. Morones, J. L. Elechiguerra, A. Camacho, K. Holt, J. B. Kouri, J. T. Ramírez and M. J. Yacaman, *Nanotechnol.*, 2005, **16**, 2346–2353.

[93]   J. Jiang, G. Oberdörster and P. Biswas, *J. Nanopart. Res.*, 2009, **11**, 77–89.

[94]   R. D. H. Murray, J. Mendez and S. A. Brown, The Natural Coumarins Occurrence, Chemistry And Biochemistry, Chichester; John Wiley and Sons Ltd.: New York, NY, USA, 1982.

[95]   B. Lake, *Food Chem. Tox.*, 1999, **3**, 412–423.

[96]   N. Mostajeran, F. A. Arshad, H. Aliyan and A. R. Massah, *Pharm. Chem. J.*, 2018, **52**, 1–7.

[97] D. Srikrishna, C. Godugu and P. K. Dubey, *Min Rev Med Chem*, 2018, **18**, 113–141.

[98] S. N. Esfahani, M. S. Damavandi, P. Sadeghi, Z. Nazifi, A. Salari-Jazi and A. R. Massah, *Sci. Rep.*, 2021, **11**, 20088.

[99] J. Hirsh, J. E. Dalen, D. R. Anderson, L. Poller, H. Bussey, J. Ansell and D. Deykin, *Chest.*, 2001, **119**, 8S-21S.

[100] K. Hodák, V. Jakesová and V. Dadák, *Cesk. Farm.*, 1967, **16**, 86–91.

[101] M. Gellert, M. H. O'Dea, T. Itoh and J. Tomizawa, *Proceedings of the National Academy of Sci.*, 1976, **73**, 4474–4478.

[102] A.D. Patil, A. J. Freyer, D. S. Eggleston, R. C. Haltiwanger, M. F. Bean, P. B. Taylor, M. J. Caranfa, A. L. Breen and H. R. Bartus, *J. Med. Chem.*, 1993, **36**, 4131–4138.

[103] R. D. Murray, *Fortschr. Chem. Org. Naturst.*, 2002, **83**, 1.

[104] J. R. Casley-Smith, R. G. Morgan and N. B. Piller, *N. Engl. J. Med.*, 1993, **76**, 1158–1163.

[105] S. Arulmurugan, H. P. Kavitha and B. R. Venkatraman, *Rasayan J. Chem.*, 2010, **3**, 385–410.

[106] J. M. Mir, S. A. Majid and A. H. Shalla, *Rev. Inorg. Chem.*, 2021, **0**, 000010151520200020.

[107] H. I. Ugras, I. Basaran, T. Kilic and U. Cakir, *J. Heterocycl. Chem.*, 2006, **43**, 1679–1684.

[108] M.A. Ashraf, K. Mahmood, A. Wajid, M. J. Maah and I. Yusoff, *Int. Conf. Chem. Chem. Proc.*, 2011, **10**, 1-7.

[109] M. K. Biyala, K. Sharma, M. Swami, N. Fahmi and R. V. Singh, *Transit. Met. Chem.*, 2008, **33**, 377–381.

[110] A. Gueiffier, S. Mavel, M. Lhassani, A. Elhakmaoui, R. Snoeck, G. Andrei, O. Chavignon, J. C. Teulade, M. Witvrouw, J. Balzarini and E. De Clercq, *J. Med. Chem.*, 1998, **41**, 5108–5112.

[111] A. F. Mohammed, G. Andrei, A. M. Hayallah, S. G. Abdel-Moty, R. Snoeck and C. Simons, *Bioorgan. Med. chem.*, 2019, **27**, 1023–1033.

[112] L. Zhao, J. Zhang, T. Liu, H. Mou, C. Wei, D. Hu and B. Song, *J. Agric. Food. Chem.*, 2019, **68**, 975–981.

[113] Y. Hu, W. Chen, Y. Shen, B. Zhu and G.-X. Wang, *Bioorganic Med. Chem. Lett.*, 2019, **29**, 1749–1755.

[114] W. C. Chen, L. Liu, Y. F. Shen, Y. Hu, F. Ling, G. X. Wang and B. Zhu, *Cell. Signal.*, 2018, **51**, 199–210.

[115] J. Balzarini, E. Keyaerts, L. Vijgen, F. Vandermeer, M. Stevens, E. De Clercq, H. Egberink and M. Van Ranst, *J. Antimicrob. Chemother.*, 2006, **57**, 472–481.

[116] Z. Chen, P. Li, D. Hu, L. Dong, J. Pan, L. Luo, W. Zhang, W. Xue, L. Jin and B. Song, *Arab. J. Chem.*, 2019, **12**, 2685–2696.

[117] H. K. Peng, W. C. Chen, J. C. Lee, S. Y. Yang, C. C. Tzeng, Y. T. Lin and S. C. Yang, *Org. biomol. Chem.*, 2013, **11**, 1858-1866.

[118] O. O. Ajani, C. A. Obafemi, O. C. Nwinyi, and D. A. Akinpelu, *Bioorg. Med. Chem.*, 2010, **18**, 214–221.

[119] M. Basanagouda, K. Shivashankar, M. V. Kulkarni, V. P. Rasal, H. Patel, S. S. Mutha and A. A. Mohite, *Eur. J. Med. Chem.*, 2010, **45**, 1151–1157.

[120] A. R. Massah, H. Adibi, R. Khodarahmi, R. Abiri, M. B. Majnooni, S. Shahidi, B. Asadi, M. Mehrabi and M. A. Zolfigol, *Bioorg. Med. Chem.*, 2008, **16**, 5465–5472.

[121] M. J. B. Mengelers, P. E. Hougee, L. H. M. Janssen and A. S. J. P. A. M. Van Miert, *J. Vet. Pharmacol. Thervc.*, 1997, **20**, 276–283.

[122] J. J. Abraham.*Br. J. Vener. Dis.*, 1948, **24**,153.

[123]   F. Zani and P. Vicini, *Arch. Pharm.*, 1998, **331**, 219.

[124]   O. A. Mascaretti, *Bacteria versus antibacterial agents: an integrated approach*, ASM Press, Washington, D.C, 2003.

[125]   G. Domagk, *Angew. Chem.*, 1935, **48**, 657–667.

[126]   A. Bermingham and J. P. Derrick, *Bioessays.*, 2002, **24**, 637–648.

[127]   S. Roland, R. Ferone, R. J. Harvey, V. L. Styles and R. W. Morrison, *J. Biol. Chem.*, 1979, **254**, 10337–10345.

[128]   E. C. Griffith, M. J. Wallace, Y. Wu, G. Kumar, S. Gajewski, P. Jackson, G. A. Phelps, Z. Zheng, C. O. Rock, R. E. Lee and S. W. White, *Front. Microbiol.*, 2018, **9**, 1369.

[129]   S. Ahmad and M. A. Farrukh, *Pak. J. Pharm. Sci.*, 2012, **25**, 839–844.

[130]   Y. Zheng and L.C. Cantley, *J. Exp. Med.*, 2018. DOI: 10.1084/jem.20181965

[131]   M. Abdul Qadir, M. Ahmed and M. Iqbal, *Biomed. Res. Int.*, 2015, **2015**, 938486.

[132]   B. C. Ranu, R. Jana and S. Sowmiah, *J. Org. Chem.*, 2007, **72**, 3152–3154.

[133]   X. Ma and D. R. Gang, *Nat. Prod. Rep.*, 2004, **21**, 752.

[134]   A. A. Altaf, A. Shahzad, Z. Gul and N. Rasool, *J. drug des. med. chem.*, 2015, **1**, 1.

[135]   Y. Hamada, in *Pyridine* ed. P. P. Pandey, *InTech.*, 2018. DOI: 10.5772/intechopen.74719

[136]   M. L. Cohen, *Nature.*, 2000, **406**, 762–767.

[137]   R. Sahu, R. Mishra, R. Kumar, C. Majee, Salahuddin, A. Mazumder and A.

Kumar, *Indian. J. Pharm. Sci.*, 2021, **83**, 162–185.

[138] H. S. Ibrahim, W. M. Eldehna, H. A. Abdel-Aziz, M. M. Elaasser and M. M. Abdel-Aziz, *Eur. J. Med. Chem.*, 2014, **85**, 480–486.

[139] D. T. Felson, J. S. Smolen, G. Wells, B. Zhang, L. H. D. van Tuyl, J. Funovits, D. Aletaha, C. F. Allaart, J. Bathon, S. Bombardieri, P. Brooks, A. Brown, M. Matucci-Cerinic, H. Choi, B. Combe, M. de Wit, M. Dougados, P. Emery, D. Furst, J. Gomez-Reino, G. Hawker, E. Keystone, D. Khanna, J. Kirwan, T. K. Kvien, R. Landewé, J. Listing, K. Michaud, E. Martin-Mola, P. Montie, T. Pincus, P. Richards, J. N. Siegel, L. S. Simon, T. Sokka, V. Strand, P. Tugwell, A. Tyndall, D. van der Heijde, S. Verstappen, B. White, F. Wolfe, A. Zink and M. Boers, *Arthritis Rheum.*, 2011, **63**, 573–586.

Chapter 2

Silver nanoparticles derived from *Albizia lebbeck* bark extract demonstrate killing of MDR-isolates of bacteria by damaging cellular architecture with antioxidant activity

Abstract:

Silver nanoparticles are synthesized and stabilized by the extract of ethnomedicine, *Albizialebbeck* bark. The extract-wrapped Ag-NP (Ag-NP-AE; AE, Aqueous Extract)is active against several multidrug-resistant (MDR) clinical isolates. The nanoparticles are characterized by different spectroscopy (spectroscopy (FTIR, UV-Vis, DLS, SEM, XRD). The antibacterial potency of Ag-NP-AE is determined by Disk diffusion, Agar and Broth dilution assays against 14 MDR isolates along with their minimum inhibitory concentration (MIC), and minimum bactericidal concentration (MBC). The growth kinetics was determined by quantification of colonies; while toxicity was by quantification of viable cells and *in vitro* free-radical scavenging activity by the DPPH method. The Ag-NP-AE shows strong free-radical scavenging activity at 15-20 μM and is non-toxic up to 50μMbut demonstrated significant antibacterial activity against all the test isolates with zone diameter of 10.4-19.5 mm and MIC of 0.5-0.84 μM (0.085-0.143 μg); while the zone diameter with AE was 10.2-15 mm and MIC of 128-1024 μg/ml, respectively, indicating that the nanoparticles are more active than the AE. The MBC was 2-4-fold higher than their MIC; while 100% killing was observed at 0.50 μM within 2-4h of exposure due to damage to cellular architectures.

2.1 Introduction:

Infections caused by the WHO listed priority pathogens of greatest threat including *Staphylococcus aureus*, *Enterococcus faecalis*, *Escherichia coli*, *Salmonella typhi*, *Klebsiella pneumonia*, *Pseudomonas aeruginosa* are ubiquitous in community and hospital settings, leading to increased mortality, morbidity, and economic burden [1, 2]. The multi-antibiotic resistant strains may cause treatment failure to death. Moreover, the biofilm formed by some pathogenic bacteria is difficult to eradicate, while growing antibiotic-resistant limits the treatment options [1,3]. One promising option is the use of ultra-fine nanoparticles (1-100 nm) of metallic silver, gold, copper, or zinc with therapeutic activities against a wide array of pathogenic bacteria [1,4]. Moreover, the development of resistance against silver nanoparticles is less because of its unique structure and multimodal mechanisms of action [5]. Silver nanoparticles (AgNP) prepared with plant extracts or phytocompounds are reported to possess antimicrobial activity against bacteria including *S. aureus*, *E. coli*, *S. typhimurium,* and *P. aeruginosa* at 2-4 ppm, fungi, and viruses [6-9]. Silver ions of AgNP not only accumulate around the cell wall but also penetrate *E. coli* and *S. aureus* cells and interact with the bacterial DNA [10]. Metal nanoparticles prepared by chemical/photochemical reduction or electrochemical methods showed better stability [11]; while synthetic methods used organic solvents as a medium due to better hydrophobicity of capping agents. The size, morphology, surface charge, and coating of AgNPs are reported to play critical roles in determining their antimicrobial activities [12]. Earlier, AgNPs synthesized with chemicals showed toxic/hazardous effects on the ecosystem; thus, plant or microbial metabolites are preferred [13], due to their eco-friendly nature, termed "Green synthesis"[14]. Moreover, the synthesis of nanoparticles from bio-metabolites is rapid with high yield and cost-effective downstream processing

[15]. A substantial amount of work has been done on the 'green synthesis' of AgNPs using plant extracts or phyto-metabolites, secondary metabolites of viruses, bacteria, fungi, and plants, due to their antioxidant activity that can reduce metal compounds in their respective nanoparticles [16].

Several species of *Albizia* (Mimosoideae) are traditionally been used as ethnomedicine in diverse communities. Among them, *Albizia lebbeck* (Linn) Benth, locally known as Siris, is a tall tropical deciduous tree distributed throughout India, parts of Asia, Africa, Australia, and Southern America. In the Unani system of medicine, the flower and stem bark are used for arthritis; while in Ayurveda the stem bark is recommended for diarrhea [17]. Traditionally *A. lebbeck* is used for inflammatory ailments including asthma, arthritis, allergies, bronchitis, gingivitis, toothache, sinusitis, fractures, and snakebite. However, studies on different parts of *A. lebbeck* showed antibacterial, antifungal, antitumor, anti-inflammatory, antifertility, anticonvulsant, anti-anaphylactic, psychoactive, antioxidant, anti-arthritic, antidiabetic, and anti-malarial activities [18- 27]. Recently it has been reported that zinc oxide nanoparticles from *Albizia lebbeck* stem bark possess antimicrobial and antioxidant activities, along with cytotoxic effect against human breast cancer cells [28]. We have used the well-known ethnomedicinal plant *Albizia lebbeck* bark extract as a stabilizer and reductant for the synthesis of silver nanoparticles (Ag-NP-AE). The characterization and purity of Ag-NP-AE were determined by spectroscopic techniques, Scanning Electron Microscopy (SEM), Transmission electron microscopy (TEM), and X-Ray diffraction (XRD) studies while safety was assayed by Cell Viability assay and oxidative ability by DPPH radical scavenging assay. The antibacterial potential of Ag-NP-AE was validated against fourteen multidrug resistants (MDR) hospital isolates of bacteria belonging to eight genera, by determining their sensitivity, inhibitory profile, growth kinetics, and mode and mechanism of action, following standard techniques.

2.2 Experimental Section

2.2.1 Reagents

Mueller-Hinton Broth (MHB), Mueller-Hinton agar (MHA), nutrient broth (NB), nutrient agar (NA), and MacConkey agar (MA), ampicillin, and gentamicin, along with the antibiotic discs of different potency were purchased from Difco, UK. The Dulbecco's Modified Eagle Medium (DMEM), fetal bovine serum (FBS), penicillin (Penicillin G sodium 100 Units/m), and streptomycin (Streptomycin sulfate 100μg/ml) were obtained from Gibco (Thermo Fisher Scientific, Grand Island, USA). While Silver nitrate (AgNO3), sodium bicarbonate, MTT [3-(4, 5-dimethylthiazol-2-yl)-2,5 diphenyl tetrazolium bromide], DPPH (2,2-diphenyl-1-picryl hydroxyl), Ascorbic acid (vitamin C), methanol, and conventional antibiotics (ampicillin, gentamicin) were procured from Sigma-Aldrich (St Louis, MO, USA).

2.2.2 Collection, processing, and extraction of plant materials

About one kilogram of *A. lebbeck* stem bark was collected from the forests of the Jangalmohal area (Belpahari, Similipal, and Jhargram), West Medinipur, West Bengal, India during March, June, and October 2018 to cover up the seasonal variation of active compounds. The collected samples were authenticated by a Botanist from the Botanical Survey of India, Shibpur Howrah, India. A voucher specimen (VU/2017-18/0025) was deposited in the host institute. The samples were thoroughly washed in tap water and then with distilled water; shade dried, mixed, pulverized, and passed through a 40-mesh sieve to get a fine powder. The powdered bark (100 gm) was macerated with sterile distilled water (500 ml) for 72 h at room temperature. The extract was filtered, condensed, and lyophilized as powder. The resultant powdered aqueous extract (AE) with a

percentage yield (w/w) of 13.2±0.21 g was stored in an airtight amber color container and kept in a desiccator for future use.

2.2.3 Micro-organisms and Cell line

Well-characterized 14 clinical isolates of eight bacterial species, containing two each of Staphylococcus aureus, *Bacillus subtilis*, Escherichia coli, *Enterococcus faecalis*, *Salmonella enterica*subspecies enterica Serovar Typhi (S. Typhi), and Pseudomonas aeruginosa; with one each of *Klebsiella pneumonia* and *Serratia marcescens*, obtained from the Department of Microbiology, Calcutta Medical College and Hospital, and the Peerless Hospital, Kolkata were used in this study. The quality control strains include *Staphylococcus aureus* ATCC 29213, *Escherichia coli* ATCC 25922, *Enterococcus faecalis* ATCC 29212, and *Klebsiella pneumonia* ATCC 700603. Bacteria were grown either on sterile nutrient agar, blood agar, or MacConkey agar plates and maintained on agar slants and stored at −80 °C with 50% glycerol. Before experimentation, a single isolated colony of the respective bacterium was aseptically picked up from 24 h old culture plates, grown on nutrient agar for the preparation of the inoculum, and checked at an optical density of 0.1 at 600nm.

For cell culture: African green monkey kidney epithelial cells (Vero cells, ATCC, USA), were grown and maintained in DMEM, supplemented with 5-10% FBS, 100 U/ml penicillin, and 100 µg/ml streptomycin at 37ºC in 5% CO_2; while EMEM with 2% FBS was served as maintenance medium.

2.2.4 Synthesis and Characterization of Silver nanoparticles using plant extract as reductant

The powdered AE of *Albizia lebbeck* stem bark (0.5 mg) was dissolved in 5.0 ml sterile double distilled water into a 50 ml round-bottom flask and mixed with 1.0 mM of AgNO3

(0.85 mg). The mixture was allowed to react by stirring at 90 °C for 2 h. The change of color from pale-yellow to deep-brown indicates the completion of the reaction with the formation of silver nanoparticles Ag-NP-AE. Characterization of biologically Ag-NP-AE was carried out using UV-Vis spectroscopy, FTIR, XRD, DLS, and SEM studies.

2.2.5 Determination of Cytotoxicity of the Silver nanoparticle by MTT assay

The cytotoxicity of Ag-NP-AE, as well as AE of A. lebbeck bark, was determined by MTT (3-[4, 5-dimethyl-thiazol-2-yl]-2,5 diphenyl tetrazolium bromide) assay in Vero cell on 96-well plates. The absorbance was read by a microplate spectrophotometer (Multiskan Go, Thermo Scientific) at 570 nm against a reference wavelength of 690 nm. The 50% cytotoxic concentration (CC_{50}) causing visible morphological changes in 50% of Vero cells concerning cell control was determined [29]. All experiments were conducted in triplicate to calculate the averages. The cell viability was calculated as: Cell viability (V) = [(At-Ab) / (Ac-Ab)] × 100%

[Where At = sample absorbance; Ab = absorbance of cell-free blank; Ac= mean control absorbance]

2.2.6 Evaluation of in vitro antioxidant activity of nanoparticles

Antioxidant activity was carried out by 2, 2-diphenyl-1-picrylhydrazyl (DPPH) radical scavenging assay using different concentrations of Ag-NP-AE (0, 0.5, 1.0, 5.0,10,15,20 µM) along with the standard antioxidant Ascorbic acid (vitamin C) in separate test tubes. The percentage free radical scavenging activity was determined by the formula [30]: % Free radical scavenging (FS) = [{(CA - BA) - (TA- BA)}/ (CA - BA)] × 100% [Where CA = absorbance of Control; BA = absorbance of blank (only methanol); TA = Mean

absorbance of DPPH radical along with the sample Ag-NP-AE/ standard   vitamin C]

2.2.7 Evaluation of the antibacterial potential of Nanoparticles and AE of *A. lebbeck* bark

Antibacterial susceptibility was determined by the disk-diffusion assay described by Kirby-Bauer, following the guidelines of the Clinical and Laboratory Standard Institute [31]. For disc diffusion assay 1.0 ml inoculum (1.8×10^6 CFU/ml) of respective bacteria from an overnight culture, was spread evenly on dried sterile MHA plates at room temperature, and incubated for 30 min at 37 ℃. Previously prepared *A. lebbeck* bark AE (0–1024 µg/ml) or Ag-NP-AE nanoparticle-impregnated discs (0–50 µM or 0–8.5 µg) were placed aseptically on the inoculated plates, with the antibiotic disc as controls, in triplicate. After overnight incubation at 37 °C, the sensitivity was recorded by measuring the clear zone of growth inhibition (in mm) on the agar surface around the discs. The zone diameter ≥10 mm for any test strain was considered antibacterial. Briefly, the sterile MHA plates prepared with a serial dilution of Ag-NP-AE (0–50 µM or 0–8.5 µg) or AE (0-1024µg/ml) were kept overnight at 4 ℃. The next day the plates were dried and inoculated with 10 µl of respective bacterium (2×10^6CFU/ml) as spot, with appropriate controls, in triplicate and incubated at 37 ℃ for 18-24 h. The plates were visually observed for the presence of growth or any colony, and the complete absence of any growth/colony in the plate will be considered an inhibitory concentration [32].

2.2.8 Determination of minimum inhibitory and minimum bactericidal concentration

The minimum concentration of test nanoparticles (Ag-NP-AE) or test extract (AE) that inhibits the growth of the test bacteria was determined by broth and agar dilution methods, following CLSI guidelines [33]. The previously prepared MHA plates containing Ag-NP-AE (0-50 μM or 0-8.5μg) or AE (0–1024 μg/ml) and Ampicillin or Gentamycin (0-30 μg) were inoculated with the test bacteria (2×10^6 CFU/ml) and incubated at 37 °C for 24 h. While for broth dilution assay sterile 96 well culture plate, each containing 90 μl of MHB with varying concentrations of Ag-NP-AE (0-50 μM or 0-8.5μg) or AE (0-1024 μg) was added with 10 μl of bacterial inoculum (2×10^6 CFU/ml) separately, to adjust bacterial density at 2×10^5 CFU/ml in a total volume of 100 μl for each well, along with antibiotic control Ampicillin or Gentamycin, in triplicate [34]. The culture plate was incubated in a shaker incubator (250 rpm) at 37°C for 24h [35], and the absorbance was recorded by a microplate reader (Multiskan Go, Thermo Scientific) at 600 nm. A graph was plotted by using OD vs concentration of Ag-NP-AE or AE for each well and the lowest concentration of the test agents having the least OD without any visible growth was considered as the MIC. To determine the minimal bactericidal concentration (MBC) 9.0 ml of sterile MHB with 1.0 ml suspension of test bacteria (2×10^6 CFU/ml) was poured in the tube(s) and added with 0 to the 4-fold MIC of Ag-NP-AE or AE along with appropriate controls, in triplicate and incubated at 200 rpm for 24 h at 37 °C. The aliquots (0.1 ml) were withdrawn at hourly intervals (0-12 h) and at 24 h to determine the OD at 540 nm with a Multiskan plate reader (Thermo, USA) as well as the colony count of treated bacteria [36].

2.2.9 Time-dependent growth inhibition by test nanoparticles

To evaluate the time-dependent rate and extent of growth inhibition with an antimicrobial activity we have evaluated the killing efficacy of Ag-NP-AE and AE of *A. lebbeck* bark against highly sensitive MDR-isolates. Briefly, an overnight culture of the three most sensitive test bacterium *E. coli*, *P.aeruginosa*, and *S. Marcescens* were diluted in MHB and incubated at 37 ℃ for 3 h in a shaker incubator at 200 rpm to achieve log-phase growth. At the mid-logarithmic phase (2×10^6 CFU/ml) of growth, the test nanoparticle Ag-NP-AE or antibiotic control was added at its MIC (0-5.0 µM) along with the bacteria control (fresh medium containing bacterial inoculum) in triplicate. Aliquots were withdrawn at half-hourly intervals (0-240 min), diluted (10^{-1}-10^{-3}) in sterile PBS to count the number of colonies, in triplicate. The mean viable count was recorded, and the Log10 CFU/ml was plotted against time [37]. The percentage of killing was calculated by dividing the difference between the CFU of control and the CFU of the test group with the CFU of the control, multiplying by 100. All experiments were performed in triplicate to get the average.

2.2.10 Morphological changes of the test bacteria exposed to Ag-NP-AE

To find out the architectural changes of test bacteria, if any, with Ag-NP-AE we have exposed two MDR-resistant bacteria *P. aeruginosa* and *S. marcescens* at 2×10^5 CFU/ml, highly sensitive to the test nanoparticle at their MBC, along with appropriate control, for 0 to 8 h, in triplicates. Cells were then centrifuged, fixed with 3% (w/v) glutaraldehyde solution, dehydrated serially with 30, 50, 70, and 90% ethanol-water for 15 min, and visualized by the SEM [37].

2.2.11 Statistical analysis

The data were presented as mean ± SD. Comparisons between two sets of tests were conducted by using Student's t-test; while one-way ANOVA was used to compare the data between three groups or more. The P-value of 0.05 was considered statistically significant.

2.3 Results

2.3.1 Green Synthesis of Ag-NP-AE and their characterization

Synthesis of Silver nanoparticles using plant extract

Albizia lebbeck stem bark AE (0.42 mg) dissolved in 5.0 ml sterile double distilled water with I mM of Silver nitrate (0.85 mg) was allowed to stir at 90 °C for 2 h. The changes in the color of the mixture from pale-yellow to deep-brown (**Fig**. **2.1**) indicate the formation of silver nanoparticles of *A. lebbeck* bark AE (Ag-NP-AE).

Fig. **2.1** *Albizia lebbeck* stem bark extract powder (A); synthesized Silver nanoparticle with Pale-yellow and deep-brown solution of Ag-NP-AE (B).

UV-Vis Spectroscopy

The formation of Ag-Np-AE is indicated by the changecolorlour of the solution from pale yellow to dark brown. The Ag-NP-AE was further studied for its optical properties using UV-Visible spectroscopy. The resultant UV spectral peak at 432 nm, presented in

Fig. **2.2**, clearly indicates the longitudinal Vibration corresponding to the silver nanoparticle. The results also indicate that there is a strong interaction between the silver nanoparticles and the aqueous extract of the plant. The shape and size of the nanoparticle along with the dielectric constant of the corresponding medium usually affect the exact peak and nature of the plasmon absorption band.
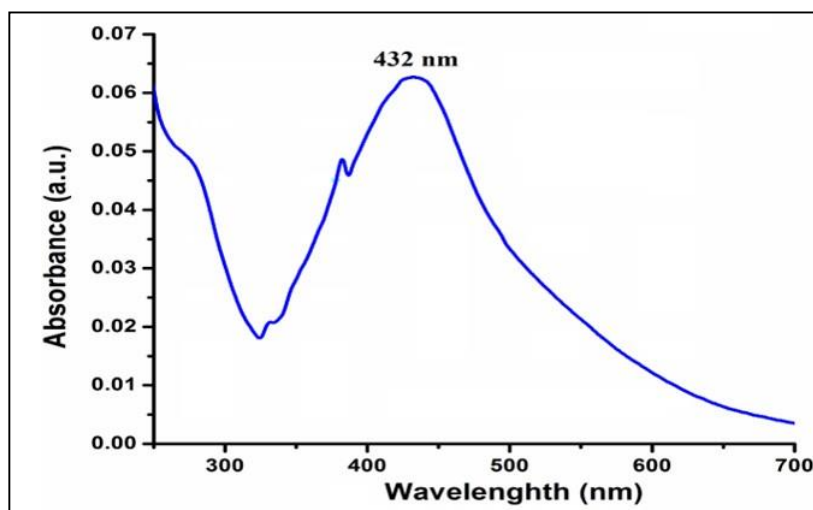
Fig. **2.2** UV-Vis spectral profile of *Albizia lebbeck* stem bark extract derived nanoparticle Ag-NP-AE (λmax = 432 nm).

FT-IR Analysis

During 'green synthesis' the silver nitrate ($AgNO_3$) is reduced to silver nanoparticles by the phytochemicals present in the plant extract, which also serve as a stabilizing or capping agent. FT-IR spectra of AE and the synthesized nanoparticle were presented in **Fig**. (2.**3**). The results revealed that the absorption peaks at 3189 cm^{-1}, 2910 cm^{-1}, 2850 cm^{-1}, 1602 cm^{-1}, and 1064 cm^{-1} of AE are associated with oxygen-containing functional groups. While the peaks at 2970 cm^{-1}, 2817 cm^{-1}, 1602 cm^{-1}, 1451 cm^{-1},and 1382 cm^{-1} are due to Ag-NP-AE. The shifting of several peaks indicates the reduction of intensity during the formation of nanoparticles with *A. lebbeck* bark AE. The IR spectra of AE

revealed an absorption peak at 3189 cm^{-1} corresponding to the o –OH/–NH group, where intensity is reduced during the formation of nanoparticles. The –OH/–NH group is mainly responsible for the reduction and stabilization of nanoparticles. Similarly, the peak at 1602 cm^{-1}, corresponds to the amide C=O group. Other shifted peaks observed were at ~2910 cm^{-1} and ~2850 cm^{-1} which correspond to the carboxylic –OH groups. Thus, by comparing the spectra of AE with the spectra of synthesized Ag-NP-AE, it can be confirmed that AE plays a dual role during the formation of nanoparticles as a reducing and stabilizing or capping agent.
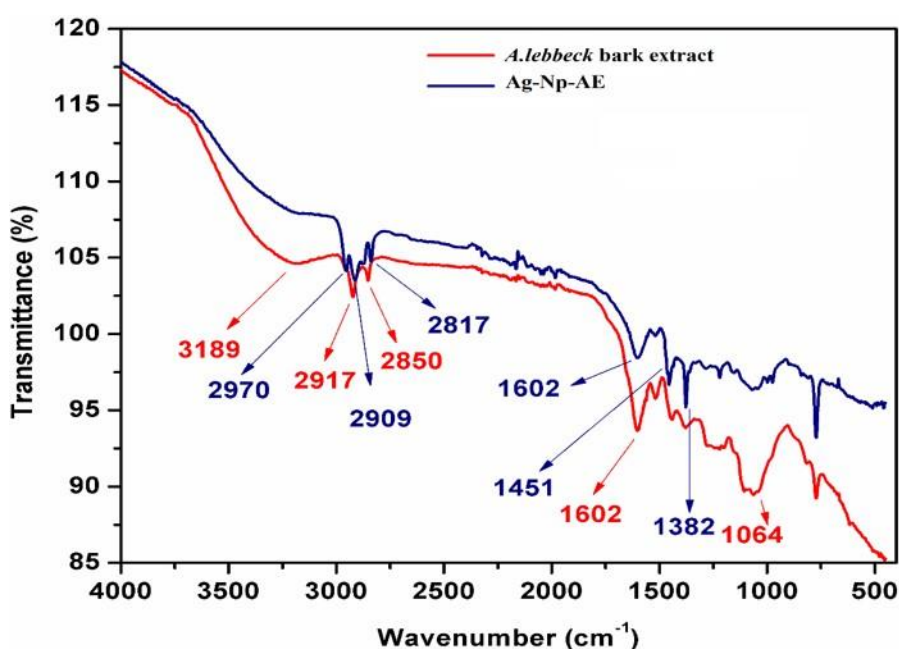
Fig. **2.3** FT-IR spectra of *Albizia lebbeck* bark aqueous extract (AE) and Ag-NP-AE.

X-Ray Diffraction Study of nanoparticles

The XRD of Ag-NP-AE was performed to confirm the structural and chemical composition. The XRD pattern of Ag-NP-AE nanoparticles presented in **Fig**. **2.4** showed five diffraction peaks at (2θ) 27.89º, 32.30º, 38.12º, 44.40º, and 46.28º. Among these 38.12º and 44.40º corresponds to (111) and (220) planes, respectively. Comparing of

standard powder diffraction card of JCPDS with silver file No. 1100136 indicates the cubic crystalline face-centered cubic structure of silver. The unassigned peaks at 27.89º, 32.30º, and 46.28º are due to the crystallization of phytochemicals present on the surface of the silver nanoparticles [69]. The stronger planes (111) that appeared in the Powder XRD plot strongly indicate that silver is a major constituent in the biosynthesis of nanoparticles.
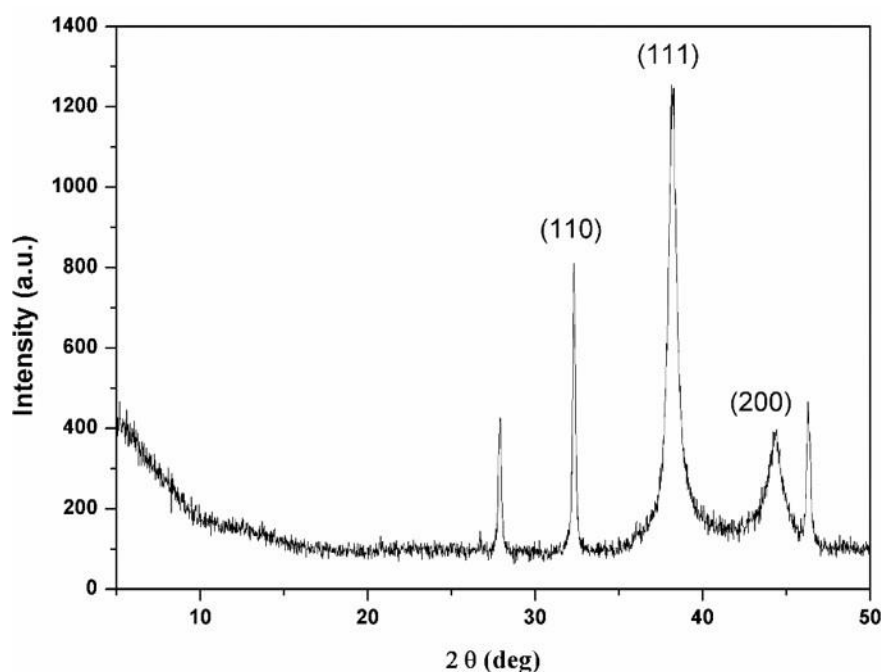
Fig. **2.4.** Powder XRD patterns of Ag-NP-AE.

Morphological studies

Dynamic Light Scattering (DLS) Analysis

DLS analysis was used for the hydrodynamic size distribution of the synthesized Ag-NP-AE. The results showed that the particle size distribution varies between 15-100 nm while the Z-average size distribution of Ag-NP-AE was around 90 nm and the average Poly Dispersity Index (PDI) was <1.5 **Fig**. **2.5**, indicating the stable colloidal dispersion. Moreover, the Ag-NP-AE solution was highly stable and there was no accumulation of

silver even after one month of storage, probably due to the presence of hydroxyl group in the AE of *A. lebbeck* bark that provides long-lasting stability of the 'green nanoparticle'. The morphological study of synthesized Ag-NP-AE by SEM, presented in **Fig**. (**2.5**), revealed the presence of compact granular nano-sized particles with square shape, varies between 20-90 nm, with an average diameter of 90 nm. The particles are disbursed as an individual particle scale, indicating the importance of using *A. lebbeck* bark as a reducing agent during nanoparticle preparation. The

TEM analysis of Ag-NP-AE showed that the nanoparticles have variable shapes as spherical shapes and the size is ranged between 10 to 60 nm with an average size of 27 nm as shown in **Fig. 2.5a**. The diffraction pattern of Ag-NP-AE appeared as lighted spots on the dark field also reflect the crystalline structure and the diffraction rings of the nanoparticles of silver. **Fig. 2.5b** shows EDX of Ag-NP-AE, which indicates the presence of silver as the major ingredient element. Due to surface plasmon resonance, metallic silver nanoparticles generally show a strong signal peak at 3 keV. The quantitative information of the presence of Cl, Si, O, and S isa key element of the bioactive AE of *A. lebbeck*.
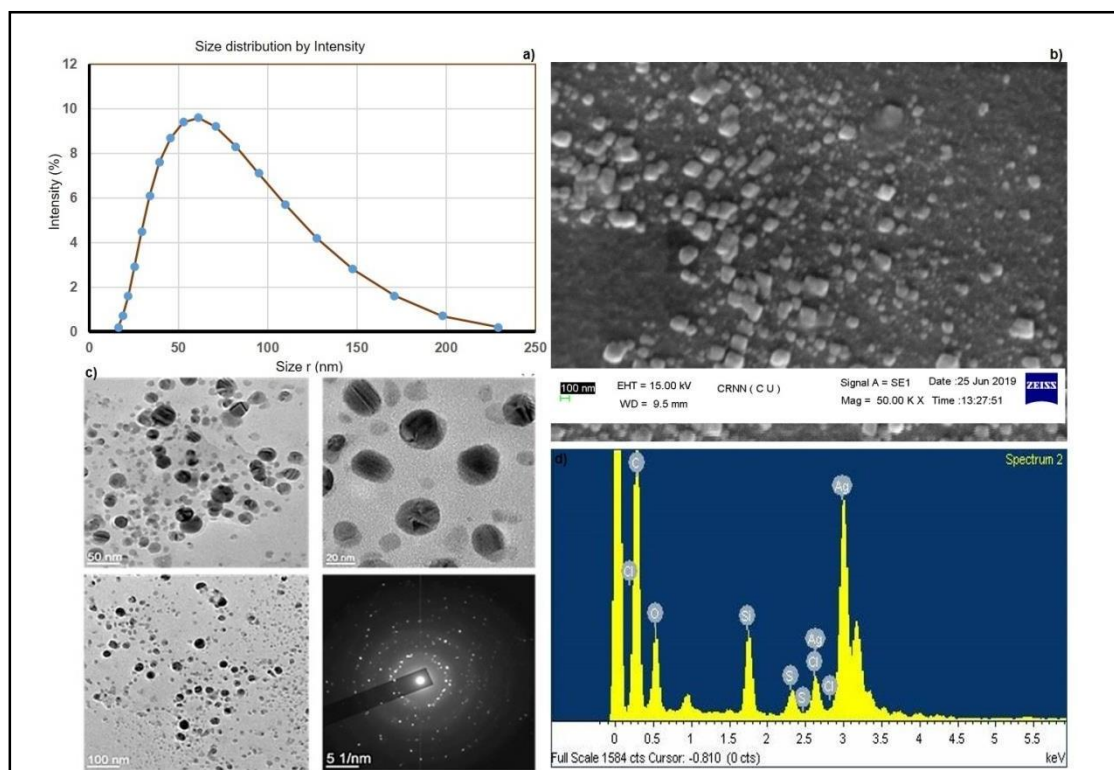
Fig. **2.5** a) Ag-NP-AE Particle size distribution. b) SEM image at magnification 50,000 ×. c) TEM micrograph shows spherical shape off Ag-NP-AE. d) Energy-dispersive X-ray spectroscopy of Nanoparticle.

Determination of Cytotoxicity of nanoparticles

It is known that nano-sized particles with an average diameter of 20-100 nm can able to penetrate living cells and tissues and may produce diverse cellular lesions including toxic manifestations. Thus, to determine the biological impacts of AgNPs and their risks to human health and the environment we have tested the cytotoxicity of Ag-NP-AE in cultured Vero cells by using the well-accepted MTT assay, at different doses (**Fig.2.6**). The results revealed that the 50% cytotoxicity (CC_{50}) of synthesized Ag-NP-AE was 11.0 µM (1.87 µg), in which about half of the Vero cells are survived.
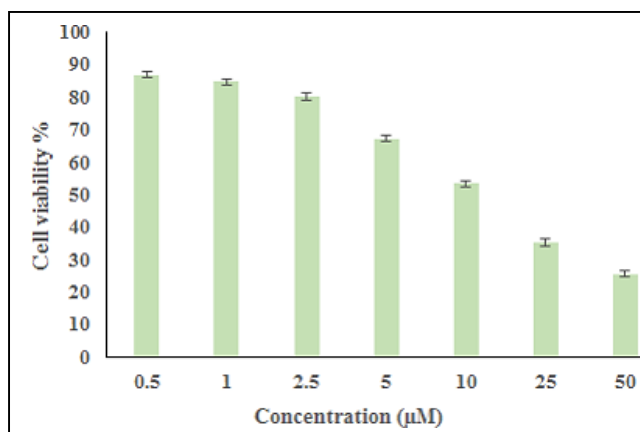
(a)
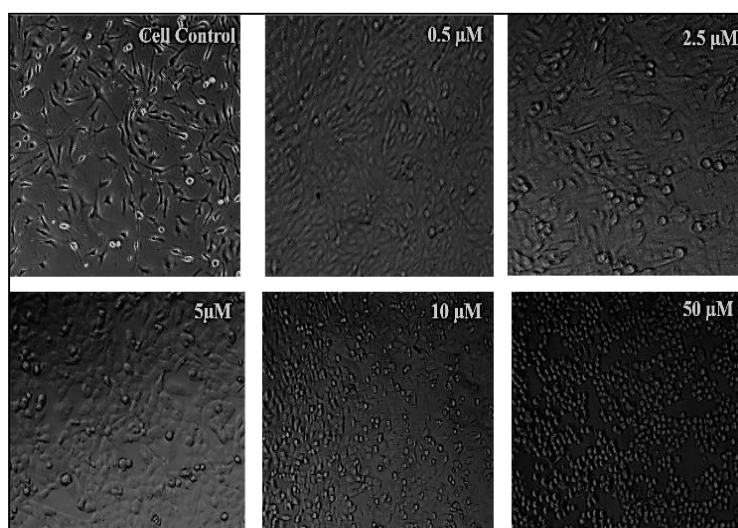
(b)

Fig. **2.6** (**a**) Cell viability assay (**b**) Vero cell morphology at different concentrations of Ag-NP-AE.

In vitro **Antioxidant activity of synthesized nanoparticles**

Free radical scavenging activity of synthesized nanoparticles was evaluated by DPPH radical scavenging assay. The results indicated that Ag-NP-AE can bleach the stable DPPH radical that contained an odd electron (with a strong absorption band at 517 nm; deep violet) which is paired off in presence of a free radical scavenger Ag-NP-AE. The

absorption vanishes and the resulting decolorization is stoichiometricconcerning the number of electrons taken up. The results further revealed that the quenching capacity of Ag-NP-AE at 20 µM (3.4 µg) is more than 50%, close to the standard ascorbic acid (20 µM = 3.4 µg) and is concentration-dependent (**Fig**. **2.7**).
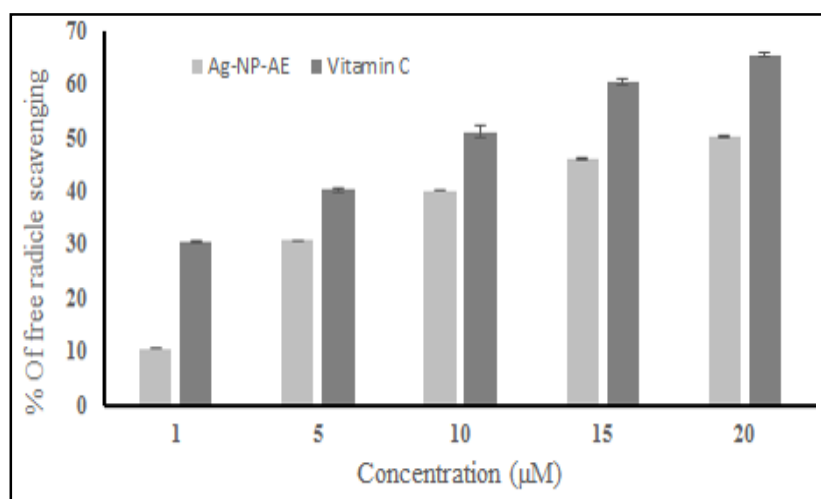
Fig. **2.7** Free radical scavenging activity of Ag-NP-AE and Ascorbic acid.

Antibacterial sensitivity profile of nanoparticles against selected MDR-isolates

The antibacterial susceptibility profile of 14 MDR-isolates of bacteria tested by disc diffusion assay, presented in **Table 1**, revealed that the synthesized nanoparticles (Ag-NP-AE) have significant antibacterial activity against all the test isolates. The results showed that the diameter of inhibition zones varies between 10.9–15.2 mm against the multi-antibiotic resistant strains of *Bacillus subtilis* and *Staphylococcus aureus*; while the zone diameter of 10 Gram-negative isolates varies between 10.4–19.5 mm. On the other hand, quality controlstrains had zone diameters between 11.5–16.2 mm. Interestingly, the zone diameter was highest with the highly resistant *Klebsiella pneumonia* (11.2-16.7 mm), *Serratia marcescens* (16.5-18.9 mm), and *Pseudomonas aeruginosa* (17.5-19.5 mm), compared to the other isolates and the quality control strains.

Further, the diameter of inhibition zones for AE (10.5-16.7 mm) was less than the test nanoparticles, even the concentration of AE was much higher, compared to the nanoparticles (**Table 1**).

Determination of MIC and MBC of Silver nanoparticles

The MIC of synthesized Ag-NP-AE or AE of *A. lebbeck* bark determined against 14-MDR isolates with corresponding quality control strains, presented in **Table 1**, showed significant inhibitory activity against all the test strains. The MIC of AE was between 128-1024 μg/ml; while it was between 64-512 μg/ml for the quality control strains. Surprisingly, the MIC of Ag-NP-AE for all the test isolates was between 0.50-0.84 μM (equal to 0.085-0.143 μg), far below the MIC of plant extract (**Table 2.1**). This indicated that the silver nanoparticles can penetrate the bacterial cell much quickly and damage the bacterial cell to cause rapid and efficient killing than the AE of *A. lebbeck* bark. **Table 2.1.** Antibacterial activity of Ag-Np-AE and AE of *Albizia lebbeck* bark against selected MDR-pathogens.

Bacteria	No	Ag-Np-AE			AE of *A. lebbeck*		Resistance profile
		MIC		Inhibition zone (mm)*	MIC (μg/ml)	Inhibition zone (mm)*	
		μM	μg				
Staphylococcus aureus	2	0.83	0.141	15.2-13.5	256	14.2-13.5	An Amc CIP, Mc, Er
Bacillus subtilis	2	0.64	0.108	12.4-10.9	128	15.4-13.9	Amp, C, Er, T, Km, SXT
Enterococcus faecalis	2	0.82	0.139	12.1-11.0	256	13.2-10.8	A CIP, Van, C, T, Er, Gm
Escherichia coli	2	0.72	0.112	11.9-10.4	512	14.4-12.2	An Amc, Gm, Er, SXT, CIP
Klebsiella pneumoniae	1	0.78	0.132	11.2-16.7	1024	16.7-11.2	A, C, NA, NOR, T, Cft, SXT
Salmonella Typhi	2	0.84	0.143	13.7-12.5	128	13.7-12.5	A, C, SXT, CIP, NA, NOR, T
Serratia marcescens	1	0.60	0.102	18.9-16.5	512	15.9-12.4	A, T, Er, CIP, C, Gm
Pseudomonas aeruginosa	2	0.50	0.085	19.5-17.5	1024	13.5-10.5	AnAMC, C, T, Er, Cft, Gm
Quality control strains							
S. aureus ATCC 29213	1	0.67	0.114	14.8-12.3	256	11.8- 10.1	Sensitive
E. coli ATCC 25922	1	0.75	0.127	14.5-13.7	128	13.5-12.2	Sensitive
E. faecalis ATCC 29212	1	0.72	0.112	12.2-11.5	256	11.4-10.9	Sensitive
K. pneumoniae ATCC 700603	1	0.65	0.110	16.2-13.4	512	15.2-14.4	Sensitive

AE, aqueous extract; Antibiotic discs of: A, ampicillin (10 μg); Amc, amoxicillin with clavulanic acid (20/10 μg); C, chloramphenicol (30 μg); CIP, ciprofloxacin (5 μg); Cft, cefotaxime (30 μg)); Er,

erythromycin (15 µg); Km, kanamycin (30 µg); Gm, gentamicin (10 µg); Mth, methicillin (10 µg); NA, nalidixic acid (30 µg); NOR, norfloxacin (10 µg); OFX, ofloxacin (5 µg); SXT, sulphamethoxazole-trimethoprim (25 µg); T, tetracycline (30 µg); Van, vancomycin (>16 µg). The lowest MIC values indicate the highest inhibitory effect. *Results are the mean of triplicate tests, measuring from three angles.

The MBC of AE was found to be 3-4-fold (512-3072 µg/ml), but for the test nanoparticles Ag-NP-AE it was 4-fold (2.0-3.36 µM or 0.34-0.562 µg) higher than their MIC values; while MBC with the control strain(s) was 2-4 folds higher. Further, the Ag-NP-AE had bactericidal activity at lower concentrations; while the AE had bacteriostatic at lower but cidal at higher concentrations, probably due to the faster penetrability and multiple actions of silver nanoparticles on the bacterial cell.
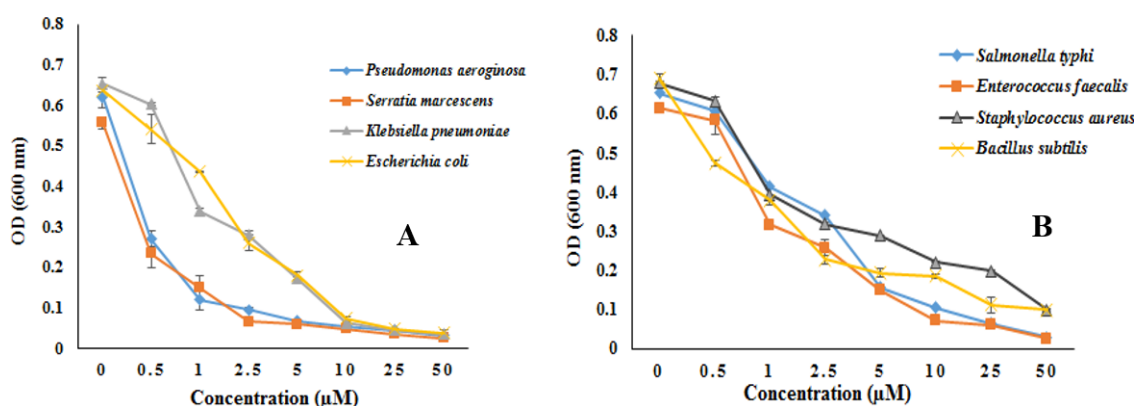
Fig. 2.8 Effect of Ag-NP-AE nanoparticle at different concentration determination by OD (600 nm) vs different concentrations of Ag-NP-AE.

To know the mode of action (cidal or static) of test nanoparticles we have assessed time-dependent growth inhibition or killing of three test bacteria *Pseudomonasaeruginosa*, *Serratia marcescens,* and *Escherichia coli*, at different concentrations of Ag-NP-AE, along with the damage inflicted [70]. The results showed significant inhibition of growth by Ag-NP-AE, with rapid reduction of viable cell numbersovertime at 2.0, 2.4, and 2.88 µM (0.34, 0.408, 0.448 µg) within 0-3 h, indicating higher sensitivity of these MDR-isolates to the test nanoparticles with MIC below 0.9 µM. While for AE it was 3072 and

2048 μg/ml within 4-6 h of exposure **Fig**. **2.8** Here, the colony count (CFU/ml) of test

bacteria were determined at every 30-480 min to find out the inhibitory potential of the

test nanoparticle, compared with the controls (**Fig**. **2.9**). In normal control, without Ag-

NP-AE, all strains had a viable count of 1×10^8 CFU/ml, which decreased exponentially

to zero within 3 h of Ag-NP-AE exposure to the test bacteria. The nanoparticle caused

the death of test bacteria *Serratia marcescens*, *Pseudomonas aeruginosa*, and

Escherichia coli rapidly at the 4 X MIC within only 3 h (**Fig**. **2.10**) indicating that the

MDR-isolates, obtained from hospital patients, are highly sensitive to the test

nanoparticles at a very low concentration, with the excellent inhibitory profile.
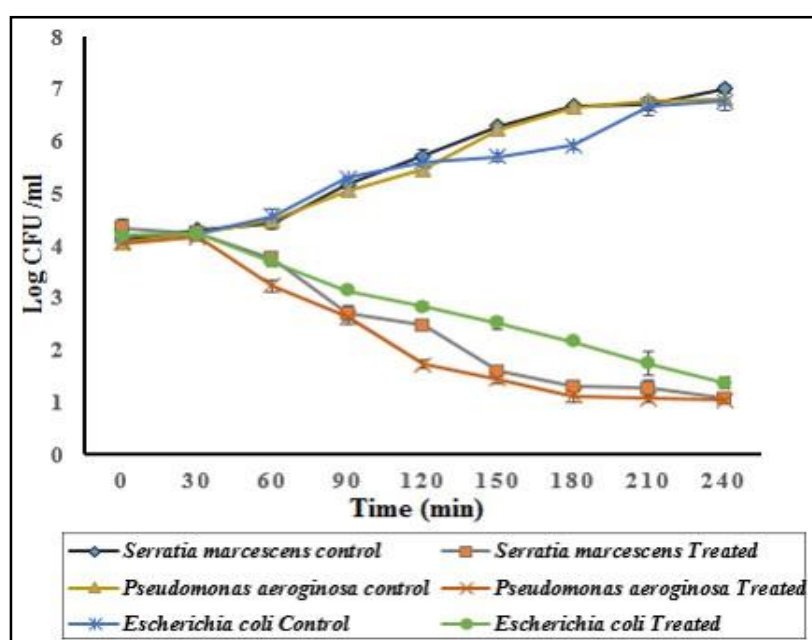
Fig. **2.9** Time-dependent killing of *Escherichia coli*, *Pseudomonas aeruginosa,* and

Serratiamarcescens at their MIC of Ag-NP-AE nanoparticle Evaluated by counting CFU

at different time intervals (0, 30, 60, 90, 120, 150, 180, 210, and 240 min).
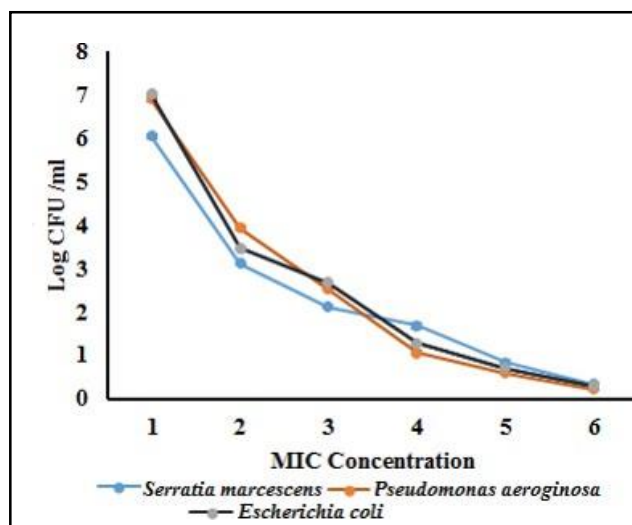
Fig. **2.10** Determination of Minimum Bactericidal Concentration (MBC) for *Escherichia coli*, *Pseudomonas aeruginosa* and *Serratia marcescens*.

The indiscriminate and over-use of antimicrobials reduced the effectiveness of common antibiotics; while the drug-resistant microbes confer resistance primarily through the alteration of the cell wall or cell membrane or through specific genes. Moreover, most antibiotics have cumulative adverse effects like hypersensitivity, neurotoxicity, and immune suppression on individuals and communities. Here, our results showed that silver nanoparticles prepared from AE of *A. lebbeck* stem bark had potent antibacterial activity against 14-MDR isolates of two Gram-positive and six Gram-negative genera confirmed by its MIC and MBCs. Thus, our study demonstrated the therapeutic potential of Ag-NP-AE against MDR-isolates of selected pathogenic bacteria.

Topography change of bacteria after treatment with Ag-NP-AE

We have used powerful scanning electron microscopy to study the morphological changes at sub-cellular resolution and comparative assessment of the effect of Ag-NP-AE to determine the possible mechanism of action. Two clinically important Gram-negative bacteria *Pseudomonas aeruginosa* and *Serratia marcescens*, isolated from a

human patient, highly sensitive to the test nanoparticles but resistant to multiple antibiotics, are used.*Pseudomonas aeruginosa* is the leading pathogens in ICU that cause pneumonia, cystic fibrosis, bacteremia, external otitis, contact lens keratitis, and traumatic endophthalmitis; while *Serratia marcescens* is a facultative anaerobe of soil and water, associated with urinary and respiratory infections, endocarditis, osteomyelitis, septicemia, meningitis, wound, and eye infections. The Electron Micrograph showed clusters of rod-shaped bacillus with normal morphology and topology in the untreated control; while the bacteria treated with Ag-NP-AE revealed altered ultrastructure, as presented in **Fig**. **2.11**, compared to the untreated control, under 25000X magnification of SEM. *Pseudomonas aeruginosa* cells, after 8 h incubation with Ag-NP-AE at 1.5 µM(0.50 µM), showed damaged cell wall and membrane with several pores and leakage of cytosolic content leading to cell lysis; while the untreated bacteria had normal rod-shaped morphology. On the other hand, *Serratia marcescens* treated with Ag-NP-AE showed complete lysis with loss of normal topography. Thus, the morphology of nanoparticles-treated isolates of *P. aeruginosa* and *S. marcescens* under SEM was different, mainly due to the differences in their sensitivity pattern (MIC 0.50 and 0.60 µM) against the test nanoparticles, along with minor variations in inoculum size, cell wall peptidoglycan content or biochemical components.
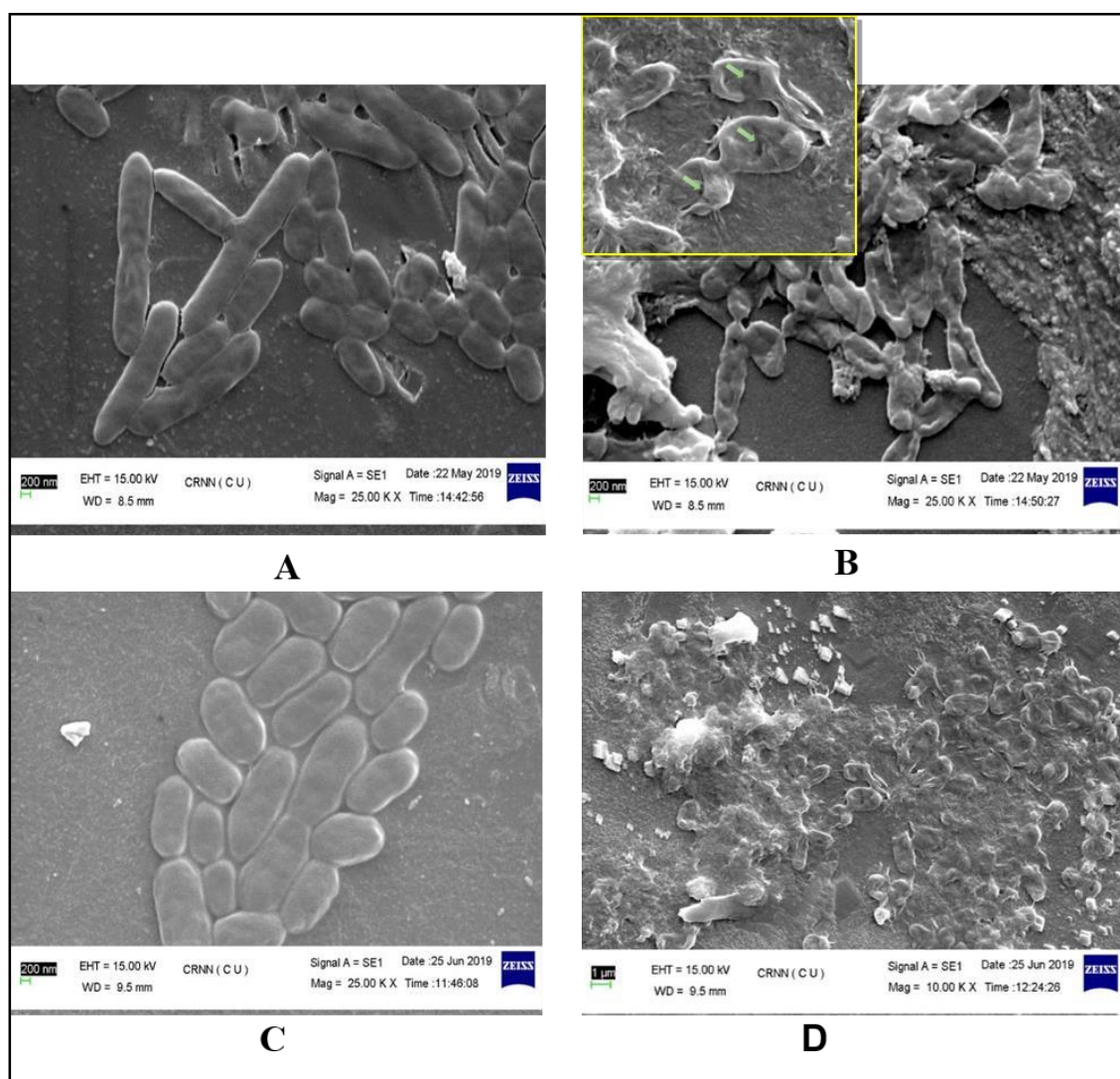
Fig. **2.11** Scanning Electron Micrograph of *Pseudomonas aeruginosa* (A, B)

and*Serratia marcescens*(C, D) before andafter treatment with Ag- NP-AE respectively,

at their MIC.

2.4 Discussion

Several studies reported the broad-spectrum antimicrobial activity of silver nanoparticles,

including the drug-resistant *S. Aureus* [5], *E. coli* [42], *E. faecalis* [43], *K.Pneumonia*

[41], *P. Aeruginosa* [44, 45], *A.Baumannii* [45], *M. tuberculosis*[46]. The silver

nanoparticles synthesized with AgNO3 and leaf extract of *Annona reticulata* showed

potent activity against *Bacillus cereus* and *Staphylococcus aureus* at 125 and 31.25

µg/ml;while it inhibits *Escherichia coli*, *Pseudomonas aeruginosa,* and *Candida albicans* at 62.5 µg/ml [47]. Similarly, the *s*ilver nanoparticles prepared with increased concentrations of *Lepidium draba* root extract showed that nanoparticles with reduced size possess strong activity against *S. aureus*, *B. cereus*, *E. coli,* and *S.Typhimurium* [48]; but silver nanoparticles from *Caesalpinia coriaria* leaf extract are active against antibiotic-resistant *S. aureus*, *E. coli*, *Klebsiella pneumonia*,and *P. aeruginosa*;while silver nanoparticles of *Helicteres isora* root extract possess antibacterial with antioxidant activity [30]; similar to our observation with silver nanoparticles of *A. lebbeck* bark extract but at extremely low concentrations.

It has been reported that the antibacterial or bactericidal properties of silver nanoparticles are shape and size-dependent and smaller particles (<30 nm) were more effective against *K. Pneumonia and S. aureus*, while spherical particles are more active than rod shape [41]. In our study, the nanoparticles Ag-NP-AE is spherical with an average diameter of 27 nm, whichmanyattributes to the release of silver ions responsible for bactericidal activity of Ag-NP-AE at extremely low concentrations (0.5-0.84 µM or 0.085-0.143µg); while AE of *A. lebbeck* bark showed anti-bacterial activity at 128-1024 µg/ml, i.e., at much higher concentrations against all the bacterial isolates tested. An earlier study with zinc oxide nanoparticles from *A. lebbeck* stem bark extract showed antibacterial activity against Gram-negative and Gram-positive bacteria with zone diameter of 10-12mm [31], however, the zone diameter with test nanoparticle Ag-NP-AE was 10.9-19.5 mm, much higher than the zinc oxide nanoparticles, possibly due to better penetrability and activity of silver ions.Further, the antibacterial activity of AgNPs also depends on cell wall peptidoglycan of bacteria, as observed with increased sensitivity of *Escherichia coli* with thin peptidoglycan layer, compared to *Staphylococcus aureus* with thick peptidoglycan layer, which prevents the penetration of Ag-NPs into the bacterial cell. Thus, the

antimicrobial activity of AgNPs is related to the interaction with the surfaces in Gram-positive, but on size, charge, and other features for Gram-negative strains.

The MIC of Ag-NP-AE against the test isolates was between 0.50-0.84 µM (0.085-0.143 µg) but it was 128-1024 µg/ml with AE, and 64-512 µg/ml for the control strains, indicating that the silver nanoparticles can penetrate the bacterial cell quickly and damage cell, cell membrane or other components to cause rapid and efficient killing than the AE. Further, we have observed maximum inhibition of MDR-isolates *P.aeruginosa*, *Serratia marcescens,* and *E.coli*at 2.0, 2.4 and 2.88 µM (0.34, 0.408, 0.448 µg) within 0-3 h; while for AE, it was at a much higher concentration within 4-6 h of exposure.To establish the mode and mechanism of action we have studied the time-dependent growth of three isolates sensitive to Ag-NP-AE and the powerful electron microscopy of nanoparticle treated cells. The time-dependent growth assay revealed significant inhibition of growth by Ag-NP-AE, with a rapid reduction of viable cell number over time, indicating its tidal nature (MIC < 0.9 µM), whichcauses cellular damage. Further, test nanoparticles caused the death of all test bacteria rapidly at the 4X MIC within only 3 h indicates that the MDR-hospital isolates are highly sensitive to the test nanoparticles below 0.9µM (up to 0.143µg), with an excellent inhibitory profile with bactericidal nature against highly antibiotic-resistant pathogens. The SEM image of AgNP-AE treated bacteria demonstrated a clear ultrastructural change in *P. aeruginosa* and *Serratia marcescens* cell morphology (**Fig. 2.11**), under 25000X magnification of SEM after 8 h incubation at 1.5 µM (0.50 µM), containing damaged cell wall (pores) and cell membrane leading to the leakage of cytosolic content to lysis, compared to the untreated bacteria with normal rod-shaped morphology, due to the differences in their sensitivity pattern (MIC 0.50 and 0.60 µM), along with variations in inoculum size, resistance level, peptidoglycan, biochemical and molecular structure as well as other components. This

suggests that Ag-NP-AE can be helpful in the management of those MDR-bacterial infections. Further, nanoparticles not only act on bacteria by direct contact, but also penetrate rapidly to interact with microbial DNA, which prevents the bacterial to develop resistance, and thus nanoparticles are less disposed to bacterial resistance [45-50].

2.5 Conclusions

Here, we are reporting the synthesis of a stable silver nanoparticle using AE of an ethnomedicinal plant *Albizia lebbeck* bark as a 'green'bioreductiont by an ecofriendly method, with a demonstration of its radical scavenging and significant bactericidal activity against 14 MDR-isolates of pathogenic bacteria, with a mechanism of action. However, further safety and efficacy studies in suitable infection models using those MDR-pathogens are required to establish its therapeutic potential.

2.6 References

[1]   N. R. Naylor, R. Atun, N. Zhu, K. Kulasabanathan, S. Silva, A. Chatterjee, G. M. Knight and J. V. Robotham, *Antimicrob. Resist. Infect. Control.*, 2018, **7**, 58.

[2]   M. Hawkey, R. E. Warren, D. M. Livermore, C. A. M. McNulty, D. A. Enoch, J. A. Otter and A. P. R. Wilson, *J Antimicrob. Chemother.*, 2018, **73**, iii02- iii78.

[3]   R. A. Brady, J. G. Leid, J. H. Calhoun, J. W. Costerton and M. E. Shirtliff, *FEMS Immunol. Med. Microbiol.*, 2008, **52**, 13–22.

[4]   J. B. Aswathanarayan and R. R. Vittal, *Pharm. Nanotechnol.*, 2017, **5**, 148–153.

[5]   J. Kang, M. J. Dietz, K. Hughes, M. Xing and B. Li, *J. Antimicrob. Chemother.*, 2019, **74**, 1578–1585.

[6]   G. Franci, A. Falanga, S. Galdiero, L. Palomba, M. Rai, G. Morelli and M. Galdiero, *Molecules.*, 2015, **20**, 8856–8874.

[7]   S. Valsalam, P. Agastian, M. V. Arasu, N. A. Al-Dhabi, A.-K. M. Ghilan, K. Kaviyarasu, B. Ravindran, S. W. Chang and S. Arokiyaraj, *J. Photochem and Photobiol B: Biology.*, 2019, **191**, 65-74.

[8]   H. H. Lara, E. N. Garza-Treviño, L. Ixtepan-Turrent and D. K. Singh, *J. Nanobiotechnol.*, 2011, **9**, 30.

[9]   F. Okafor, A. Janen, T. Kukhtareva, V. Edwards and M. Curley, *Int. J. Environ. Res. Public Health.,* 2013, **10**, 5221–5238.

[10] Q. L. Feng, J. Wu, G. Q. Chen, F. Z. Cui, T. N. Kim and J. O. Kim, *J. Biomed. Mater. Res.*, 2000, **52**, 662–668.

[11] W. Chen, W. Cai, L. Zhang, G. Wang and L. Zhang, *J. Colloid Interface Sci.*, 2001, **238**, 291–295.

[12] T.-H. Kim, M. Kim, H.-S. Park, U.S. Shin, M.-S. Gong and H-W. Kim, *J Biomed Mater Res A.*, 2012, **100**, 1033–1043.

[13] P. Raveendran, J. Fu and S. L. Wallen, *J. Am. Chem. Soc.*, 2003, **125**, 13940–13941.

[14] J. Umashankari, D. Inbakandan, T. T. Ajithkumar and T. Balasubramanian, *Aquat. Biosyst.*, 2012, **8**, 11.

[15] S. Ahmed, M. Ahmad, B. L. Swami and S. Ikram, *Journal of Advanced Res.*, 2016, **7**, 17–28.

[16] V. K. Sharma, R. A. Yngard and Y. Lin, *Adv. Colloid Interface Sci.*, 2009, **145**, 83–96.

[17] S. E. Besra, A. Gomes, L. Chaudhury, J. R. Vedasiromoni and D. K. Ganguly, *Phytother Res.*, 2002, **16**, 529–533.

[18] S. K. Lam and T. B. Ng, *Phytomedicine.*, 2011, **18**, 601–608.

[19] A. K. Das, F. Ahmed, S. C. Bachar, J. Kundu and S. Dev, *J Biol Sci.*, 2003, **3**, 685–687.

[20] R. S. Gupta, J. B. S. Kachhawa and R. Chaudhary, *Asian J. Androl.*, 2004, **6**, 155–159.

[21] R. S. Gupta, R. Chaudhary, R. K. Yadav, S. K. Verma and M. P. Dobhal, *J. Ethnopharmacol.*, 2005, **96**, 31–36.

[22] C. C. Baruach, P. P. Gupta, G. K. Patnaik, D. K. Kul-Shreshtha and B. N. Dhawan, *Indian J. Vet Med.*, 1997, **21**, 127–132.

[23] S. D. Chintawar, R. S. Somani, V. S. Kasture and S. B. Kasture, *J. Ethnopharmacol.*, 2002, **81**, 299–305.

[24] C. R. Resmi, M. R. Venukumar and M. S. Latha, *Indian J. Physiol. Pharmacol.*, 2006, **50**, 297–302.

[25] N. Pathak, P. Gohil, N. B. Patel, S. Kasture, N. Jivani and Y. Bhalodia, *Int. J. Pharm Sci Drug Res.*, 2009, **1**, 183–187.

[26] D. Kumar, S. Kumar, S. Kohli, R. Arya and J. Gupta, *Asian Pacific Journal of Tropical Medicine*, 2011, **4**, 900–903.

[27] S. Kalia, N. Walter and U. Bagai, *Indian J. Med. Res.*, 2015, **142**, 101.

[28] H. Umar, D. Kavaz and N. Rizaner, *IJN.*, 2018, **14**, 87-100.

[29] P. Bag, D. Ojha, H. Mukherjee, U.C. Halder, S. Mondal, A. Biswas, A. Sharon, L. Van Kaer, S. Chakrabarty, G. Das, D. Mitra and D. Chattopadhyay, *Antivir. Res.*, 2014, **105**, 126–134.

[30] S. Bhakya, S. Muthukrishnan, M. Sukumaran and M. Muthukumar, *Nanosci.*, 2016, **6**, 755–766.

[31] Clinical Laboratory Standards Institute (*CLSI*). 2019.M7-A7, **26**(2).

[32] D. Chattopadhyay, T. Mukherjee, P. Pal, B. Saha and R. Bhadra, *J. Antimicrob. Chemother.*, 1998, **42**, 83-86.

[33] Clinical and Laboratory Standards Institute (*CLSI*). 2015.M7-A10, **35** (2).

[34] A. O Oluduro, *Malaysian J Microbiol.*, 2012.

[35] S. D. Sarker, L. Nahar and Y. Kumarasamy, *Methods.*, 2007, **42**, 321–324.

[36] D. Chattopadhyay, D. Ojha, H. Mukherjee, P. Bag, S.P. Vaidya and S. Dutta, *Biomed. Pharmacother.*, 2018, **99**, 286–289.

[37] L. P. Watson, A. E. McKee and B. R. Merrell, *Scan. Electron Microsc.*, 1980, 45–56.

[38] M. Balouiri, M. Sadiki and S. K. Ibnsouda, *Journal of Pharmaceutical Analysis.*, 2016, **6**, 71–79.

[39] P. D. Lister, D. J. Wolter and N. D. Hanson, *Clinical Microbiology Reviews.*, 2009, **22**, 582–610.

[40] J. R. Morones, J. L. Elechiguerra, A. Camacho, K. Holt, J. B. Kouri, J. T. Ramírez and M. J. Yacaman, *Nanotechnology.*, 2005, **16**, 2346–2353.

[41] D. Acharya, K. M. Singha, P. Pandey, B. Mohanta, J. Rajkumari and L. P. Singha, *Sci Rep.*, 2018, **8**, 201.

[42] K. Maruthai, K. Vallayyachari, T. Ravibalan, S.A. Philip, A.V. Samrot and M. Muthuraj, *Prog Biosci Bioeng.*, 2017,1.

[43] K. Halkai, J. Mudda, V. Shivanna, V. Rathod and R. Halkai, *Contemp Clin Dent.*, 2018, **9**, 237.

[44] S. Liao, Y. Zhang, X. Pan, F. Zhu, C. Jiang, Q. Liu, Z. Cheng, G. Dai, G. Wu, L. Wang and L. Chen, *IJN.*, 2019, **14**, 1469–1487.

[45] M. Chen, X. Yu, Q. Huo, Q. Yuan, X. Li, C. Xu and H. Bao, *J. Nanomater.*, 2019, **2019**, 1–7.

[46] K. Punjabi, S. Mehta, R. Chavan, V. Chitalia, D. Deogharkar and S. Deshpande, *Front. Microbiol.*, 2018, **9**, 2207.

[47] E. Parthiban, N. Manivannan, R. Ramanibai and N. Mathivanan, *Biotech Reports.*, 2019, **21**, e00297.

[48] F. Benakashani, A. Allafchian and S. A. H. Jalali, *Green Chem Letters and Reviews.*, 2017, **10**, 324–330.

[49] K. Jeeva, M. Thiyagarajan, V. Elangovan, N. Geetha and P. Venkatachalam, *Ind. Crops Prod.*, 2014, **52**, 714–720.

[50] G.V. Vimbela, S.M. Ngo, C. Fraze, L. Yang and D. A. Stout, *Int. J. Nanomedicine.*, 2017, **12**, 3941-3965

Chapter 3

Silver Nanoparticles synthesized from an aqueous extract of *Oxalis corniculata* demonstrate significant anti-biofilmfim and anti-microbial activity by damaging the bacterial cell membrane

Abstract

The silver nanoparticles OC-AgNPs, synthesized from the aqueous extract of *Oxalis corniculata* (OC), showed moderate antiviral activity against herpes simplex virus-1 (HSV-1), but significant anti-biofilm, and antibacterial activities against human isolates of six multi-drug resistant (MDR) bacteria *Staphylococcus aureus*, *Streptococcus pyogenes*, *Escherichia coli, Klebsiella pneumonia*, *Salmonella typhi,* and *Pseudomonas aeruginosa*. The nanoparticle was characterized by UV-Vis and FTIR spectroscopy; while its morphology and distribution were determined by transmission electron microscopy (TEM). The cytotoxicity and safety of OC-AgNP were evaluated by MTT assay in Vero cells, and triple-negative human breast cancer MDA-MB-468 cells. To test the antiviral activity against HSV-1F we have used the plaque reduction assay. The anti-biofilm activity was assessed by crystal violet staining, followed by light and confocal microscopy; while the antibacterial activity was determined by conventional disk-diffusion and broth-dilution methods. Moreover, the mechanism of anti-biofilm and antibacterial activity was examined by Field Emission Scanning Electron Microscopy (FESEM). The results revealed that the biogenic OC-AgNPs are spherical in shape with an average diameter of 40 nm and showed a UV-Vis peak at 445 nm. The cytotoxicity (CC_{50}) on Vero cells was found to be 300μg/ml; while the survival percentage of MDA-MB-468 cells was 27.12 and 80.97% at 100 and 20μM of OC-AgNPs, respectively. The OC-AgNP showed moderate antiviral activity (EC_{50}) against HSV-1F at 25μg/ml, but significantly inhibited the biofilm of *P. aeruginosa* and *E. coli* at 25-50μg/ml; while at 30-50μM we observed the dose-dependent lowering of fluorescence intensity, under light and confocal microscope. Interestingly, the OC-AgNPs demonstrated significant antibacterial activity against *Pseudomonas aeruginosa* (20 mm), *Klebsiella pneumonia* (15 mm), *Escherichia coli* (12 mm), *Salmonella typhi* (10 mm), *Streptococcus pyogenes* (11 mm), and *Staphylococcus aureus* (10 mm) with Minimum Inhibitory Concentration (MIC) of 0.65 to 0.90 μM (0.11- 0.153μg), respectively. Further, the FESEM micrograph showed disruption of membrane structure with the damage of cell membrane integrity of *P. aeruginosa* at its MIC.

3.1 Introduction

Silver nanoparticles (Ag-NPs) have a broad range of biomedical applications, particularly as antimicrobial and anticancer agents, drug-delivery carriers, diagnostics, imaging probes, etc.[1]. Different methods are now available to monitor the shape size, and yield of AgNPs, such as physical (ball milling, laser ablation, electrical arc, and vapor condensation), chemical (Ag^+ reduction by $NaBH_4$. Na-citrate), electrochemical, photochemical, microwave-assisted, sonochemical, micro-organism assisted and plant-mediated [2]. Considering the sustainable development and environmental fortification the plant-mediated methods of synthesis of AgNPs are the most favorable ones. Synthesis of silver nanomaterials by using plant extract(s) is found to be more useful because of their natural, less-toxic, eco-friendly, cost-effective, scalable, and more reliable nature. Moreover, the plant-based nanoparticle synthesis is quick, and it can replace the capping agents used in chemical reduction methods [3, 4, 5]. More importantly, the diverse bioactive metabolites of plants including enzymes, amino acids, vitamins, polysaccharides, flavonoids, alkaloids, quinines, oils, terpenoids, and phenolics, present in plant extracts [6, 7], may help to reduce Ag^+ ions to AgNPs in a greener way. The antimicrobial efficacy of AgNPs depends upon the morphology of nanoparticles and the nature of protecting agents [8, 9], as nanoparticles can easily attach to microbial membrane surfaces [10] to block the respiration and membrane permeability of bacteria. Thus, smaller AgNPs are more bactericidal than larger ones [11, 12]. Biofilms of bbacteriaclustersrs of bacterial colonies implanted in a self-secreted exo-polysaccharide (EPS) matrix that protects them from the adverse environment within the host cells and helps in lateral gene transfer [13]. Biofilms also help bacteria to adapt t ecological stresses, as well as protect from antibiotics, and biocides[14]. The AgNPs were reported to block the biofilm development and destroy the bacteria inside the

cluster, suggesting their use in the management of biofilm-related infections [15, 16]. It is reported that the plastic catheters coated with AgNPs can prevent biofilm formation by *Enterococcus faecalis*, *E. coli*, *P. aeruginosa*, *S. aureus,* and *Candida albicans* with significant *in vitro* antimicrobial activity [17, 18].

The herbaceous plant *Oxalis corniculata* Linn(Oxalidaceae), known as sleeping beauty or creeping woodsorrel, is a medicinal plant grown in moist shady places of subtropical and tropical reregionsnd is traditionally used in diverse ailments thatatti-booti". In India, the plant is known asCangeri (Sanskrit), Tinpatiya (Hindi), Amrool (Bengali), Teltupp (Kannada), Amabile(Marathi), Sialthur (Oriya), etc. The medicinal usages of *Oxalis corniculata* are described in diverse traditional systems of medicines including Ayurveda, Unani, and Siddha [19]. Chemically the plant contains diverse phytochemicals including tannins, palmitic acid, a mixture f oleic, linoleic, linolenic and, stearic acids, glyoxylic-, pyruvic-, and oxalic acids, vitexin, neutral and glycolipids, β-carotene, niacin, and vitamin C; while glycosides, phytosterols, phenolics, flavonoids, and volatile oils are isolated from its alcoholic (methanol and ethanol) extracts [20, 21]. The whole plant is a rich source of carbohydrates, lipids, proteins, with diverse minerals including sodium, potassium, calcium, magnesium, and nitrogen that help in regulating metabolic pathways in living cells [22] and thus, used as an alternative vegetable. Pharmacologically *Oxalis corniculata* possess antibacterial, anti-helminthic, analgesic, anti-inflammatory, astringent, diuretic ,relaxant, styptic, stomachic, and febrifuge activities. Thus the plant is used in ddiarrhea enteritis, fever, burn, skin eruptions, influenza, urinary tract infections, traumatic injuries, scurvy, sprains, insect and snake bites; while its infusion help to expel hookworms [23, 24]. Contemporary literature revealed that methanolic extract of *Oxalis corniculata* and its fractions can scavenge free

radicals, with antifungal and hepatoprotective activities, and may play a significant role in anticancer therapeutics [25, 26, 27].

Here, OC-AgNP has been synthesized by using the aqueous extract (AE) of *Oxalis corniculata* as a reductant of $AgNO_3$ and as the natural stabilizer. We have used various spectroscopic and microscopic techniques to characterize OC-AgNPs; while cytotoxicity and cell viability were tested in Vero and human breast cancer cells MDA-MB-468, respectively. The anti-bacterial and anti-biofilm potential of OC-AgNPs were evaluated against six multi-drug resistant (MDR) clinical isolates of bacteria, by determining the sensitivity, inhibitory activity, growth kinetics, and mode or mechanism of action, following standard techniques [28].

3.2 Experimental section

3.2.1 Plant materials preparation

The fresh *Oxalis corniculata* L (OC) herb was collected from the Jangalmohal forest area of Paschim Medinipur District, West Bengal, and washed under running tap water to make it mud and dust-free and then dried in a shaded airy room. The dried plants were powdered in a grinder, and passed through a 40-mesh sieve to obtain fine powder. About 500 gm of powdered samples were defatted with petroleum ether at room temperature and then extracted with water by cold maceration for 72h at 28-30°C [29]. The whole extract was filtered by Whatman filter paper No. 2 (6 mm) and subjected to solvent evaporation to dryness at 35-40°C under decreased pressure in an EYELA Centrifugal Evaporator (Japan).

3.2.2 Standardization of extract by RP-HPLC

Standardization of plant extract(s) was achieved via High-performance liquid chromatography (HPLC), while the quality evaluation was done by a photo-markerferulic acid and validated by the Reverse Phase (RP)-HPLC. The Shimadzu RP-HPLC system (Shimadzu Prominence, Kyoto, Japan) consists of two reciprocating pumps LC-20 AD UFLC, a variable SPD-M20A Prominence PDA detector, and a Rheodyne manual injector was used. The analysis was done by Isocratic elution with a C_{18} reverse-phase column (4.6 mm width ×250 mm length) with a particle size of 5 μm (Phenomenex-Luna C18, Torrance, CA, USA). All the samples were filtered (0.45 μM syringe filter, Whatman NYL0.45) and the volume of each sample was 20 μl. Then 1.0 ml of each sample was injected into the injector RP-HPLC port for 1 min at a maintenance temperature of 25°C. The lyophilized extract was then dissolved in methanol at a 5 mg/ml concentration, while the standard solution was prepared by dissolving ferulic acid (0.5 mg/ml) in methanol. All the samples were sonicated before the experiment. The mobile phase was maintained by Methanol: Water (1% glacial acetic acid) in the ratio 3:2, after adjusting its pH (Orion 3 Star pH Meter, Thermo-Scientific); and analyzed at a wavelength of 320 nm. All the samples were sonicated before the experiment. LC solution software was utilized for peak area calculation. While the standard calibration curve was plotted by the corresponding peak area of the standard versus the concentration of standards, using linear regression. The quantification of ferulic acid as standard was determined by the constructed standard calibration curve. Following the International Conference on Harmonization guidelines, the above method was validated for sensitivity, accuracy, and specificity [30].

3.2.3 Preparation and characterization of OC-AgNPs

About 0.5 mg of the aqueous extract (AE) of *Oxalis corniculata* (OC) was added with 1.0 mM of $AgNO_3$ (0.85 mg) in a 50 ml round-bottom flask. The mixture was allowed to agitate at 90°C for 2h. The pale yellow solution was shifted to deep-brown, indicating the completion of the reaction with the preparation of OC-AgNPs. The OC-AgNP was characterized by UV–Visible spectra at a range of 250–700 nm with a Perkin-Elmer Lambda 25 Spectrometer. To distinguish the functional group and formations of OC-AgNP, by change of color, from AE of OC we have used FTIR spectra (Model: Perkin Elmer spectrum 100). To determine the actual size and shape of OC-AgNP we have used High-Resolution TEM (HR-TEM) by spotting the sample on carbon-coated copper grids, and subsequently, air-dried before microscopy. The arrangements of selected area electron diffraction (SAED) were collected by using 2100 KeVJEOL Ultra High-Resolution Field Emission Gun (UHR-FEG) TEM with 200 KeVvoltage.

3.2.4 Microorganism and Cell culture

Well-characterized bacterial species of *Bacillus subtilis*, *Staphylococcus aureus*, *Escherichia coli*, *Enterococcus faecalis*, *Salmonella enterica* subspecies *enteric* Serovar Typhi (*S.* Typhi), *Pseudomonas aeruginosa*, *Klebsiella pneumonia* and *Serratia marcescens*, obtained from the Microbiology Department, Calcutta Medical College and Hospital, and the Peerless Hospital, Kolkata were used in this study. The quality control strains include *E. coli* ATCC 25922, *S. aureus* ATCC 29213, *E. faecalis* ATCC 29212, and *K. pneumoniae* ATCC 700603. All the cultures were maintained in agar slants and stored at −80°C with 50% glycerol and cultured in sterile MacConkey agar, nutrient agar, or blood agar plates, as and when required. Before experimentation, a single isolated colony of the respective bacterium was aseptically picked up from a 24 h old culture

plates, grown on nutrient agar for the preparation of the inoculum, and checked at an optical density of 0.1 at 600 nm.

Kidney epithelial cells from African green monkey (Vero cells, ATCC, USA) and human breast cancer cells (triple-negative) MDA-MB-468, acquired from the National Center for Cell Science (NCCS) Pune, India were grown in DMEM containing 10% FBS (Fetal Bovine Serum), with penicillin/streptomycin (100 Units/ml) in 5% CO_2 at 37ºC. Experiments were conducted with the cells in the exponential growth phase.

3.2.5 Cell survival assay

Cytotoxicity and cell survival ability of OC-AgNPs was studied on Vero and MDA-MB-468 cells, following standard procedure [31]. In brief, the cellular toxicity of OC-AgNPs, after treatment with different concentrations, was calculated by MTT assay. The cells (1×10^4 cells/well) were seeded in 96well plates and exposed to OC-AgNPs at 0, 20, 40, 60, 80, and 100 µM, respectively for 24h. Then the cells were washed with PBS and reincubated in 5% CO_2 with MTT solution for 3h at 37ºC. MTT solubilization buffer was used to solubilize formazan crystals and the absorbance was examined at 570 nm in a photometer (BioTek)along with the absorbance of the control.

3.2.6 *In vitro* Antibacterial activity

Bacterial strains: Fully characterized MDR-isolates of six bacterial species, responsible for causing difficult-to-treat infections, were used. For *antibacterial susceptibility testing* the AE and OC-AgNPs were exposed to the bacterial isolates to determine the inhibitory zone diameter (IZD) by a modified agar diffusion method [29, 32] using commercial antibiotic discs (Difco, UK) and DMSO (0.1%) as control. The antibacterial efficacy of test extract and nanoparticles were firmed for each bacteria in terms of zone diameter. On each Mueller Hinton agar (MHA, Difco, UK) plate 1.0 ml of bacterial culture (2×10^6

CFU/ml) was spread uniformly, and the extractor OC-AgNPs impregnated discs (0-1000 μg/disc) were placed aseptically on each inoculum-containing plate; and subsequently incubated overnight at 37°C. The test agent with IZD ≥ 10 mm against one of the test bacteria was considered a promising antibacterial agent [33].

3.2.7 Determination of MIC and MBC

The broth dilution method was used to determine the MICs [29, 32]. A standardized suspension of bacteria at 2×10^6 CFU/ml in MHB containing test agents (0-500 μg/ml) was incubated in a shaker incubator (200 rpm) at 37°C for 24h. The lowest concentration of the tube without noticeable growth was recorded as the MIC; while the MBC was determined with the standardized suspension (1.0 ml) of test bacteria in MHB containing test agents at 0- to 4-fold MIC at 37°C overnight. The aliquots (0.1 ml) at hourly intervals were collected to measure the OD at 600 nm and plated to count the viable bacterial colony [33].

3.2.8 Growth inhibitory potential of test agents

The overnight culture of test bacteria diluted with fresh MHB was incubated for 3h, and at the mid-logarithmic phase (10^6 CFU/ml) the culture was exposed to OC-AgNPs at their MIC along with the drug-free bacteria-inoculated medium. Samples were collected at 1h interval (0- 24h) for colony count [28, 29]. Experimental data in triplicate was recorded to evaluate the mean viable bacterial counts, while the Log_{10} CFU/ml was plotted with respect to time [33].

3.2.9 Anti-biofilm activity by Crystal Violet assay

To determine the effectiveness of OC-AgNPs against the formation of biofilm network by the test bacteria, the overnight cultures of each isolate were diluted in Luria-Bertani (LB) broth to 1×10^6 CFU/ml for colorimetric measurements of crystal violet

incorporated biofilm-forming cells [34]. The diluted bacterial samples in a sterile flat-bottom 96-well microplate were incubated for 5h at 37ºC. After the incubation period, the culture was added with fresh medium containing various concentrations of OC-AgNPs, without disturbing the biofilm, and preincubated for 24h at 37°C. The medium was discarded and the cultures were carefully washed with sterile distilled water to take out the planktonic bacterial cells for drying at room temperature for 30 min. The biofilm was stained with 0.1% (v/v) crystal violet solution for 20 min, washed with sterile distilled water three times, and allowed to dry at room temperature for 1h. The excess stain was removed by adding 200 µl of absolute ethanol to each wellwiyj 15 min agitation, and the OD was measured at 590 nm by an ELISA reader. The percentage of anti-biofilm activity was calculated using the formula: $[1 - (A_{590}$ of treated cells $/A_{590}$ of non-treated control)$]\times 100$ [35, 36]. Experiments were conducted three times to obtain the statistical means $\pm$ SD.

3.2.10 Biofilm Microscopy

Light Microscopy: Sterileslides (1×1cm) were aseptically placed on each well of a 24-well polystyrene plate and added with *P. aeruginosa* culture (1×10^6 CFU/ml). The culture media was replaced with fresh media containing OC-AgNPs at its MIC and incubated for 5h at 37°C. After incubation, suspended cells were removed. Biofilms formed on the slides were stained with crystal violet for 5 min, gently washed with PBS, and dried for another 5 min. The biofilm was then examined under a Carl Zeiss Axiovert inverted light microscope at a magnification of 40X, and images were captured [36].

3.2.11 Confocal Microscopy

To visualize the surface topology of *P.aeruginosa* biofilm on a glass slide, placed on a 24-well polystyrene coated microtiter plate, Confocal Laser Scanning Microscope (CLSM) was used [37]. To determine the effects of OC-AgNPs on mature biofilms the test drugs, AE (OC), OC-AgNPs, or antibiotics (as control) were added at their MIC. The drug-treated biofilms on glass slides were then incubated overnight at 37°C, and washed with PBS, followed by staining with acridine orange to detect the biofilm morphology under CLSM (Carl Zeiss LSM700, Jena, Germany) [37].

3.2.12 *In vitro* Antiviral assay

3.2.12.1 Antiviral activity by plaque reduction assay

The cytopathic effect of OC-AgNPson HSV-1F was examined by MTT assay; while antiviral activity was validated by the plaque reduction assay (PRA). Monolayers of Vero cell infected with 100 plaque-forming units (PFU/well) of HSV-1Fwas treated with doubling concentrations of OC-AgNPs followed by the addition of 1% methyl-cellulose (overlay medium) and incubated for 72h in a CO_2 incubator at 37ºC. Using paraformaldehyde (4%) as a fixing agent, the cells were stained with 0.03% crystal violet (in 70% methanol) for plaque count. The EC_{50} (50% effective concentration) for antiviral activity of OC-AgNPs was calculated [38].

3.3 Results and Discussion

3.3.1 Chemistry: Green synthesis of AgNPs using *Oxalis corniculata* Aqueous extract

The HPLC–PDA quantitative analysis was performed in isocratic conditions using a validated RP-HPLC method by the standard calibration technique [39]. The content of

the standard pyhtomarker in the OC-AE was analyzed by a comparative study with the retention time of the standards. Ferulic acid showed good linearity within 20-100 µg/ml of the calibration curve and the Correlations coefficient (r2) was found to be >0.99. The chromatograms obtained from RP-HPLC of the OC-AE and standard Ferulic acid, presented in **Fig**. **3.1**, showed that the retention time (Rt) for Ferulic acid present in OC-AE was 2.69 min; and the concentrations of Ferulic acid, determined from the standard calibration curve, was0.145 % (w/w). Ferulic acid is one of the active constituents of *Oxalis corniculata* [40].
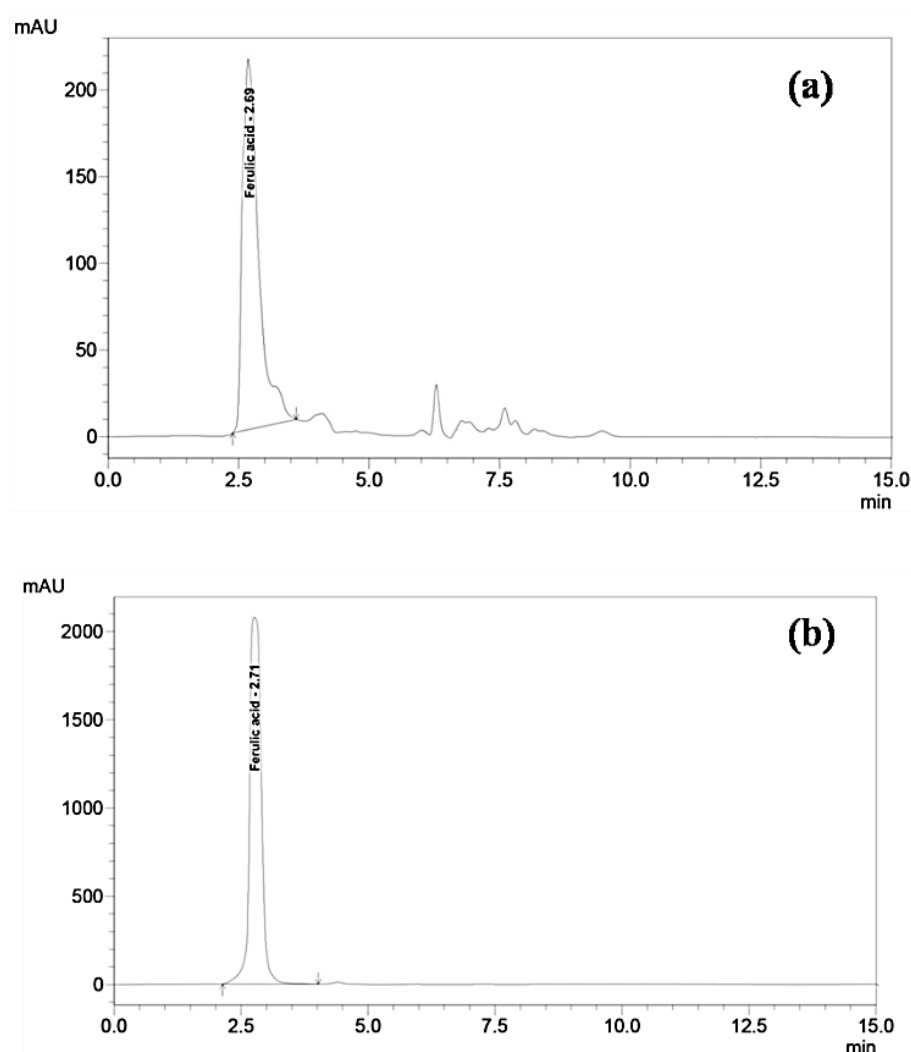
Fig. **3.1.** RP-HPLC Chromatogram of Standard Ferulic acid (**a**); *Oxalis corniculata* Aqueous extract (**b**).

In this work, biogenic nanoparticles OC-AgNPs were synthesized using the aqueous extract of *O. corniculata* as bioreduction. The conformation of OC-AgNPs nanoparticle synthesis was indicated by the color change from pale-yellow to deep brown. The observed UV-Vis spectrum peak at 445 nm clearly designates the longitudinal Vibration related to the silver nanoparticle(s) and this band is associated with oscillation of the electron on the surface of the nanoparticle, upon excitation in the determined wavelength (**Fig**. **3.2a**). The presence of different functional groups in plant extract(s) or biomolecules and their function towards nanoparticles can be clearly understood by FT-IR spectra of AE-OC and OC-AgNP, shown in **Fig**. **3.2b**. The AE-OC contains the absorption peaks at 3244 cm^{-1} which approaches the existence of O-H/N-H bond of alcohol or amine groups, 2933 cm^{-1} for aliphatic C-H bond, 1586 cm^{-1} for C=C bond, 1390 cm^{-1} for C-O bond, 1299 cm^{-1} for C-N bond of amine, and 770 cm^{-1} for C-Cl bond, shifted at 3224 cm^{-1}, 2925 cm^{-1}, 1609 cm^{-1}, 1382 cm^{-1}, 1329 $cm^{-1,}$ and 823 cm^{-1} after the interaction of OC-AgNPs. Comparing the IR spectra of AE and OC-AgNPs, can be concluded that the extract contains mainly alcoholic, OH, amines, C=C that could reduce Ag^+ to Ag (0), and the biopolymer matrix has stabilized AgNPs.
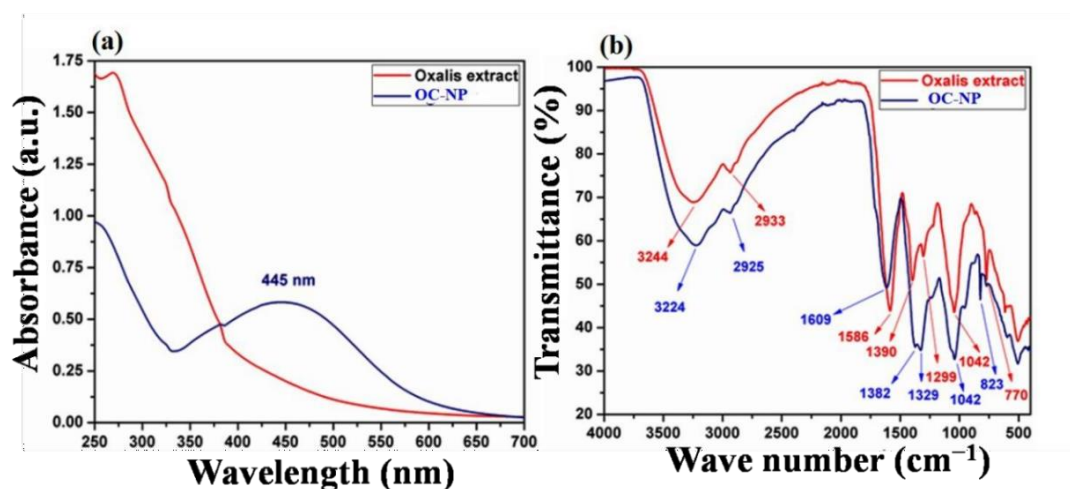
Fig. **3.2**. UV-Vis profile of OC-AgNP (λmax 445 nm) (**a**); FT-IR spectrum ofOC-AgNP and *Oxalis corniculata* aqueous extract (**b**).
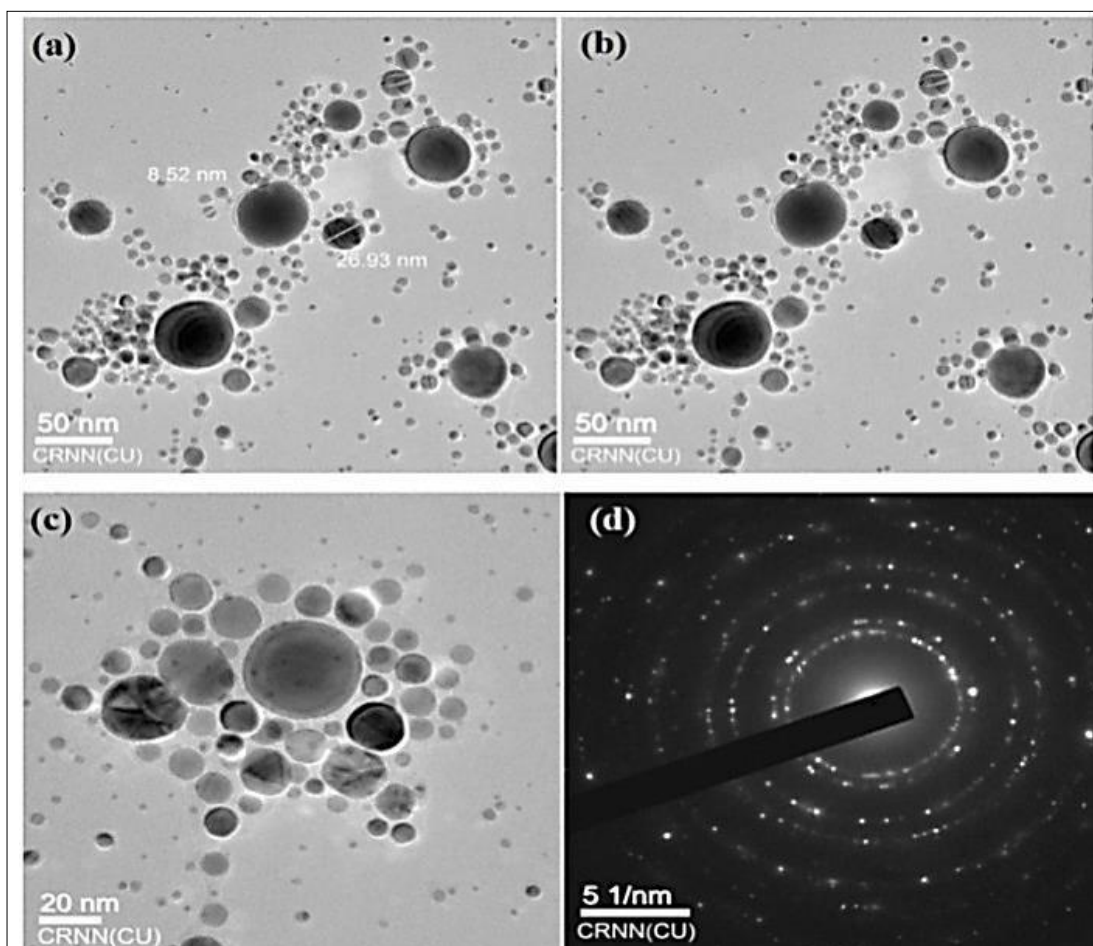
Fig. **3.3** HR-TEM micrograph showing spherical OC-AgNPs at different scales (**a-c**). JEOL 2100 KeV Ultra High-Resolution Field Emission Gun (UHR-FEG) TEM collected SAED at voltage 200 KeV(**d**).

The distribution and size of synthesized OC-AgNPs were studied by transmission electron microscope (TEM). The OC-NPs solution was drop cast on a carbon-coated copper grid and dried under ambient conditions. The high-resolution transmission electron micrograph revealed a particular selected area electron diffraction pattern of OC-AgNPs (**Fig**. **3.3**), obtained by acceleration at the voltage of 200 KeV. The micrographs presented in **Fig**. **3.3** suggest that the particles were of consistent spherical morphology with 40 nm in size.

3.3.2 Bioactivity studies

3.3.2.1 Cytotoxicity of synthesized silver nanoparticles

The cytotoxicity of OC-AgNP was examined on Vero cells, and cell viability on breast cancer cells MDA-MB-468, using MTT assay. The cells were exposed to different concentrations of OC-AgNPsfor 24h. Results depicted a significant dose-dependent reduction of cell viability. The 50% cytotoxicity of OC-AgNP was 300μg/ml, where 50% of cells remained alive. The survival percentage of MDA-MB-468 cells treated with 20, 40, 60, 80, and 100 μM of OC-AgNP was found to be 80.97, 65.98, 50.00, 32.45, and 27.12%, respectively. While the 50% inhibitory concentration (IC_{50}) for MDA-MB-468 cells was found to be 60 μM. Interestingly, the percentage of cell survival was low with the increasing concentrations of OC-AgNPs.
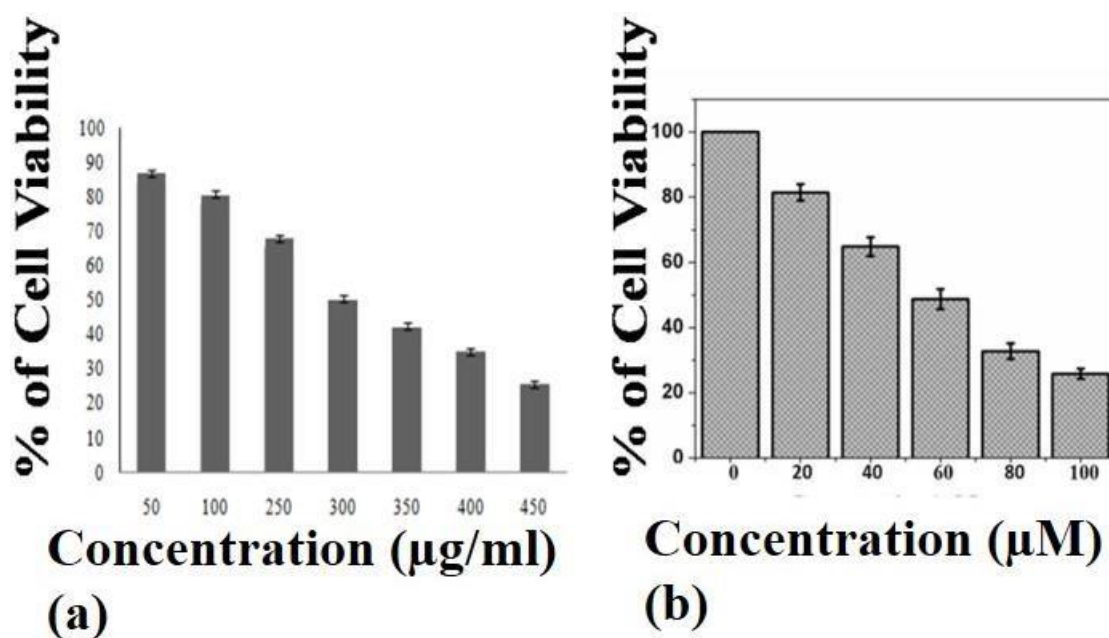
Fig. 3.4 Cytotoxicity of OC-AgNP on Vero cell (**a**); and breast cancer cell MDA MB-468 (**b**) by MTT assay.

3.3.2.2 Antibacterial activity against pathogenic bacteria with an evaluation of MIC and MBC

The data from the zone of inhibition, MIC were presented in **Table 3.1**. The results revealed that the test extract (AE-OC) and the synthesized nanoparticles (OC-AgNPs) have a bactericidal effect. The MIC of AE-OCwas between 108-800μg/ml for MDR-isolates; while it was 255-650μg/ml for the quality control strains. On the other hand, the MIC of OC-AgNP for all the pathogenic isolates was between 0.65-0.90 μM (equals to 0.11-0.153 μg); which is significantly lower than the MIC of the parent extract (**Table 3.1**). This indicated that OC-AgNPs may invade the microbial cell quickly and damage the cell more rapidly than the AEof*O. corniculate*. Further study on growth kinetics of *E. coli* and *P. aeruginosa* in the presence or absence of OC-AgNP revealed that bacterial viability or number of viable cells was drastically reduced at 2-4 fold-higher concentrations of its MIC.

| Bacteria | No | OC-AgNP | | Aqueous extract of *O.corniculata* (OC-AE) | | Resistance profile[1] |
		MIC (µM)	Zone of inhibition (mm)	MIC (µg/ml)	Zone of inhibition (mm)	
Pseudomonas aeruginosa	2	0.65	20.10-19.0	108	15.9-12.4	Amc, A, C, T, Er, Cft
Bacillus subtilis	2	0.69	12.1-11.0	345	10.4-9.9	Amp, C, Er, T, Km
Enterococcus faecalis	1	0.82	11.9-10.4	289	9.4-8.2	A, CIP, Van, C, T, Er
Escherichia coli	1	0.72	12.7-11.2	208	10.3-16.7	Er,A, Amc, Gm, SXT
Klebsiella pneumoniae	2	0.78	15.7-14.5	380	13.7-2.5	A, C, NA, NOR, T
Streptococcus pyogenes	1	0.84	10.9-9.0	560	8.7-7.9	T, Er, CIP, C
Staphylococcus aureus	1	0.76	10.5-10.2	800	8.5-7.3	Amc, CIP, Er
Quality control strains						
S. aureus ATCC 29213	1	0.114	14.8-12.3	300	11.8- 10.1	Sensitive
K. pneumoniae ATCC 70(	1	0.127	14.5-13.7	245	13.5-12.2	Sensitive
E. faecalis ATCC 29212	1	0.112	12.2-11.5	255	11.4-10.9	Sensitive
E. coli ATCC 25922	1	0.110	16.2-13.4	650	15.2-14.4	Sensitive
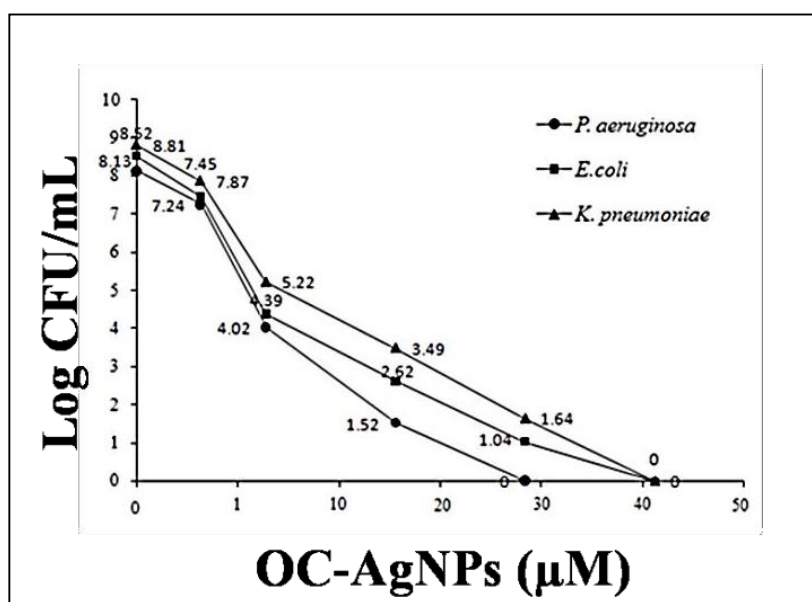
Fig. 3.5 The antimicrobial spectrum of OC-AgNPs against selected microbes.

[1]Antibiotic discs of: A, ampicillin (10 µg); Amc, amoxicillin with clavulanic acid (20/10 µg); C, chloramphenicol (30 µg); CIP, ciprofloxacin (5 µg); Er, erythromycin (15 µg); Km, kanamycin (30 µg); Gm, gentamicin (10 µg); NA, nalidixic acid (30 µg); NOR, norfloxacin (10 µg); SXT, sulphamethoxazole-trimethoprim (25 µg); T, tetracycline (30 µg); Van, vancomycin (>16 µg). Lowest MIC values indicate the highest inhibitory effect. *Results are the mean of triplicate tests, measuring from three angles.

To know the possible mode of action i.e., bacteriostatic or bactericidal effect of OC-AgNPs on bacterial growth, we performed a growth curve analysis in the presence or absence of nanoparticles. The most sensitive strains of *E. coli* and *P. aeruginosa* (**Fig. 3.6**), treated with OC-AgNPs, demonstrated maximum growth inhibition at their MICwithin 2-8 h of exposure indicating that OC-AgNPs have an inhibitory effect on bacterial cell division. Thus, OC-AgNPthe green synthesized nanomaterial can serve as an attractive antimicrobial candidate against diverse human pathogens, as reported earlier [41].
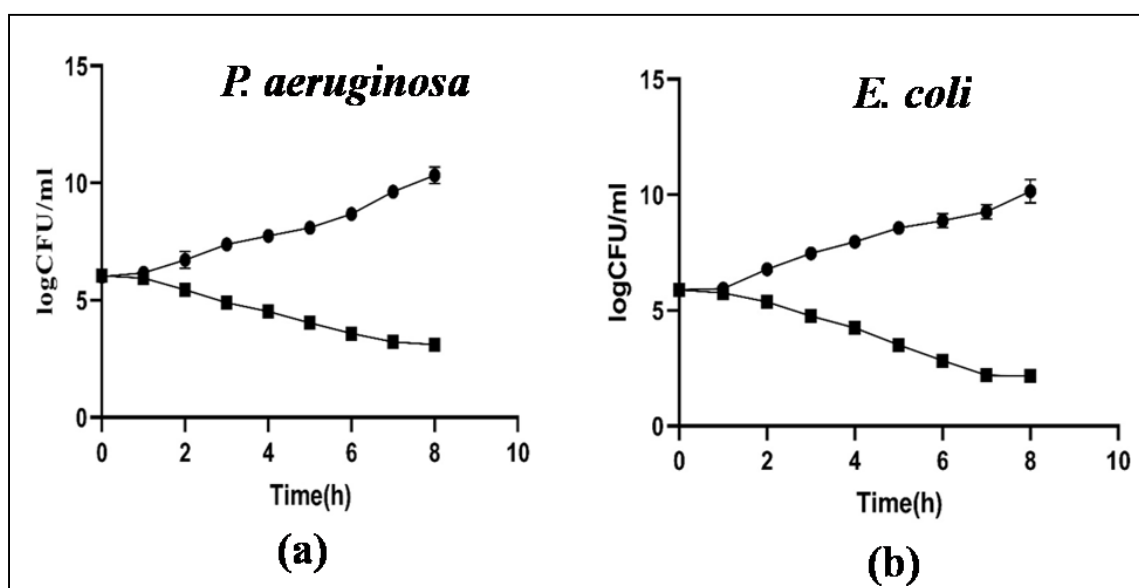
Fig. 3.6 Growth curve of *P.aeruginosa* (**a**), and *E. coli* (**b**) in the presence and absence of OC-AgNPs.

3.3.2.3 Potency of synthesized nanoparticle OC-AgNPs on biofilm formation of test bacteria

The potency of OC-AgNPs against the formation of biofilm by *P. aeruginosa* and *E. coli*, presented in **Fig. 3.7**, revealed that nanoparticles at 10 µM and 50 µM concentrations inhibit >50% and >80% of biofilm formation of *P. aeruginosa*. While at 50 µM, it

prevents 80% biofilm formation of *E. coli*. Thus, OC-AgNPs were more effective against *P.aeruginosa* biofilm formation than the *E. coli* isolate tested.
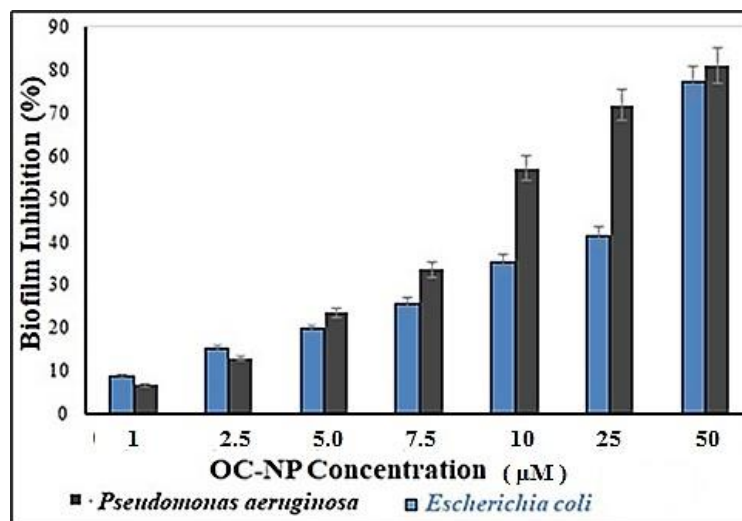
Fig. 3.7 Effect of OC-AgNPs on biofilm inhibition of *P.aeruginosa* and *E.coli*.

We have studied the effect of OC-AgNP on biofilm construction by two bacteria *E. coli* and *P. aeruginosa* using 96-well plates for biofilm formation. **Fig. 8** showed that OC-AgNPs can inhibit the biofilm formation of *P. aeruginosa* and *E. coli* isolates at 25 and 50 µM, respectively. Further, the anti-biofilm activity of OC-AgNPs was studied by Zeiss Axiovert inverted light microscope. The micrograph of the biofilm(s), control and test-set, revealed that OC-AgNPs caused the maximum reduction of biofilm constituents (**Fig**. 3.**8a** and **3.8b**), probably due to its better penetration of the biofilm matrix, and interferes with the metabolic process of bacteria including the constituents that form biofilm. Additionally, the quantitative assay of biofilm development on 96-well plates using an automated Micro ELISA reader (Thermo Scientific, Pittsburgh, PA) revealed that by preventing colonization of bacteria in the biofilm matrix, OC-AgNP decreases the growth and progression of the biofilm formed by *P. aeruginosa*. This evidence indicated that the biofabricated nanoparticle is effective in disrupting bacterial biofilm by reducing the pathogenic bacterial load/concentration.

91
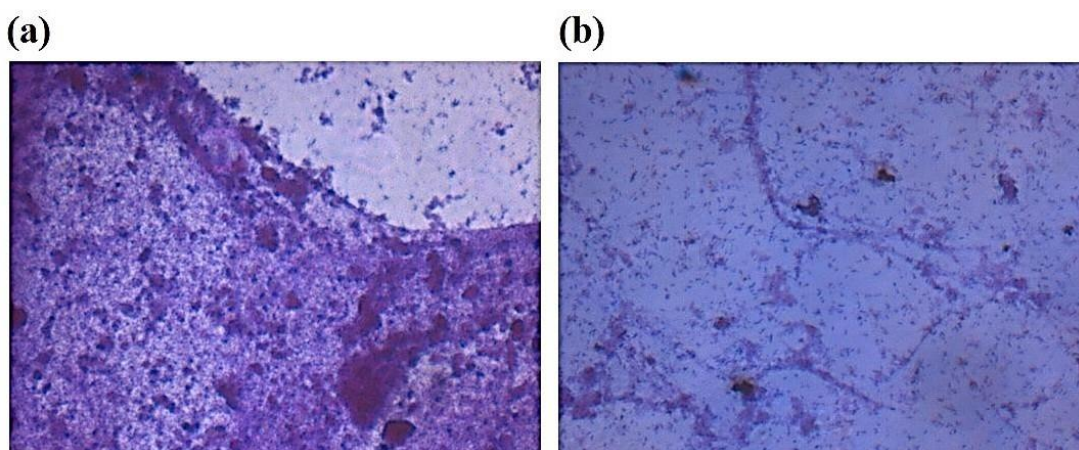
Fig. 3.8 Inverted Light Microscopic Image of biofilm of *P. aeruginosa*, stained with 0.1% crystal violet, on OC-AgNP coated glass surface before treatment (**a**), and after treatment (**b**) at their MIC.

3.3.2.4 Quantification of live bacteria in the biofilm

To compute the percentage of destruction of live bacteria in the thebiofilmwe conducted live-dead staining of *P. aeruginosa* biofilm (**Fig**. **3.9**) and examined it under a confocal microscope. The confocal microscopic image of visible biofilm after treatment with OC-AgNP (30 µM and 50 µM), presented in **Fig**. **3.9b** and **3.9c**, clearly demonstrated lower fluorescence intensity with increasing concentration of OC-AgNP; while the biofilm of untreated control bacteria appears green due to the presence of live green cells.
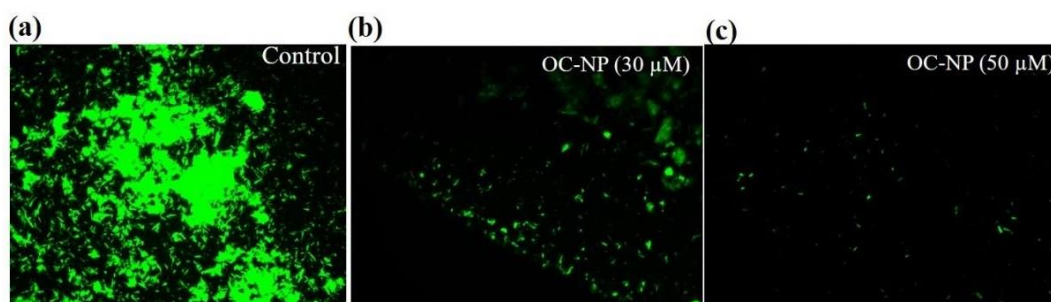
Fig. 3.9 Confocal micrograph of *P. aeruginosa* biofilm. (a) Untreated biofilm of *P. aeruginosa* (Positive control); (b) Biofilm treated with OC-AgNP at 30 µM; (c) Biofilm incubated with OC-AgNP at 50 µM.

Previously, it was reported that silver nanoparticles have potential anti-biofilm activity and not only suppress the embedded biofilm but also kill the bacterial cells [42,43]. Many bacteria produce their polymer matrix on living tissue or abiotic surfaces as biofilm, that are more difficult to destroy than planktonic bacterial cell [44]. Here the exposure OC-AgNPs to biofilm developed by *P. aeruginosa* and *E. coli* resulted in the inhibition of bacterial growth in a dose-dependent manner (**Fig**. **3.8** and **3.9**).

The field emission (FE)-SEM images under 25,000X magnification (**Fig**. **3.10**) showed that control cells are even and unchanged. On the other hand, OC-AgNP treated *P. aeruginosa* cells revealed evidence of maximum membrane abrasion. Thus, our study demonstrated that the OC-AgNP treatment at its MIC unusually damages the bacterial membrane integrity with disruption of the cytoplasm membrane.
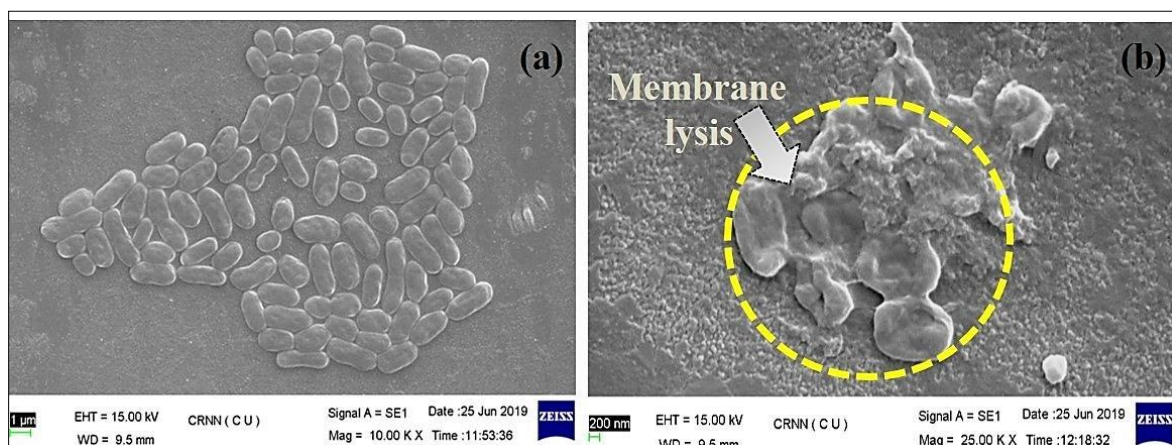
Fig. 3.10 Morphology of untreated *P. aeruginosa* by FE-SEM (**a**); FE-SEM image of OC-AgNPs treated *P. aeruginosa* cells at MIC showing membrane lysis (**b**).

Treatment with OC-AgNPs may damage the bacterial membrane to facilitate the release of cellular contents from the bacterial cells, like biogenic silver nanoparticles from *Albizia lebbeck* bark [42] and *Pandanus odorifer* leaf extract [45].

3.3.2.5 Cytotoxicity and antiviral activity of AE of OC and its nanoparticles OC-AgNPs

The cytotoxicity assay revealed that the 50% cytotoxicity (CC_{50}) of AE of *Oxalis corniculata* and OC-AgNP was 450.6±3.22 and 300.5±4.84 µg/ml. While the anti-HSV activity determined by plaque reduction assay showed that 50% effective concentration (EC_{50}) of OC-AE and OC-AgNPsagainst HSV-1F was 107.2±4.1 and 61.0±3.6 µg/ml, compared to acyclovir 129.8 ± 0.44 µg/ml; with selectivity index (SI) of 4.2 and 5.0 (**Table 3.2**). Thus, *Oxalis corniculata* AE had EC_{50} at a higher concentration with low SI, than its nanoparticle (**Table 3.2**).

Table 3.2. Cytotoxicity and Antiviral activity of AE of *O. corniculata* and its nanoparticle, OC-AgNP, against HSV-1F.

Test Drug	CC_{50}[a] (µg/ml)	EC_{50}[b] (µg/ml)	Selectivity index (SI)[c]
		HSV-1F (MOI:1)	HSV-1F
O. corniculata AE	450.6 ± 3.22	107.2 ± 4.1	4.2
OC-AgNP	300.5 ± 4.84	61.0 ± 3.6	5.0
Acyclovir (ACV)	129.8 ± 0.44	2.1 ± 0.1	61.5

Further, the 99% effective concentration (EC_{99}) to inhibit viral growth was achieved at 186.4 and 94.6 µg/ml by OC-AE and OC-AgNPagainst HSV-1F, respectively.

3.4 Conclusion

Oxalis corniculata aqueous extract was used to synthesize and stabilize AgNPs (OC-AgNPs) which was characterized by spectral data, and TEM. OC-AgNPs displayed significant inhibition of MDA-MB-468 breast cancer cells; with cytotoxicity (CC_{50}) at 300µg/ml. The nanoparticle possesses moderate antiviral activity (EC_{50}) against HSV-1F at 25µg/ml. Interestingly, the anti-biofilm activity was significant at 25-50 µg/ml against *P. aeruginosa* and *E. coli*; while the antibacterial activity against six MDR-isolates was between 0.65-0.90 µM, equal 0.11 to 0.153 µg. Further study revealed that OC-AgNP can disrupt bacterial integrity with lysis of cell membrane.

3.5 References

[1] S.P. Deshmukh, S.M. Patil, S.B. Mullani and S.D. Delekar, *Mater. Sci. Eng. C. Mater. Biol. Appl.*, 2019, **97**, 954–965.

[2] L. Xu, Y.-Y. Wang, J. Huang, C.-Y. Chen, Z.-X. Wang and H. Xie, *Theranostics.*, 2020, **10**, 8996.

[3] M. Huhtala, J. Heino, D. Casciari, A. de Luise and M.S. Johnson, *Matrix Biol.*, 2005, **24**, 83–95.

[4] M. Shaik, M. Khan, M. Kuniyil, A. Al-Warthan, H. Alkhathlan, M. Siddiqui, J. Shaik, A. Ahamed, A. Mahmood, M. Khan and S. Adil, *Sustainability.*, 2018, **10,** 913.

[5] M. Yadi, E. Mostafavi, B. Saleh, S. Davaran, I. Aliyeva, R. Khalilov, M. Nikzamir, N. Nikzamir, A. Akbarzadeh, Y. Panahi and M. Milani, *Nanomed. Biotechnol.*, 2018, **46**, S336–343.

[6] O. Collera-Zúñiga, F. García Jiménez and R. Meléndez Gordillo, *Food Chem.*, 2005, **90**, 109–114.

[7] S. Ghosh, V.S. Meli, A. Kumar, A. Thakur, N. Chakraborty, S. Chakraborty, A. Datta, *J. Exp. Bot.*, 2011, **62**, 571–582.

[8] A. J. Kora and R. B.Sashidhar, *J. Antibiot.*, 2014, 1–10.

[9] T.-H. Kim, M. Kim, H.-S. Park, U.S. Shin, M.-S. Gong and H.-W. Kim, *J. Biomed. Mater. Res.*, 100A (2012) 1033–1043.

[10] H. E. Webb, D. M. Brichta-Harhay, M. M. Brashears, K. K. Nightingale, T. M. Arthur, J. M. Bosilevac, N. Kalchayanand, J. W. Schmidt, R. Wang, S. A. Granier, T. R. Brown, T. S. Edrington, S. D. Shackelford, T. L. Wheeler, G. H. Loneragan, *Front. Microbiol.*, 2017, **8**, 2214.

[11] L. Kvítek, A. Panáček, J. Soukupová, M. Kolář, R. Večeřová, R. Prucek, M. Holecová, R. Zbořil, *J. Phys. Chem.*, C. 2008, **112**, 5825–5834.

[12] A. Melaiye, Z. Sun, K. Hindi, A. Milsted, D. Ely, D.H. Reneker, C.A. Tessier, W.J. Youngs, *J. Am. Chem. Soc.*, 2005, **127**, 2285–2291.

[13] C.C. Goller, T. Romeo, Springer Berlin Heidelberg, Berlin, Heidelberg, 2008, 37–66.

[14] A. Kumar, A. Alam, M. Rani, N. Z. Ehtesham, S. E. Hasnain, *Int. J. Med. Microbiol.*, 2017, **307**, 481–489.

[15] F. Martinez-Gutierrez, L. Boegli, A. Agostinho, E. M. Sánchez, H. Bach, F. Ruiz and G. James, *Biofouling*., 2013, **29**, 651–660.

[16] P.Lehours, E.Siffré, F.Mégraud, *BMC gastroenterology*., 2011, **11**, 1–5.

[17] Z. Khatoon, C. D. McTiernan, E. J. Suuronen, T.-F. Mah and E. I. Alarcon, *Heliyon*., 2018, **4**, 01067.

[18] R. M. Donlan and J. W. Costerton, *Clin. Microbiol. Rev.*, 2002, **15**, 167–193.

[19] H. Badwaik, M. K.Singh, D. Thakur, T. K. Giri and D. K.Tripathi, *Inter. J. Phytomedicine*., 2011, **3**, 01.

[20] N. P. Manandhar, *Contrib. Nepal. Stud.*, 1993, **20**, 183–196.

[21] M. P. Raghavendra, S. Satish, K. A. Raveesha, My science, 2006, **1**, 72–78.

[22] Q. J. Groom, J. Van der Straeten and I. Hoste, *PeerJ*., 2019, **7**, e6384.

[23] A. Rehman, A. Rehman and I. Ahmad, *Int. J. Anal. Chem.*, 2015, **2015**, 1.

[24] M. Srikanth, T. Swetha and B.Veeresh, *Int. J. Med. Microbiol.*, 2012, **3**, 4077–4085.

[25] M. R. Khan, A.Marium, M.Shabbir, N.Saeed, J.Bokhari, *Afr. J. Pharmacy Pharmacol.*, 2012, **6**, 2255–2267.

[26] S. Mukherjee, H. Koley, S. Barman, S. Mitra, S. Datta, S. Ghosh, D. Paul and P. Dhar, *J. Med. Food.*, 2013, 16, 801–809.

[27] R. A. Sharma and A.Kumari, *Int. J. Pharm Pharm Sci.*, 2014, **3**, 6–12.

[28] D. Chattopadhyay, D. Ojha, H. Mukherjee, P. Bag, S.P. Vaidya, S. Dutta, *Biomed. Pharmacother.*, 2018, 99, 286–289.

[29] D. Chattopadhyay, K. Maiti, A.P. Kundu, M.S. Chakraborty, R. Bhadra, S.C. Mandal, A.B. Mandal,Journal of Ethnopharmacology 77(2001), 49–55.

[30] Guideline I.H.T, Validation of analytical procedures: text and methodology, Q2 (R1). 1(2005) 5.

[31] L. El Khalki, V. Maire, T. Dubois and A. Zyad, *Molecules*, 2020, **25**, 506.

[32] D. Chattopadhyay, T. Mukherjee, P. Pal, B. Saha, R. Bhadra, *J. Antimicrob. Chemother.*, 1998, **42**, 83-86.

[33] Clinical and Laboratory Standards Institute, Methods for Dilution Antimicrobial Susceptibility Tests for Bacteria That Grow Aerobically. Approved Standard M07-A10, 35 (2) (2015) 20-25, Clinical and Laboratory Standards Institute, Wayne, PA 19087, USA, 2015.

[34] K. Kalishwaralal, S. BarathManiKanth, S. R. K. Pandian, V. Deepak and S. Gurunathan, Colloids Surf. B: Biointerfaces. 2010, **79**, 340–344.

[35] E. Haney, M. Trimble, J. Cheng, Q. Vallé and R. Hancock, Biomolecules. 2018, **8**, 29.

[36] C. I. Extremina, L. Costa, A.I. Aguiar, L. Peixe and A.P. Fonseca, *J. Microbiol. Methods.*, 2011, **84**, 167–173.

[37] G. D. Christensen, W. A. Simpson, J. J. Younger, L. M. Baddour, F. F. Barrett, D. M. Melton and E. H. Beachey, *J. Clin. Microbiol.*, 1985, **22**, 996–1006.

[38] P. Bag, D. Ojha, H. Mukherjee, U.C. Halder, S. Mondal, A. Biswas, A. Sharon, L. Van Kaer, S. Chakrabarty, G. Das, D. Mitra, D. Chattopadhyay, *Antivir. Res.*,

2014, **105**, 126–134.

[39]   A. Acheampong, W.O. Gyasi, G. Darko, J. Apau, S. Addai-Arhin, SpringerPlus.
       2016, **5**, 1–8.

[40]   S. Mukherjee, S. Pal, R. Chakraborty, H. Koley, P. Dhar, *Indian J. Exp. Biol.*,
       2018, **56**, 239–243.

[41] K. Karimzadeh, Elhamsharifi, N. Bakhshi and M. Ramzanpoor, *J. Drug Deliv. Sci.
       Technol.*, 2019, **54**, 101263.

[42]   A. Das Mahapatra, C. Patra, J. Mondal, C.R. Sinha, P. Sadhukhan, D.
       Chattopadhyay, *Chemistry Select.*, 2020, **5**, 4770–4777.

[43]   Y. K. Mohanta, K. Biswas, S/K. Jena, A. Hashem, E. F. Abd-Allah, T. K.
       Mohanta, *Front. Microbiol.*, **11**, 1143.

[44]   Z. Khatoon, C. D. McTiernan, E. J. Suuronen, T.-F. Mah and E.I. Alarcon,
       Heliyon. 2018, **4**, e01067.

[45] X. Yan, B. He, L. Liu, G. Qu, J. Shi, L. Hu and G. Jiang, *Metallomics.*, 2018, **10,**
       557–564.

Chapter 4

Exploration of synthetic potential Anti-HSV nucleoside and non-nucleoside analogues, their mechanism of action, and control of efficacy by structure regulation

Abstract

Nucleoside analogues acyclovir, valaciclovir, and famciclovir are used as golden drugs against human herpes simplex viruses (HSVs). However, these agents filed to remove the viruses from the host, nor prevent repeated infections. While the viruses may frequently develop resistance against these agents. Thus, new antivirals are necessary to tackle this age-old viral disease. We have synthesized two non-nucleoside amide analogues 2-Oxo-2H-chromene-3-carboxylic acid [2-(pyridine-2-ylmethoxy)-phenyl]-amide (**HL1**), 2-hydroxy-1-naphthaldehyde-(4-pyridine carboxylic) hydrazone (**HL2**) and (7-Hydroxy-4- methyl-2 O-2*H*-chromen-8-yl) methylene) isonicotinihydrazide (**HL3**) as the potential antiviral lead against HSV-1. These three promising candidates **HL1**, **HL2**, and **HL3** have been characterized by different physicochemical methods including basic elementary analysis, mass spectra, and ^{1}H–NMR; while determining their cytotoxicity (CC_{50}) and antiviral activity (EC_{50}) we have used the MTT and plaque reduction assay. Our results showed that both **HL1** and **HL2** possess significant antiviral activities against HSV-1F at EC_{50} of 38 and 64 μg/ml respectively, at non-cytotoxic concentrations (CC_{50}) with a Selectivity Index (SI) of 11. The mode of action studies revealed that these amide derivatives block the early stage of the HSV-1F life-cycle, just after viral attachment and entry to the Vero cells. Further, the plaque number was also decreased by suppressing the activity of the virions, when the infected Vero cells were exposed to **HL1** and **HL2** for a short period, following attachment.

4.1 Introduction

Among the human viruses, the herpes viruses HSV-1 and HSV-2 are major pathogens [1]. HSV-1 is usually spread by oral-to-sexual contact and infects upper parts of the body around the mouth as oral herpes [2], or sometimes genitalia [3]. The HSV-2 is most efficiently transmitted through genital-to-genital contact during sex, causing genital or anal herpes [4]. To develop anti-HSV leads the general strategy is to identify agents that specifically target the structural components of virions or viral multiplication. One of the competent strategies is to recognize compounds that may interrupt the essential communications between the virus and the host cells. People of different ages have been infected by Herpes viruses since time immemorial. Among these two types, HSV-1 is more frequent than HSV-2; while the seroprevalence of the latter tends to increase in different populations with age [1]. After establishing the primary infection these viruses tend to transport to the local ganglia, where they remain latent for an indeterminate period and can re-infect the host time-to-time [5, 6]. Another antiviral foscarnet inhibits the viral DNA polymerase of herpes viruses by binding near to the pyrophosphate binding site required for polymerase activity [7]. However, both viruses can attack the Central Nervous System (CNS) and replicate in nerve ganglia to start a latent infection, particularly in dorsal root ganglia [8]. Latent genomes of these viruses can be activated at various times throughout the host's life, resulting in lytic infections, which may manifest as sores, whitlow, skin lesions, keratitis, or other mucocutaneous diseases [9]. Often HSV causes encephalitis or systemic infections, in immune-compromised individuals. Therefore, antiviral medications need to be administered in serious cases [10]. Currently, the most preferred anti-HSV drugs include nucleoside analogues acyclovir (ACV) and ganciclovir which specifically target the viral thymidine kinase (TK) [11]. These antiviral agents can heal skin lesions, caused by HSV-1 and HSV-2,

usually in 4-5 days [12]. The effect and the selectivity of nucleoside drugs are decreased in immune-compromised patients, if the TK gene is altered (TK^a), or the virion does not express functional TK, as found in TK$^-$ viruses [13,14]. Those TK$^-$ viruses have been treated by non-nucleoside pyrophosphate foscarnet and deoxycytidine analogue cidofovir that inhibit Herpes viral DNA polymerase activity [15]. Till date, known antiviral drugs are not capable of neither eradicating the viruses nor preventing recurrences or repeated infection while strong resistance is generated in the virus [16, 17].

An earlier study reported that the synthetic derivatives of 2-aminobenzamide SNX-25a, SNX-2112, and SNX-7081 possess significant anti-HSV activities by selective binding with the N-terminal ATP pocket of heat shock protein 90 (HSP90) of HSV-1 and HSV-2 at non-cytotoxic concentrations in Vero cells, with EC$_{50}$ close to the standard drug ACV [18]. Further, 0.1% or 0.025% of eye gels of SNX-25a demonstrated antiviral activity in the herpes simplex keratitis (HSK) rabbit model with the highest efficacies against HSV-1 infection, better than 0.1% ACV; while SNX-2112 and SNX-7081 gels were effective at different concentrations [18]. Further, a ribosomally synthesized lantibiotic peptide Labyrinthopeptin-A1 showed broad anti-HSV activity [19]. Two recent studies showed that Hsp90 inhibitors prevent HSV-1 replication by targeting the UL42-Hsp90 complex [20] and inhibit the entry of HSV-1 into neuron cells by varying cofilin-mediated F-actin reorganization [21]. Pyridine derivatives have a considerable role in diverse therapeutic areas, and thus, many novel bioactive compounds with pyridine scaffold have been synthesized. Pyridine moiety-enclosed natural products have also been effective against cancer [22]; hence, we choose to synthesize pyridine backbone bearing **HL1** and **HL2** as a promising anti-HSV candidate. Moreover, purely synthesized compound 5-[(3'-aralkyl amido/amino-alkyl) phenyl]-1, 2, 4-triazole [3, 4-

103

b]-1, 3, 4-thiadiazole have anti-Herpes activity [23]. The high-throughput screening identified iron-cheater 2-hydroxy1-naphthaldehyde isonicotinoyl hydrazone as a novel anticancer, anti-plasmodial, and antiviral agent [24-28]. Earlier studies revealed that the two important immune modulators Imiquimod and Resiquimod can inhibit HSV-polymerase, while Thiazolyl phenyl and Thiazolyl amide are inhibitors of herpes viral helicase [29-31], that received significant attention. Another unique antiviral molecule 4-Hydroxyquinoline-3-carboxamide prevents HSV-1 infraction by inhibiting late and immediate-early transcripts [32].

This chapter deals with *in vitro* evaluation of cytotoxicity and antiviral activity of 2-Oxo-2H-chromene-3-carboxylic acid [2-(pyridine-2-ylmethoxy)-phenyl]-amide (**HL1**) and 2-hydroxy-1-naphthaldehyde-(4-pyridine carboxylic) hydrazone (**HL2**). To design these two anti-viral compounds, we have used pyridine moiety as common, with coumarin derivatives, as Pyridine derivatives have a significant role in diverse therapy. Several novel compounds containing pyridine scaffolds have been synthesized and proven to be biologically effective, as observed with pyridine-containing natural products having anticancer activity [22] with diverse pharmacological properties. Coumarins are reported to have antitumor, anticancer, and anti-microbial effects [33-36]. Thus, our study focused on the biological significance of these molecules to validate the *in vitro* anti-HSV-1 potency of **HL1** and **HL2**, for the first time.

4.2 Experimental section

4.2.1 Materials and Methods

Throughout the study, all reagents used were procured from available suppliers; while all aqueous solutions were prepared using Milli-Q water (Millipore). The Coumaric acid, 2-(chloromethyl) pyridine hydrochloride, and tetrahydrofuran were purchased from

Sigma-Aldrich, India; while Thionyl Chloride, Ethyl Acetate, 2-Hydroxy-1-naphthaldehyde, Dimethyl sulfoxide (DMSO) were from E. Merck, Germany. The FTIR spectra (KBr disk, 4000–400 cm^{-1}) were taken by a Perkin-Elmer LX-1FTIR spectrophotometer; and the NMR spectra were obtained on a Bruker (AC) 300 MHz FT-NMR spectrometer, using TMS as an internal standard. The ESI mass spectra were recorded from a Water HRMS model- XEVOG2QTOF# YCA351 Spectrometer. All of the measurements were conducted at room temperature. A detailed description of spectroscopic techniques is described in **Chapter 2**.

4.2.2 Synthesis of compounds:

Synthesis of 2-Oxo-2H-chromene-3-carboxylic acid [2-(pyridine-2-ylmethoxy)-phenyl]-amide (HL1):

Step-1: 1 mmol of Coumaric acid (190 mg) with 25ml dry tetra hydro furan (THF) was taken in a 100 ml round bottom (RB) flask and added with one drop of DMF. Approximately 1.5 mmol of SOCl$_2$ was added drop-wise into this mixture, followed by refluxing for approximately 2 h. The mixture was cooled at room temperature, and after cooling the solvent was vacuum evaporated. Finally, an acid chloride was collected from the solids.

Step-2: 1mmol of 2-nitrophenol (139 mg), 2 mmol of K$_2$CO$_3$, and 1 mmol of 2-(chloromethyl pyridine hydrochloride (164 mg) were mixed in a 100 ml RB flask and was refluxed about 4 h. Then it was poured into ice-water, the product was collected with Ethyl Acetate and it was reduced by Hydrazine-hydrate and palladium charcoal produce describe earlier.

Step-3: In a 100 ml RB flask, 1 mmol of compound from Step-1, and 1 mmol of compound from Step-2 with 1.2 mmol of tri-ethyl amine were taken and stirred for 1 h. The light yellowish-green precipitation was collected (yield, 70%). The Synthetic scheme is presented as **Scheme 4.1**. *Micro-analytical data*: $C_{22}H_{16}N_2O_4$; Calcd. (Found): C, 70.96 (70.92); H, 4.33 (4.36); N, 7.52 (7.57) %. ^{1}H NMR (CDCl$_3$, 400 MHz) δ:11.39 (s, 1H), 9.02 (s, 1H), 8.59 (t, J = 6.4 Hz, 2H), 7.98 (d, J =7.6 Hz, 1H), 7.82 (d, J= 7.6 Hz, 1H), 7.73 (d, J =7.6 Hz, 1H). 7.67 (d, J =7.2 Hz, 1H), 7.42 (t, J = 5.6 Hz, 2H), 7.07 (t, J = 7.6 Hz, 1H), 7.02 (t, J = 8 Hz, 2H), 5.34 (s, 2H), 3.1 (s, 2H). (**Fig**. **4.1**). Mass: $(M+Na)^+$ 395.08 (**Fig.4.2**). IR: 3454 cm^{-1} (amido, N-H), 1700 cm^{-1} (lactone C=O), 1602 cm^{-1} (amido, C=O) (**Fig.4.3**).

Synthesis of 2-hydroxy-1-naphthaldehyde-(4-pyridine carboxylic) hydrazone (Compound -HL2):

Step-1: 2.1 g of 2-naphthol and 2.5 g of Hexamethylenetetramine (HMTA) were heated in 20 ml of acetic acid for 1 h at 60 ℃. Then H$_2$SO$_4$ (98%, 4 ml) was added drop-wise to the above solution and the mix was refluxed for 10 h. After cooling, the ice-water mixture was added and the crude product was collected, and then recrystallized from ethanol to get a yellow solid, with a yield of 82%.

Step-2: 2-Hydroxy-1-naphthaldehyde (0.86 g) and 4-pyridine carboxylic hydrazide (0.68 g) was refluxed in 30 ml ethanol for 8 h, under N$_2$. After cooling to room temperature, the precipitate was collected and the final product was recrystallized from ethanol to give a yellow solid (yield, 90%). This synthetic scheme is presented as **Scheme 4.1**. *Micro-analytical data*: $C_{17}H_{13}N_3O_2$; Calcd. (Found): C, 70.09 (70.12); H, 4.50 (4.46); N, 14.42 (14.37) %. ^{1}H NMR (DMSO-d$_6$, 300MHz) δ:12.54 (s, 1H), 12.42 (s, 1H), 9.49 (s, 1H), 8.94 (d, J = 5.7 Hz, 2H), 8.57 (d, J = 8.7 Hz, 1H), 7.96 (d, J = 9 Hz, 2H). 7.90 (d, J = 1.8

Hz11, 1H), 7.89 (d, J = 1.5 Hz, 1H), 7.25 (d, J = 9 Hz, 1H), 7.43 (t, J = 7.2 Hz, 1H), 7.64

(m, 1H) (**Fig. 4.4**). Mass: (M+Na)$^{+}$ 314.14 (**Fig. 4.5**). IR: 3427.79 cm^{-1} (aromatic -OH),

1678.84 cm^{-1} (amido C=O), 1623 cm^{-1} (Schiff's bass, C=N) (**Fig. 4.6**).
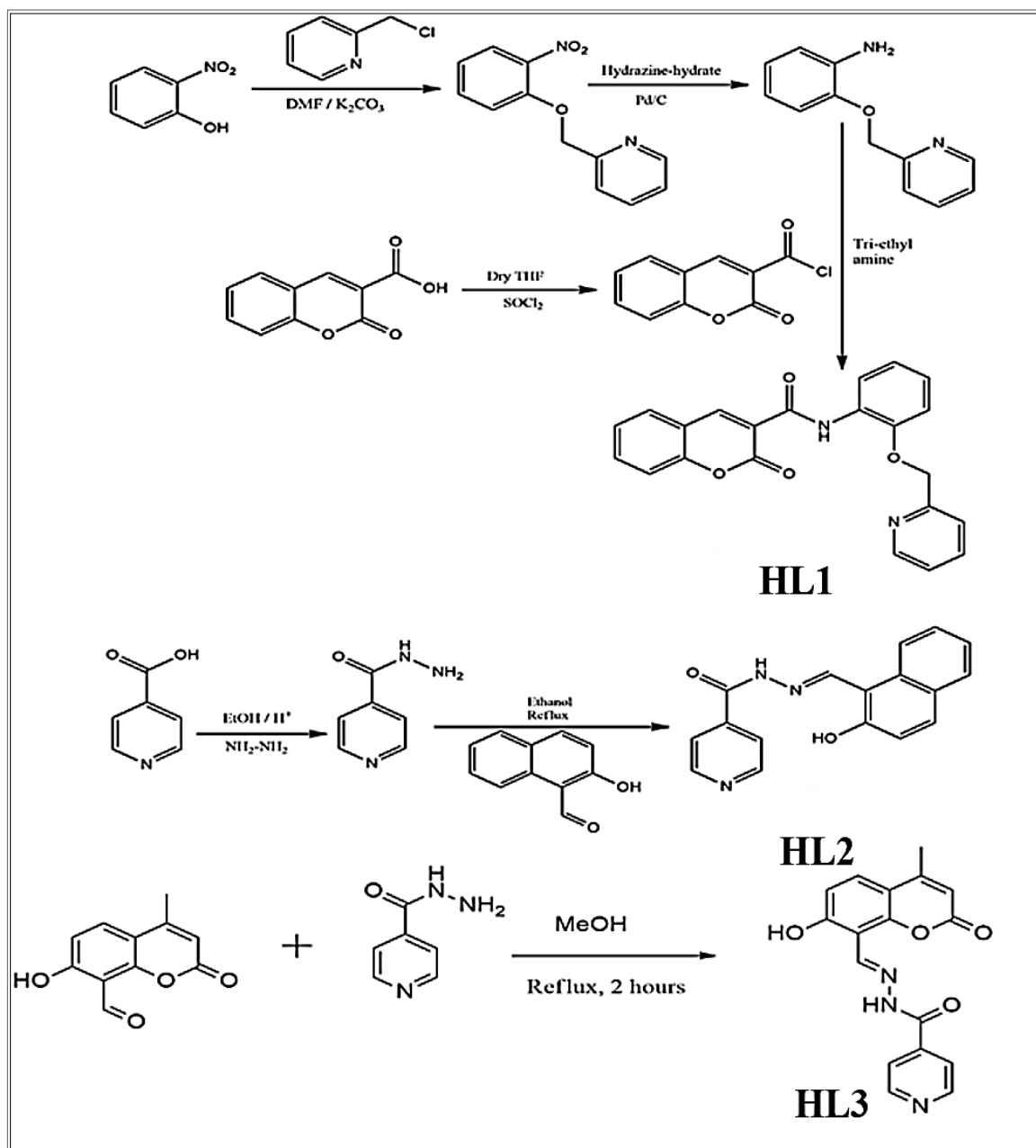
Scheme 4.1. Chemical Synthesis Scheme of 2-Oxo-2H-chromene-3-carboxylic acid [2-

(pyridine-2-ylmethoxy)-phenyl]-amide (**HL1**) and 2-hydroxy-1-naphthaldehyde-(4-

pyridine carboxylic) hydrazone (**HL2**) and **HL3**.

4.2.3 Viruses and the Cell line:

The experimental cells were grown using African green monkey kidney cells (Vero cells, ATCC, Manassas, VA, USA) and maintained in DMEM with 10% FBS (Invitrogen, USA), using 100 U/ml penicillin, and 100 μg/ml streptomycin at 37 ℃ in 5% CO_2. The standard strain of HSV-1F (ATCC VR-733), purchased from the ATCC-USA, was used. The virus was grown and the virus stocks were stored at −80 ℃ using plaque purified samples for future use in vials, and whenever required the virus stocks were grown on Vero cells to determine the titter (s) by plaque assay and used for further study [17].

4.2.4 Determination of Cytotoxic Concentration (CC_{50}):

To measure the cellular toxicity of two synthesized molecules, we have analyzed their effect on Vero cell morphology. Vero cell monolayers were cultured onto 96 well plates at 1.0×10^5 cells/well. After incubation at 37 ℃ in 5% CO_2 for 6 h, different concentrations of HL1 and HL2 and standard drug ACV were added to each culture well, at a final volume of 100 μl, in triplicate, using DMSO (0.1%) as a negative control. The drug-treated cells were incubated at 37 ℃ with 5% CO_2 for 2 days. After 48 h of incubation, MTT reagent (10 μl) was added to each well and incubated for 4 h at 37 °C. Then, the formazan was solubilized by adding diluted HCl (0.04 N) in isopropanol and the absorbance was measured at 570 nm with a reference wavelength of 690 nm by an ELISA reader. Data were calculated as the percentage of cell viability using the following formula:

[(**sample absorbance – cell-free sample blank)/mean media control absorbance)]/100%**.

The 50% cytotoxic concentration (CC_{50}) causing visible morphological changes in 50% of Vero cells concerning cell control was determined [17].

4.2.5 Determination of Antiviral activity using Plaque reduction assay:

The antiviral activity of **HL1** and **HL2** against HSV-1F was evaluated by a standard Plaque reduction assay. Vero cell monolayers were seeded onto 96 well plates with a concentration of 1.0×10^5 cells/well. After incubation at 37 °C in 5% CO_2 for 4-6 h, the virus (at 0.5 MOI) was added and incubated (1 h) for viral adsorption. Different concentrations of **HL1** and **HL2** (25, 50, 100, 150, and 200 µg/ml) were added to culture wells in duplicate at the final volume of 100µl. Different concentrations of ACV (0- 6 µg/ml) and DMSO (0.1%) were also added into the marked wells, as a positive and negative control, respectively. After 3 days of incubation at 37 °C in 5% CO_2, the plaque assay was carried out as described previously [33].

4.2.6 Docking Study:

Molecular docking is a tool used to find interactions between small and macromolecules [37, 38]. This structural information can be utilized to find a pharmacophore against the target protein, identify a target protein, and understand protein inhibition mechanisms through the analysis of interactions [39]. The docking study was used here to find the interactions between the synthesized small molecules (**HL1** and **HL2**) and viral glycoprotein B (gB) and glycoprotein D (gD). The choice of the protein was based on the time response assay. The structural coordinates of gB and gD were acquired from the protein data bank (PDB ID: 5v2s[4] for gB and 2c36[5] for gD). Molecular docking of energy minimized the structure of **HL1** and **HL2** with the data bank proteins by AutoDock Vina [40, 41]. For gB, a 126 x 126 x 126 grid box at x = 59, y = -34, z = 125 was selected and

for gD, it was 60 x 60 x 60 grid box at x = 55, y = 37, z = 85. The results found from the docking study were represented by Chimera 1.10.2 and Discovery Studio 4.1 Client.

4.2.7 Dose-response assay by Plaque reduction assay:

Vero cells seeded in 6-well plates (5 x 10^6 cells per well) were treated with serial dilutions of the test compounds **HL1 and HL2** (0- 200 μg/ml) for 15 min at 37 °C and then challenged with HSV-1 (100 PFU/well) for 1 h. Viruses and drugs were subsequently removed from the wells, and the cells were washed with PBS twice and overlaid again with different dilutions of the test compounds. After further incubation for 72 h, the supernatant was removed, and the wells were fixed with methanol and stained with Giemsa stain (Sigma, USA). Viral inhibition (%) was calculated as:

[1 - Exp (number of plaques) / control (number of plaques)] X 100%,

where "Exp (number of plaques)" indicates the plaque counts from virus infection with test compound(s) treatment and "control (number of plaques)" indicates the number of plaques derived from virus-infected cells with control treatment (HSV-1F with DMSO only) [34]. The 50% effective concentration (EC_{50}) for antiviral activity was defined as the concentration of antiviral compounds that produced 50% inhibition of the virus-induced plaque formation [17, 35].

4.2.8 Time response assay:

A time response assay was used to investigate the mechanism of inhibition of the infection of HSV-1F by **HL1** and **HL2** at various time periods, up to 12 h. To assess the effect of pre-treating cells with compounds, Vero cell monolayers seeded in 96-well plates were treated with newly synthesized HL1 or HL2 (100 μg/ml) for 24 h (long term) or 1 h (short term) and then washed with PBS before challenging with HSV-1F (MOI: 1)

in DMEM (**pre-infection**). To study the effect of the above molecules and virus concurrently, Vero cells were treated simultaneously with HSV-1 (MOI: 1) and HL1 and **HL2** (100 µg/ml) or ACV (5 µg/ml). After incubation for 1 h at 37°C, the virus-drug mixture was removed, and cells were washed prior to overlay with media (**co-infection**). To evaluate whether the molecules had any effects after viral entry, Vero cells were challenged with HSV-1 for 1 h, and after removal of the virus inoculum, infected cells were washed and subsequently overlaid with media containing them (100 µg/ml) or ACV (5 µg/ml) (**post-infection**). For the continuous drug treatment, cells were pre-treated for 1 h with HL1 or HL2, challenged with HSV-1 in the presence of the drugs, and overlaid with media containing the test compounds after viral entry (**throughout infection**). For all of the above experiments, MTT assays were carried out following a total incubation of 48 h post-infection (p.i.). DMSO (0.1%) treatment was included as a control in each condition [33].

4.2.9 Changing of mRNA expression by quantitative RT-qPCR :

The HSV-1F (1.0 MOI) infected Vero cells were treated with **HL1** and **HL2** ($2 \times EC_{50}$) for 1, 2, 4, 6, and 8 h pre-infection and co-infection. HL1 and HL2 were added to HSV-1F infected Vero cells at 2, 4, and 6 h post-infection so that the cells were exposed to the compounds from 2-8 h, 4-8 h, and 6-8 h p.i., respectively. The RNA was isolated after 8 h of infection, using the RNeasy Mini kit (Qiagen, Germany), following the manufacturer's protocol. The total RNA (0.1 mg/ml) in RNase-free water containing 20 µl of RT-mix was subjected to cDNA synthesis by using the Revert Aid First Strand cDNA Synthesis Kit (Thermo Scientific, USA) with the help of a PCR system (BIORAD, Thermocycler). The qPCR was performed with those products using SYBR Green PCR Master Mix (Qiagen, Germany), following manufacturer protocol in an ABI Prism 7000 sequence detection system (Applied Biosystems, CA, USA). The PCRs were done in

triplicate with an initial denaturation at 95°C for 10 min then 40 cycles (15s at 95°C then and 60s at 60°C) in triplicate [36]. The sequences of primers used were presented in **Table 4**.1.

Table 4.1. List of primers with their sequences used for RT-qPCR study

Serial no	Name of Gene	Sequences of Primer	Tm
1	GAPDH	F-5'GAGAAGGCTGGGGCTCATTT-3'	59.4
		R-5'GCTGACGATCTTGAGGCTGT-3	59.4
2	HSV-1 ICP4	F-5'GGCGACGACGACGATAAC-3'	58.2
		R-5'-CGAGTACAGCACCACCAC-3 '	58.2
3	HSV-1 ICP8	F-5'-GCTCGGACAAGGTAACCATAG-3 '	55.7
		R-5'-CACGAGGAAGAAGCGGTAAA-3 '	53.7
4	HSV-1 gB	F-5'-GGAACACAAGGCCAAGA-3'	57.3
		R-5'-GTTGGGAACTTGGGTGT-3'	57.9
5	HSV-1 DNA Pol	F-5'-GAACATCGACATGTACGGGATTA-3'	58.9
		R-5'-GGTCCTTCTTCTTGTCCTTCAG-3'	60.3

4.2.10 Statistical analysis:

Results were expressed as SEM ($n = 6$) and the statistical analysis was performed with a one-way analysis of variance (ANOVA), followed by Dunnett's test. A value of $p < 0.05$ was considered to be statistically significant, compared with the respective control.

4.3 Results:

4.3.1 The characterization of HL1, HL2 and HL3

2-Oxo-2H-chromene-3-carboxylic acid [2-(pyridine-2-ylmethoxy)-phenyl]-amide (compound -**HL1**) was successfully synthesized by using the acid chloride derivative of coumaric acid with amine derivative and the compound has been characterized by spectroscopic data including NMR, Mass and FTIR (**Fig**. **4**–**3**). The molecular ion peak $(M + Na)^+$ at 395.08 supports the molecular identity along with 3454 cm^{-1} (amido, N-H), 1700 cm^{-1} (lactone C=O), 1602 cm^{-1} (amido, C=O) of the IR spectrum. The ^{1}H NMR spectrum of compound-HL1 (300 MHz, DMSO-d6) demonstrates singlet at 11.39 ppm, corresponding to N-H proton of amido linkage and other aromatic protons appearing at 9.02–7.02 ppm. Similarly, the compound **HL2** (2-hydroxy-1-naphthaldehyde-(4-pyridine carboxylic) hydrazone) is synthesized by the condensation reaction between 2-Hydroxy-1-naphthaldehyde (0.86 g) and 4-pyridine carboxylic hydrazide and the resultant compound is characterized by spectroscopic analysis of NMR, Mass and FTIR (**Fig**. **4**–**6**). IR spectrum shows a peak at 3427.79 cm^{-1} corresponding to aromatic -OH, 1678.84 cm^{-1} for amido C=O), 1623 cm^{-1} for Schiff's bass, C=N, and from mass spectra, peak at $(M+Na)^+$ 314.14 which is its molecular peak. The ^{1}H NMR (DMSO-d$_6$, 300MHz) spectrum shows singlet δ (OH) at 12.54 ppm, δ (NH, amido) at12.42, imine-H, δ (CH=N) at 9.49 ppm, and other aromatic protons have been assigned based on their spin-spin interaction.

Compound (**HL-3**) was prepared by condensation between 1 mmol of 8-formyl-7-hydroxy-4-methylcoumarin (204 mg) and 1 mmol of Isoniazid (137 mg) were taken in 50 ml methanol. The light yellowish green precipitation was collected (yield, 81%). The synthetic scheme is presented as **Scheme 4.1**. Micro-analytical data: $C_{17}H_{13}N_3O_4$; Calcd.

(Found): C, 63.16 (63.18); H, 4.05 (4.02); N, 13.00 (12.98) %. ^{1}H NMR (DMSO-d_6, 300MHz) δ: 12.69 (s, 1H), 12.66 (s, 1H), 9.19 (s, 1H), 8.85 (d, J = 6 Hz, 2H), 7.94 (d, J = 6 Hz, 2H), 7.88 (d, J = 9 Hz, 1H), 7.01 (d, J = 9 Hz, 1H), 6.30 (s, 1H), 2.43 (s, 3H) (**Fig**.**4.7**).
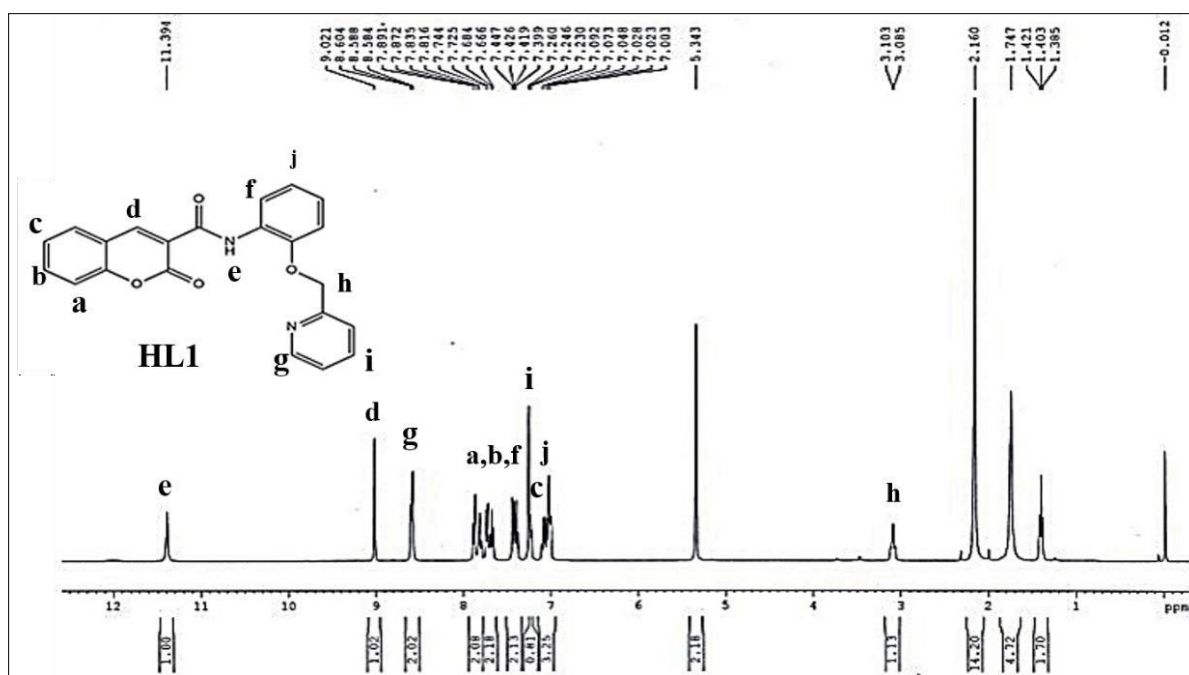
Fig. **4.1**. ^{1}HNMR spectra of **HL1** in CDCl$_3$.
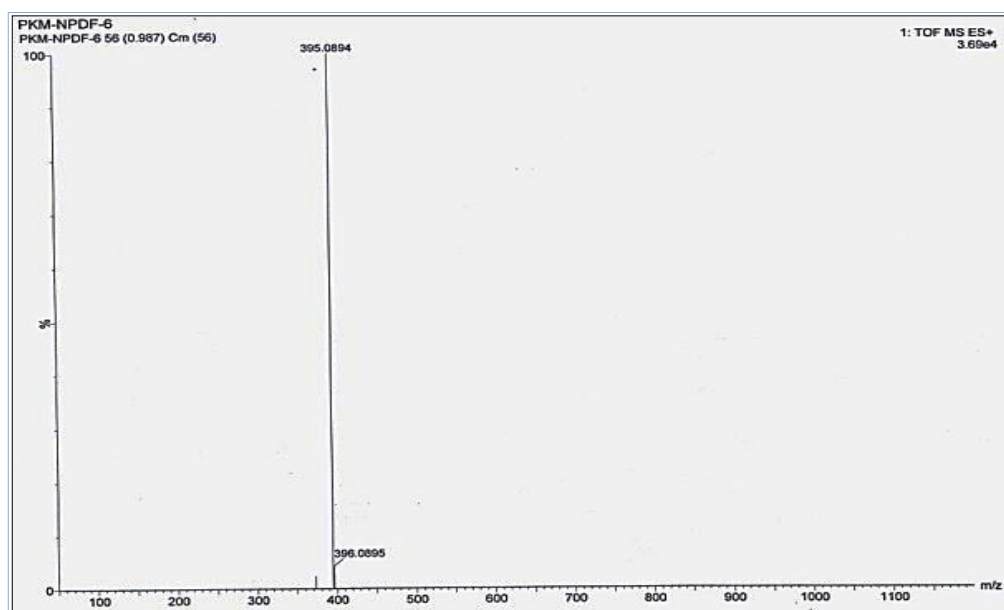
Fig. 4.2. Mass spectra of **HL1**.
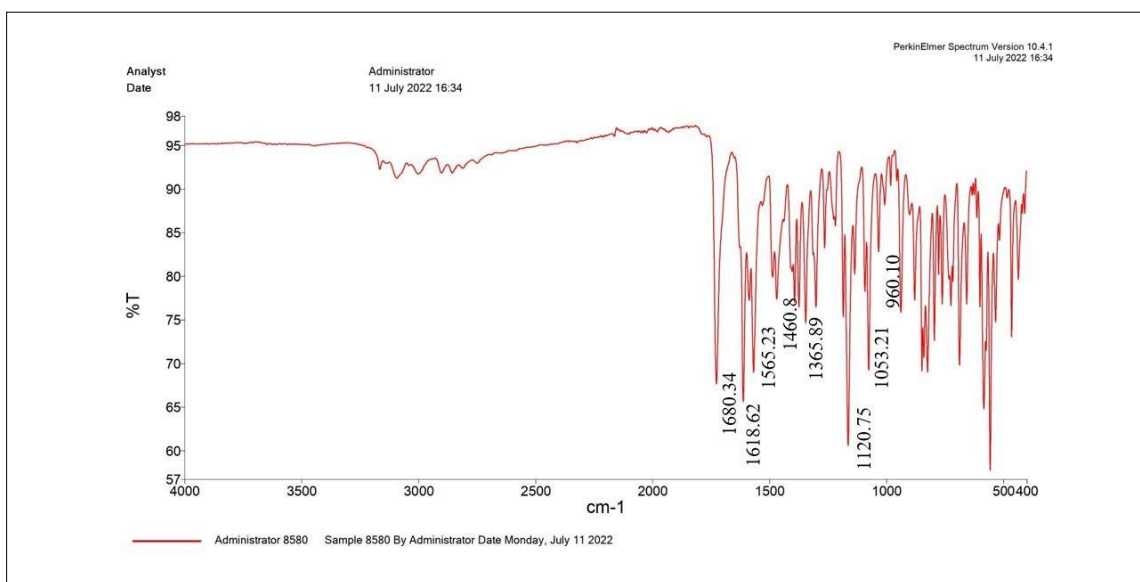
Fig. 4.3 IR spectrum of Compound-**HL1**.
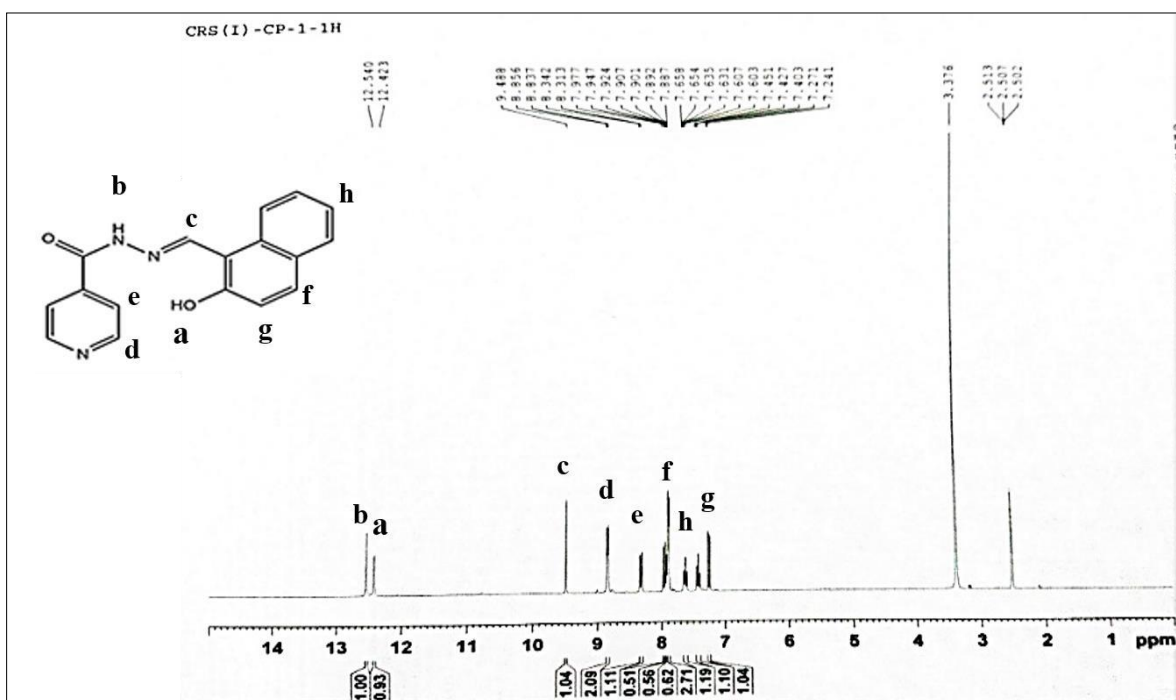
Fig. 4.4 ^{1}HNMR spectra of compound-**HL2** in DMSO-d$_6$.

314.1402

314.1475

292.1602

%

0

100   200   300   400   500   600   700   800   900   1000   1100   m/z
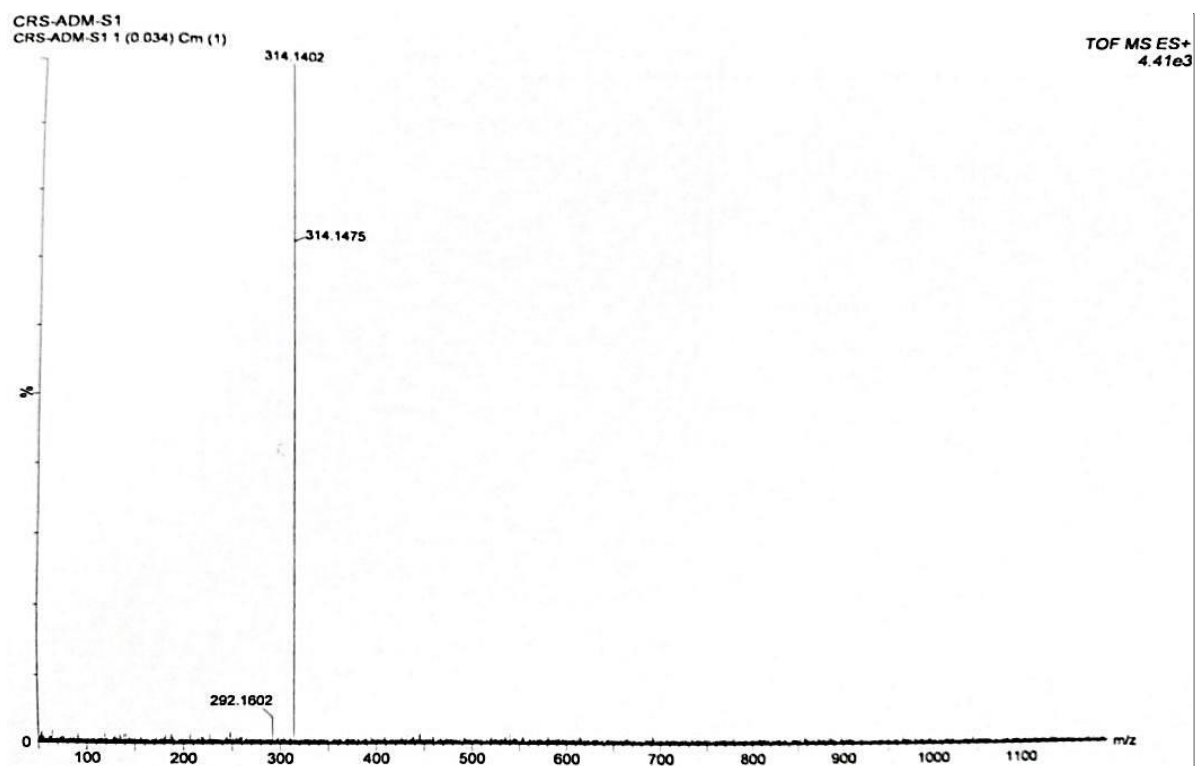
Fig. **4.5** Mass spectrum of **HL2**.

ADMS1

3427.79

1678.84
1575.13
1551.63
1469.56
1415.30
1328.48
1285.02
1241.61
1623.79
1390.37
1192.70
1167.76
953.08
815.26
741.05
686.17

%T

Wavenumbers (cm-1)
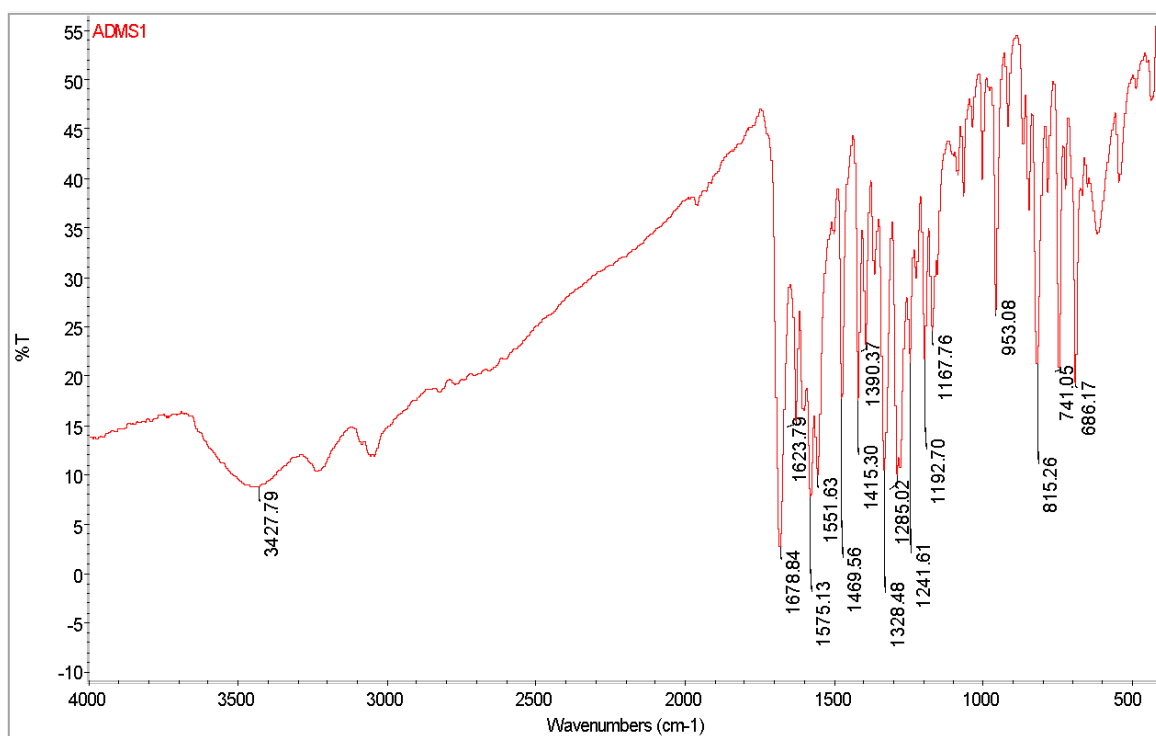
Fig. **4.6** IR spectrum of **HL2**
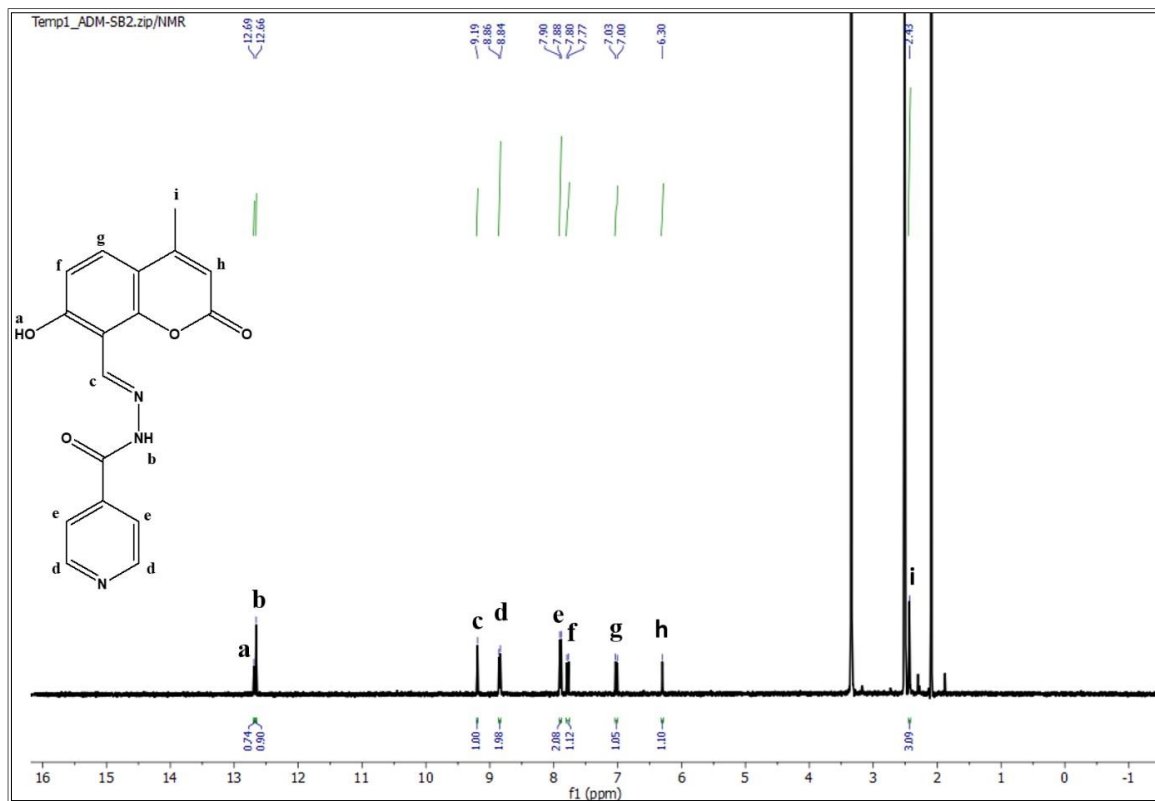
Fig. **4**.7. ^{1}HNMR spectrum of **HL3.**

4.3.2 Cell viability study:

Both HL1 and **HL2** were tested for cytotoxicity at different doses, using a conventional MTT assay on Vero cells (**Fig 4.8**). The results revealed that the 50% cytotoxicity (CC$_{50}$) of **HL1 HL2** and **HL3** was 362, 278.4, and 58.5 µg/ml respectively, in which about half of the Vero cells survived.
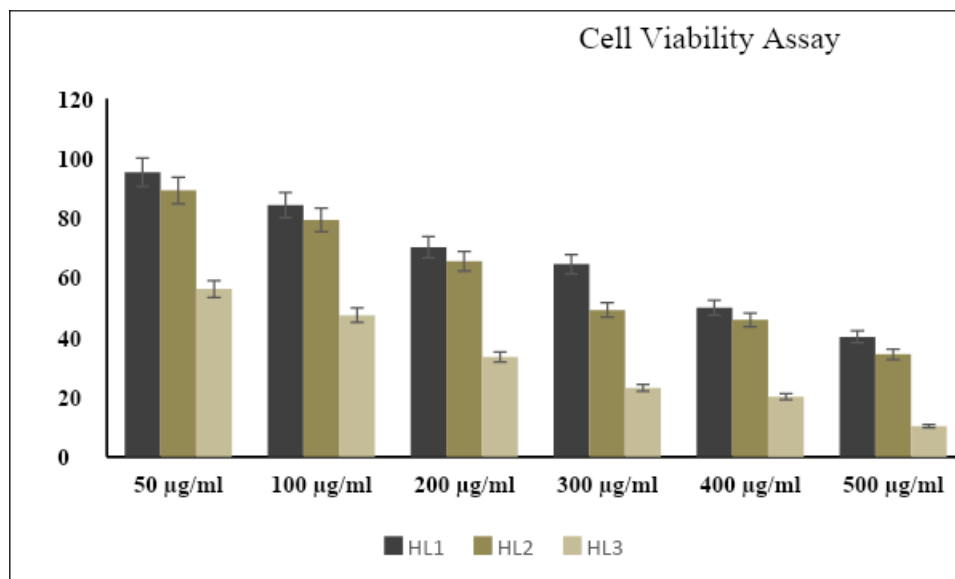
Fig. **4.8** Determination of Cytotoxic concentration of **HL1, HL2,** and **HL3**.

4.3.3 Assessment of anti-HSV-1F activity of HL1 and HL2

The synthetic analogues **HL1** and **HL2** were added at different time points of the virus life cycle (**pre-infection**, **co-infection**, and **post-infection**), **using an MTT assay**. Results demonstrated that HL1 and HL2 were unable to protect Vero cells pre-infected with HSV-1F. However, the compounds were effective in preventing the Cytopathic effect (CPE) during co-infection, and also immediately after viral entry.

Table 4.1. Assessment of anti-HSV-1F activity of **HL1** and **HL2**

Test drug	CC_{50}*	EC_{50}**	Selectivity index (SI)***
HL2	362.6 ± 2.5	37.2 ± 2.8	9.7
HL1	270.4 ± 3.2	63.4 ± 3.0	4.3
HL3	58.05 ± 1.5	34.9 ± 2.0	1.5
Acyclovir	128.8 ± 3.4	2.8 ± 0.1	49.3

* 50% cytotoxic concentration (CC_{50}) for Vero cells at µg/ml.

† Concentration of synthetic compound (µg/ml) producing 50% inhibition of virus-induced CPE (EC_{50}) in three separate experiments. ‡ Selectivity index (SI) = CC_{50}/EC_{50}.

118
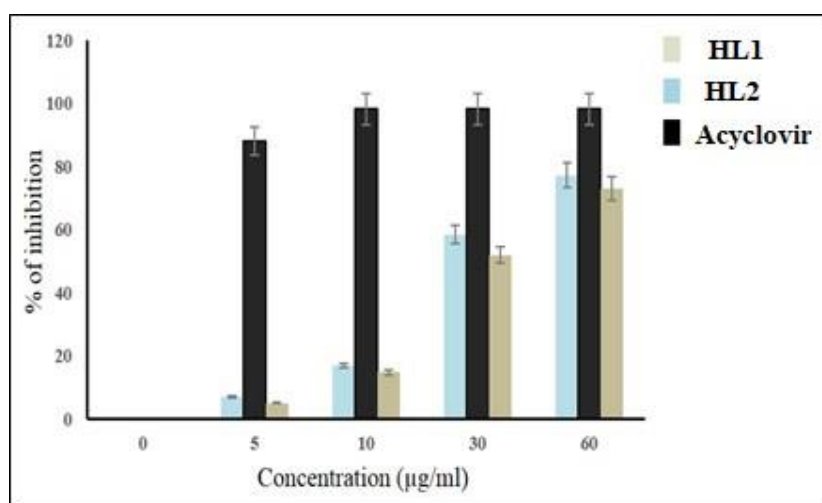
Fig. **4.9** Dose-response Assay of synthetic antiviral compounds (**HL1**, **HL2,** and Acyclovir) against HSV-1F.
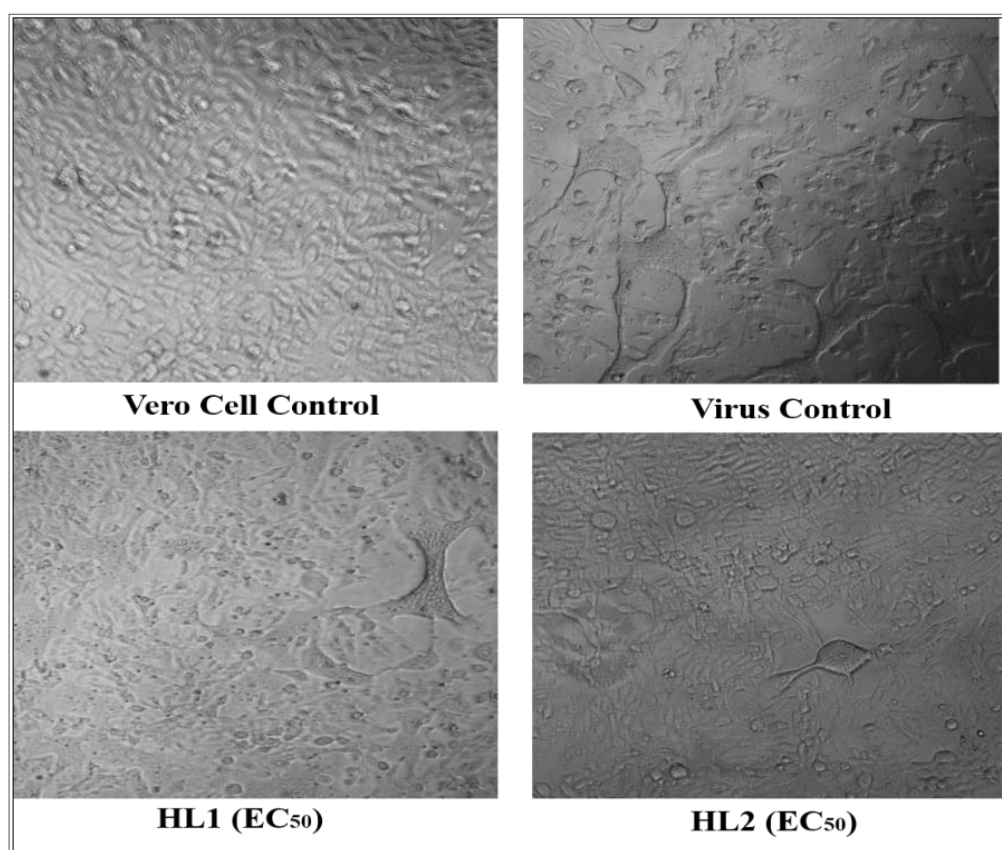
Fig. **4.10** Cytopathic effect (CPE) of HSV-1 infected Vero Cells under an inverted light microscope. The uninfected Vero cells served as a control.

We tried to compare the four possible couples of the biological samples: control cells and HSV-1 infected cells; HSV-1 infected cells treated with **HL1** and **HL2** respectively at their EC_{50} concentration and HL3 has higher cytotoxicity and low SI index. So, **HL1** and **HL2** are chosen for further study.

The results of the docking studies show that the **HL2** has a better binding affinity toward the viral glycoproteins concerning the **HL1**. The change of free energy in the interaction of **HL1** with gB and gD proteins were -7.5 and -7.7 kcal mol^{-1}, respectively, whereas these values were -8.3 and -8.2 kcal mol^{-1} for **HL2** with HSV-glycoproteins, respectively. Therefore, **HL2** is a better inhibitor of these envelop proteins of HSV-1 than that **HL1**.

The **HL2** can interact with both the glycoproteins almost equally intensely. The gB consists of three identical peptide chains (red, blue, and green) through self-assembly (**Fig**. **4.11**). The docking results sho that **HL2** can bind at the Ecto-region of the glycoproteins (**Fig**. **4.11**) through conventional and non-conventional H-bond. Here, only one H-bond was observed between the oxygen of phenolic OH and H-N of I114 residue. The aromatic C-H beside N of pyridine is involved in C=O…H-C type of non-conventional H-bod with three Q101 residues of each chain (**Fig**. **4.11**). Similar interactions were also observed between imine C-H and C=O of I114. In gD, the molecule binds at the surface near the C-terminal region (**Fig**. **4.11**). Hydrogen bonding was observed between pyridine N of **HL2** and S276 as well as Q278, individually, and amide C=O of **HL2** and I202 residue (**Fig**. **4.11**). The P275 residue is involved in the hydrophobic interaction with the pyridine ring. The ortho-hydrogen of pyridine nitrogen was found to interact with H273, I274, and D279 residues via non-conventional H-bond. Another non-conventional H-bond was found to be involved between amide C=O and F201.
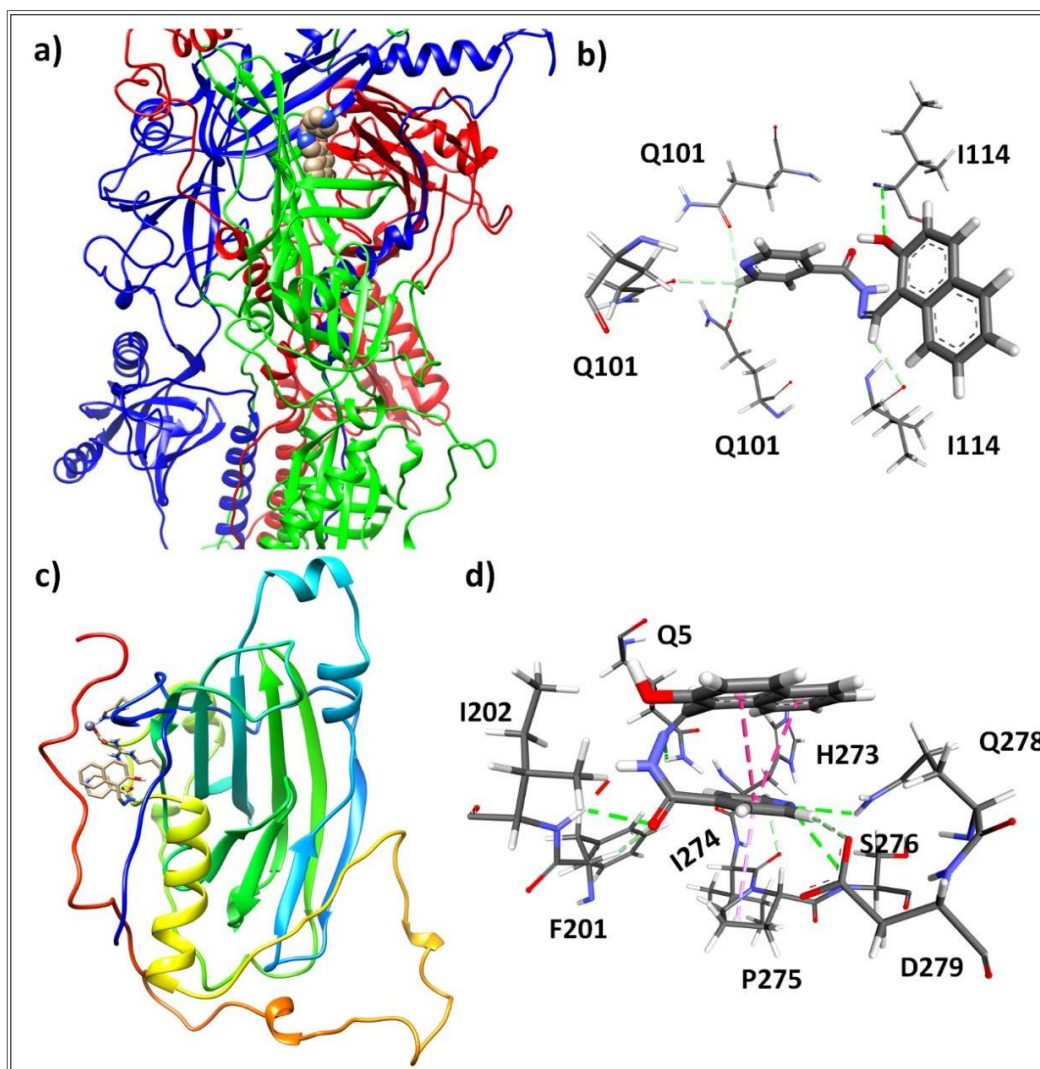
Fig.**4.11** Docking pose of **HL2**: (a) of gB; and (b) interactions between amino acids of gB and **HL2**; docking pose of **HL2**: (a) of gD and (b) interactions between amino acids of gD and **HL2.**

To investigate the possible stage of the viral life cycle affected by **HL1** and **HL2** we conducted the time of-addition assay. However, both can prevent plaque formation when added during virus adsorption and in the early stages of replication, after entry (**Fig**. **4.13**). Further, HSV-1 infection was severely hindered when test compound(s) were present at the time of infection, suggesting that the antiviral activity of synthesized test compound(s) is not due to their direct effects on Vero cells but on the viral particles to inhibit its entry into host cells. This result accounts that both **HL2** (38 μg/ml) and **HL1**

(64 µg/ml) significantly inhibit HSV-1 within 1–6 h post-infection; this implies that the effect starts at an early stage of virus infection (**Fig**. **4.10**). Whereas **HL1** and **HL2** were unable to inhibit the virus during pre-infection or co-infection. Viral internalization or penetration was assessed by incubating the pre-chilled (4°C, 1h) Vero cell monolayer (1×10^6 cells/well) in a six-well plate with HSV-1F (100 PFU/well) for 3 h at 4 °C for viral adsorption.
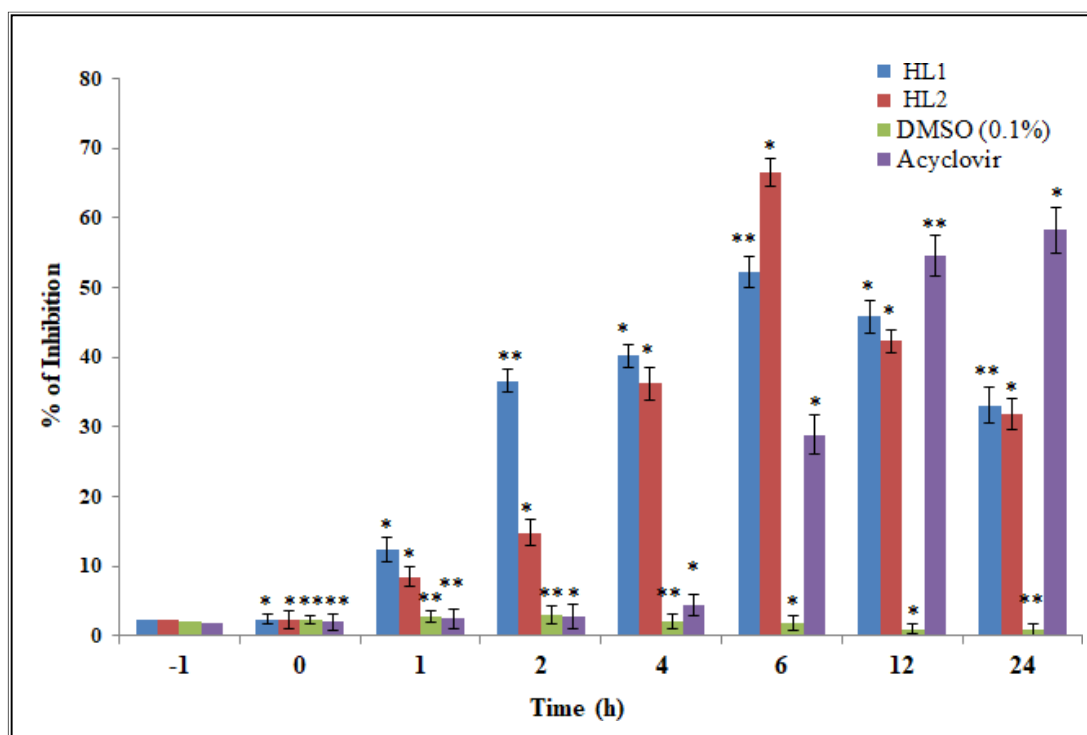
Fig. **4.12** Inhibitory effect of **HL1** and **HL2** (EC_{50}) on HSV-1 infected Vero cells at various time intervals during pre-infection (-1 h), co-infection (0 h), or post-infection (2-6 h), after 3 days of infection by MTT assay, followed by Plaque-reduction assay and expressed as the inhibition rate.
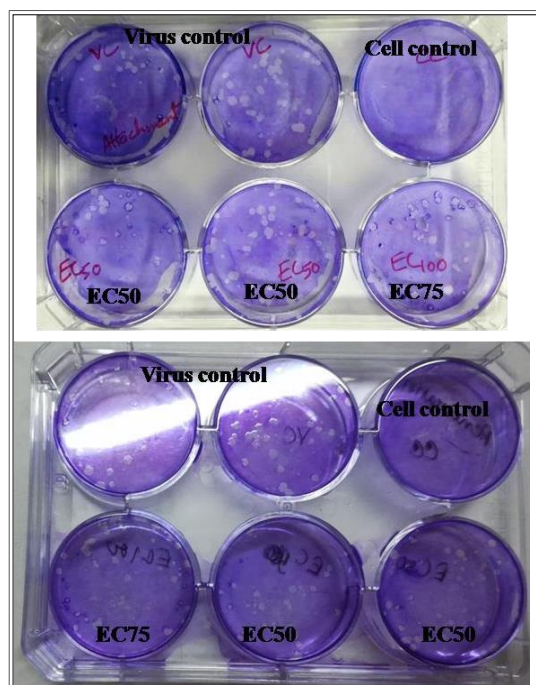
Fig. **4.13** Representative Photograph showing plaque reduction assays in the presence or absence of **HL1** and HL2, during virus attachment/ and internalization/penetration.

A

B
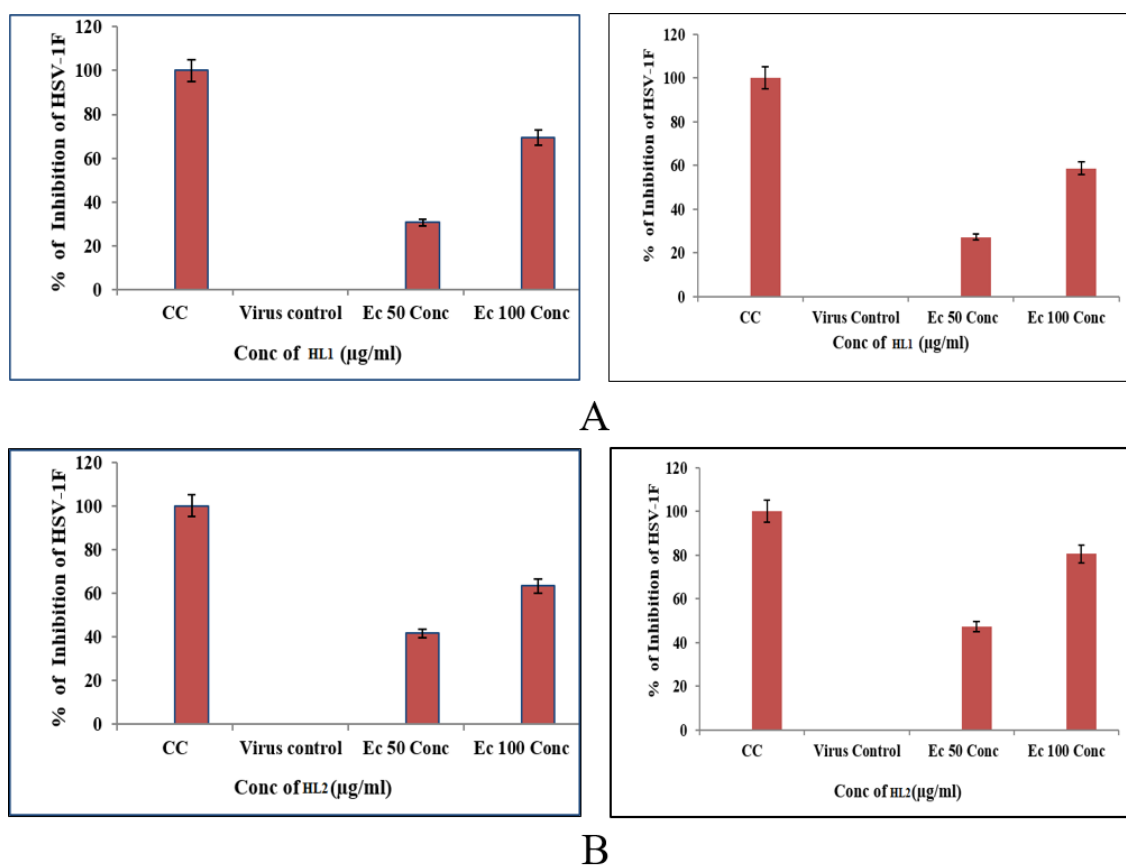
Fig. **4.14** Effect of **HL1** and **HL2** on the   entry of HSV-1F in Vero cells by Virus attachment/ internalization assay (A) and (B), respectively.

4.3.4 Action of Compounds HL1 or HL2 on HSV-1 gene expression

To determine whether the **HL1** and **HL2** treatment inhibited early replication, we measured the expression of viral ICP4, ICP8, DNA polymerase, and envelope gB in pre-treatment (1-8 h), co-treatment, and post-treatment (2-6 h), after infection. The kinetic study reported that the immediate-early (IE) gene transcripts (ICP4) are expressed at 1-2h p.i, the early (E) gene transcripts (ICP27, DNA-pol) at 3-4 h p.i, and the late (L) gene transcripts after 4h p.i [42]. Thus, we have isolated the RNA from virus-infected **HL1** and **HL2** treated and untreated cells after 8h of infection. A time point of 8 h was chosen for measurable levels of immediate early (IE) and early (E) transcripts, as well as increasing levels of late (L) transcripts. The time-of-addition assay and a gene expression study jointly suggested that the attachment and/or internalization of viruses by **HL1** and **HL2** might be inhibited either by interfering with the host cell surface receptor or by direct neutralization of the virus. The results of RT-qPCR showed that the viral mRNA expression was diminished by these two molecules. DNA transcripts were meaningfully decreased by pre-treatment for 1-8 h pre-treatment and by co-treatment within the appearance of the molecules, while at post-treatment from 2-8 h had little effect as the reduction was insignificant (**Fig**. **4.13**).
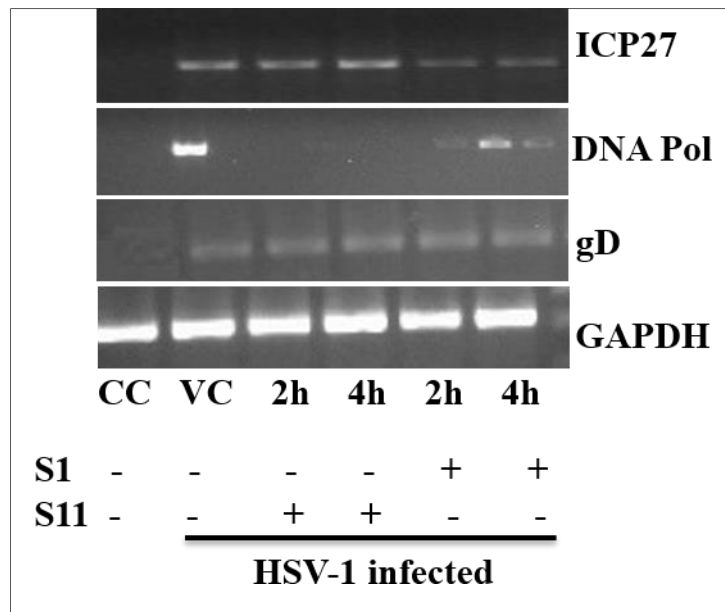
Fig. **4.15**. Effect of **HL1** and **HL2** on HSV-1-induced ICP27, DNA polymerase, and gD gene expression, isolated from uninfected and HSV-1 infected Vero cells. Lane 1: Cell control; lane 2: Cell+HSV-1; Lane 3,4: Cells + HSV-1 + **HL2** at 2 h and 4 h post-infection; Lane 5,6: Cells + HSV-1 + **HL1** at 2 h and 4 h post-infection. The data are expressed as Mean ± SEM from triplicate experiments yielding similar results (*, $P<0.05$; **, $P<0.01$).

HL1 and **HL2** have been analyzed for their effect on the expression of viral mRNA after the entry of HSV-1F to address the time-of-addition assay's consequences. Our purpose was to assess the consequences of the time-of-addition assay on viral mRNA expression after entry of the HSV-1F. Citrate buffer was used to inactivate HSV-1F-infected Vero cells for 1 h, along with washing and exposing the cells to **HL1** and **HL2** at 1, 2, and 4 h post-inoculation. Total cellular RNA was then isolated. Results revealed that **HL1** and **HL2** down-regulated the viral mRNA expression, as levels of immediate-early (ICP27), early (DNA-Pol), and late (gD) gene transcripts failed to express at 2 and 4 h p.i. in presence of **HL1** and **HL2** while at 1 h p.i. the gene expression was insignificant. These

findings demonstrate that both **HL2** and **HL1** prevent the early phase of HSV-1 transcription after host cell penetration.

4.4 Discussion

The 50% cytotoxic concentration (CC_{50}) of **HL1** and **HL2** were found to be at 362.6 µg/ml and 270 µg/ml, respectively, and the Concentration of **HL1** and **HL2** (µg/ml) produced 50% inhibition of virus-induced CPE (EC_{50}) were 37 µg/ml and 63 µg/ml. Thus, the selectivity index (SI) = CC_{50}/EC_{50} of **HL2** and **HL1** were 9.7 and 4.28. Compound **HL1** and **HL2** contained pyridine moieties with amide linkage as a common structural part indicating better anti-HSV potential. We still do not know enough about molecular identification and what it proceeds for a ligand to trigger an indicator on a receptor, and drug discovery is much more difficult. It has been reported that numerous novel synthesized chalcone derivatives containing pyridine moieties revealed antiviral activities against cucumber mosaic virus at 500 µg/mL [43]. Again, synthesized 1, 5-benzothiazepine derivatives, containing pyridine moiety demonstrated *in vivo* antiviral activity against TMV [44]. Elgemeie *et al.*, reported that synthesized pyridine thioglycosides had an anti-HSV activity with EC_{50} of 6.3 µg/100 µl [45]. The herpes virus is a lytic virus because after infection the virus kills the host cells by inhibiting cellular protein synthesis and destroying cellular DNA [46- 48]. A similar type of *in vitro* experiment has been performed with other viruses [49, 50], predominantly on RNA viruses, rather than DNA viruses. It is known that heterocyclic compounds having a pyridine backbone had broad-spectrum antiviral activities. Comparing the basic structure of these two compounds **HL1** and **HL2**, which contains either pyridine moieties or amide linkage or both, may enhance anti-HSV activities and at a low cytotoxicity effect. Pyridine rings present in both of the compounds may attribute to the activity of **HL1** and

HL2, similar to the fact that Pyridine-based molecules have multiple biological potentials. At 2 and 4 h post-infection, **HL1** and **HL2** also down-regulated viral mRNA expression, as levels of immediate early (ICP27), early (DNA-Pol), and late (gD) gene transcripts failed to express.

4.5 Conclusion

Urgently Novel antiviral candidates are desirable, which are certainly essential for the treatment of various deadly viral infections. Heterocyclic compounds are considered much important in the field of medicinal chemistry because of their physiological activities, among them, pyridine derivatives are especially attractive. These results may contribute to a better understanding of the prerequisites for the further design of new, more efficient pyridine-containing antiviral lead. Because to date, neither any effective vaccine, nor any non-toxic drug that eradicates HSV from the host cell, or prevents latency or resistance development is available. The failure of vaccine and 'magic bullet' is due to the establishment of viral latency and reactivation that occurs during cell-mediated and humoral immunity.

4.6 References

[1]   L. Corey and P. G. Spear, *N. Engl. J. Med.*, 1986, **314**, 686–691.

[2]   Y. Chang, E. Cesarman, M. S. Pessin, F. Lee, J. Culpepper, D. M. Knowles and P. S. Moore, *Science*, 1994, **266**, 1865–1869.

[3]   D. J. McGeoch and D. Gatherer, *J. Virol.*, 2005, **79**, 725–731.

[4]   R. J. Whitley and B. Roizman, *Lancet*, 2001, **357**, 1513–1518.

[5]   T. Valyi-Nagy, D. Shukla, H. H. Engelhard, J. Kavouras and P. Scanlan, *Springer, Boston. MA.*, 2007, 1–36.

[6]   L. Jin, W. Peng, G. C. Perng, D. J. Brick, A. B. Nesburn, C. Jones and S. L. Wechsler, *J. Virol.*, 2003, **77**, 6556–6561.

[7]   C. L. Poole and S. H. James, *Clin. Ther.*, 2018, 40, 1282–1298.

[8]   L. F. Duarte, M. A. Farías, D. M. Álvarez, S. M. Bueno, C. A. Riedel and P. A. González, *Front. Cell. Neurosci.,* 2019, **13**, 46.

[9]   F. M. Cowan, R. S. French, P. Mayaud, R. Gopal, N. J. Robinson, S. A. de Oliveira, T. Faillace, A. Uusküla, M. Nygård-Kibur, S. Ramalingam, G. Sridharan, R. El Aouad, K. Alami, M. Rbai, N. P. Sunil-Chandra and D. W. Brown, *Sex. Transm. Infect.*, 2003, **79**, 286–290.

[10]   K. Erlich, J. Mills, P. Chatis, J. Mertz, D. Busch, S. Follansbee, R. Grant and C. Crumpacker, *N. Engl. J. Med.*, 1989, **320**, 293–296.

[11]   G.B. Elion, *Angew Chem. Int. Ed. Engl.*, 1989, **28**, 870–878.

[12]   T. G. Evans, D. I. Bernstein, G. W. Raborn, J. Harmenberg, J. Kowalski and S. L. Spruance, *Antimicrob. Agents Chemother.,* 2002, **46**, 1870–1874.

[13] J. Englund, M. Zimmerman, E. Swierkosz, D. Goodman, D. Scholl and H. Balfour, *Ann. Intern. Med.*, 1990, **112**, 416–422.

[14] J. Pottage and H. Kessler, *Agents Dis.*, 1995, **4**,115–124.

[15] M. J. Hitchcock, H. S. Jaffe, J. C. Martin and R. J. Stagg. *Antivir. Chem. Chemother.*, 1996, **7**,115–127.

[16] J. Piret and G. Boivin, *Antimicrob. Agents. Chemother.*, 2011, **55**, 459–472.

[17] P. Bag, D. Ojha, H. Mukherjee, U. C. Halder, S. Mondal, N. S. Chandra, S. Nandi, A. Sharon, M. C. Sarkar, S. Chakrabarti and D. Chattopadhyay, *PLoS ONE.*, 2013, **8**, e77937.

[18] Y.-F. Xiang, C.-W. Qian, G.-W. Xing, J. Hao, M. Xia and Y.-F. Wang, *Bioorg. Med. Chem. Lett.*, 2012, **22**, 4703–4706.

[19] A. I. Khodair, A. M. Attia, E. A. Gendy, Y. A. Elshaier, M. A. El-Magd, *Int. J. Hematol.*, 2020, **1**.

[20] V. K. Pandey, Z. Tusi, S. Tusi and M. Joshi, *ISRN Organic Chemistry*, 2012, **2012**, 1–7.

[21] P. Ponka, D. Richardson, E. Baker, H. M. Schulman and J. T. Edward, *Biochim. Biophys. Acta.*, 1988, **967**, 122–129.

[22] D. A. Green, W. E. Antholine, S. J. Wong, D. R. Richardson and C. R. Chitambar, *Clin. Cancer Res.*, 2001, **7**, 3574–3579.

[23] Z. Debebe, T. Ammosova, M. Jerebtsova, J. Kurantsin-Mills, X. Niu, S. Charles, D. R. Richardson, P. E. Ray, V. R. Gordeuk and S. Nekhai, *Viro.*, 2007, **367**, 324–333.

[24] A. Walcourt, M. Loyevsky, D. B. Lovejoy, V. R. Gordeuk and D. R. Richardson, *Int. J. Biochem.*, *Cell Biol.*, 2004, **36**, 401–407.

[25] M. W. Wathen, *Rev. Med. Virol.*, 2002, **12**, 167–178.

[26] M. Jurk, F. Heil, J. Vollmer, C. Schetter, A. M. Krieg, H. Wagner, G. Lipford and S. Bauer, *Nat. Immunol.*, 2002, **3**, 499.

[27] H. Hemmi, T. Kaisho, O. Takeuchi, S. Sato, H. Sanjo, K. Hoshino, T. Horiuchi, H. Tomizawa, K. Takeda and S. Akira, *Nat. Immunol.*, 2002, **3**, 196–200.

[28] N. L. Oien, R. J. Brideau, T. A. Hopkins, J. L. Wieber, M. L. Knechtel, J.A. Shelly, R. A. Anstadt, P. A. Wells, R. A. Poorman, A. Huang and V. A. Vaillancourt, *Antimicrob. Agents Chemother.*, 2002, **46**, 724–730.

[29] P. K. Jain, H. Joshi, *J. Appl. Pharm. Scie.,* 2012, **2**, 236–240.

[30] M.-H. Lin, C.-H. Cheng, K.-C. Chen, W.-T. Lee, Y.-F. Wang, C.-Q. Xiao and C.-W. Lin, *Chem. Biol. Interact.*, 2014, **218**, 42–49.

[31] S. Kawaii, Y. Tomono, K. Ogawa, M. Sugiura, M. Yano and Y. Yoshizawa, *Anticancer Res.*, 2001, **21**, 917–923.

[32] N. S. Al-Abbas and N. A. Shaer, *Heliyon.*, 2021, **7**, e06255.

[33] D. Ojha, H. Mukherjee, S. Ghosh, P. Bag, S. Mondal, N. S. Chandra, K. C. Mondal, A. Samanta, S. Chakrabarti and D. Chattopadhyay, *J. Appl. Microbiol.*, 2013, **115**,1317–1328.

[34] H. Mukherjee, D. Ojha, P. Bag, H. S. Chandel, S. Bhattacharyya, T. K. Chatterjee, P. K. Mukherjee, S. Chakraborti, D. Chattopadhyay. *Microbiol. res*., 2013, **168**, 238–44.

[35] D. Chattopadhyay, M. C. Sarkar, T. Chatterjee, R. Sharma Dey, P. Bag, S. Chakraborti and M. T. H. Khan, *N. Biotechnol.*, 2009, **25**, 347–368.

[36] J. Mondal, A. D. Mahapatra, K. C. Mandal and D. Chattopadhyay. *Arch. Virol.*, 2021, **26**, 1–2.

[37] J. M. Harkness, M. Kader and N. A. DeLuca, *J. Virol.*, 2014, **88**, 6847–6861.

[38] Z. Chen, P. Li, D. Hu, L. Dong, J. Pan, L. Luo, W. Zhang, W. Xue, L. Jin and B. Song, *Arab. J. Chem.*, 2019, **12**, 2685–96.

[39] T. Li, J. Zhang, J. Pan, Z. Wu, D. Hu, B. Song, *Eur. J. Med. Chem.*, 2017, **125**, 657–662.

[40] M. A. Abu-Zaied, S. F. Hammad, F. T. Halaweish and G. H. Elgemeie, *ACS. Omega*, 2020, **5**, 14645–14655.

[41] V. Erukhimovitch, E. Bogomolny, M. Huleihil and M. Huleihel, *Analyst.*, 2011, **136**, 2818–2824.

[42] R. Vogel, M. Seyffert, R. Strasser, A. P. de Oliveira, C. Dresch and D. L. Glauser, *J. Virol.*, 2012, **86**, 143–155.

[43] N. C. Elde, S. J. Child, M.T. Eickbush, J. O. Kitzman, K. S. Rogers, J. Shendure, A. P. Geballe and H. S. Malik. *Cell.*, 2012, **150**, 831–841.

[44] E. Hildebrandt, J. R. Dunn, S. Perumbakkam, M. Niikura and H. H. Cheng, *J. Virol.*, 2014, **88**, 6232–6242.

[45] K. R. Cone, Z. N. Kronenberg, M. Yandell and N. C. Elde, *J. Virol.*, 2017, **91**, e01428–16.

Chapter 5

Comparative study of Chromone

Sulfonamide derivatives: antibacterial agent

Abstract

Sulfonamide derivatives are a broad range of multi-target bioactive representatives for multifaceted diseases. These compounds have been used in numerous pharmaceutical applications due to their antibacterial, antiviral, antimalarial, antifungal, anticancer, antidepressant, or other properties. In Medicinal Chemistry Sulfonamide,-structural motifs are frequently seen. The structural flexibility of sulfonamide derivatives makes them an excellent candidate for the advancement of new multi-target agents in the rising field of pharmacology. The functionalization of established or tested drugs for the manufacture of less toxic more competent medicine is a recently undertaken program. 7-Hydroxy-4-methyl-2-oxo-2H-chromene-8-carbaldehyde and different sulfonamides (Sulfapyridine, Sulfathiazole, Sulfamethoxazole, and Sulfamerazine) are used to synthesize Schiff bases, **1a**–**1d**, those are potentially active against both Gram-positive and Gram-negative bacteria. The Schiff bases have been spectroscopically characterized. Two of these four Schiff bases, **1a,** and **1b** are found to be reasonably more activities related to **1c** and **1d**. The plausible mechanism of drug action at the cellular level is attempted to explore in this research.

5.1 Introduction

Antibiotics either inhibit or stop the essential enzymatic functions of pathogens. Plausible mechanism of action of antibiotics on four major pathways : (i) inhibition of cell wall synthesis and corrupt its functionality; (ii) inhibition of Nucleic Acid synthesis and disruption of their functions; (iii) hindrance to folate synthesis; and (iv) inhibition of protein synthesis [1-5]. From the very beginning age of antibiotics, bacteria have tried to develop resistance to antibiotics [3]. The number of antibiotic-resistant bacteria has increased gradually and caused a global public health threat. Developing new drugs by Pharmaceutical Industries is one way out to overcome the crisis of antibiotic resistance [6]. During the 1920-30s staphylococcal and streptococcal infections were the large killers, even minor scratches and scrapes could be deadly, while pneumonia and tuberculosis killed young adults in Europe and USA [7]. Prontosil (Kl730), a Sulfonamide dye, noted as anti-bacterial in 1900's by German Pathologist Gerhard Domagk, a Nobel laureate in 1939, to save his daughter from streptococci infection, when he observed its selective ability to prevent the infectious bacteria [8]; while Ernest Fourneau in 1936 discovered that pro-drug prontosil converted into active antibacterial Sulfonamide in the human body [9]. The discovery triggered more anti-bacterial agents from the Sulfa group including sulfapyridine for the treatment of pneumonia (1938), sulfacetamide prescribed for the handling of urinary tract infections (1941), and succinoyl-sulfathiazole given to patients suffering from gastrointestinal tract infections (1942); of which sulfathiazole was used for wound infection during Second World War. Sulfonamides are employed on large scale for preventive and chemotherapeutic purposes against various ailments. More than thirty different types of sulfa drugs are utilized as antibacterial, antiprotozoal, antifungal anti-inflammatory, nonpeptidic vasopressin receptor antagonists, and translation initiation inhibitors [10, 11, 12].

134

Sulfonamides block the synthesis of folic acid by replacing *p*-amino benzoic acid (PABA) and hamper DNA or RNA synthesis in bacteria [12]. The selectivity of sulfonamides depended on the enzymatic action of dihydropteroate synthase (DHPS) [13]. While hypersensitivity of sulfonamides is due to fractional oxidation of the aromatic-NH_2 group of sulfonamides to hydroxylamine (SF-NHOH) and/or nitroso derivative (SF-NO) by human Cytochrome-P450 that results in cellular toxicity [14]. Sulfonamides are employed on large scale for preventive and chemotherapeutic purposes against various elements. More than thirty different types of sulfa-drugs are utilized as antibacterial, antifungal, antiprotozoal, anti-inflammatory, non-peptidic vasopressin receptor antagonists, and translation initiation inhibitors [15, 16, 17]. Some important Sulfonamide compounds are also used as carbonic anhydrase inhibitors [18]. Coumarins, secondary metabolites of a wide variety of plants, are specific classes of compounds having significant biological activities [19] and their activities or roles may differ based on different substituents. In Coumarins, the benzene ring is fused with the pyrone ring having diverse activities including antibacterial, antifungals, anticoagulant, antioxidant, anti-inflammatory, and anticancer [20]. Coumarins are highly active against both Gram-negative and Gram-positive bacteria, but more potent against Gram-negative bacteria, by deforming the bacterial outer membrane. Some plants produce secrete coumarin-like active molecules phytoalexins that provide a defensive mechanism to counter the attack from phytopathogens which are environmentally benign and are not vulnerable to bacterial resistance development [21, 22]. A compound with a sulfonamide functional group was found to inhibit the activity of carbonic anhydrase; thus, when conventional antibiotics are ineffective, sulfonamide derivatives are useful as a pharmaceutical agent [23]. Primary amines and active carbonyls react with each other to form an azomethine group (-C=N-), known as Schiff bases, to honor Hugo Schiff (1834-1915) [24]. Aromatic

135

Schiff bases are weak nucleophiles and weak bases. Schiff's bases are utilized in the ink dye industry, as well as to prepare superconducting polymers that are highly resistant to oxidation, heat, and light [25]. Most aromatic Schiff bases are sparingly water-soluble. Schiff bases have exhibited significant activity such as antibacterial, fungicidal, antioxidant, anti-inflammatory, antitumor, anti-cancer and herbicidal properties [26-28]. In view of the biological significance of these pharmacological active compounds, the present work aims to synthesize new Schiff bases 1a to 1d by using 7-Hydroxy-4-methyl-2-oxo-2H-chromene-8-carbaldehyde and different sulfonamides (Sulfapyridin, Sulfathiazole, Sulfa-methoxazole, and Sulfamerazine) as potential less-toxic antibacterial agents. As microbial resistance has evolved sharply over last five-six decades, most antimicrobial drugs lost their 'magic-bullet' like effectiveness. This profit disparity is further exacerbated as the result of a crowded generic market and the increasing extent of bacterial resistance [29, 30]. It is important to exploit the diverse natural products those can lead to more competent less toxic antimicrobial drugs. The safety of the molecules can be judged by toxicity studies in a suitable animal model, and also in isolated ex-vivo. The side effects of the molecules might be studied in comparison to direct toxicity upon animal cells. This work aimed at representing the comparative therapeutic aptitude of **1a**, **1b**, **1c**, and **1d**.

5.2 Experimental Section

5.2.1 Reagents and solvents

Required AR grade chemicals were procured from Merck (India), HiMedia (India), SRL (India) and TCI. Some of the important compounds were purchased from Sigma. High purity water was collected from Milli-Q water (Millipore) for use in this research. 8-Formyl-7-hydroxy-4-methyl coumarin in methanol was prepared as per the published

article [31]. Sulfonamides were purchased from HiMedia (India), Bombay, India. Thin-layer chromatography was performed by using Al sheets (Merck) coated with silica gel 60F254. FTIR spectra on KBr discs 4000–400 cm^{-1}) was taken from Bruker ALPHA II spectrometer in an attenuated total reflectance (ATR) mode. The ^{1}H NMR spectra were recorded with Bruker (AC) 300 MHz FT-NMR spectrometer in DMSO-d$_6$ using TMS as an internal standard; while ESI mass spectra were verified by a Water HRMS XEVOG2QTOF#YCA351 Spectrometer.

Culture Media

Nutrient broth (NB; Oxoid), Peptone water (PW; Oxoid brand, UK.), Luria broth (LB; Oxoid), Triple sugar iron Agar (TSI, Difco, Detroit, USA), MacConkey Agar (Difco, Detroit, USA), Mueller Hinton broth (MHB; Difco, Detroit, USA) and other basic media was obtained from the commercial suppliers, Himedia. Peptone agar (PA), nutrient agar (NA), and Mueller Hinton agar (MHA) were prepared in the laboratory by adding the appropriate amount of agar in the individual liquid media and sterilize.

5.2.2 Synthesis of Compounds (1a-1d)

To methanol (30 ml) solution of 8-formyl-7-hydroxy-4-methyl coumarin (0.204 g, 1 mmol), sulfapyridine (0.249 g, 1 mmol) was added and refluxed for 4 h. A reddish coloured precipitate was collected by filtration, washed with cold methanol, and dried (yield, 90%). Other Schiff bases were prepared by using 8-formyl-7-hydroxy-4-methyl coumarin and sulfathiazole, sulfathiazole, sulfamerazine, respectively. The synthetic scheme is presented in **Scheme 5.1**. Detail characterization of the compounds are given in the Results section.

5.2.3 Determination of the antibacterial activity

The compounds **1a**–**1d** were screened *in vitro* for their antibacterial activity against Gram-negative *Escherichia coli* ATCC 29212 and *Salmonella typhi* MTCC 734, and five Gram-positive *Staphylococcus aureus* ATCC 29213, methicillin resistance *S. aureus* (MRSA), *S. aureus*, Coagulase negative *Staphylococcus aureus* (CONS), *Enterococcus faecalis* ATCC 25922 and *Enterococcus faecalis* PH007^R bacterial strains. The antimicrobial susceptibility or resistance of all the strains against the commercially available common antibiotic discs was determined by the standard disc diffusion method following the guidelines of the Clinical and Laboratory Standards Institute [32, 33]. (All ATCC and MTCC are quality control strains). A stock solution (1 mg/ml) was prepared by dissolving 1 mg of compound(s) in 1.0 ml sterile distilled water; or in 100 μl of 0.1% DMSO and diluted in sterile distilled water. To get compound (drug) impregnated disc of various potency (0-1000 μg/ml), different amount of stock solution was added to the sterile filter paper (Whatman No 3) discs (5.25 mm diameter) and dried at room temperature. The disks of the desired potency were then aseptically placed on the MHA plate seeded with the test and control bacterium (10^6 CFU/ml) and incubated at 37 ^{o}C for 24 h. The activity was recorded by measuring the clear zones of growth inhibition on the agar surface around the discs [34-36].

5.2.4 Determination of MIC and growth inhibition assay

Minimum inhibitory concentration (MIC) of the compound was determined by treating with all the test strains, by broth and agar dilution methods, using MRSA and CONS, following the National Committee for Clinical Laboratory Standards guidelines [32, 33], compounds at two-fold dilutions were added in each tube containing MHB at room temperature. Bacterial isolates were grown overnight in MHB at 37 °C and diluted with

the fresh media at a density of 10^6 CFU/ml to add in each tube containing different concentrations of the test drugs. Aliquots (100 µl) of culture removed from the incubated tubes were inoculated onto an MHA plate to determine the CFU per ml to record viable counts. The agar dilution test was conducted on MHA plated prepared with a two-fold concentration of the test compounds along with 10^6 CFU/ml of inoculum of each bacterium and incubated overnight at 37 °C. The colony count of the plates was made in each dilution. Both the test was repeated three times to calculate the mean count of each dilution [33].

5.2.5 Determination of Minimal Bactericidal Concentration (MBC)

The MBC was determined by the broth dilution method [35]. Freshly made MHA plates containing different concentrations (0–1000 µg/ml) of test compounds were inoculated with the respective bacterial strains at a density of 10^6 cfu/ml. The mixtures were incubated at 37°C for 18 h with shaking (200 rpm) on a platform shaker. The growth of the bacterium was determined by measuring the optical density of the culture in a colorimeter at 600 nm. The lowest concentration of the molecules which did not show any visible growth after overnight incubation in MHA plates was considered as the MBC [36].

5.2.5 Tolerance level

The MIC and MBC values usually provide a clear indication about the tolerance levels of each test molecule for selective recognition and killing of pathogenic drug-resistant or MDR strains like MRSA. The tolerance level was measured with the help of the formula: Tolerance level = MBC/ MIC [37].

5.2.6 Growth inhibition study of test compounds on MRSA and CONS

The rate and extent of bacterial growth, treated with **1a-1d**, were studied by growth inhibition assay and subsequent growth curve analysis. Growing cultures (10^6 CFU/ml)

of the most susceptible MRSA and CONS isolates in MHB were exposed to the test compounds at their MIC, along with a drug-free inoculated medium plate as growth control. Samples were removed for colony counts at hourly intervals (0-12 h) and at 24 h. Viable counts were determined by the serial dilution method after 24 h of incubation and plates containing 30 to 300 CFU/ml for each dilution were counted [35]. The procedure was repeated three times for each test organism to record the mean readings, and Log_{10} CFU/ml *vs*. time (t) was plotted. Antibiotic carryover was prevented by serial dilution of the testing antibiotic. An antimicrobial agent was considered bactericidal when its lowest concentration can reduce the original inoculum by >3 log_{10} CFU/ml (99.9%); while it will be bacteriostatic when the original inoculum was reduced by 0-3 log_{10} CFU/ml [36].

5.2.7 Morphology changes of bacterial cells

The bacterial isolates were grown in 5 ml culture media and were incubated in agitating phase at 198 rpm at 37 °C for 12 h. MBC of **1a** was added to the culture. The untreated cells were taken as negative control. Following centrifugation at 5000 rpm for 5 minutes, the cells were systematically washed with PBS and centrifuges to accumulate the pellets. The cells were fixed with 2.5% glutaraldehyde and washed three times with sterile PBS. A drop of solution was placed on the glass plate and dried using a vacuum oven. After coating, the cell morphology was recorded by scanning electron microscopy (SEM, EVO 18 Special Edition, Carl Zeiss, Germany).

Molecular Docking Study has been performed by using the methods described in Chapter 4**.**

5.3 Results

5.3.1 Synthesis and formulation

Four compounds 4-[(7-Hydroxy-4-methyl-2-oxo-2*H*-chromen-8-ylmethylene)-amino]-*N*-pyridin-2-yl-benzenesulfonamide(**1a**), 4-[(7-Hydroxy-4-methyl-2-oxo-2*H*-chromen-8-ylmethylene)-amino]-*N*-(4-methyl-thiazole-2-yl)-benzenesulfonamide (**1b**), 4-[(7-Hydroxy-4-methyl-2-oxo-2*H*-chromen-8-ylmethylene)-amino]-*N*-(4-methoxazole-2-yl)-benzenesulfona-mide (**1c**) and 4-[(7-Hydroxy-4-methyl-2-oxo-2*H*-chromen-8-ylmethylene)-amino]-*N*-(4-methyl-pyrimidin-2-yl)-benzenesulfonamide (**1d**) were successfully synthesized by the condensation reaction between 8-formyl-7-hydroxy-4-methylcoumarin and the corresponding of sulph-amines (sulfapyridine, sulfathiazole, sulfathiazole, sulfamerazine) separately, and their characterization were performed by spectroscopic data (NMR, Mass, FTIR). The ^{1}H NMR spectral data of Compound-**1a** (DMSO-D$_6$) showed characteristic signals at 14.47 ppm which corresponding to a coumarinyl -OH proton, a sharp singlet at 9.27 ppm indicating the imine (–CH=N–) proton, at 2.50 ppm coumarinyl–CH$_3$ and other Ar-Hs appear at 6.29–7.77 ppm. The molecular ion peak at 458.00 (M+Na)$^+$ (add calculated Mass) from the mass spectrum also supports the molecular identity. The structural characterization was established by IR spectral data which report characteristic signals corresponding to 3443.9 cm^{-1} (aromatic -OH), 1731.4 cm^{-1} (lactone C=O), 1632.2 cm^{-1} (Schiff's bass, C=N), and 1388.3 cm^{-1} (S=O). All the observations strongly support and confirmed the formation of compound-**1a**. Similarly, confirm the structural identification was observed for compound-**1b**, **1c**, and **1d**.

Micro-analytical data of **Compound-1a**: C$_{22}$H$_{17}$N$_3$O$_5$S; Calcd. (Found): C, 60.68 (60.62); H, 3.93 (3.96); N, 9.65 (9.71)%. ^{1}H-NMR (300 MHz, DMSO-d$_6$). δ 14.47 (s, 1H), 9.27 (s, 1H),7.77 (d, 4H, J = 8.4), 7.66 (d, 1H, J = 8.7), 7.75 (s, 1H), 7.39 (d, 2H, J = 2.8), 7.21

(s, 1H), 6.97 (m, 2H, J = 9), 6.29 (s, 1H), 2.50 (s, 3H), (**Fig**. **5.1**). Mass: (M+Na)$^+$ 458.00 (**Fig**. **5.2**). IR: 3443.9 cm^{-1} (aromatic -OH), 1731.4 cm^{-1} (lactone C=O), 1632.2 cm^{-1} (Schiff's bass, C=N), 1388.3 cm^{-1} (S=O) (**Fig**. **5.3**).

Synthesis of 1b-1d

All the compounds were synthesized by same procedure as described for Compound-**1a** which is presented in **Scheme 1.1**. *Micro-analytical data* of **Compound-1b**: $C_{20}H_{15}N_3O_5S_2$; Calcd. (Found): C, 54.41 (54.38); H, 3.42 (3.46); N, 9.52 (9.51)%. ^{1}H-NMR (300 MHz, CDCl$_3$). δ 14.33 (s, 1H), 9.33 (s, 1H),7.99 (d, 2H, J = 7.3), 7.61 (d, 1H, J = 6), 7.40 (d, 2H, J = 8.8), 7.13 (d, 1H, J = 4.8), 6.93 (d, 2H, J = 9), 6.55 (d, 1H, J = 4.8), 6.14 (s, 1H), 2.42 (s, 3H), (**Fig**. **5.4**). Mass: (M+Na)$^+$ 458.00 (**Fig**. **5.5**). IR: 3458.9 cm^{-1} (aromatic - OH), 1719.4 cm^{-1} (lactone C=O), 1634 cm^{-1} (Schiff's bass, C=N), 1391.1 cm^{-1} (S=O). Melting point of 1a and 1b are 185°C 189°C respectively (**Fig**. **5.6**).

Micro-analytical data of **Compound-1c**: $C_{21}H_{17}N_3O_6S$; Calcd. (Found): C, 57.40 (57.41); H, 3.90 (3.92); N, 9.56 (9.52)%. ^{1}H-NMR (300 MHz, DMSO-d$_6$).δ 14.33 (s, 1H), 11.51 (s, 1H), 9.26 (s, 1H),7.92 (d, 2H, J = 9.3), 7.85 (d, H, J = 9),7.69 (d, 2H, J = 8.3), 6.96 (d, 1H, J = 8.97), 6.27 (s, 1H), 6.15 (s, 1H),2.26 (s, 3H),2.06 (s, 3H) (**Fig**. **5.7**) Mass**:** (M+H)$^+$ 440.00 (**Fig**. **5.8**). IR: 3445 cm^{-1} (aromatic -OH), 1729.8 cm^{-1} (lactone C=O), 1644.4 cm^{-1} (Schiff's bass, C=N), 1345.8 cm^{-1} (S=O), Melting point of 1c is 179°C (**Fig**. **5.9**).

Micro-analytical data of **Compound-1d**: $C_{22}H_{18}N_4O_5S$; Calcd. (Found): C, 58.66 (58.67); H, 4.03 (4.01); N, 12.44 (12.41)%. ^{1}H-NMR (300 MHz, DMSO-d$_6$). δ 14.45 (s, 1H), 10.45 (s, 1H),8.089 (d, 1H, J=7.8),8.339 (d, 1H, J = 3.6),7.873 (d, 1H, J = 9),7.68 (d, 1H, J = 9.1),7.626 (d, 1H, J = 8.7), 6.994 (d, 1H, J = 9), 6.926 (d, 1H, J = 4. 5), 6.557 (d, 1H, J = 8.4), 6.313 (s, 1H), 5.98 (s, 1H),2.439 (s, 3H), 2.344 (s, 3H) (**Fig**. **5.10**). IR:

3445 cm^{-1} (aromatic -OH), 1729 cm^{-1} (lactone C=O), 1618 cm^{-1} (Schiff's bass, C=N), 1341cm-1 (S=O). The melting point of 1d is 170°C (**Fig**. **5.11**).
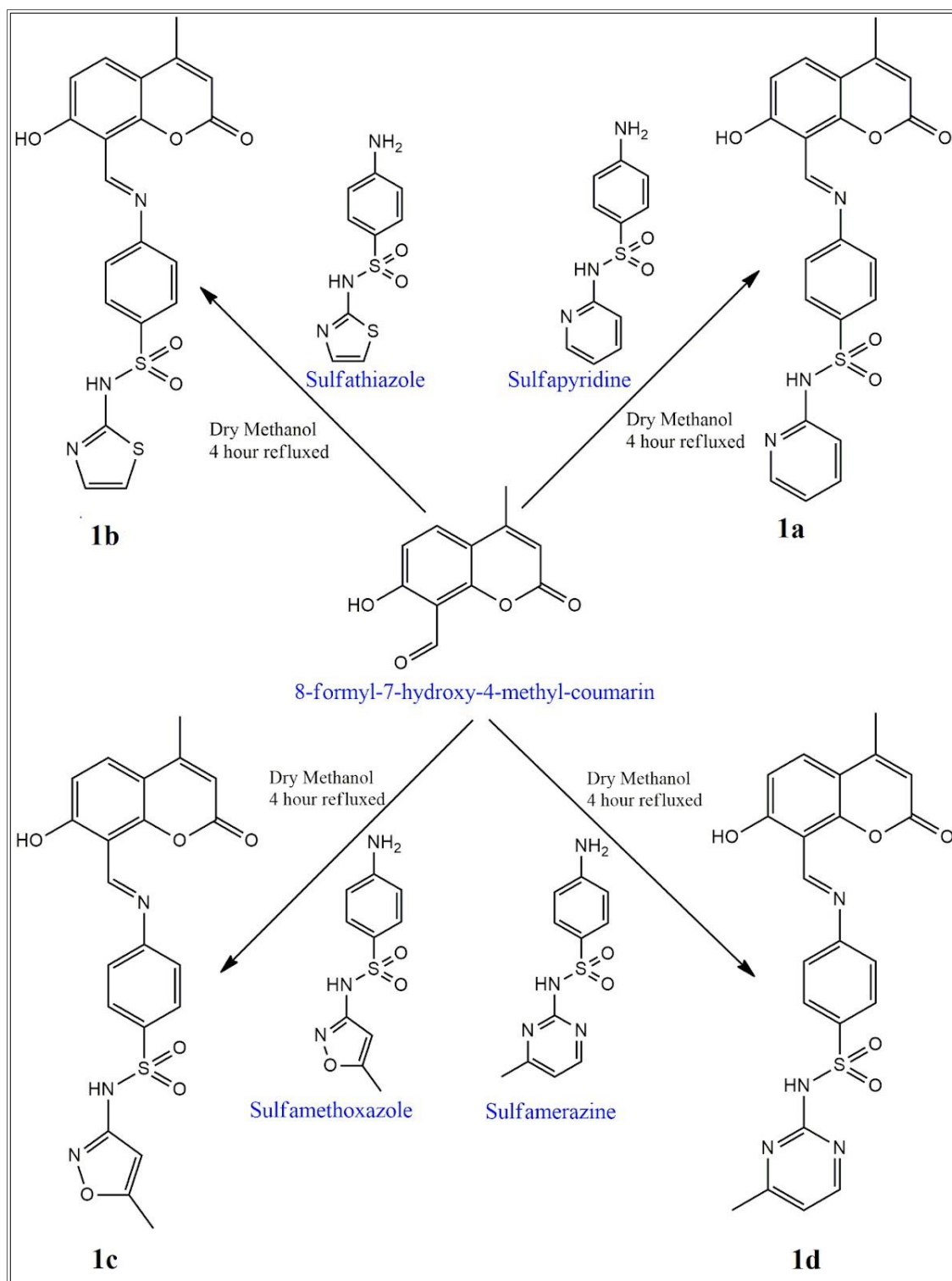
Scheme 5.1 Synthesis of Compound-1a, 1b, 1c, and 1d.
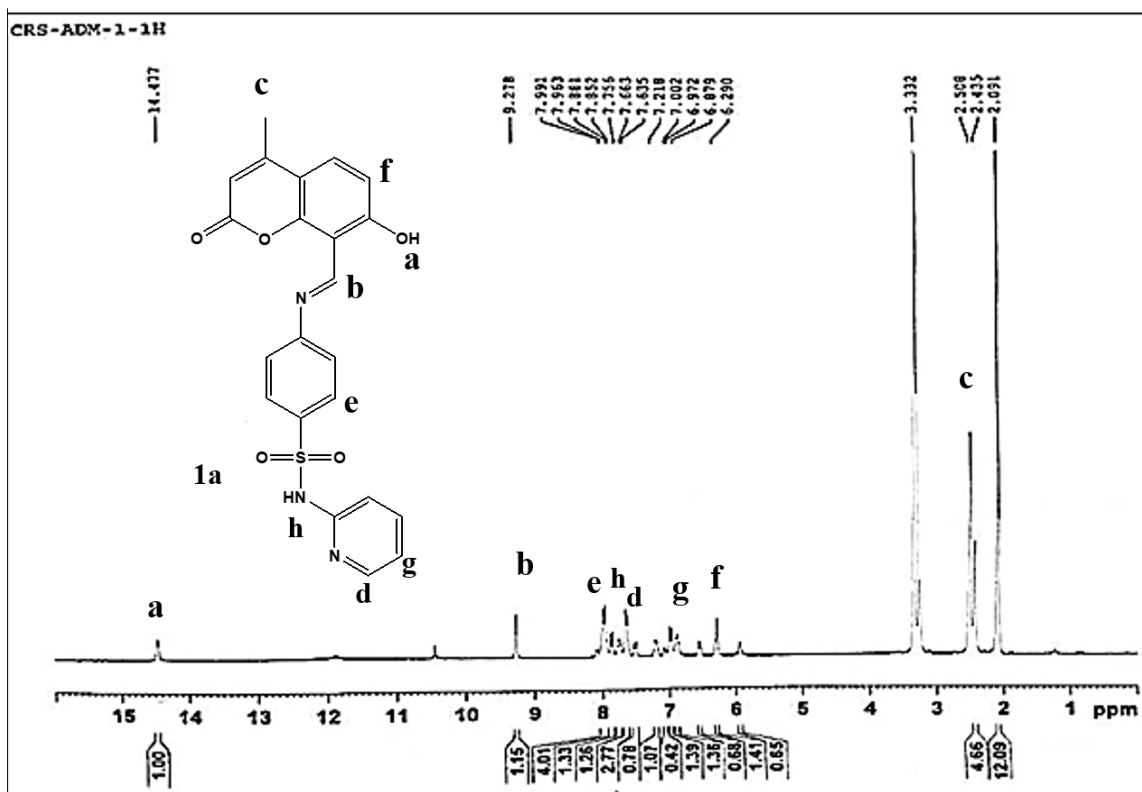
Fig. 5.1 ^{1}HNMR spectrum of 1a in DMSO-d$_6$
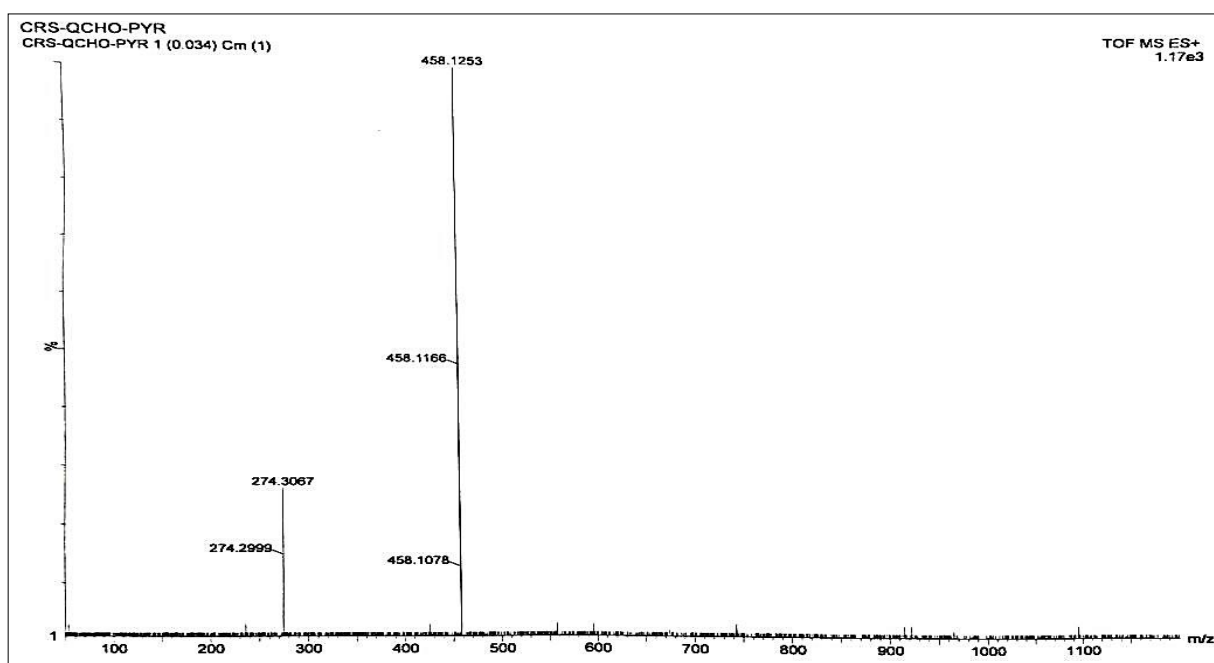
Fig. 5.2 Mass spectrum of Compound-1a.

144
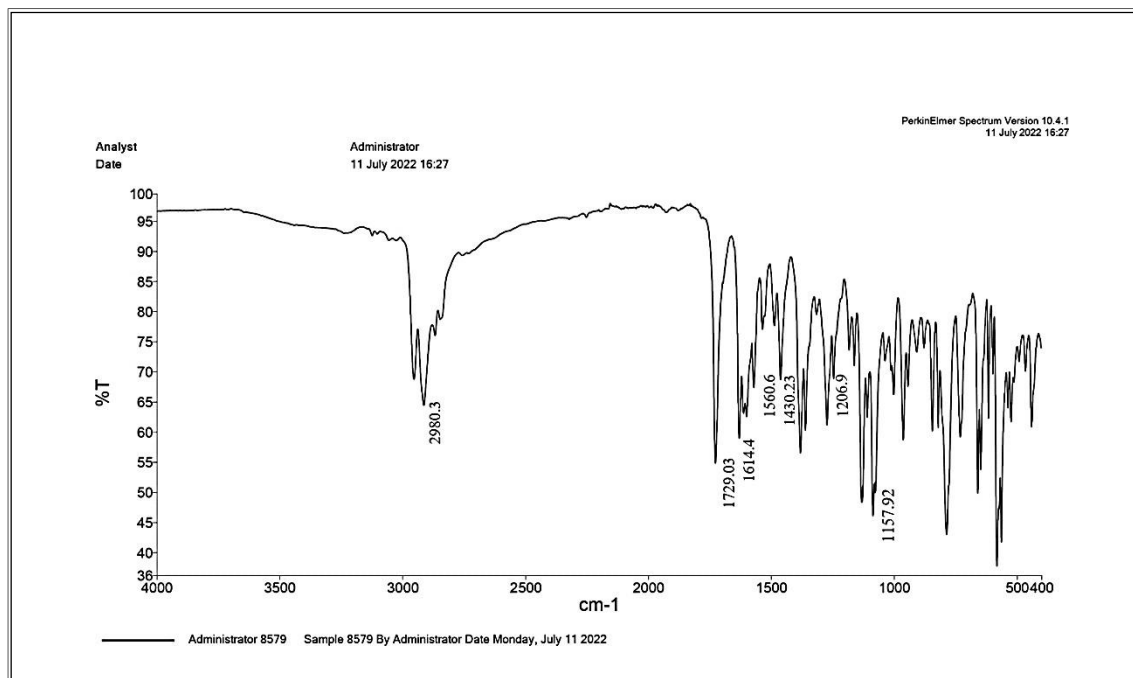
Fig. 5.3 IR spectrum of Compound-1a.
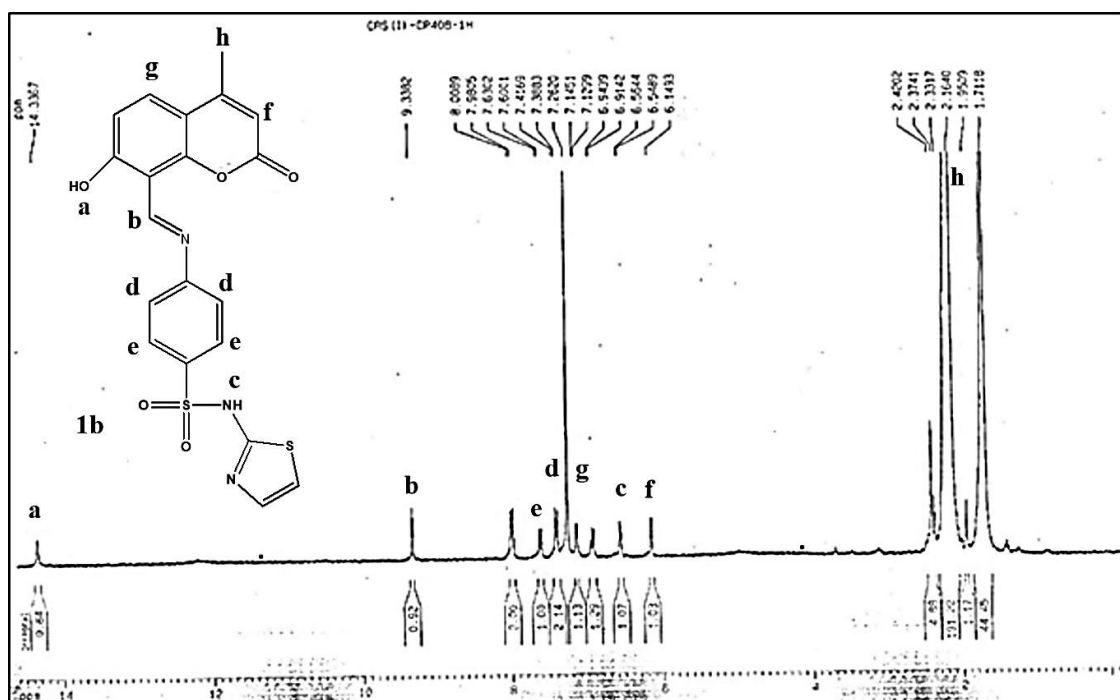
Fig. 5.4 ^{1}HNMR spectrum of Compound-1b in CDCl$_3$
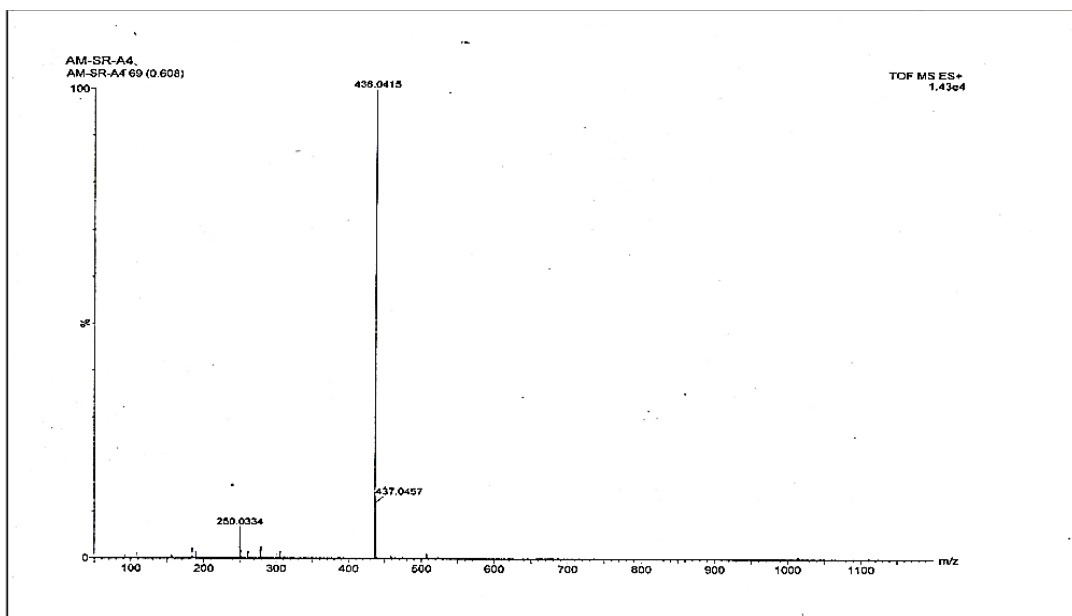
Fig. **5.5** Mass spectrum of the compound -1b.
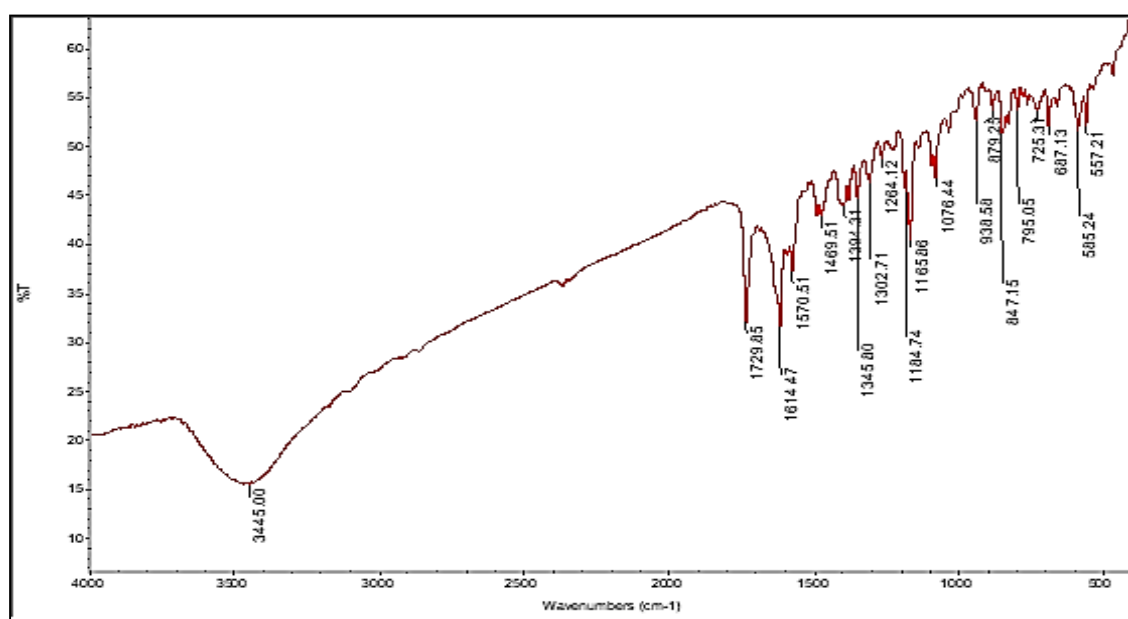
Fig. 5.6 IR spectrum of Compound-1b.

146
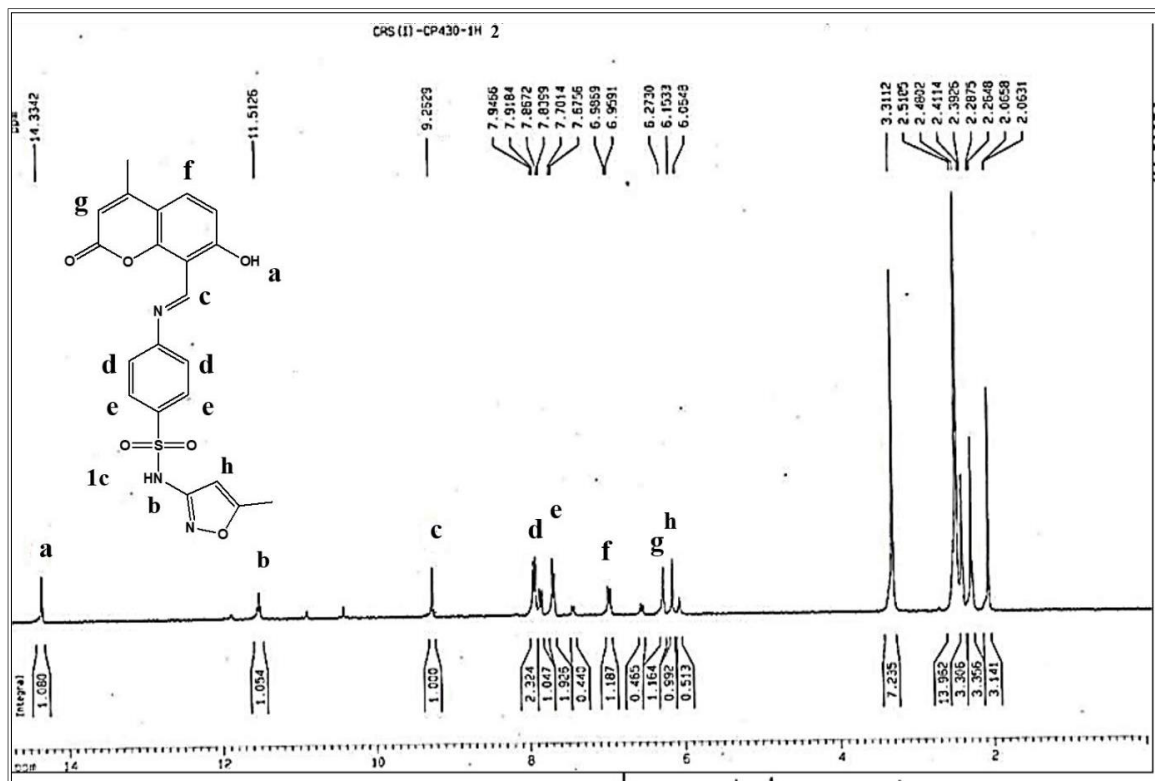
Fig. **5.7** ^{1}HNMR spectrum of the compound -1c in DMSO-D$_6$
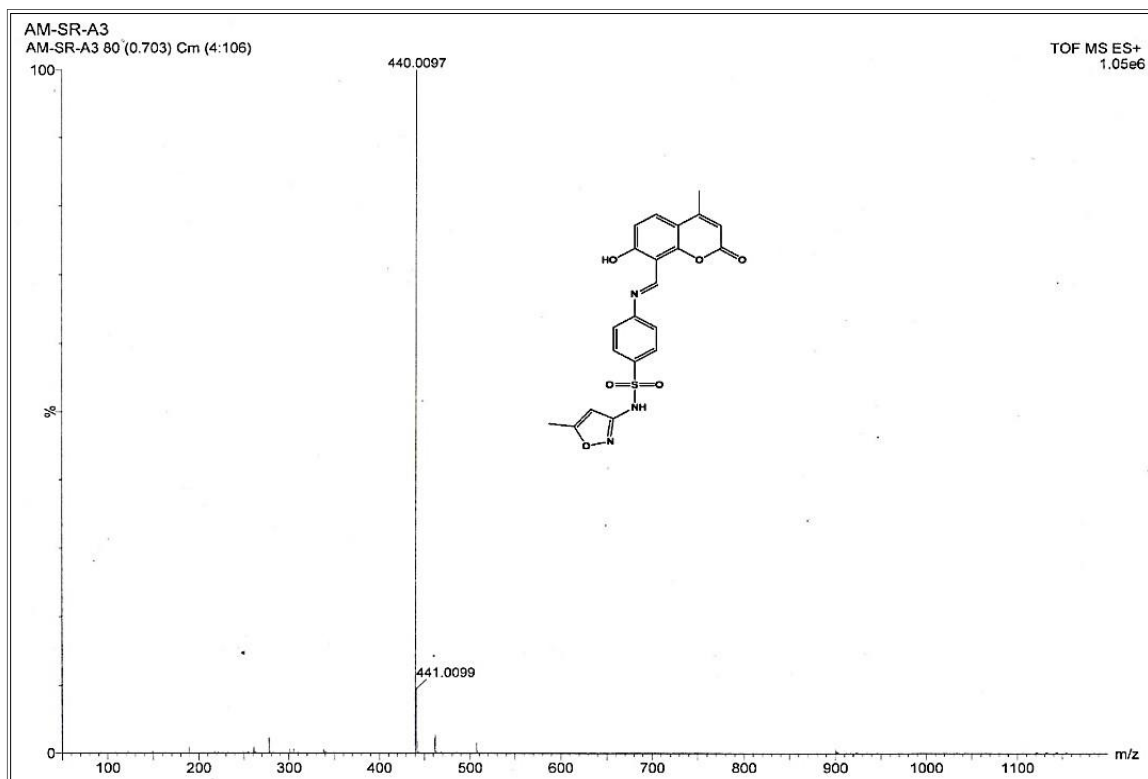
Fig. **5.8** Mass spectrum of the compound -1c.

147
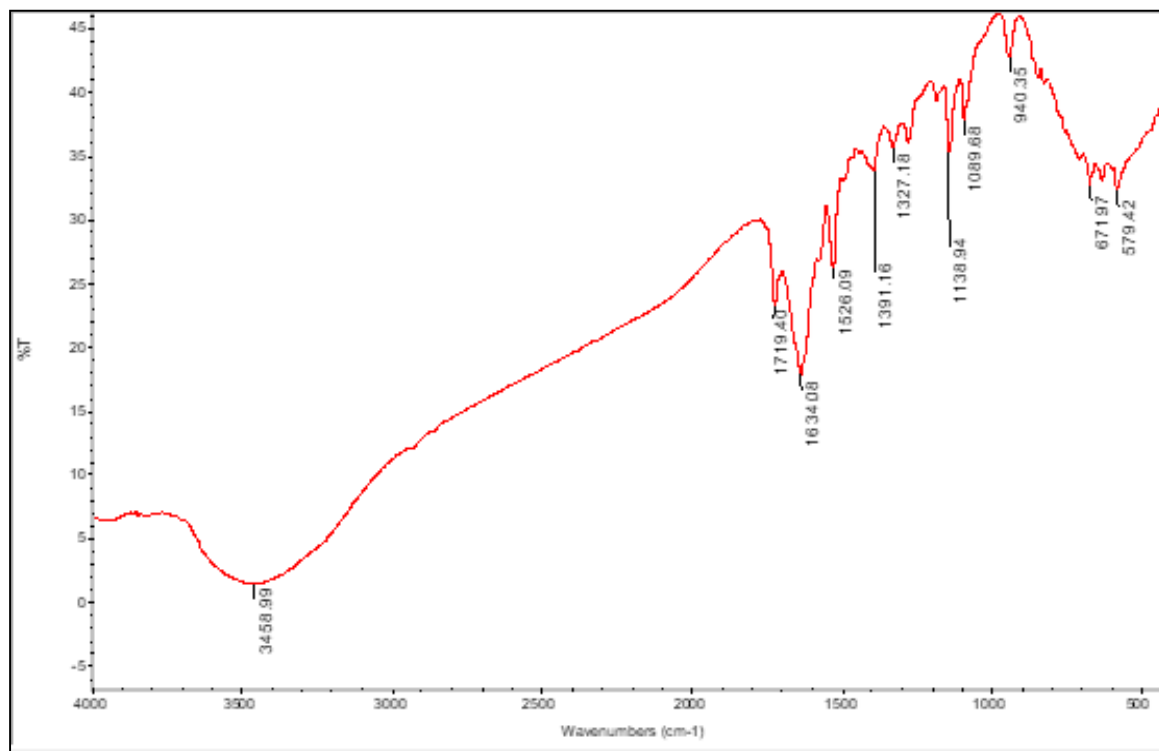
Fig. 5.9 IR spectrum of Compound-1c
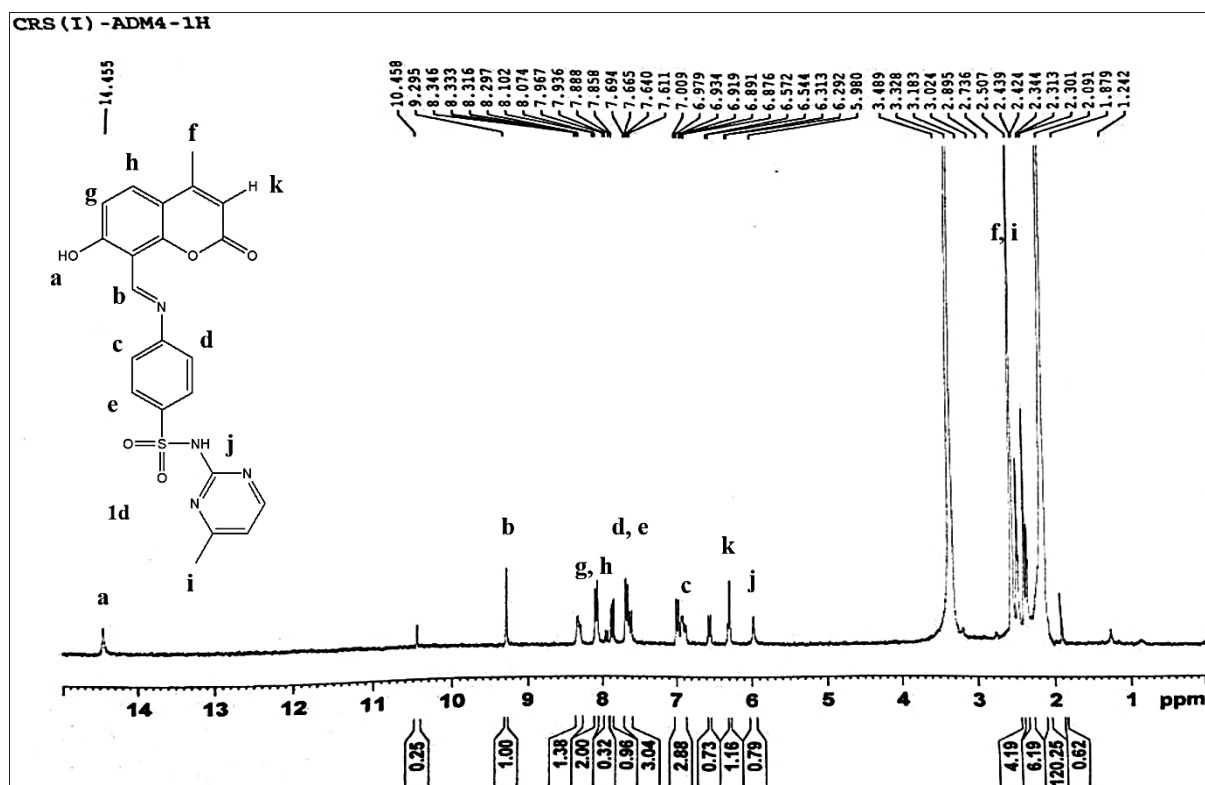
Fig. **5.10** ^{1}HNMR spectrum of the compound -1d in DMSO-D[6]
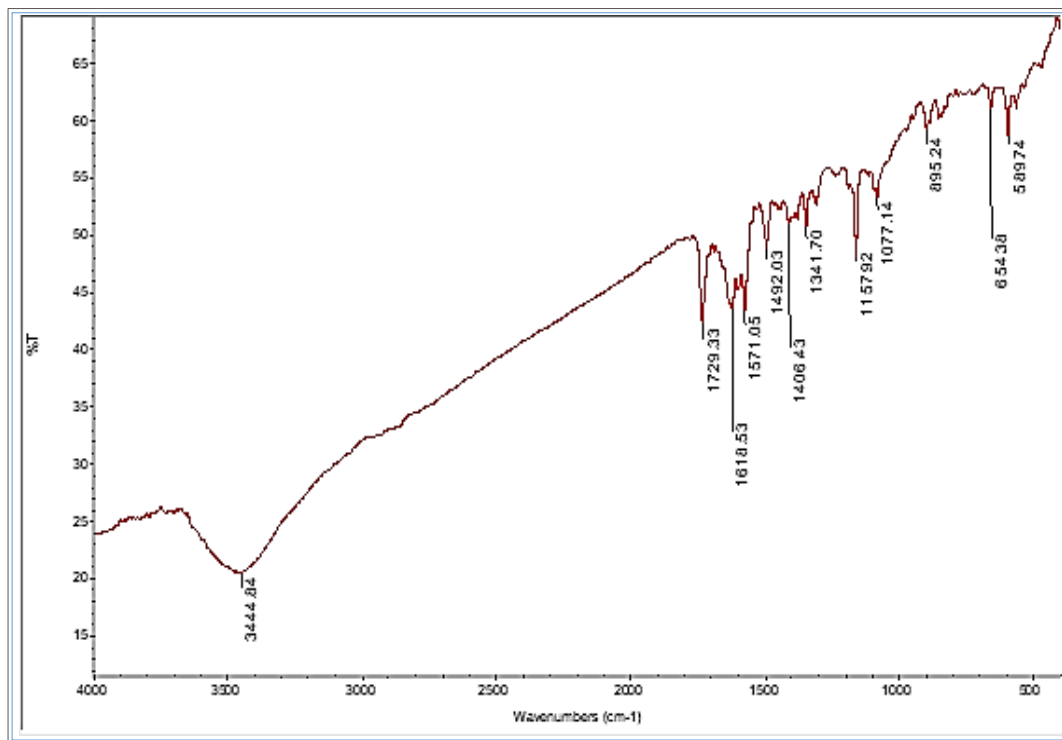
Fig.**5.11** IR spectrum of Compound-1d.

5.3.2 Biological evaluation

Determination of cytotoxicity by MTT assay

The MTT (3-[4,5-dimethylthiazol-2-yl]-2,5 diphenyl tetrazolium bromide) is used to assess toxicity of the drugs, **1a-1d**, on Vero cell morphology (MTT 2003, Sigma-Aldrich, MO, USA). Following the procedure, 10×10^6 Vero cells per well were cultured onto 96-well plates, and the test drugs (**1a-1d**) of different concentrations were added to each well at a final volume of 100 µl, in triplicate using DMSO (0.1%) as a negative and positive control, respectively. The drug-treated cells were incubated at 37 °C in 5% CO_2 for 2 days, and then the MTT reagent (10 µl) was added to each well [38]. Formazan was solubilized by adding MTT solubilization solution equal to the original culture media volume after 4 h of incubation, and the absorbance was recorded at 570 nm with a reference wavelength of 690 nm by an ELISA reader. Data were calculated as the

percentage (%) of cell viability by the formula: [(sample absorbance cell - free sample blank)/mean media control absorbance)]/100%. The fifty cytotoxic concentration (CC_{50}) causing observable morphological changes in 50% of Vero cells concerning cell control was evaluated (**Fig 5.13**).
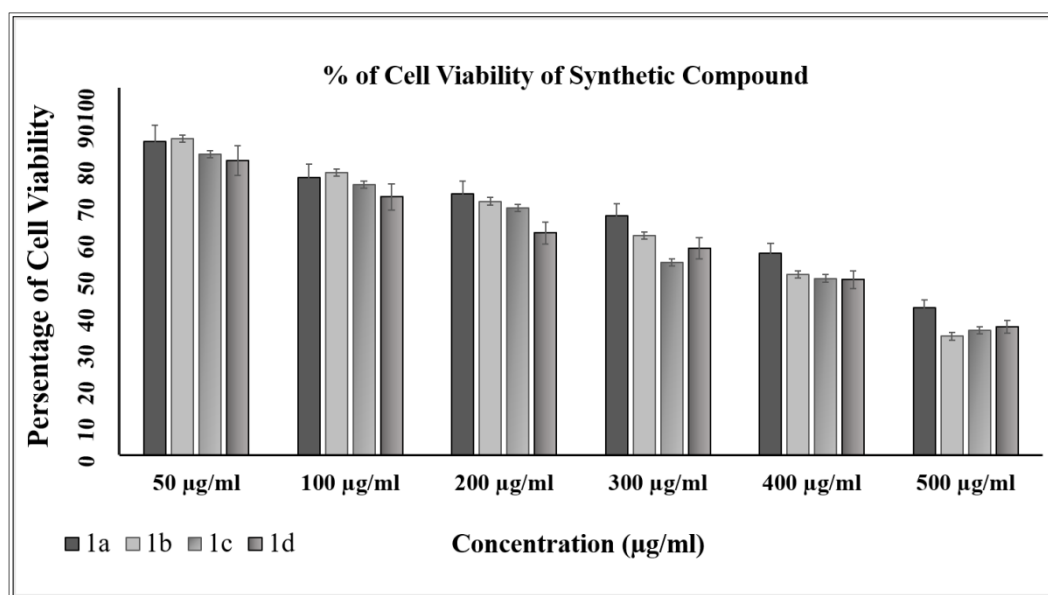
Fig. 5.13 Cytotoxicity of coumarin functionalized **1a**, **1b**, **1c**, and **1d** by MTT Assay. Vero cell morphology does not seem to be affected at CC_{50} concentration of Schiff base (**1a**) by exposure compared to control.

Cell Control   **CC50**   **Cytotoxic concentration**
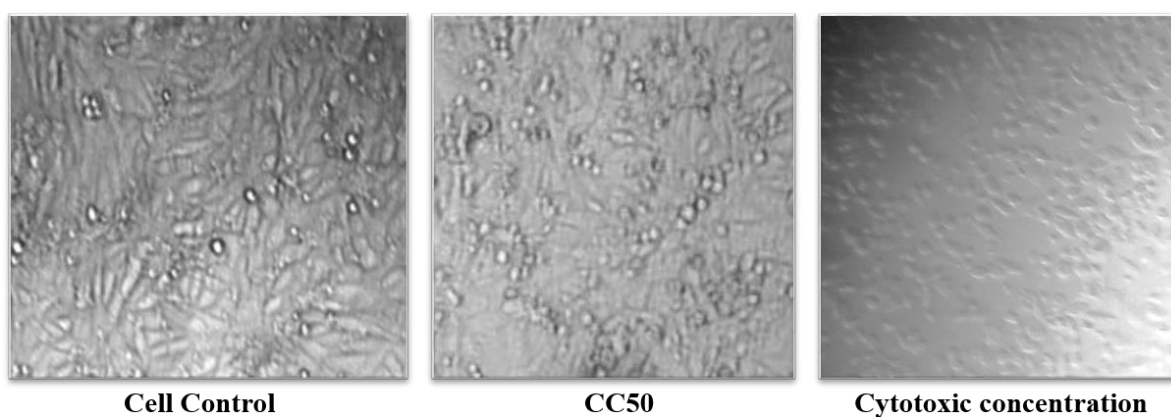
Fig. **5.14** Change of Vero cell morphology before and after treatment with **1a**; (a) Cell control, (b) CC_{50} dose, (c) Vero cell at cytotoxic concentration.

Table 5.1: **Antibacterial activity of Coumarin functionalized derivatives 1a-1d and sulfadrug**

Bacteria	1a	Sulfa pyridine	1b	Sulfa thiazole	1c	Sulfathiazole	1d	Sulfamerazine
	Inhibition Zone dia[#] (mm)	Inhibition Zone dia[#] (mm)	Inhibition Zone dia[#] (mm)	Inhibition Zone dia[#] (mm)	Inhibition Zone dia[#] (mm)	Inhibition Zone dia[#] (mm)	Inhibition Zone[#] (mm)	Inhibition Zone dia[#] (mm)
Staph aureus PH217(MRSA)[R]	15.9	13.5	10.5	9.5	8.0	7.5	9.2	8.0
Staph aureus (CONS)	18.2	16.8	9.0	9.6	5.5	7.6	7.4	7.6
Staph aureus ATCC29213	17.7	15.7	12.5	10.3	9.0	8.4	9.2	8.3
Escherichia coli ATCC29212	15.0	13.8	7.4	10.4	8.5	8.3	7.7	7.0
Enterococcus faecalis PH007[R]	10.5	10.5	9.7	8.7	7.3	7.6	8.2	6.3
nterococcus faecalis ATCC25922	12.5	10.8	8.0	8.6	7.3	6.3	8.9	7.1
Salmonella typhi MTCC 734	11.3	10.5	8.5	5.5	9.5	7.3	7.5	8.3
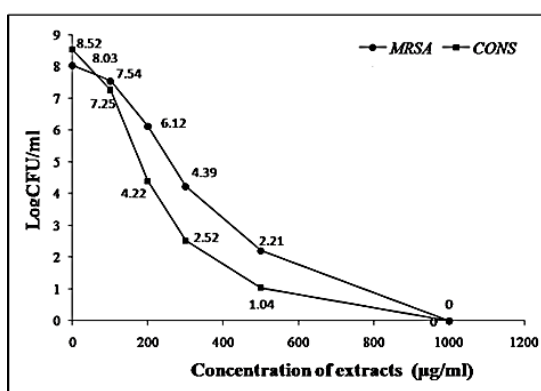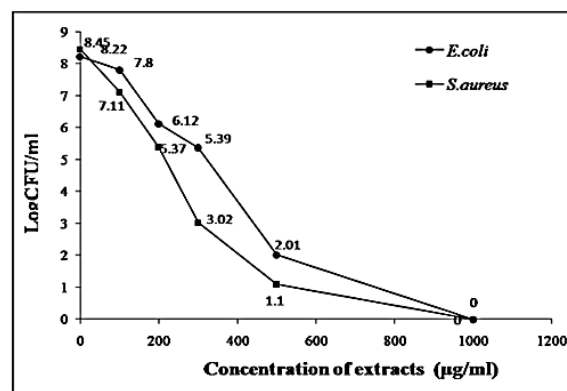
Fig. 5.15 Antibacterial activity spectrum of 1a against MRSA and CONS (**A**) and *E. coli*, *S. aureus* (**B**).

Antimicrobial susceptibility testing by disc diffusion method

The antimicrobial susceptibility of *S. aureus*, MRSA, CONS, and *E. coli* against test common antibiotics revealed that most of the strains are resistant against wide variety of antibiotics tested, suggesting that the test isolates are multidrug resistance (MDR). Interestingly the disc containing **1a** produces a significant zone of growth inhibition between 17.7-15.2 mm and 15.9-13.3 mm against *S. aureus* and human isolates of MRSA respectively. However, some lower disc potency with 1b produced zone diameter (12.5-8.0 mm) and (8.5-7.2 mm) against the same organisms (**Table 5.1**). Diameters of growth inhibition zones of the tested microorganisms were measured and compared to ciprofloxacin and amoxicillin, used as standard reference drugs.

Growth inhibition study with determination of MIC of the test compounds

The minimum inhibitory concentration (MIC) of the **1a** was found to be 250-300 µg/ml against *S. aureus* standard strain, 150-200 µg/ml against MRSA, 550-600 µg/ml against *E. coli* ATCC 25922, 175-225 µg/ml against *CONS*, when inoculum size was 10^6CFU/ml (**Table 5.1**). From the results of the susceptibility study, it is clear that **1c** and **1d** have antimicrobial activity in moderate high concentrations against the selected bacteria (**Table 5.1**). However, further antibacterial study was carried out with **1a** and **1b** as it has better activity against the selected species.
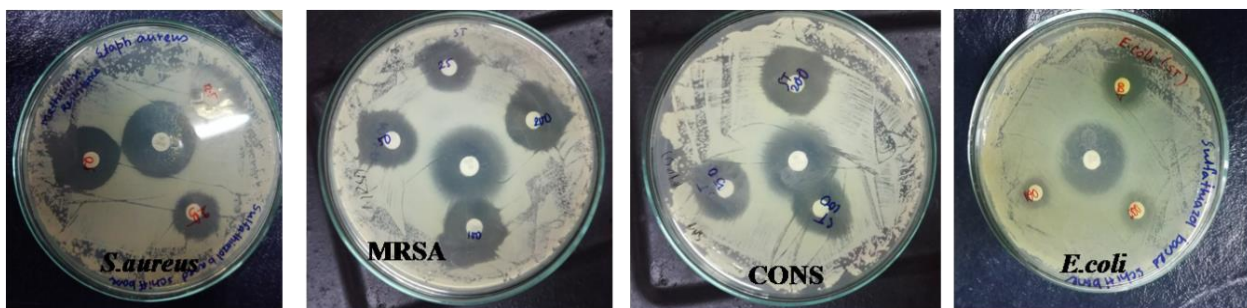
Fig. **5.16** Zone of inhibition of four bacterial isolates against **1a**.
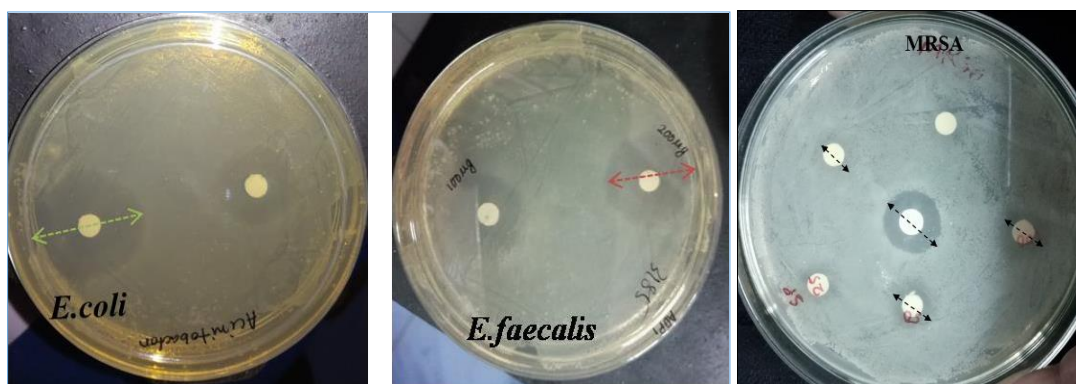
Fig. **5.17** Zone of inhibition of three bacterial isolates against **1b**.
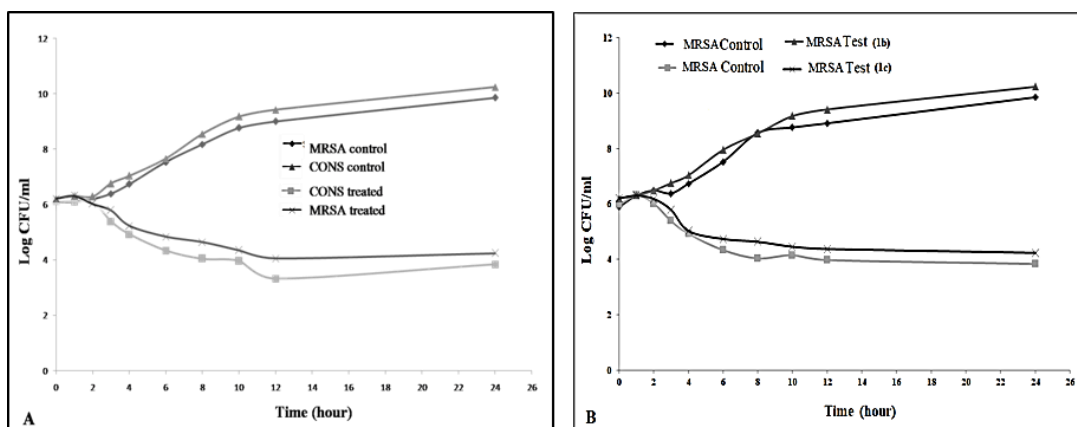
Fig. 5.18 Growth curve of MRSA and CONS in presence or absence of 1a **(A)**, 1b and

1c **(B)**.

Mechanistic insights of antibacterial activity of the test compound 1a

Surface morphology of the bacterial cell wall was examined by SEM analysis; the surface

structure alterations at sub-cellular level of magnification and comparative assessment of

the effect of the drug, **1a** was used to suggest the plausible mechanism of action. Quality

control strain of Gram-negative *E. coli* (MDR) is highly sensitive to **1a**. The Electron

Micrograph demonstrated rod-shaped bacteria with normal topology and morphology in

untreated control; while the bacteria treated with **1a** showed altered ultra-structure, as

presented in **Figure 5.19**, compared to the untreated control, under 25000X

magnification of SEM [39].
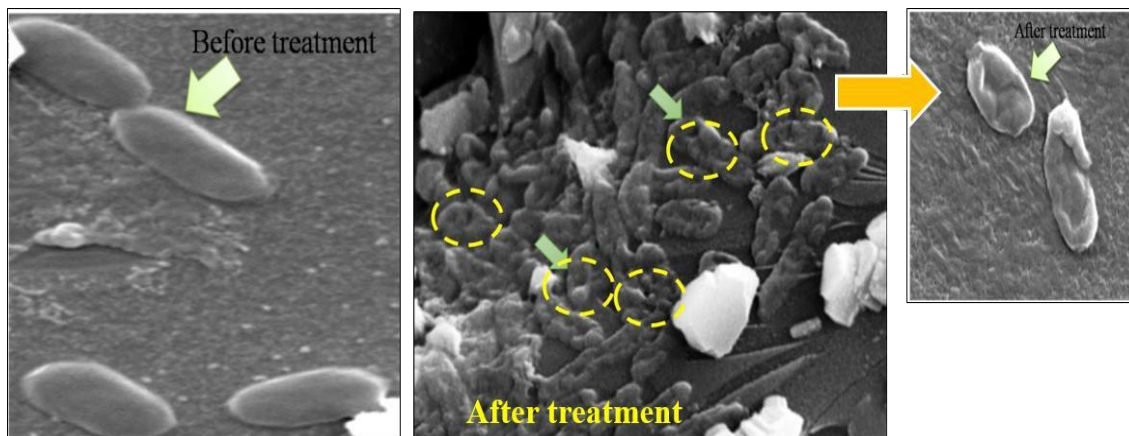
Fig. 5.19 Cellular morphology of untreated *E. coli*; and **1a** treated *E. coli* cells at MIC by FE-SEM.

The antimicrobial activity spectrum of Schiff's bases against a few Gram-positive and Gram-negative bacterial isolates was evaluated by disc diffusion assay is presented in **Table 5.1**. Overall, we found that the sulfapyridine-based Schiff base (**1a**) exhibited the highest antibacterial activity, with inhibitory activity against *S. aureus* proliferation similar to the positive control. Thus, these complexes could reasonably be used in planning more effective antibacterial agents for the treatment of some common diseases caused by *E. coli*, *S. aureus*, MRSA, CONS.

Molecular Docking Study

To realize the effect of the investigating compounds on their anti-bacterial activities, molecular docking was used. Commonly, sulphonamide drugs can inhibit dihydropteroate synthetase enzyme. It is the reason for the choice of the dihydropteroate synthetase (PDB id: 1DHS) for molecular docking study in this case. The study shows that the coumarin derivative of known sulphonamide drugs have higher binding ability with respect to the corresponding sulphonamide drug. All the binding energy data have been tabulated in the following table 5.2. Based on the binding energy, the compound **1a**

154

was found to be the best. The theoretical observation also corroborate with the

experimental results.

Table 5.2: Binding energy of sulphonamide drugs and their coumarin derivatives obtained from their molecular docking with the dihydropteroate synthetase.

Compound	ΔG (kcal/mol)	Compound	ΔG (kcal/mol)
8-formyl-7-hydroxy-4-methylcoumarin	-5.8		
Sulfathiazole	-5.6	Sulfamethoxazole	-5.9
1b	-7.3	**1c**	-7.5
Sulfapyridine	-5.8	Sulfamerazine	-6.1
1a	-7.7	**1d**	-7.4
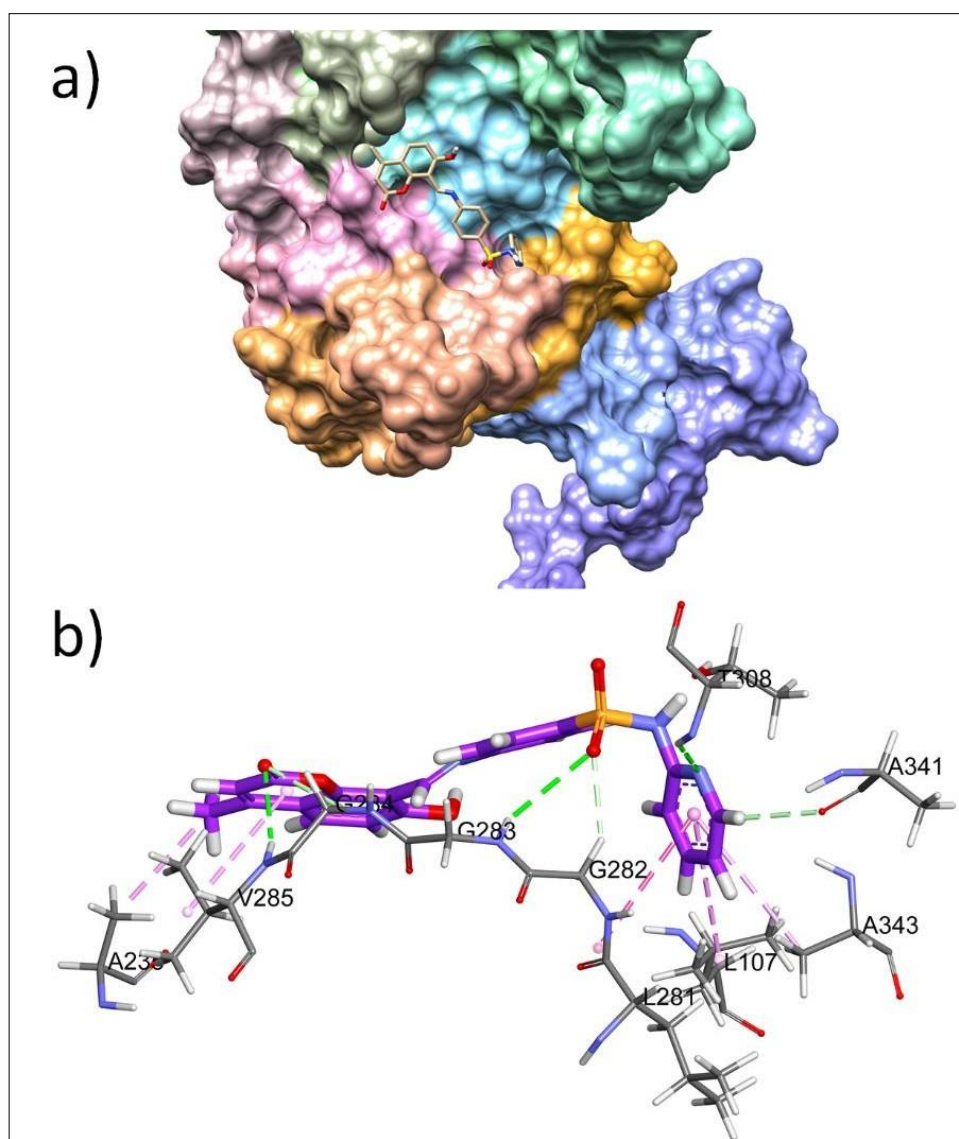
Fig. 5.20 (a) Docking pose of **1a** with DHPS and (b) non-covalent interactions between **1a** and DHPS.

5.4 Discussion

After tetracyclines, second broadly used class of veterinary antibiotics are Sulfa drugs [40]. Sometimes these agents are used to treat human diseases, but more commonly used in veterinary medicine, especially on animal and fish farms. However, the spread of antibiotic resistance has raised questions about the environmental implications of sulfonamides [41, 42]. Haemolytic streptococcus has been treated with sulfapyridine and sulfathiazole, which are used here as the precursor molecules of 1a and **1b**, respectively [43]. Additionally, Zhu *et al*. reported the fungicidal activity of macrolactones and macrolactams with a Sulfonamide side chain [44, 45]. The Sulfonamide family of compounds is known to cause several toxic symptoms, including anorexia, dizziness, mental confusion, nausea, cyanosis, dermatitis, and hepatitis [46]. In addition, coumarin analogues have antibacterial properties as well, which is consistent with our findings that our synthetic compounds can be effective against both Gram-positive and Gram-negative bacteria [47]. Moreover, coumarin analogues had been reported for other antibacterial activities which were consistent with our result that it could increase the activity against both Gram-staining positive and Gram-negative bacteria. Thus, we can conclude that the antimicrobial activities of different types of sulfonamide derivatives might be related to their structure-activity relationship. Upon binding to the cell membrane, **1a** is internalized in *E. coli* (MDR) cells and damages the cellular integrity, as shown in the SEM study of the test bacteria. On the other hand, compound **1a** binds at the nicotinamide-adenine-dinucleotide binding site of the DHPS protein. The site is on the surface of the protein (5.20.a). Coumarin C=O, sulphonamide S=O and pyridine nitrogen are involved in hydrogen bonding with V285, G283, and T308, respectively. The first two fragments are also found in non-classical hydrogen bonding with G284 and G282, respectively. Amino acid residue A341 interact with pyridine hydrogen through non-

classical hydrogen bonding. Other aromatic parts of the molecule interact with A238, V285, G282, L281, L103, and A343 with the help of π-stacking, π-alkyl, and hydrophobic interactions respectively.

5.5 Conclusion

Antibiotics became one of the great discoveries of 20th century. But the reality is the rise of antibiotic resistance in hospitals, communities, and the environment concomitant with their use. The MTT assay indicates that our synthesized compounds are relatively low-toxic and the four novel Schiff bases of sulfonamides are moderately safe. Compared to parent sulfonamide, their cytotoxic efficacy was much better in the *in vitro* study. Their effectiveness against MRSA and CONS shows that they work much better than parent Sulfa drugs. We therefore conclude that our synthesized biocompatible **1a** is a promising agent against a wide range of multidrug-resistant bacterial infections that plague our society today.

5.6 References

[1]   D. Kahne, C. Leimkuhler, W. Lu and C. Walsh, *Chem. Rev.*, 2005,**105**, 425–48.

[2]   C. Walsh and T. Wencewicz, Antibiotics: Challenges, Mechanisms, Opportunities, ASM Press, Washington, DC, USA, 2016, 16–32.

[3]   P.A. Lambert, *Adv. Drug Deliv. Rev.*, 2005, **57**, 1471–85.

[4]   R.J. Fair and Y. Tor, *Perspect. Medicinal Chem.*, 2014, **6**, 25–64.

[5]   S. Sengupta, M.K. Chattopadhyay and H.P. Grossart, *Front. Microbiol.*, 2013, **4**, 47.

[6]   I.M. Gould and A.M. Bal, *Virulence*, 2013, **4**, 185–191.

[7]   D. Domagk, *Ann NY Acad Sci.,* 1957, **69**, 380–384.

[8]   M. Wainwright and Jette E. Kristiansen, *Dyes and Pigm.*, 2011, 88, 231–234.

[9]   G. Domagk, Chemotherapie der streptokokken-infektionen *Klin Woch.,* 1936, **15**, 1585–1590

[10]   J.E. Lesch. The first miracle drugs: how sulfa drugs transformed medicine. *New York: Oxford University Press,* 2007*, 364*.

[11]   D. Kishore and A. Pareek. *Int. J. Pharma and Biosciences*., 2013, **4**, 812-820.

[12]   R.L. Then, *Rev. Infect. Dis.*, 1982, **4**, 261–269.

[13]   O. Sköld, *Drug Resist. Updat.*, 2000, **3**, 155–160.

[14]   D. J. Naisbitt, J. Farrell, F.S. Gordon, L.J. Maggs, C. Burkhart, J.W. Pichler, M. Pirmohamed and K.B. Park*, Mol. Pharmaco.*, 2002, **62**, 628–637.

[15]   M. Abdul Qadir, M. Ahmed and M. Iqbal. *Biomed Res. Int.*, **2015**, 2015.

[16] P. Bhaiya, S. Roychowdhury, P. M. Vyas, M. A. Doll, D. W. Hein and C. K. Svensson, *Toxicol. Appl. Pharmacol.*, 2006, **215**, 158-167.

[17] I.R. Ezabadi, C. Camoutsis, P. Zoumpoulakis, A. Geronikaki, M. Soković, J. Glamočilija and A. Ćirić, *Bioorg. Med. Chem.*, 2008, **16**, 1150–1161.

[18] Z.H. Chohan, A.U. Shaikh, A. Rauf and C.T. Supuran. *J Enzyme Inhib Med Chem.* 2006, **21,** 741–748.

[19] T. M. Pereira, D.P. Franco, F. Vitorio and A. E. Kummerle. *Curr. Top. Med. Chem.*, 2018, **18**,124–48.

[20] K.P. Barot, S.V. Jain, L. Kremer, S. Singh and M. D. Ghate, *Med Chem Res.*, 2015, **24**, 2771–2798.

[21] M. Saleem, M. Nazir, M.S. Ali, H. Hussain, Y.S. Lee, N. Riaz and A. Jabbar, *Nat. Prod. Rep.*, 2010, **27**, 238–54.

[22] Y.M. Yu, The antibacterial effects and mechanism of several botanical compounds against *Ralstonia solanacearum* (Doctoral dissertation, Master's Thesis, Southwest University, Chongqing, China). 2015.

[23] M. El-Gaby, Y.A. Ammar, M. IH El-Qaliei, M.A. Ali, F. Hussein M and A.F. Faraghally, *Egypt. J. Chem.*, 2020, **63**, 5289–327.

[24] H. Schiff, *Annal. Chem.*, 1864, **131**, 118–119.

[25] A.A. Numan, Synthesis and biological activity of Some amino acid and Barbituric acid derivatives via Schiff's bases (Doctoral dissertation, Ministry of Higher Education), 2008.

[26] S.B. Desai, P.B. Desai and K.R. Desai, *Heterocycl. Comm.*, 2001, **7**, 83–90.

[27] T.Y. Fonkui, M.I. Ikhile, D.T. Ndinteh and P.B. Njobeh, *Trop. J. Pharm. Res.*, 2018, **17**, 2507–2518.

[28] P.G. More, R.B. Bhalvankar and S.C. Pattar, *J. Indian Chem. Soc.*, 2001, **78**, 474–475.

[29] M. P. Crespo, N. Woodford, A. Sinclair, M. E. Kaufmann, J. Turton, J. Glover, J. D. Velez, C.R. Castaneda, M. Recalde and D.M. Livermore, *J. Clin. Microbiol.*, 2004, **42**, 5094–6101.

[30] T.D. Gootz and A. Marra. *Expert Rev. Anti Infect. Ther.*, 2008, **6**, 309–325.

[31] C. Patra, A.K. Bhanja, C. Sen, D. Ojha, D. Chattopadhyay, A. Mahapatra and C. Sinha, *Sens. Actuators B Chem.*, 2016, **228**, 287–294.

[32] Clinical and Laboratory Standards Institute. Performance Standards for Antimicrobial Disk Susceptibility Tests. Approved Standards. CLSI document M2-A7. Wayne, Pa, USA, 2001.

[33] Clinical and Laboratory Standards Institute (CLSI), Fifteenth International Supplement, CLSI Document M100-S15, CLST, Wayne, pa, USA, 2005.

[34] D. Chattopadhyay, S. G. Dastidar and A. N. Chakrabarty, *Arzneimittel Forschung.*, 1988, **38**, 869–872.

[35] D. Chattopadhyay, B. Sinha and L.K. Vaid, *Fitoterapia.*, 1998, **69**, 365–367.

[36] D. Chattopadhyay, K. Maiti, A.P. Kundu, M.S. Chakrabarty, R. Bhadra, S.C. Mandal and A.B. Mandal, *J. Ethnopharmacol.*, 2001, **77**, 49–55.

[37] J. May, K. Shannon and A. King, *J. Antimicrob. Chemother.*, 1998, **42**, 189–97.

[38] P. Bag, D. Chattopadhyay, H. Mukherjee, D. Ojha, N. Mandal, M.C. Sarkar, T. Chatterjee, G. Das and S. Chakraborti, *Virol. J.*, 2012, **9**, 98.

[39] P.D. Lister, D.J. Wolter and N.D. Hanson, *Clin. Microbiol. Rev.*, 2009, **22**, 582–610.

[40] A. K. Sarmah, M.T. Meyer and A.B.A. Boxall, *Chemosphere.*, 2006, **65**, 725–759.

[41] H. Heuer and K. Smalla, *Environ. Microbiol.*, 2007, **9**, 657–666.

[42] H. Schmitt, H. Haapakangas and P. van Beelen, *Soil Biol. Biochem.*, 2005, 37, 1882–1892.

[43] E.A. Bliss and E. Ott, *Proceedings of the Society for Exp. Bio. Med.*, 1940, **43**, 706–709.

[44] W. J. Zhu, P. Wu, X.M. Liang, Y.H. Dong, J.J. Zhang, H.Z. Yuan, S.H. Qi, X.Q. Meng, J. P. Wu, F. H. Chen and D. Q. Wang, *J. Agric. Food Chem.*, 2008, **56**, 6547–6553.

[45] K. Rehman, S. H. Kamran and M. S. Akash, In Antibiotics and Antimicrobial Resistance Genes in the Environment, *Elsevier*, 2020, 234–252.

[46] W. R. Taylor and N.J. White, *Curr. Drug Saf.*, 2004, **27**, 25–61.

[47] C. L. Céspedes, J.G. Avila, A. Martínez, B. Serrato, J.C. Calderón-Mugica and R. Salgado-Garciglia, *J. Agric. Food Chem.*, 2006, **54**, 3521–3527.

Chapter 6

Structural characterization and biological studies of Au (III) complex of 2-(3-phenyl-1H-1, 2, 4-triazol-5-yl) pyridine

Abstract

2-(3-Phenyl-1H-1, 2, 4-triazol-5-yl) pyridine acts as bidentate N, $N^{/}$-chelator and forms Au(III) complex, [**Au** (2-ptp)$_2$]Cl (**1**). The structure has been characterized by single-crystal X-ray diffraction technique and other spectroscopic data. Presence of different noncovalent interactions leads to the formation of 3D supramolecular structure. The complex **1** exhibits antibacterial activity against Gram-positive (MIC) (*Staphylococcus aureus* (240 µg/ml), *Bacillus subtilis* (645 µg/ml) and Gram-negative (*Escherichia coli* (270 µg/ml), *Enterococcus faecalis* (820 µg/ml), *Klebsiella pneumonia* (785 µg/ml)) bacteria. Also, the toxicity of **1** has been checked by MTT assay. The complex shows promising anticancer activity against Vero cells and the CC$_{50}$ is 405 µg/mL.

6.1 Introduction

1,2,4-Triazole and its derivatives are potential pharmacological agents and show many biological activities like herbicidal, insecticidal, antifungal, anticancer properties [1]. Pyridyl substituted triazoles offer a planar aromatic system of strong π−π stacking and have been used to synthesize metal complexes with various geometries [2]. Triazole is an exceptional building block to constitute coordination polymer and supramolecular geometries like cages, cylinders etc. along with diverse applications in catalysis, drug development, metal ion sensing, imaging etc. [3-7]. Au(III) chemistry of polydentate N-heterocycles is an under developing research area compared to their Au(I) counter parts [8, 9] along with other coinage metals [10]. The square planar Au (III) complexes may have a higher ability to intercalate into the DNA structure than linear structure of Au (I) complex and might have high biological efficiency [11-15]. In this work, 2-(3-phenyl-1H-1, 2, 4-triazol-5-yl) pyridine (2-ptp) has been used to synthesize Au (III) complex and the single crystal diffraction analysis is used for the confirmation of the structure where ligand, 2-ptp, acts as bidentate chelating ligand. The complex has been used to examine the antimicrobial property and out of five bacteria two stains (*Staphylococcus aureus* (240 μg/ml), *Escherichia coli* (270 μg/ml)) show better efficiency.

6.2 Experimental Section

6.2.1 Materials and Methods

The chemicals were purchased from Sigma–Aldrich ($HAuCl_4$, $3H_2O$; 2-Cyanopyridine; H_2N-NH_2), TCI (N, N-Dimethyl formamide (DMF), Acetonitrile, MeOH, Dimethylacetamide (DMA), Ethylene glycol) and were used as received. The ligand, 2-(3-Phenyl-1H-1,2,4-triazol-5-yl)pyridine (2-ptp) was prepared in two steps following reported method [16] $KAuCl_4$ was prepared from $HAuCl_4$ by adding KCl in aqueous

solution as per reported procedure and further purified by crystallization from aqueous solution.

Micro–analytical data (C, H, N) were collected on Perkin-Elmer 2400 CHNS/O elemental analyzer. Spectroscopic data were obtained using the following instruments: FTIR spectra (KBr disk, 4000–400 cm^{-1}) from a Perkin Elmer RX–1 FTIR spectrophotometer. Electronic absorption spectra were recorded on a PerkinElmer UV/VIS Spectrophotometer (LAMBDA 35). NMR spectra were measured on Bruker 300 MHz spectrometer for 1H NMR. X-Ray powder diffraction was performed using a Bruker D8 ADVANCE X-ray diffractometer. Scanning electron microscope (SEM) and energy dispersive X-ray (EDX) were collected from ZEISS EVO-MA 10 having resolution of 3 nm with W filament and Sb as sources, Operated at EHT = 15 kV, WD = 8.5 mm and mag = 2.51–30 K. The absorption spectrum of synthesized material was recorded using a UV-Vis spectrophotometer (Perkin Elmer, Lambda 365). Thermal analysis (TGA) was carried out on a Perkin-Elmer Pyris Diamond TG/DTA thermal analyzer under nitrogen atmosphere (flow rate: 50 cm^3 min^{-1}) at the temperature range of 30−800°C with a heating rate of 10°C/ min.

6.2.2 Synthesis of 2-(3-Phenyl-1H-1, 2, 4-triazol-5-yl) pyridine (2-ptp)

The ligand was prepared in two steps following reported method [16].
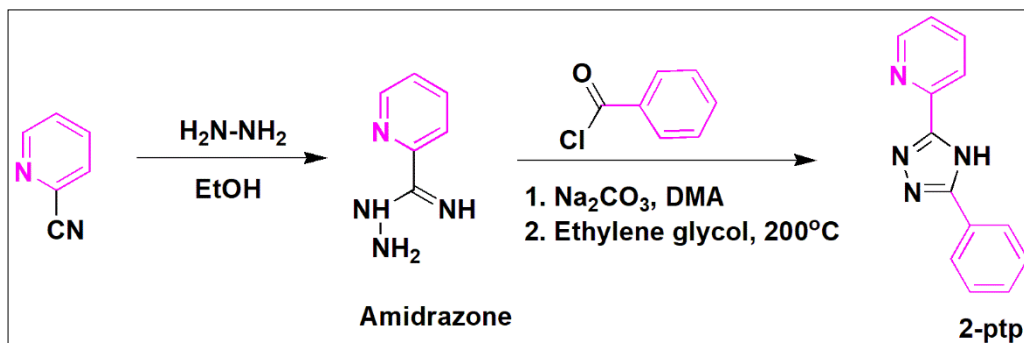
Scheme 6.1. Synthetic key route of **2-ptp.**

6.2.3 Synthesis of Complex, [Au (2-ptp)₂] Cl, 1

KAuCl₄. 2H₂O (0.2 mmol, 0.083 g) was dissolved in acetonitrile (10 ml) solution in a round bottom flask and reflux for 30 min followed by the addition of 2-(3-phenyl-1H-1,2,4-triazol-5-yl) pyridine (2-ptp) (0.2 mmol, 0.045 g) in methanol. Upon refluxing the reaction mixture for 4 h yellow precipitate was appeared, which filtered and dried than the powered product was soluble in DMF for crystallization. After 9-10 days yellow rod-shaped crystalline compound (0.054 g, yield 65%) was isolated and taken for single crystal X-Ray diffraction measurement. Elemental analysis calculated for $C_{26}H_{18}AuClN_8O_4$ (**1**) : C, 41.37; H, 2.36; N, 15.44; Found: C, 41.44; H, 2.41; N, 15.30 %. IR (KBr pellet, cm^{-1}): 3106, $v_{(Aromatic\ N-H)}$;1622, $v_{(Aromatic\ ring,C=N)}$ (**Figure 6.1a, 6.1b**). ^{1}H-NMR (300 MHz, CDCl₃) spectrum are summarized in **Figure 6.2 and 6.3**.
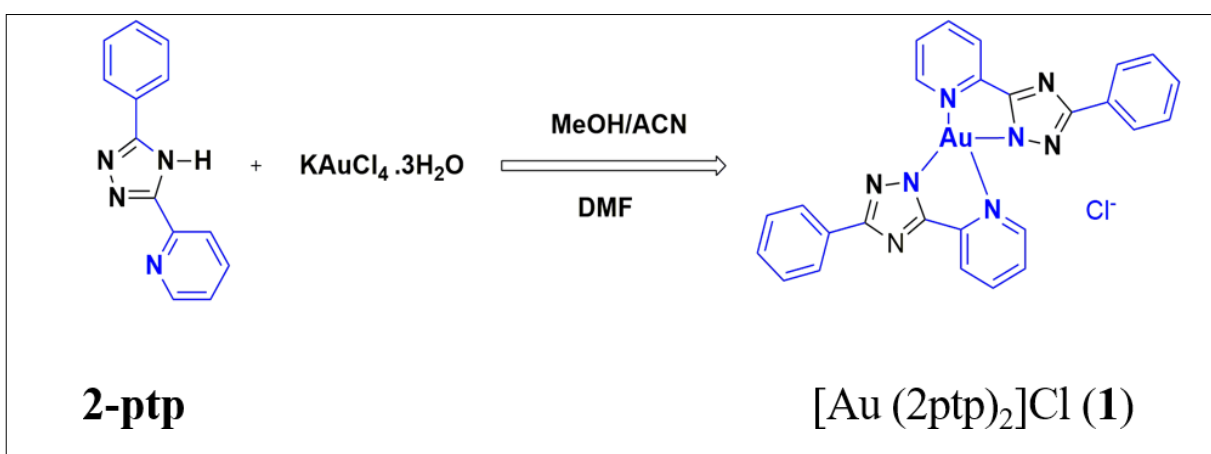
Scheme 6.2. Synthetic key route of [Au (2ptp)₂] Cl (**1**)

6.2.6 X-ray Crystallography

A rod-shaped yellow-colored single crystal of complex **1** was taken for Single X-Ray Diffraction data collection using a Bruker SMART APEX-II CCD diffractometer furnished with graphite-monochromatic Mo-Kα radiation (λ=0.71073 Å). The structure of the complex was solved with the direct method and was refined by full-matrix least

squares on F^2 using the SHELXL-2016/6 [17] program package. The non-hydrogen atoms present in the architecture were well-refined with an isotropic thermal parameter. The hydrogen atoms were positioned in their geometrically idealized positions and controlled to ride on their parent atoms. Least squares refinements of all reflections within the hkl range $-43 \leq h \leq 43$, $-16 \leq k \leq 16$, $-16 \leq l \leq 16$ were utilized to carry out the unit cell parameters and crystal-orientation matrices. Collected data ($I > 2\sigma(I)$) of crystal was integrated by employing the SAINT program [18] and the absorption correction was performed through SADABS [19]. The crystallographic data and refinements are briefly given in the Table **6.1**.

Table **6.1**. Crystal data and refinement parameters for complex **1**.Complex	Complex**1**
CCDC No.	2078225
empirical formula	$C_{26}H_{18}AuClN_8O_4$
formula weight	738.90
crystal system	Monoclinic
space group	$C2/c$
a(Å)	33.688(4)
b(Å)	12.5276(14)
c(Å)	13.2293(15)
$\beta(^o)$	103.069(3)
V(Å^3)	5438.6(11)
T(K)	298(2)
Z	8
D_{calcd}(Mg/m^3)	1.851
μ(mm^{-1})	5.562
λ(Å)	0.71073
θ range (°)	1.740-27.131
total reflections	6007
unique reflections	4787
refine parameters	370
R_1^a [$I > 2\sigma$ (I)]	0.0401
wR_2^b	0.1360
goodness-of-fit	0.990

$^aR_1=\Sigma||F_o|-|Fc||/\Sigma|F_o|$, $^bwR_2=[\Sigma w\ (F_o^2-Fc^2)^2/\Sigma wF_o^2)^2]/2$, $w = 1/[\sigma^2(Fo^2) + (0.0350P)^2 + 0.9811P]$, where P= $(F_o^2 +2Fc^2)/3$

6.2.4 Biological Applications

6.2.4.1 Antibacterial Activity

The compounds (**2-ptp** and [Au(2-ptp)$_2$]Cl (**1**)) were screened for antibacterial activity against Gram positive [*Staphylococcus aureus* (ATCC 25923), *Bacillus subtilis* (ATCC 14579)], and Gram-negative bacteria [*Escherichia coli* (ATCC 25922), *Enterococcus faecalis* (ATCC 29212) and *Klebsiella pneumoniae* (ATCC 700603)] at the concentrations of 1000, 500, 200, 100, 50, 25, 12.5 μg/ml. Antibacterial susceptibility was determined by disk-diffusion assay described by Kirby-Bauer, following the guidelines of Clinical and Laboratory Standard Institute [20]. For disc diffusion assay 1.0 ml of inoculum (1.8 × 10^6 CFU/ml) of respective bacteria from an overnight culture, was spread evenly on dried sterile MHA plates at room temperature, and incubated for 30 min at 37°C. The stock solution of ligand and the complex **1** were prepared by using 0.01% of DMSO solution and then the disc was placed aseptically on the inoculated plates, with antibiotic disc as controls, in triplicate [21]. The plates were incubated at 37°C overnight, and the sensitivity was recorded by measuring the clear zone of growth inhibition (in mm) on agar surface around the discs.

6.2.4.2 Determination of Cytotoxicity by MTT Assay

The toxicity test was carried out by MTT (3-[4,5-dimethylthiazol-2-yl]-2,5 diphenyltetrazolium bromide) assay on an African green monkey kidney cell, known as Vero cell. The cells were cultured onto 96-well plates at 10 × 10^6 cells per well and different concentrations at a final volume of 100 μl, in triplicate using DMSO (0.1%) as a negative for the **2-ptp** and the complex **1**. The remaining part of the assay was done according to the literature procedure [22]. Data were calculated as the percentage of cell viability by the formula:

168

$$\text{The percentage of cell viability} = \frac{\text{(Sample absorbance cell free sample blank)}}{\text{(Mean media control absorbance)}} \times 100$$

6.2.5 DFT Computation

To explain the spectral findings of the ligand and complex, DFT and TD-DFT calculation were conducted. The molecular geometry of ligand and Au-complex were optimized with coordinates obtained from structural formula and single crystal structure respectively, using DFT/B3LYP method with LanL2MB as basis set of Gaussian Program Package 09 [23-25]. The vibrational frequency related calculation has been completed to confirm that the optimized geometries are represented the local minima and the only positive Eigen values are taken. Gauss-sum calculation was carried out for the fractional contribution of groups of molecular components to the Molecular orbitals [26].

6.3 Results and Discussion

6.3.1 Structural description of Au (III) complex (1)

The analysis of Single Crystal X-Ray Diffraction data revealed that the Au(III)-complex crystallizes in Monoclinic crystal system having space group C2/c and Z=8. The structure is distorted square planar about Au(III) with AuN_4 coordination sphere where two **2-ptp** ligands are chelated with the triazolyl-N and pyridyl-N centres and Au is placed at the distorted square centre. Positive charge of the complex is neutralized with Cl^- counter ion. Water of crystallization also appears in the structure. The ligand shows the chelate binding mode of two **2-ptp** ligands around the central Au(III) ion (Au01-N1, 1.981(6); Au01-N5, 1.991(6); Au01-N8, 2.043(5); Au01-N4, 2.043(6) Å) and the corresponding bond angles N1-Au01-N5, 178.9(2)°; N1-Au01-N8, 99.9(2)°; N5-Au01-N8, 79.4(2)°; N1-Au01-N4, 79.7(2)°; N5-Au01-N4, 100.9(2)°; N8-Au01-N4, 178.34(19)° (**Table 6.2**). The bond parameters are comparable with reported data of Au (III)-N (sp^2) chelated system [10].

169
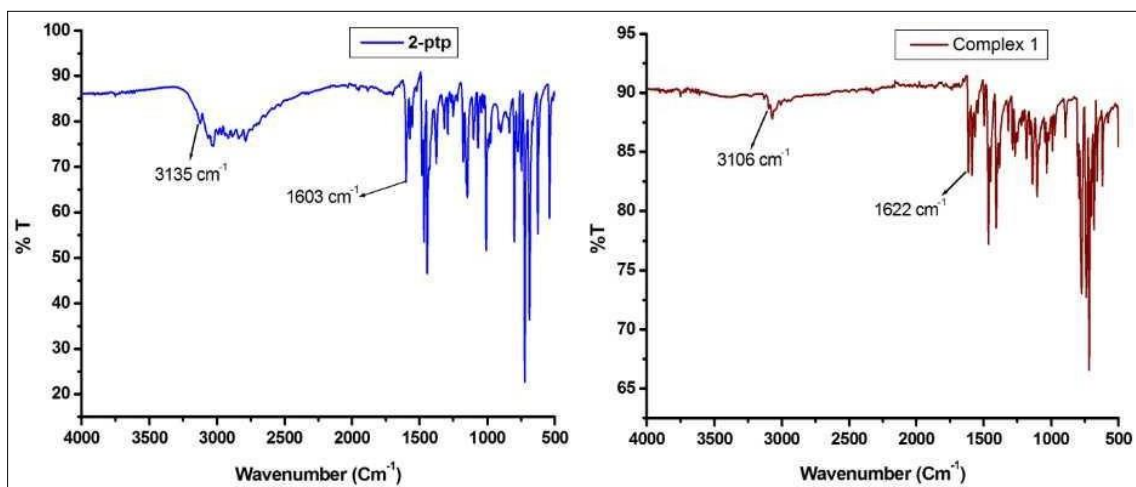
Figure 6.1 IR spectroscopy of **(a)** 2-(5-Phenyl-2H-1, 2, 4-triazol-3-yl) pyridine (**2-ptp**) and **(b) Complex 1**.
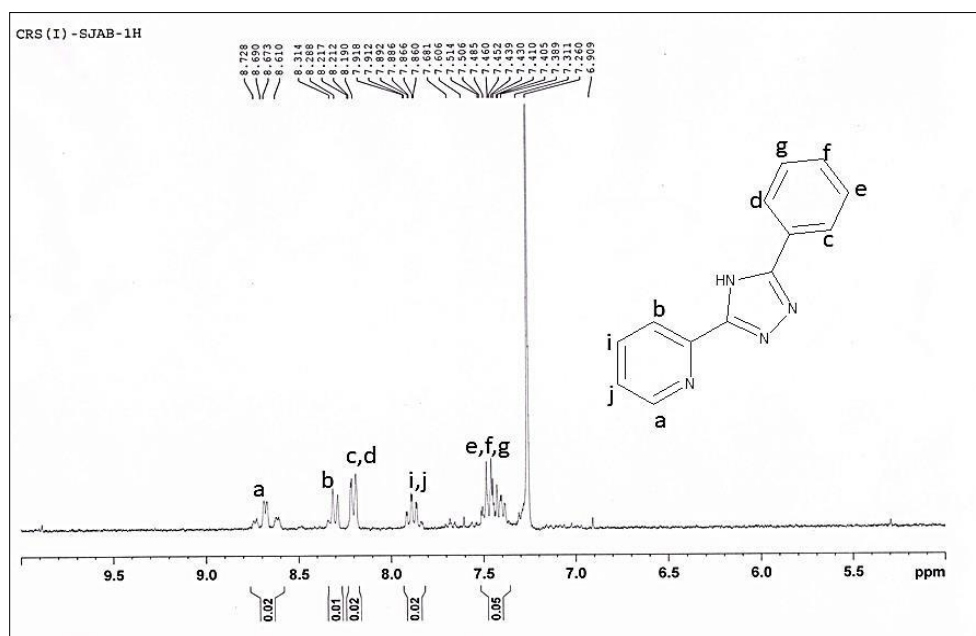
Figure 6.2 ^{1}H-NMR spectroscopy of 2-(3-phenyl-1H-1, 2, 4-triazol-5-yl) pyridine (**2-ptp**).
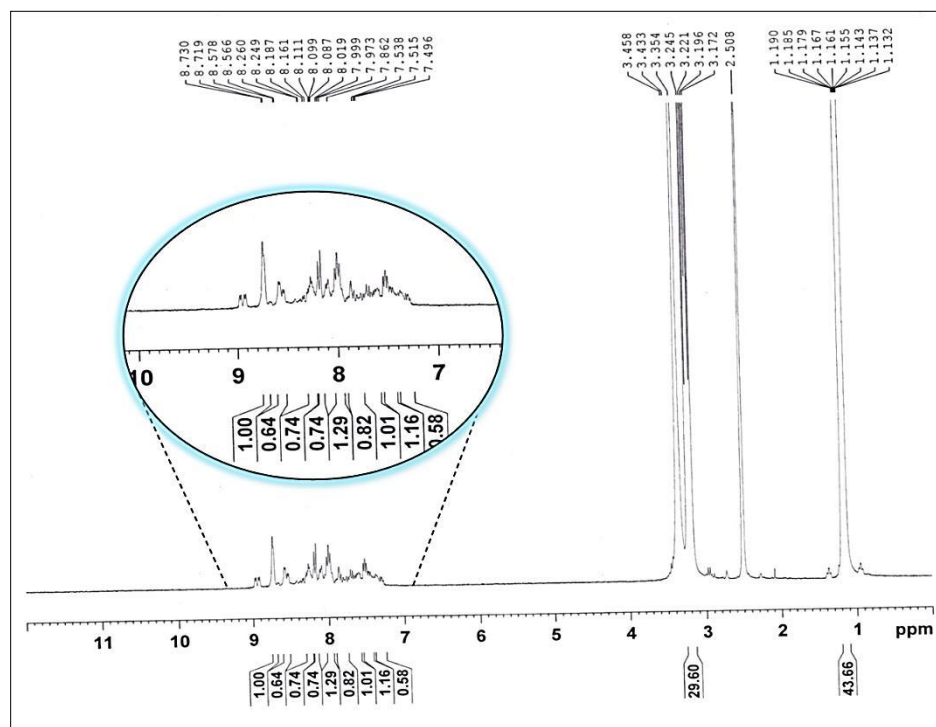
Figure 6.3 ^{1}H-NMR spectroscopy of Au (III) Complex 1.

Table 6.2. List of selected bond lengths and bond angles of Complex**1**.

Complex 1			
Bond Lengths	(Å)	Bond Angles	(°)
Au01-N1	1.981(6)	N1-Au01-N5	178.9(2)
Au01-N5	1.991(6)	N1-Au01-N8	99.9(2)
Au01-N8	2.043(5)	N5-Au01-N8	79.4(2)
Au01-N4	2.043(6)	N1-Au01-N4	79.7(2)
		N5-Au01-N4	100.9(2)
		N8-Au01-N4	178.34(19)
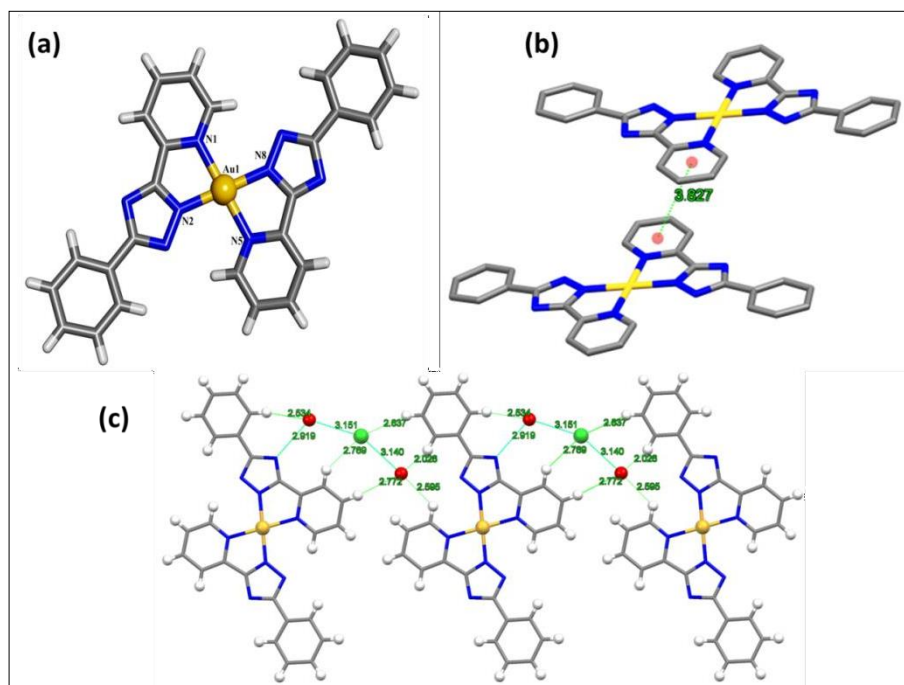
Figure 6.4 (a) Single unit of complex **1** (solvent molecules removed for clarity), **(b)** intermolecular π−π stacking between two consecutive Au (III) complex, and **(c)** supramolecular assembly *via* Cl⁻ and guest water molecules.

Hydrogen bonding interactions of **2-ptp** (pyridyl and pendant Phenyl rings) (C00H-H---O(H₂), 2.032 Å and C00P-H00P, 2.777 Å) and O-atom(O4) of aqua molecule and also the secondary interactions of Cl⁻ at 2.826 Å (H00X···Cl1) and 2.770 Å (H00U···Cl1) make higher dimensional supramolecular geometry. Again, the pyridyl rings are arranged in parallel manner to make π···π interactions ensuring distance 3.827 Å. Therefore, these non-covalent interactions construct supramolecular assembly and induces flexible cavity.
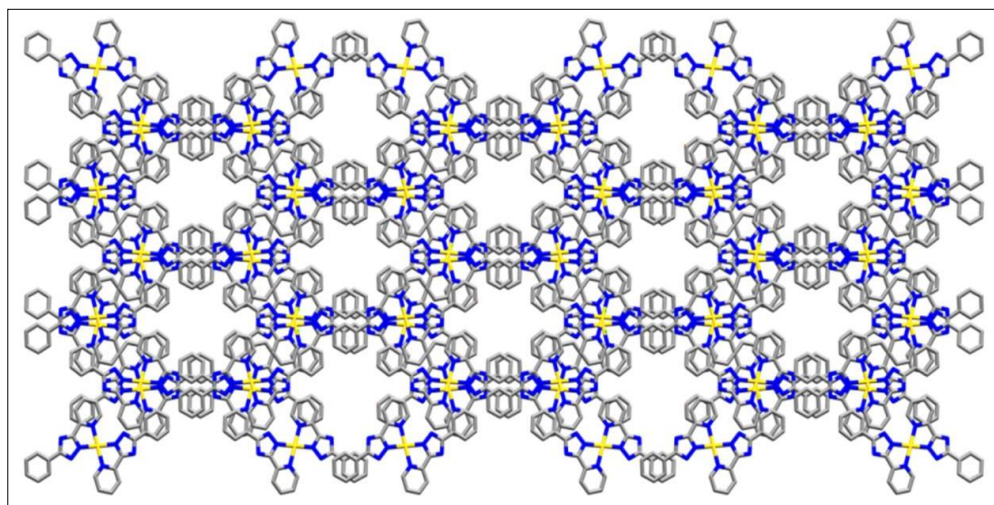
Figure 6.5 Supramolecular aggregated 3D packing of **1**.

6.3.2 Thermal stability and Morphology Analysis

The thermal stability of **1** was verified by thermo-gravimetric-analyses (TGA) within the temperature range of 32-800°C under an N_2 atmosphere (**Figure 6.6**). TGA analysis reveals that after significant loss of water molecules at the temperature of 84°C the complex**1** attains the plateau of the stable region of the structure up to ~210°C. Bulk purity of the synthesized crystalline gold complex was verified by PXRD analysis and shows the most of the crystalline phases were well matched with the simulated pattern (**Figure 6.7**).
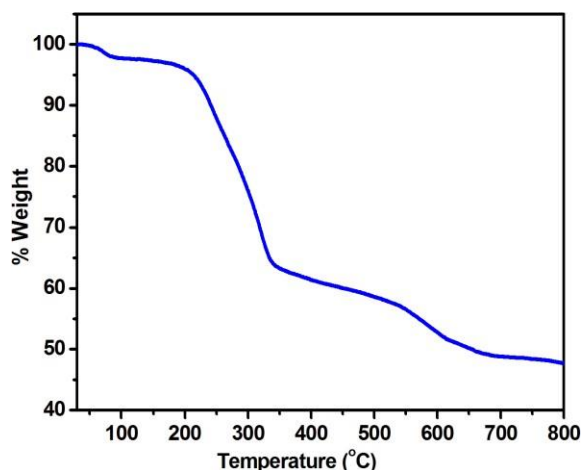
Fig.6.6 TGA plot of {[Au (2-ptp)]$_2$·(H$_2$O)$_4$·Cl} (complex **1**)
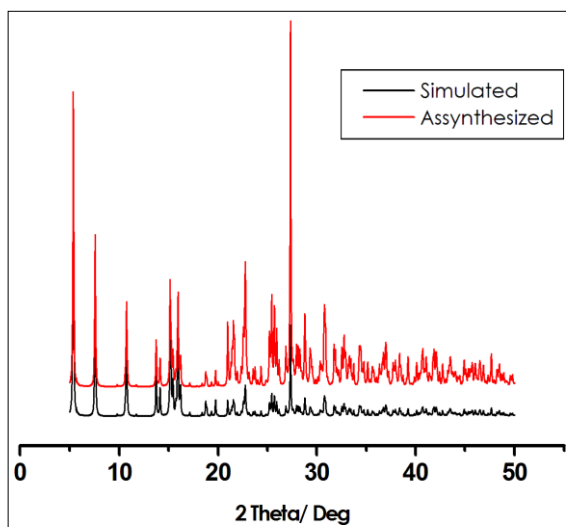
Fig. 6.7 PXRD plot of complex **1.**

The SEM images of **1** were captured using crystalline samples (**Figure 6.9a and 6.9b**) followed by well grinded powder samples (**Figure 6.9c** and **6.9d**). Well organized structure of complex **1** was confirmed from the microphotographs in which flower like structure and aggregations endowed prevalence of noncovalent interactions within the supramolecular microstructures. In addition, presence of Au (III) has been confirmed from EDX spectrum (**Figure 6.8**). Additionally, morphology of pulverized material shows variable nano-sized particle (**Figure 6.9c** and **6.9d**) that insisted to use for biological applications, such as antibacterial activity, microbial action detector, and cancer cell treatment.
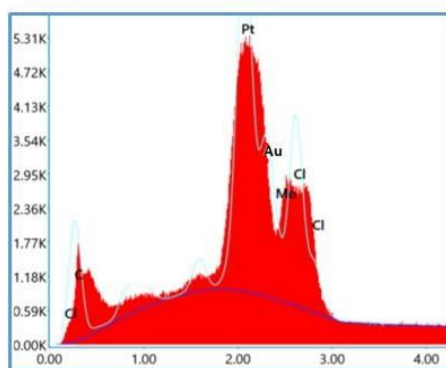
Fig. 6.8 EDX spectrum of Complex **1**.

174
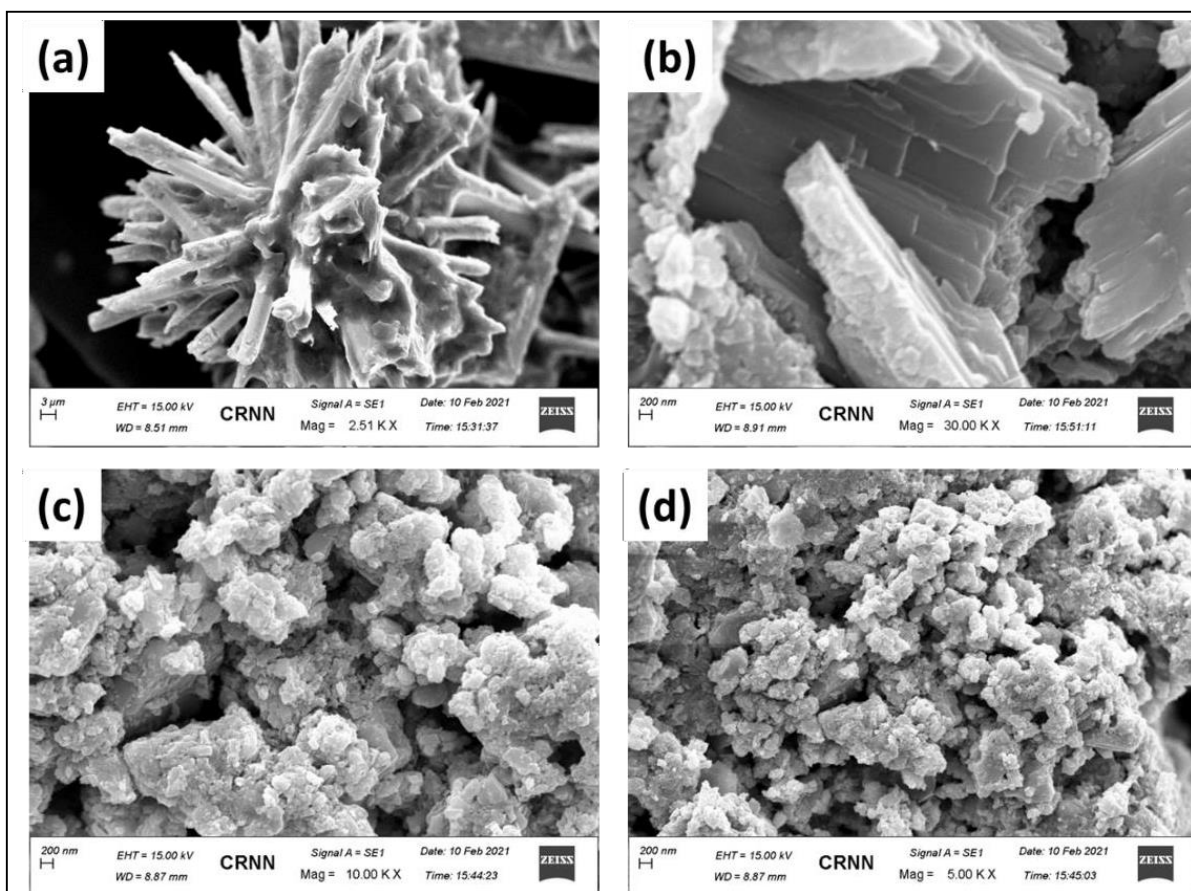
Fig.6.9 SEM microphotographs of (**a, b**) crystalline and (**c, d**) grinded powder samples of **1** at electron high tension 15 kV.

6.3.3 Biological activity of 2-ptp and [Au (2-ptp)₂]Cl (1)

Standardized suspension (1 ml) of bacteria (2×10^6 CFU/ml) was added into MH broth containing the complex **1** and ligand to a final concentration between 0-1000 µg/ml and incubated at 37°C for 18 h with shaking at 200 rpm. The complex **1** and ligand, 2-ptp, were added at mid-logarithmic phase of growth and aliquots of 1.0 ml were withdrawn at intervals to record OD_{540} and colony count. From the above finding it was cleared that complex **1** and **2-ptp** gave activity from 240-480 µg/ml against a series of microorganisms (**Table 6.2**).

175

Table 6.2. Antibacterial activities of 2-ptp and [Au (2-ptp)₂] Cl (**1**)against selected pathogens

Bacteria	Strain Quality	MIC (µg/mL)		Inhibition zone (mm)	
		2-ptp	[Au(2-ptp)₂]Cl	2-ptp	[Au(2-ptp)₂]Cl
Staphylococcus aureus	ATCC 25923	289.25	240	9.2±0.50	10.50±0.10
Bacillus subtilis	ATCC 14579	333.25	298.65	5.60±0.50	5.9±0.40
Enterococcus faecalis	ATCC 29212	-	480	-	7.2±0.40
Escherichia coli	ATCC 25922	243.50	270	11.2±0.30	10.4±0.20
Klebsiella pneumoniae	ATCC 700603	-	322	-	7.2±0.70

According to several studies, gold complexes are likely to exert their antimicrobial efficiency as a result of their ability to form complexes with soluble extracellular proteins or cell walls, or even because of their lipophilicity, which may damage their cells and cause their membranes to rupture [10, 27]. Further, the loss of ions and the reduction of its potential are also associated with the permeability of the cell membrane of bacteria [28]. It may cause damages that can result in the extravasation of macromolecules, causing a collapse of the cell's functions, resulting in bacterial death [29]. It is evident from the MIC values for metal complex **1** that the ligand shows an increase in antimicrobial activity after interacting with Au ions, which may support that the compound and its ligand share the same mechanism. In tests against a variety of strains, the synthetic ligand **2-ptp** displayed a relatively good antimicrobial activity, inhibiting the growth of the bacteria at low concentrations, with MIC values of 250 and 500 g/ml, respectively.
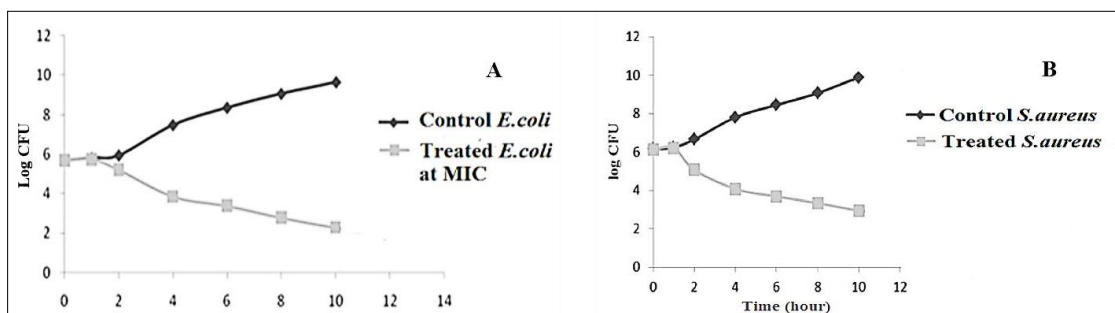
Figure 6.10. Time dependent growth curve of *E. coli* (A) and *S. aureus* presence or, absence of complex **1** at its MIC (B).

6.3.4 Cytotoxicity determination

The cytotoxicity of **1** has been examined in cultured Vero cells by using the MTT assay, at different doses (**Figure 6.11**). The result reveals that the 50% cytotoxicity (CC_{50}) of 2-ptp and [Au(2-ptp)$_2$]Cl (**1**) are 405 and 389.90 µg/ml, respectively.
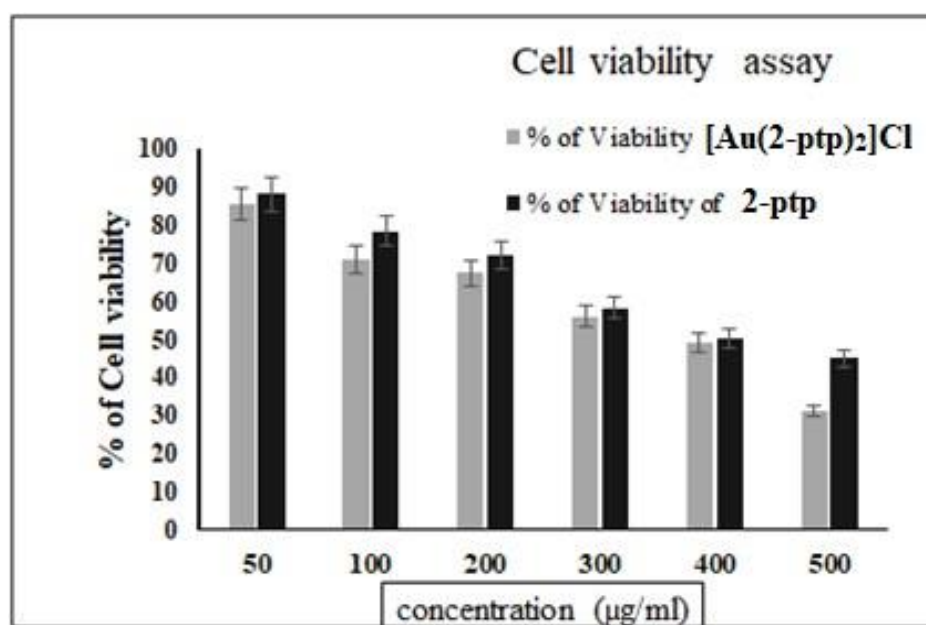
Figure 6.11 Cytotoxicity of 2-ptp and [Au (2-ptp)$_2$]Cl (**1**) against Vero cell.

3.5 Optical spectrum and DFT computation

Thin film of well dispersion of the complex **1** in DMF shows high intense band at UV region (**Figure 6.12**).
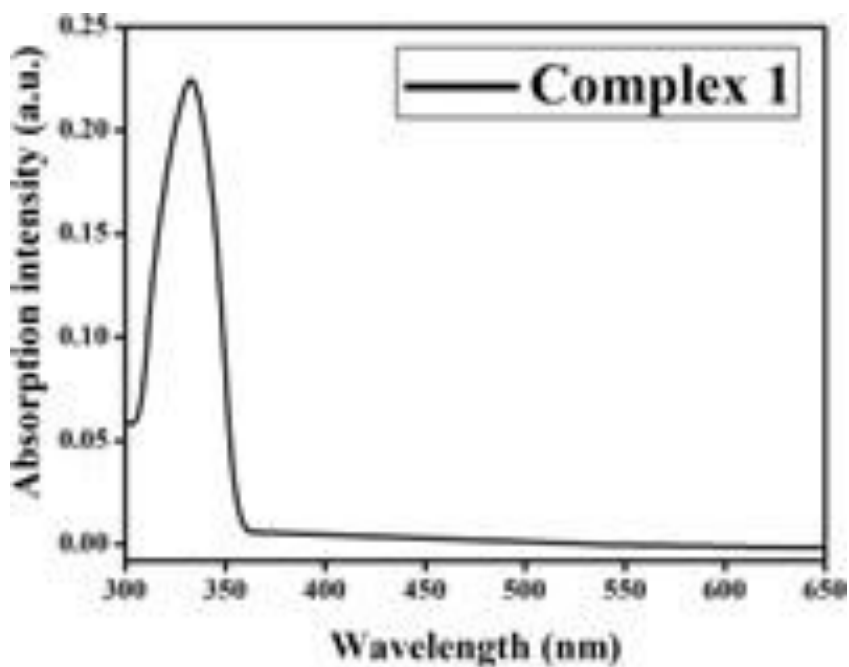
Fig. 6.12 UV-vis absorption spectrum of the Complex **1**.
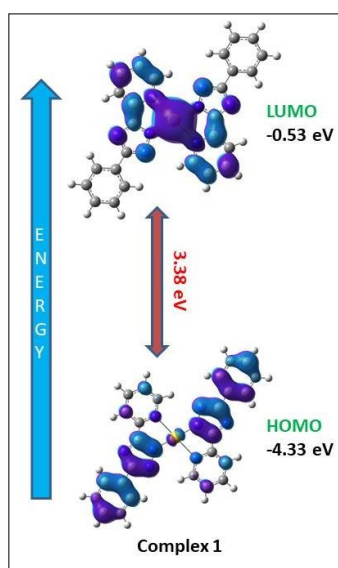
Fig. 6.13 The energy diagram of HOMO and LUMO by DFT computation of complex **1**.

The optimization of structural geometry of the complex **1** has been performed by DFT computation. The optimized structure of the complex is used to calculate energy of HOMO (-4.33 eV) and LUMO (-0.53 eV) and hence the ΔE ($E_{LUMO} - E_{HOMO}$, 3.80 eV) (**Fig. 6.13**) and is much lower than band gap of **2-ptp** (4.87 eV) (**Fig. 6.14**).
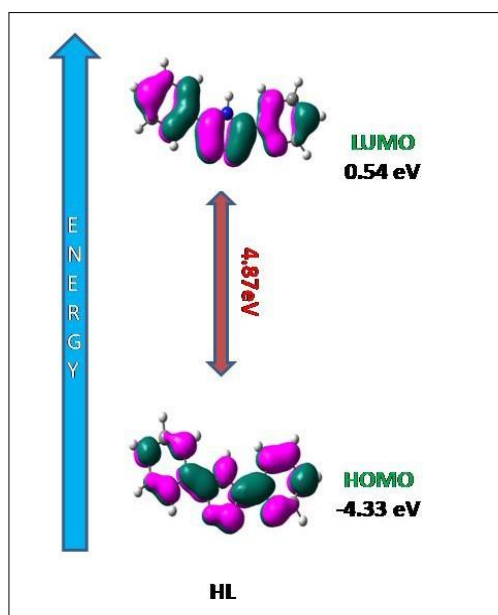
Fig. 6.14 DFT-computed energy of molecular orbitals and the energy difference between highest occupied molecular orbital (HOMO) and lowest unoccupied molecular orbital (LUMO) of **2-ptp**.

6.4 Conclusion

2-(3-Phenyl-1H-1,2,4-triazol-5-yl)pyridine (2-ptp) is a monoanionic bidentate chelating ligand and forms mononuclear Au(III) complex, $[Au(2\text{-ptp})_2]^+$. The structure exhibits distorted square-planar arrangement and the molecular units are assembled through hydrogen bonding and π---π interactions to form supramolecular aggregate. Interestingly, the compound has potential against Gram-positive (*S. aureus*) and Gram-negative (*E. coli*) bacterial species. The results have displayed that the growth of *E. coli* and *S. aureus* ATCC 25923 have been diminished with increasing time at MIC of $[Au(2\text{-ptp})_2]Cl$. The toxicity of complex has been checked by MTT assay and satisfactory result achieved.

179

The electrical conductivity under dark condition has been estimated as 7.42×10^{-5} Sm^{-1} and under illumination condition the value has been improved to 2.45×10^{-4} Sm^{-1} for complex **1** fabricated device. Therefore, our synthesized material may be utilized for next generation functional molecule.

6.5 References

[1]   A. M. Ahmed, E, Reedy and N. K. Soliman, *Sci. Rep.,* 2020, **10**, 6137.

[2]   M. H. Klingele and S. Brooker, *Chem. Rev.,* 2003, **241**, 119 – 132.

[3]   B. Schulze and U. S. Schubert, *Chem. Soc. Rev.*, 2014, **43**, 2522 –2571.

[4]   J. D. Crowley and D. A. McMorran, *J., Ed. Springer-Verlag Berlin Heidelberg.*, 2012, **28**, 31 –84.

[5]   L. Suntrup, M. Kleoff and B. Sarkar, *Dalton Trans.*, 2018, **47**, 7992 –8002.

[6]   Q. V. C. van Hilst, N. R. Lagesse, D. Preston and J. D. Crowley, *Dalton Trans.*, 2018, **47**, 997 –1002.

[7]   D. Schweinfurth, L. Hettmanczyk, L. Suntrup, B. Sarkar and *Z. Aonrg. Allg. Chem.*, 2017, **643**, 554 –584.

[8]   H. Beucher, S. Kumar, R. Kumar, E. Merino, W.-H. Hu, G. Stemmler, Cuesta- S. Galisteo, J. A. González, L. Bezinge, J. Jagielski, C.-J. Shih and C. Nevado, *Chem. Eur. J.*, 2020, **26**, 17604 –17612.

[9]   A.C. Reiersølmoen and A. Fiksdahl, *Eur. J. Org. Chem.*, 2020, 2867-2877.

[10]   I. Eryazici, C. N. Moorefield and G. R. Newkome, *Chem. Rev.,* 2008, **108**, 1834–1895.

[11]   T.N. Solvi, A. C. Reiersølmoen, A. Orthaber and A. Fiksdahl, *Eur. J. Org. Chem.*, 2020, **2020**, 7062-7068.

[12]   S. P. Fricker, *Met.-Based Drugs,* 1999, **6**, 291 –300.

[13]   L. Messori, F. Abbate, G. Marcon, P. Orioli, M. Fontani, E. Mini, T. Mazzei, S. Carotti, T. O'Connell and P. Zanello, *J. Med. Chem.,* 2000, **43**,3541 –3548.

[14]   N. S. Radulović, N. M. Stojanović, B. Ð. Glišić, P. J. Randjelović, Z. Z. Stojanović-Radić, K. V. Mitić, M. G. Nikolić and M. I. Djuran, *Polyhedron.,* 2018, **141**, 164 –180.

[15]   A. P. Martins, A. Ciancetta, A. de Almeida, A. Marrone, N. Re, G. Soveral and A. Casini, *ChemMedChem.*, 2013, **8**, 1086-1092.

[16]   J. Pons, A. Chadghan, J. Casabo, A. Alvarez-Larena, J. Francesc Piniella, and J. Ros, *Inorg, Chem. Commun.*, 2000, **3**, 296–299,

[17]   G. M. Sheldrick, SHELXL 2014, SHELXL-2016/6 and SHELXL-2017/1, Program for Crystal Structure Solution, University of Göttingen., 2014, **2016**, 2017.

[18]   SMART and SAINT; Bruker AXS Inc.: Madison, WI, 1998.

[19]   Bruker. SADABS. Bruker AXS Inc., Madison, Wisconsin, USA., 2001.

[20]   Clinical Laboratory Standards Institute. Performance Standards for Antimicrobial Susceptibility Testing 29[th]Edition, No: 1, CLSI Supplement M 100, ISBN 978-1-68440-032-4. 1-281, Wayne, Pennsylvania 19087, USA, 2019.

[21]   D. Chattopadhyay, K. Maiti, A.P. Kundu, M.S. Chakraborty, R. Bhadra, S.C. Mandal and A.B. Mandal, *J. Ethnopharmacol.*, 2001,**77**,49-55.

[22]   A. Das Mahapatra, C. Patra, J. Mondal, C. Sinha, P. C. Sadhukhan and D. Chattopadhay, *Chemistry Select.*, 2020, **5**, 4770-4777.

[23]   M. J. Frisch, G. W. Trucks, H. B. Schlegel, G. E. Scuseria, M. A. Robb, J. R. Cheeseman, G. Scalmani, V. Barone, B. Mennucci, G. A. Petersson, H. Nakatsuji, M. Caricato, X. Li, H. P. Hratchian, A. F. Izmaylov, J. Bloino, G. Zheng, J. L. Sonnenberg, M. Hada, M. Ehara, K. Toyota, R. Fukuda, J. Hasegawa, M. Ishida,

T. Nakajima, Y. Honda, O. Kitao, H. Nakai, T. Vreven, J. A. Montgomery Jr., J. E. Peralta, F. Ogliaro, M. Bearpark, J. J. Heyd, E. Brothers, K. N. Kudin, V. N. Staroverov, R. Kobayashi, J. Normand, K. Raghavachari, A. Rendell, J. C. Burant, S. S. Iyengar, J. Tomasi, M. Cossi, N. Rega, J. M. Millam, M. Klene, J. E. Knox, J. B. Cross, V. Bakken, C. Adamo, J. Jaramillo, R. Gomperts, R. E. Stratmann, O. Yazyev, A. J. Austin, R. Cammi, C. Pomelli, J. W. Ochterski, R. L. Martin, K. Morokuma, V. G. Zakrzewski, G. A. Voth, P. Salvador, J. J. Dannenberg, S. Dapprich, A. D. Daniels, O. Farkas, J. B. Foresman, J. V. Ortiz, J. Cioslowski and D. J. Fox, Gaussian 09, Revision D.01, Gaussian Inc., Wallingford, CT, 2009.

[24] A. D. Becke, *J. Chem. Phys.,* 1993, **98**, 5648–5652.

[25] W.R. Wadt and P.J. Hay, *J. Chem. Phys*., 1985, **82**, 299-310.

[26] N. M. O'Boyle, A. L. Tenderholt and K. M. Langner, *J. Comput. Chem.,* 2008, **29**, 839–845.

[27] M. R. K. Sartori, Dissertação de Mestrado Acadêmicoem Ciências farmacêuticas. Universidade do Vale do Itajaí, 2005.

[28] D. Trombeta, F. Castelli, M. G. Sarpietro, V. Venuti, M. Cristani, C. S. Daniele, G. Mazzanti and G. Bisignanano. *Agents Ch.,* 2005, **49**, 2474-2478.

[29] G.J. Tortora, B.R. Funke, C.L. Case, Ed. Porto Alegre: Artmed.*Microbiologia.* **2003**.

[30] A. Dey, S. Middya, R. Jana, M. Das, J. Datta, A. Layek and P. P. Ray, *J. Mater. Sci. Mater. Electron.,* 2016, **27**, 6325–6335.

[31] S. Roy, S. Halder, A. Dey, K. Harms, P. P. Ray and S. Chattopadhyay , *New J. Chem*., 2020, **44**, 1285-1293.

[32] S. Konar, A. Dey, S. R. Choudhury, K. Das, S. Chatterjee, P. P Ray, J. Ortega-Castro, A. Frontera and S. Mukhopadhyay, *J. Phys. Chem. C.,* 2018, **122**,8724–8734.

[33] E. H. Rhoderick, Metal Semiconductors Contacts. Oxford University Press, Oxford. **1978**.

[34] S. K. Cheung and N. W. Cheung, *Appl., Phys. Lett.,* 1986, **49**, 85–87.

[35] A. Dey, A. Layek, A. Roy chowdhury, M. Das, J. Datta, S. Middya, D. Das and P. P. Ray, *RSC Adv.*, 2015, **5**, 36560–36567.

[36] R. K. Gupta and F. Yakuphanoglu, *Sol. Energy.,* 2012, **86**, 1539–1545.

[37] X. Miao, S. Tongay, M. K. Petterson, K. Berke, A. G. Rinzler, B. R. Appleton and A. F. Hebard, *Nano Lett.*, 2012, **12**, 2745– 2750.

[38] P. W. M. Blom, M. J. M. de Jong and M. G. van Munster, *Phys. Rev.,* 1997, **55**, 656– 659.

SUMMARY

7.1 Summary

Antimicrobial potential of diverse nature-based synthetic analogs and bio-fabricated nanoparticles derived from ethnomedicinal plants *Albizia lebbeck* and *Oxalis corniculata*

With respect to emerging, re-emerging, and ever-increasing drug-resistant microbial infection we have developed nature-based synthetic analogues and bio-fabricated nanoparticles derived from ethnomedicinal plants **Albizia lebbeck** and **Oxalis corniculata**. Since 1961 FDA approved Sulfamethoxazole (SMX, 4-Amino-*N*-(5-methylisoxazol-3-yl)-benzenesulfonamide) combined with trimethoprim in a 5:1 ratio in co-trimoxazole for the treatment of bacterial infections. Investigation of the cellular mechanism of action of SMX has shown that it hampers the synthesis of folic acid by substituting *p*-aminobenzoic acid (PABA) in the dihydropterate synthease (DHPS) and resists the growth of bacteria. However, prolonged administration of sulfonamide (SF-NH_2) causes toxicity including liver disease, loss of appetite, fever, skin rashes, lung infection, kidney damage, hemolytic anemia, etc. Hypersensitivity results from the partial oxidation of aromatic-NH2 groups of sulfonamide to hydroxylamine (SF-NHOH) or the nitrous derivative (SF-NO) via Cytochrome P450. Due to the resistance of drugs in twenty-first century researchers are synthesizing new drugs which are less toxic and more efficient. In order to minimize or diminish bacteria's toxicity and antibiotic resistance, sulfonamides need to be functionalized. The results of this research demonstrate the antimicrobial activity of a series of functionalized sulfonamides including nucleoside molecules and two distinct green synthesized nano particles named Ag-NP-AE and OC-Ag-NP.

It has been summarized in **Chapter 2** and **C**hapter 3 that the overall pharmacological evaluation of both green synthesized nanoparticles **Ag-NP-AE** and **OC-Ag-NP** respectively derived from the plants *Albizia lebbeck* and *Oxalis corniculata* correspondingly exposed and that has anti-microbial and excellent anti-oxidant activity, probably due to presence of a number of bioactive phytoconstituents. OC-Ag-NP is more active against cell line MDA-MB-468 than its parent drug. Thus, these plant extracts perform as both reducing and capping agents during the synthesis of silver nanoparticles. It may help to consider the development of a natural lead for primary health care and further bioprospecting. The result was seen by the scanning electron microscopy imaging analyses of *Serratia marcescens* after treatment with *A. lebbeck*-derived AgNps might give valuable information about the status of the bacteria with feasible treatment. Our observation under scanning electron microscopy for two different bacteria was dissimilar. Lysed cells were observed for *Serratia marcescens* after 8 h of incubation in the presence of Ag-NP-AE.

This thesis deals with the pharmacological evaluation of two green synthesized nanoparticles **Ag-NP-AE** and **OC-Ag-NP** used against ailments for microorganisms (antibacterial and antiviral) and related anti-biofilm, anti-oxidant activities for bioprospecting.

Nature-based synthetic analogs Coumarin and sulfonamide based four drugs derivative (**Chapter-5**) and Nucleoside derivatives (**Chapter-4**) have been prepared. All the compounds have been characterized by spectroscopic studies *viz*. IR, UV-Vis, Mass spectrum and NMR. The biological activities such as antimicrobial, DNA interaction, toxicity effect have been evaluated. The **MIC** against gram positive and gram negative bacteria of the drugs (**1a** to **1d**) have been summarized in **Chapter 5** and data reveal that the antibacterial activity is improved and cytotoxicity has been

decreased to their precursor. The **EC$_{50}$** data in **Chapter 4** also exposes that amide derivatives (**HL1** and **HL2**) is more potent against HSV-1F. The mechanistic investigation of anti-HSV efficiency proves the destruction of virus entering into Vero cell wall due to interaction with Glycoprotein.

In **Chapter 6,** 2-(3-Phenyl-1H-1,2,4-triazol-5-yl)pyridine (2-ptp) is a monoanionic bidentate chelating ligand and forms mononuclear Au(III) complex, $[Au(2\text{-ptp})_2]^+$. The biological application of the coordination polymer shows effective antibacterial activity. Thus, our compound may be the active member in the club of multifunctional material.

■ Biological Chemistry & Chemical Biology

Silver Nanoparticles Derived from *Albizia lebbeck* Bark Extract Demonstrate Killing of Multidrug-Resistant Bacteria by Damaging Cellular Architecture with Antioxidant Activity

Ananya Das Mahapatra,[a] Chiranjit Patra,[a] Joy Mondal,[a] Chittaranjan Sinha,[b] Provash Chandra Sadhukhan,[a] and Debprasad Chattopadhyay*[a, c]

Silver nanoparticles (Ag-NP-AE) are synthesized and stabilized by the extract of an ethnomedicine, *Albizia lebbeck* bark aqueous extract (AE). Ag-NP-AE is active against several multi-drug-resistant (MDR) clinical isolates. The nanoparticles are characterized by UV-vis spectroscopy, Fourier-transform infra-red spectroscopy (FTIR), Dynamic light scattering (DLS), Scanning electron microscope (SEM), Transmission electron microscope (TEM) and X-ray diffraction (XRD) studies. The antibacterial potency of Ag-NP-AE is determined by Disc diffusion, Agar and Broth dilution assays against 14 MDR isolates along with their minimum inhibitory concentration (MIC), and minimum bactericidal concentration (MBC). The growth kinetics was determined by quantification of colonies; while toxicity by quantification of viable cells. The Ag-NP-AE shows free-radical scavenging activity at 15–20 μM and is non-toxic up to 50 μM but demonstrated significant antibacterial activity against all the test isolates with zone diameter of 10.4–19.5 mm and MIC of 0.5–0.84 μM (0.085-0.143 μg); while the zone diameter with AE was 10.2–15 mm and MIC of 128–1024 μg/mL, respectively; while 100% killing was observed at 0.50 μM within 2–4 h of exposure due to damage of cellular architectures.

1. Introduction

Infections caused by the WHO listed priority pathogens of greatest threat including *Staphylococcus aureus, Enterococcus faecalis, Escherichia coli, Salmonella typhi, Klebsiella pneumoniae, Pseudomonas aeruginosa* are ubiquitous in community and hospital setting, leading to increased mortality, morbidity and economic burden.[1,2] The multi-antibiotic resistant strains may cause treatment failure to death. Moreover, the biofilm formed by some pathogenic bacteria is difficult to eradicate, while growing antibiotic-resistant limits the treatment options.[1,3] One promising option is the use of ultra-fine nanoparticles (1-100 nm) of metallic silver, gold, copper, or zinc with therapeutic activities against a wide array of pathogenic bacteria.[1,4] Moreover, the development of resistance against silver nanoparticles is less because of its unique structure and multimodal mechanisms of action.[5] Silver nanoparticles (AgNP) prepared with plant extracts or phytocompounds are reported to possess antimicrobial activity against bacteria including *S. aureus, E. coli, S. Typhimurium* and *P. aeruginosa* at 2–4 ppm, fungi and viruses.[6–9] Silver ions of AgNP not only accumulate around the cell wall but also penetrate to bacterial cells and interact with the bacterial DNA.[10] Metal nanoparticles prepared by chemical/photochemical reduction or electrochemical methods showed better stability;[11] while synthetic methods used organic solvents as a medium due to better hydrophobicity of capping agents. The size, morphology, surface charge, and coating of AgNPs are reported to play critical roles in determining their antimicrobial activities.[12] Earlier, AgNPs synthesized with chemicals showed toxic/hazardous effect on the ecosystem; and thus, plant or microbial metabolites are preferred,[13] due to their eco-friendly nature, termed as "Green synthesis".[14] Moreover, the synthesis of nanoparticles from bio-metabolites is rapid with high yield and cost-effective downstream processing.[15] A substantial amount of work has been done on 'green synthesis' of AgNPs using plant extracts, secondary metabolites of virus, bacteria, fungi, and plants, due to their antioxidant activity that help to reduce metal compounds in their respective nanoparticles.[16]

Several species of *Albizia* (Mimosoideae) are traditionally been used as ethnomedicine of diverse communities. Among them, *Albizia lebbeck* (Linn) Benth, locally known as Siris, is a tall tropical deciduous tree distributed throughout India, parts of Asia, Africa, Austalia, and Southern America. In the Unani

[a] A. Das Mahapatra, Dr. C. Patra, J. Mondal, Dr. P. Chandra Sadhukhan, Dr. D. Chattopadhyay
Virus Labortory Department
ICMR-National Institute of Cholera and Enteric Diseases
CIT Rd., Kolkata-700010, (India)
E-mail: debprasadc@yahoo.co.in
[b] Prof. C. Sinha
Department of Chemistry
Jadavpur University
Kolkata 700 032, (India)
[c] Dr. D. Chattopadhyay
ICMR-National Institute of Traditional Medicine
Nehru Nagar, Belagavi 59010 I, (India)
E-mail: debprasadc@yahoo.co.in

Green synthesis of AgNPs from aqueous extract of *Oxalis corniculata* and its antibiofilm and antimicrobial activity

Ananya Das Mahapatra [a], Chiranjit Patra [a], Kunal Pal [c], Joy Mondal [a], Chittaranjan Sinha [b,*], Debprasad Chattopadhyay [a,d,**]

[a] *ICMR-National Institute of Cholera and Enteric Diseases, Kolkata, India*
[b] *Department of Chemistry, Jadavpur University, Kolkata 700032, India*
[c] *Department of LifeScience & Biotechnology, JadavpurUniversity, Kolkata, 700032, India*
[d] *ICMR-National Institute of Traditional Medicine, Nehru Nagar, Belagavi, 590010, India*

ARTICLE INFO	ABSTRACT
	The silver nanoparticles OC-AgNPs, synthesized from the aqueous extract of *Oxalis corniculata* (OC), showed antiviral activity against Herpes Simplex Virus-1 (HSV-1), and anti-biofilm, and antibacterial activities against human isolates of six multi-drug resistant (MDR) bacteria - *Staphylococcus aureus*, *Streptococcus pyogenes*, *Escherichia coli*, *Klebsiella pneumoniae*, *Salmonella typhi*, and *Pseudomonas aeruginosa*. The OC-AgNP was characterized by UV-Vis and FTIR spectroscopy; while its morphology and distribution were determined by transmission electron microscopy (TEM). The results revealed that the biogenic OC-AgNPs are spherical with an average diameter of 40 nm and has shown UV-Vis peak at 445 nm. The cytotoxicity and safety of OC-AgNP has been evaluated by MTT assay in Vero cells and triple-negative human breast cancer MDA-MB-468 cells. The plaque reduction assay has been used to test the antiviral activity against HSV-1F. The anti-biofilm activity was assessed by crystal violet staining, followed by light and confocal microscopy; while the antibacterial activity was determined by conventional disk-diffusion and broth-dilution methods. Moreover, the mechanism of anti-biofilm and antibacterial activity was examined by Field Emission Scanning Electron Microscopy (FESEM). The CC_{50} (cytotoxicity) on Vero cells was 300 μg/ml; while the survival percentage of MDA-MB-468 cells was 27.12% at 20 μM and 80.97% at 100 μM of, respectively. The OC-AgNP showed moderate antiviral activity against HSV-1F at EC_{50} of 25 μg/ml; but significantly inhibited the biofilm produced by *Pseudomonus aeruginosa* and *Escherichia coli* at 25-50 μg/ml; while at 30-50 μM we observed the dose-dependent lowering of fluorescence intensity under light and confocal microscope. Interestingly, the OC-AgNPs demonstrated significant antibacterial activity against *Pseudomonas aeruginosa* (20 mm), *Klebsiella pneumoniae* (15 mm), *Escherichia coli* (12 mm), *Salmonella typhi* (10 mm), *Streptococcus pyogenes* (11 mm) and *Staphylococcus aureus* (10 mm) with Minimum Inhibitory Concentration (MIC) of 0.65–0.90 μM (0.11- 0.153 μg), respectively. Further, the FESEM micrograph showed disruption of membrane structure with the damage of cell membrane integrity of *Pseudomonus aeruginosa* at its MIC.

1. Introduction

Silver nanoparticles (Ag-NPs) have a broad range of biomedical applications, particularly as antimicrobial and anticancer agents, drug-delivery carriers, diagnostics, imaging probes, etc. [1]. Different methods are now available such as physical (ball milling, laser ablation, electrical arc, and vapor condensation), chemical (Ag$^+$ reduction by NaBH$_4$, Na-citrate), electrochemical, photochemical, sonochemical, microwave-and microorganism assisted, and plant-mediated [2] procedure to monitor the shape, size, stability and yield of AgNPs. Considering sustainable development and environmental fortification, the plant-mediated methods of synthesis of AgNPs are the most favorable ones. Synthesis of silver nanomaterials by using plant extract(s) is found to be more useful because of their natural, less-toxic, eco-friendly, cost-effective, scalable, and more reliable nature. Moreover, plant-based nanoparticle synthesis is quick, and it can replace the capping agents

---

RESEARCH ARTICLE

Supramolecular assembly of an Au(III) complex of 2-(3-phenyl-1H-1,2,4-triazol-5-yl)pyridine: Structure, biological studies and charge transportation

Manik Shit[1,2] | Arka Dey[3] | Ananya Das Mahapatra[4] |
Basudeb Dutta[1,5] | Kaushik Naskar[1] | Partha Pratim Ray[3] |
Chittaranjan Sinha[1]

[1]Department of Chemistry, Jadavpur University, Kolkata, India

[2]Narajole Raj College, Paschim Medinipur, Narajole, India

[3]Department of Physics, Jadavpur University, Kolkata, India

[4]ICMR Virus Unit, Infectious Diseases & Beliaghata General Hospital, Kolkata, India

[5]Department of Chemical Sciences, Indian Institute of Science Education and Research Kolkata, Mohanpur, West Bengal, India

Correspondence
Chittaranjan Sinha, Department of Chemistry, Jadavpur University, Kolkata 700032, India.
Email: crsjuchem@gmail.com

Abstract

An Au(III) complex, [**Au**(2-ptp)$_2$]Cl (**1**) (**2-ptp** = 2-(3-phenyl-1H-1,2,4-triazol-5-yl)pyridine), has been characterized by single-crystal X-ray diffraction technique and other spectroscopic data. Presence of different noncovalent interactions leads to the formation of 3D supramolecular structure. The complex **1** exhibits antibacterial activity against Gram-positive (MIC) (*Staphylococcus aureus* [240 μg/ml], *Bacillus subtilis* [645 μg/ml]) and Gram-negative (*Escherichia coli* [270 μg/ml], *Enterococcus faecalis* [820 μg/ml], *Klebsiella pneumonia* [785 μg/ml]) bacteria. Also, the toxicity of **1** has been checked by MTT assay. The complex shows promising anticancer activity against Vero cells and the CC$_{50}$ is 405 μg/ml. The complex also shows improved conductivity (Λ) by one order difference on illumination (Λ_{dark}, 7.42×10^{-5} Sm^{-1} and $\Lambda_{illumination}$, 2.45×10^{-4} Sm^{-1}).

KEYWORDS

antibacterial activity, Au(III) complex, conductivity measurements, DFT calculation

1 | INTRODUCTION

1,2,4-Triazole and its derivatives are potential pharmacological agents and show many biological activities like herbicidal, insecticidal, antifungal, and anticancer properties.[1] Pyridyl-substituted triazoles offer a planar aromatic system of strong π–π stacking and have been used to synthesize metal complexes with various geometries.[2] Triazole is an exceptional building block to constitute coordination polymer and supramolecular geometries like cages and cylinders along with diverse applications in catalysis, drug development, metal ion sensing,

imaging, and so forth.[3–7] Au(III) chemistry of polydentate N-heterocycles is an underdeveloped research area compared with their Au(I) counter parts[8,9] along with other coinage metals.[10] The square planar Au(III) complexes may have a higher ability to intercalate into the DNA structure than linear structure of Au(I) complex and might have high biological efficiency.[11–15] In this work, 2-(3-phenyl-1H-1,2,4-triazol-5-yl)pyridine (2-ptp) has been used to synthesize Au(III) complex and the single crystal diffraction analysis is used for the confirmation of the structure where ligand, 2-ptp, acts as bidentate chelating ligand. The complex has been used to examine the antimicrobial property and out of five bacteria two stains (*Staphylococcus aureus* [240 μg/ml],

ORIGINAL ARTICLE

An extract of Stephania hernandifolia, an ethnomedicinal plant, inhibits herpes simplex virus 1 entry

Joy Mondal[1,2] · Ananya Das Mahapatra[1] · Keshab C. Mandal[2] · Debprasad Chattopadhyay[1,3]

Abstract

Stephania hernandifolia (Nimukho), an ethnomedicinal herb from rural Bengal, has been used traditionally for the management of nerve, skin, urinary, and digestive ailments. Here, we attempted to confirm the antiviral potential of aqueous, methanol, and chloroform extracts of *S. hernandifolia* against herpes simplex virus type 1 (HSV-1), the causative agent of orolabial herpes in humans, and decipher its underlying mechanism of action. The bioactive extract was standardized and characterized by gas chromatography-mass spectroscopy, while cytotoxicity and antiviral activity were evaluated by MTT and plaque reduction assay, respectively. Two HSV strains, HSV-1F and the clinical isolate VU-09, were inhibited by the chloroform extract (CE) with a median effective concentration (EC_{50}) of 4.32 and 4.50 µg/ml respectively, with a selectivity index (SI) of 11. Time-of-addition assays showed that pre-treatment of virus-infected cells with the CE and its removal before infection reduced the number of plaques without lasting toxicity to the cell, indicating that the CE affected the early stage in the viral life cycle. The number of plaques was also reduced by direct inactivation of virions and by the addition of CE for a short time following attachment of virions. These results together suggest that modification of either the virion surface or the cell surface by the CE inhibits virus entry into the host cell.

Abbreviations

ATCC	American Type Culture Collection
CC_{50}	Median cytotoxic concentration
CE	Chloroform extract
CPE	Cytopathic effect
DMEM	Dulbecco's modified minimum essential medium
DMSO	Dimethyl sulfoxide
EC_{50}	Median effective concentration
FBS	Fetal bovine serum
gB	Glycoprotein B
gC	Glycoprotein C
gD	Glycoprotein D
GC-MS	Gas chromatography-mass spectroscopy
HSV	Herpes simplex virus
MTT	3-(4,5-Dimethylthiazol-2-yl)-2,5-diphenyl tetrazolium bromide
PFU	Plaque-forming unit
PRA	Plaque reduction assay
RT-qPCR	Quantitative real-time polymerase chain reaction
SH	*Stephania hernandifolia*
SI	Selectivity index

✉ Debprasad Chattopadhyay
debprasadc@yahoo.co.in

1. ICMR-NICED Virus Unit, ID and BG Hospital, GB-4, First Floor, 57 Dr. Suresh C Banerjee Road, Beliaghata, Kolkata 700010, India

2. Department of Microbiology, Vidyasagar University, Midnapore, West Bengal, India

3. ICMR-National Institute of Traditional Medicine, Nehru Nagar, Belagavi 590010, India

Introduction

Herpes simplex virus (HSV), a very common viral pathogen, usually infects the skin and mucosa and is classified into two types (1 and 2). HSV-1 causes herpes labialis, keratitis, and encephalitis in the upper part of the body, while HSV-2 is the causative agent of herpes genitalis in the lower body parts [1, 2]. The virus is transmitted silently from an infected person through sex, body fluids, cuts, and wounds. HSV is a unique contagious virus due to its ability to cause mild to severe infection, latency in nerve ganglia with asymptomatic shedding, periodic reactivation, and silent epidemic potential with hide-and-seek nature [3]. After entry, HSV

⚫ Springer

191

Abstract

Aim Validation of antiviral activity of Stephania hernandifolia against HSV-2. Background Ethnomedicinal plant Stephania hernandifolia, traditionally used for the management of skin, digestive and nerve ailments demonstrated significant anti-HSV-1 activity; similar to Stephania cepharantha having neuroinflammatory and anti-HSV activities. Objectives Thus, the present study was aimed to validate the potential of the most active fraction-2 (F-2) of S. hernandifolia against HSV-2 in vitro, along with the underlying mode or mechanism of action. Methods The standardized F-2 was characterized by GC-MS, 1H-NMR, Mass and FTIR spectroscopy. Cytotoxicity (CC50) and antiviral activity (EC50) was evaluated by MTT and Plaque reduction assay. To determine the mode of action, we have used time-of-addition, virus inactivation, and entry (attachment and penetration) assays, followed by semiquantitative PCR. Furthermore, the protein expression levels of immediate early (IE) and early (E) gene products of drug-treated virions were measured by Western blot. Results The results showed that HSV-2G and ICMR/VU-2012/20, the clinical isolate of HSV-2, were inhibited by F-2 at EC50 of 20.0 and 20.43 µg/ml respectively, with Selectivity Index (SI) of 12. Time-of-addition assay showed that F-2 significantly inhibited HSV-2 infection in Vero cells at 4-8 h post-treatment. The infectivity of the virion was lost within 1h of exposure to F-2 (EC50 and EC99). Furthermore, semi-Q-PCR, and Western blot studies demonstrated significant downregulation of IE and E gene products. The characterization revealed that 2-chloroethyl linoleate is

192

A bio-compatible pyridine–pyrazole hydrazide based compartmental receptor for Al³⁺ sensing and its application in cell imaging †

Check for updates

Bhriguram Das, [ID] ab Malay Dolai, [ID] c Avijit Ghosh, [ID] d Anamika Dhara, e Ananya Das Mahapatra, f Debprasad Chattopadhyay, fg

Subhabrata Mabhai, h Atanu Jana, [ID] *i Satyajit Dey [ID] *b and Ajay Misra [ID] *a

Author affiliations

Abstract

For practical applications, the development of bio-compatible organic molecules as p-block ion chemosensors is critical. Herein, we report the single crystal (SC) of new pyridine–pyrazole derived Al³⁺ sensor **H₂PPC** [(Z)-N'-(2,3-dihydroxybenzylidene)-5-methyl-1-(pyridin-2-yl)-1H-pyrazole-3-carbohydrazide] as well as its Cu-complex SC. The probe exhibits an "off–on" fluorescence response towards Al³⁺ ions, and this has been modulated with different solvents. For selective detection of Al³⁺ ions, a special coordination pocket in the structural backbone is advantageous. The chemosensor exhibits a submicromolar detection level (LOD = 4.78 μM) for Al³⁺. The density functional theory (DFT) and time-dependent DFT (TD-DFT) calculations of **H₂PPC** and **[Al(HPP)₂]⁺** (**1**) reveal that a change of the structural conformation of probe **H₂PPC** upon complexation causes the pyrazole and pyridine units to create a specific cavity to tether Al³⁺, and consequently **H₂PPC** proves to be a promising molecule for Al³⁺ detection. Furthermore, the probe has been successfully used to evaluate Al³⁺ as a low-cost kit using filter paper strips, and the *in situ* Al³⁺ ion

193

▌Inorganic Chemistry

A Phenyl Thioether-Based Probe: Zn²⁺ Ion Sensor, Structure Determination and Live Cell Imaging†

Sunanda Dey,[a] Suvendu Maity,[a] Ananya Dasmahapatra,[a] Debprasad Chattopadhyay,[b] and Chittaranjan Sinha*[a]

3,3′-((1Z,1′Z)-(((Propane-1,3-diylbis(sulfanediyl))bis(2,1-phenyl-ene))bis(azanyyldiene))bis(methanylylidene))bis(2-hydroxy-5-methylbenzaldehyde) (H₂-SAP), characterized by different spectroscopic data, exhibits yellow emission (λ_{em}, 560 nm) when binds with Zn²⁺ in H₂O-MeOH (1:9 v/v, HEPES buffer, pH 7.4) in a mixture of seventeen biologically important other metal ions. The limit of detection (LOD) is 9.0 nM which is far below the World Health Organization (WHO) recommended data. The composition of the complex, 1:1 Zn²⁺:SAP²⁻, is supported by Job's plot, ESI-MS and single crystal X-Ray crystallographic structure. Intracellular Zn²⁺ ion is detected in Vero Cells (African Green Monkey Kidney) by using the probe, H₂-SAP, in the cell lines under fluorescence microscope. The probe has successfully been applied to recover Zn²⁺ in surface water.

Introduction

Zinc, the first element in group 12 of the Periodic Table and the second-most essential metal ion in human body, is an essential nutrient[1] to the baby at the mother's womb and also to the postnatal development.[2] Because of redox innocent feature, rapid ligand exchange ability and brilliant Lewis acidity[3–6] zinc has been chosen for hydrolytic enzyme catalyzed reactions.[7–10] Zinc deficiency is the reason for growth retardation, delayed sexual development, infection liability, and diarrhea for children.[11] Excess zinc is also injurious and can cause lethargy, induces copper deficiency, ataxia, Alzheimer's and Parkinson's diseases.[12,13] So quantitative estimation of trace amount of zinc in drinks, food, beverages and also in living body is one of the important research in analytical chemistry. The WHO recommended permissible limit of Zn in drinking water is 76 μM.[14] There are different analytical techniques for precise and selective determination of trace levels of zinc such as atomic absorption spectroscopy,[15] inductively coupled plasma mass spectroscopy,[16] gel electrophoresis,[17] and reverse-phase liquid chromatography.[18] For the recognition of ions (cations, anions) small molecular fluorescence is one of the most prevailing simple and sensitive analytical methods.[19] Luminescent Metal−Organic Frameworks are also useful for a sensitive and selective fluorescence sensing of molecules and ions.[20–22] Chemical sensing via fluorescence signal recognition has been first established during 1980s.[23] Since then researchers are engaged to design various types of fluorogenic sensors to detect Zn²⁺ in different environment including intracellular measurements, Fluorogenic motifs like naphthyl,[24] Diformyl derivative,[25] terpyridyl,[26] quinoline,[27,28] imidazoylpyridyl,[29,30] bipyridyl,[31,32] pyrenyl derivatives,[33] terphenyl-based motif,[34] pyrimidinyl attached Schiff-base,[35] pyrazolyl,[36,37] BINOL,[38] rhodamine,[39,40] catechol appended Schiff base,[41] coumarinyl Schiff base,[42] thiazolyl derivative[43] etc. have successfully been used. Our group is also engaged in the design of vanillinyl thioether Schiff base,[44] diformyl thioether Schiff base.[45]

Herein we report, a diformyl thioether based fluorescent chemosensor, H₂-SAP, prepared by simple Schiff base condensation procedure (Scheme S1) which displays selective fluorescence sensitivity towards Zn²⁺ by chelation enhancement fluorescence effect (CHEF) process in presence of large number of ions and could identify Zn²⁺ in nM level, much lower than so far reported results.[26–45] The composition of the complex formed between Zn²⁺ and H₂-SAP has been supported by spectroscopic data (Mass, Job's plot) and single crystal X-ray crystallography. Theoretical computation of the probe and its Zn²⁺ complex has been used for the explanation of the electronic properties. For the practical applicability, the ligand (H₂-SAP) has been checked in Vero cells (African green monkey kidney cells, ATCC, Manassas, VA, USA) to determine the exogenous zinc ions by fluorescence cell imaging processes.

Results and Discussion

Synthesis and structural formulation

3,3′-((1Z,1′Z)-(((Propane-1,3-diylbis(sulfanediyl))bis(2,1-phenyl-ene))bis(azanylylidene))bis(methanylylidene))bis(2-hydroxy-5-methylbenzaldehyde) (H₂-SAP) is characterized by the mass ion peak at 583.6974 which corresponds to (M+H)⁺ (Figure S1). The ¹H NMR spectrum (CDCl₃) shows characteristic peaks at 13.85 ppm (singlet) corresponds to phenolic-OH; aldehyde-H (CH=O) appears at 10.5 ppm (singlet); imine-H (CH=N) is found

[a] S. Dey, Dr. S. Maity, A. Dasmahapatra, Prof. Dr. C. Sinha
    Department of Chemstry, Jadavpur University, Kolkata-700 032, India
    E-mail: crsjuchem@gmail.com
[b] Dr. D. Chattopadhyay
    ICMR Virus Unit, Infectious Diseases & Beliaghata General Hospital, GB-4, 57,S. C. Bannerjee Road, Beliaghata, Kolkata-700 010, India

194

An azine-based carbothioamide chemosensor for selective and sensitive turn-on-off sequential detection of Zn(II) and $H_2PO_4^-$, live cell imaging and INHIBIT logic gate

Rakesh Purkait,[a] Ananya Das Mahapatra,[b] Debprasad Chattopadhyay,[b] Chittaranjan Sinha*[a]

[a]Department of Chemistry, Jadavpur University, Kolkata 700 032, India
[b]ICMR Virus Unit, Infectious Diseases & Beliaghata General Hospital, GB-4, 57, S. C. Bannerjee Road, Beliaghata, Kolkata – 700 010

Abstract

Hydrazino-carbothioamide, **1**, serves as a turn-on fluorescent chemosensor to Zn^{2+} and the mixture shows green emission (λ_{em} 492) in presence of large number of ions with impressive limit of detection (LOD), 0.59 nM. Intense fluorescence of Zn-complex is selectively turn-off upon adding $H_2PO_4^-$ only to the limit of detection, 26 μM, while other anions remain silent. The sensing mechanism of **1** is established by suppressing the ESIPT of **1** and complexation with Zn^{2+} (CHEF) is supported by Job's plot, ^{1}H-NMR, and HR-MS data. Turn-on-off sequential detection of Zn^{2+} and $H_2PO_4^-$ also have successfully been employed for the engineering of INHIBIT molecular logic gate. The sensor is non-toxic and has been used in identifying Zn^{2+} in the intracellular region of African green monkey kidney cells (Vero cells).

Keywords : Hydrazino-carbothioamide sensor; turn-on-off detection, Zn(II) and $H_2PO_4^-$, INHIBIT logic gate, live cell imaging.

For correspondence : crsjuchem@gmail.com (C. Sinha)

Research Paper

A visible light excitable chromone appended hydrazide chemosensor for sequential sensing of Al+3 and F− in aqueous medium and in Vero cells

Rakesh Purkait[a], Chiranjit Patra[a], Ananya Das Mahapatra[b], Debprasad Chattopadhyay[b], Chittaranjan Sinha[a,*]

[a] Department of Chemistry, Jadavpur University, Kolkata 700 032, India
[b] ICMR Virus Unit, Infectious Diseases & Beliaghata General Hospital, GB-4, 57,S. C. Bannerjee Road, Beliaghata, Kolkata − 700 010, India

A B S T R A C T

A probe, quinoline-2-carboxylic acid (4-oxo-4H-chromen-3-ylmethylene)-hydrazide, (HL), acts as selective and specific fluorogenic sensor to Al+3 in the visible light (435 nm) excitation in presence of biologically available large number of cations and emission appears at (λ_{em}) 520 nm. The limit of detection (LOD) for Al+3 is 7.6 nM in aqueous medium which is less than 10^{-3} times of WHO recommended data (7.41 mM). The Job's plot and mass spectral data support 1:1 composition of the complex [Al(HL)(OH)H₂O](NO₃)₂. The strongly emissive complex turns off upon addition of F− and is detected at the level of (LOD) 7.4 nM. Thus, F−, a harmful water pollutant, could be identified at much lower level of WHO recommended toxic limit (3.68 μM). The absorption and emission spectral features of HL and its Al+3-complex have been explained by DFT computation of optimized geometries and calculation of molecular functions. The devised receptor is non-toxic and has been used in detecting Al+3 in the intracellular region of African green monkey kidney cells (Vero cells) and exhibits an INHIBIT logic gate with Al+3 and F− as chemical inputs by monitoring the emission mode at 520 nm.

© 2017 Elsevier B.V. All rights reserved.

1. Introduction

Aluminium, a non-essential element and significantly available on the earth's crust (8.3% of total mass), is useful in the manufacturing of household utensils, water purification instruments, electrical wirings, and is entering into human body through foods and beverages [1]. It causes Al-related bone disease (ARBD), encephalopathy, myopathy and various neurodegenerative diseases such as, Alzheimer's disease, Parkinsonism dementia etc. in human body and can also damage plant roots [2–5]. World Health Organization (WHO) has assigned Al+3 as prime food pollutants with limiting concentration 200 μg/litre (7.41 mM) and has recommended that tolerable weekly dietary human intake is 7.0 mg/kg body weight [6–8]. Thus detection of Al+3 in water is of urgent important for monitoring human health. Exploration of selective and sensitive chemosensor for detection of ions in solution has been of considerable attention with biological and environmental interest [9–14]. Schiff base ligands have gained recent interest as fluorescent sensors for metal ions including Al+3 due to their relatively easy one step synthesis [15–24]. However, sensing of aluminum in aqueous medium have been rarely reported [25,26], mainly due to sparing or insolubility of organic probe in aqueous media. Therefore it is a challenging task today to develop new sensors for selectively detecting Al+3 in aqueous solutions.

Besides, emissive Al+3-complexes are serving as anion sensor, especially to F− [27–30]. Among the entire range of biologically useful anions, F− possesses significant potential in the prevention of dental caries and treatment for osteoporosis [31,32]. Conversely presence of excess of fluoride in the human body may be dumped as fluorapatite in the bones and teeth leading to osteoporosis, osteosclerosis, dental fluorosis and skeletal fluorosis [33–35]. Thus, it is quite important to develop an efficient F− sensor. The design of dual sensor which is capable to detect sequentially Al+3 and F− by fluorescence ON−OFF signaling response is highly effective. Recently, coumarin based molecular switch for the sequential detection of Al+3 followed by its use for F− sensing is reported [27,28]. Besides, rhodamine based [29] and quinaldine appended [30] chemosensors are also available for the detection of Al+3 and

196

Boswellia serrata oleo-gum-resin and β-boswellic acid inhibits HSV-1 infection *in vitro* through modulation of NF-κB and p38 MAP kinase signaling

Debayan Goswami[a,b], Ananya Das Mahapatra[a], Subhadip Banerjee[b], Amit Kar[b], Durbadal Ojha[a], Pulok K Mukherjee[b], Debprasad Chattopadhyay[a]

[a] ICMR Virus Unit, ID and BG Hospital, General Block 4, 57 Dr. Suresh Chandra Banerjee Road, Beliaghata, Kolkata 700010, India.
[b] School of Natural Product Studies, Department of Pharmaceutical Technology, Jadavpur University, Kolkata700032, India.

Short Title: Inhibition of HSV-1 by *Boswellia serrata*

Corresponding Author(s)

Debprasad Chattopadhyay
ICMR Virus Unit, ID & BG Hospital
General Block 4, First Floor
57 Dr Suresh Chandra Banerjee Road, Beliaghata,
Kolkata 700010, India
Email: debprasadc@yahoo.co.in

1

Spectroscopic characterization, antimicrobial activity and Molecular Docking Study of novel azo-imine functionalized sulphamethoxazoles

Nilima Sahu, Sudipa Mondal , Kaushik Naskar, Anyna Das Mahapatra, Suvroma Gupta,

Alexandra M. Z. Slawin , Debprasad Chattopadhyay and Chittaranjan Sinha[*]

Sulfamethoxazolyl-azo-imine derivatives (**1**, **2a-f**) have been examined against gram positive bacteria, *B. subtillis* and gram negative *E. coli* and have found effective selectively on *B. subtillis*. Some of them also show antiviral activity against HSV-1Finfection. The structures of the compounds are supported by different spectroscopic data and single crystal X-ray structure of **2c**. The compounds have been docked in the DHPS protein cavity to examine their binding strength and **2c** shows highest binding strength.
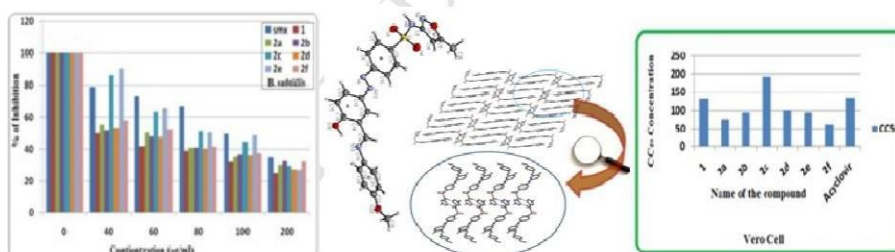
Pyridylthioether-hydroxycoumarin Schiff base as selective Zn^{2+} fluorescence sensor, application in life cell imaging and uses of resulting complex as secondary probe for ATP sensing

Chiranjit Patra,[a] Chandana Sen,[a] Ananya Das Mahapatra,[b] Debprasad Chattopadhyay,[b] Ambikesh Mahapatra,[a] and Chittaranjan Sinha[a]*

[a]Department of Chemistry, Jadavpur University, Kolkata 700 032, India, c_r_sinha@yahoo.com

[b]ICMR Virus Unit, Infectious Diseases & Beliaghata General Hospital, GB-4, 57, S. C. Bannerjee Road, Beliaghata, Kolkata – 700 010, debprasadc@gmail.com

Book Chapter

CHAPTER 3

Ethnomedicinal Wisdom: An Approach for Antiviral Drug Development

Ananya Das Mahapatra[1], Priyanka Bhowmik[1], Anwesha Banerjee[1], Apurba Das[1], Durbadal Ojha[1] and Debprasad Chattopadhyay[1,2]
[1]ICMR–Virus Unit Kolkata, ID & BG Hospital Campus, Kolkatta, West Bengal, India
[2]ICMR–National Institute of Traditional Medicine, Belagavi, Karnataka, India

3.1 ETHNOMEDICINE: A BOON

A famous quote of Norwegian Artist Edvard Munch "*Nature is not all that is visible to the eye... also includes the inner pictures of the soul*" speaks many things about the mother "Nature" and her creation. For the past 100 years, mankind have been trying to unravel the secrets of nature, yet continue to be surprised by its revelations day by day. Nature is vast in its resources which not only provide food, clothes, shelter, and antiques but also provide medicine since ages. Out of these resources the greatest gift of nature is her atmosphere with food and medicine, which not only to help mankind to sustain but also to grow, develop, and survive, particularly from the diseases and sufferings. The study of natural resources traditionally used to cure or manage ailments in diverse ethnic culture is collectively termed as "Ethnomedicine" (Chattopadhyay, 2010; Chattopadhyay et al., 2009a).

Scientifically, "Ethnomedicine" is the study of "traditional medicine" of ethnic communities, their knowledge and practices that transmitted orally over centuries, and evolved over millennia of human existence (Chattopadhyay, 2009, 2010). The indigenous people of India till date used their medicaments or "so called medicines" which might be more appropriately defined as the use of plants in the treatment of diseases and should be more accurately termed as "Ethnobotanical medicine" (Fabricant and Farnsworth, 2001). For a considerable period of time, traditional medicine and ethnomedicine were ignored by the clinicians and biomedical practitioners due to a number of factors including the

35

ScienceDirect

Evidence-Based Validation of Herbal Medicine (Second Edition)

Translational Research on Botanicals

2022, Pages 251-281

Chapter 10 - Validation of antiviral potential of herbal ethnomedicine

Amit Kar [a], Ananya Das Mahapatra [b], Barun Das Gupta [c], Debprasad Chattopadhyay [b, d]

[a] Institute of Bioresources and Sustainable Development (IBSD), Department of Biotechnology, Ministry of Science and Technology, Government of India, Takyelpat, Imphal, Manipur, India
[b] ICMR-National Institute of Cholera and Enteric Diseases Virus Research Laboratory, I.D. & B.G. Hospital, Kolkata, West Bengal, India
[c] School of Natural Product Studies, Department of Pharmaceutical Technology, Jadavpur University, Kolkata, West Bengal, India
[d] ICMR-National Institute of Traditional Medicine (ICMR-NITM), Belagavi, Karnataka, India

Available online 15 July 2022, Version of Record 15 July 2022.

Show less ∧

≡ Outline | ⤝ Share | 🗦 Cite

203

JOHN WILEY AND SONS LICENSE
TERMS AND CONDITIONS

Dec 08, 2021

This Agreement between Jadavpur University -- Ananya Das Mahapatra ("You") and John Wiley and Sons ("John Wiley and Sons") consists of your license details and the terms and conditions provided by John Wiley and Sons and Copyright Clearance Center.

License Number	5204090344120
License date	Dec 08, 2021
Licensed Content Publisher	John Wiley and Sons
Licensed Content Publication	ChemistrySelect
Licensed Content Title	Silver Nanoparticles Derived from Albizia lebbeck Bark Extract Demonstrate Killing of Multidrug-Resistant Bacteria by Damaging Cellular Architecture with Antioxidant Activity
Licensed Content Author	Debprasad Chattopadhyay, Provash Chandra Sadhukhan, Chittaranjan Sinha, et al

---

SPRINGER NATURE

An extract of Stephania hernandifolia, an ethnomedicinal plant, inhibits herpes simplex virus 1 entry

Author: Joy Mondal et al
Publication: Archives of Virology
Publisher: Springer Nature
Date: May 26, 2021

Copyright © 2021, The Author(s), under exclusive licence to Springer-Verlag GmbH Austria, part of Springer Nature

Quick Price Estimate

This service provides permission for reuse only.
If you do not have a copy of the article you are using, you may copy and paste the content and reuse according to the terms of your agreement. Please be advised that obtaining the content you license is a separate transaction not involving RightsLink.

⚑ Selection of non-commercial (non-profit) signifies you will reuse content in non-commercial (non-profit) settings. Reuse not permitted in for-profit settings including, but not limited to: textbook publishing, medical communication companies, or pharmaceutical organizations.